Fossil Energy Program Annual Progress Report

Oak Ridge National Laboratory
MANAGED BY UT-BATTELLE FOR THE DEPARTMENT OF ENERGY

ORNL 2002-031194/vlc

ORNL/TM-2002/122

Fossil Energy Program Annual Progress Report for April 2001 Through March 2002

Roddie R. Judkins
Program Manager

Paul T. Carlson
Technical Assistant

July 2002

Prepared for the
DOE Office of Fossil Energy
(AA, AB, AC, AW, AZ, SA)

Prepared by the
OAK RIDGE NATIONAL LABORATORY
Oak Ridge, Tennessee 37831-6285
managed by
UT-BATTELLE, LLC
for the
U.S. DEPARTMENT OF ENERGY
under Contract DE-AC05-00OR22725

CONTENTS

CONTENTS

CONTENTS

COMBUSTION RESEARCH

We would like to thank the ORNL Creative Media Solutions group for its assistance in this project. Vickie Conner, in Graphics Services, designed the cover; Sandra Lyttle, in Publishing Services, formatted the papers and created the PDF file.

FOSSIL ENERGY PROGRAM ANNUAL PROGRESS REPORT FOR APRIL 2001 THROUGH MARCH 2002[1]

Roddie R. Judkins, Program Manager
Paul T. Carlson, Technical Assistant
Oak Ridge National Laboratory

INTRODUCTION

The mission of the Fossil Energy Program is to conduct research and development that contribute to the advancement of fossil energy technologies. The Oak Ridge National Laboratory Fossil Energy Program research and development activities, performed for the Department of Energy Assistant Secretary for Fossil Energy, cover the areas of coal, clean coal technology, gas, petroleum, and support to the Strategic Petroleum Reserve.

Projects on the ORNL Fossil Energy Program are supported by the U.S. Department of Energy Office of Fossil Energy, the DOE National Energy Technology Laboratory, the DOE Fossil Energy Clean Coal Technology Program, the DOE National Petroleum Technology Office, and the DOE Fossil Energy Office of Strategic Petroleum Reserve.

The ORNL Fossil Energy Program shares with DOE Oak Ridge Operations technical management responsibility for all activities on the DOE Fossil Energy Advanced Research Materials Program. The Advanced Research Materials Program includes research at other DOE and government laboratories, at universities, and at industrial organizations.

[1]Research sponsored by the U.S. Department of Energy, Office of Fossil Energy, under contract DE-AC05-000R22725 with UT-Batttelle, LLC.

CORROSION RESISTANT COATINGS FOR CERAMICS

B. L. Armstrong, M. P. Brady, K. M. Cooley, J. A. Haynes, and H-T. Lin
Oak Ridge National Laboratory

INTRODUCTION

Silicon based ceramics such as silicon carbide (SiC) are attractive for use in hot-gas filters, heat exchangers, and other devices for advanced energy producing systems due to their higher temperature capability relative to metals, high thermal conductivity, retention of mechanical properties at operating temperatures, and excellent thermal shock resistance. Typically, a slow growing, silica scale protects the SiC material. This scale limits oxygen diffusion and thus prevents further attack of the substrate. A major drawback of SiC ceramics is the susceptibility of the silica scale to volatilization and corrosion by alkali salts such as Na_2SiO_4 and steam at high temperatures, which limits the applicability for extended service in many fossil energy conversion and combustion system environments. Thus, the use of protective coatings or the development of material with improved stability in these harsh environments becomes necessary. To address this issue, the development of novel coatings for SiC ceramics utilizing low-cost aqueous based processing methods such as screen-printing and dip coating is being pursued. Mullite was deposited on to SiC substrates and was evaluated for feasibility, specifically the thickness, density, microstructure and stability of the coating. Additionally, a processing approach is being developed for materials that form other types of protective scales such as the direct conversion of metal coatings to form alumina scales. Interim results for all of these approaches will be discussed.

The purpose of this program is to develop ceramic coatings with enhanced corrosion resistance through improvements in the composition and processing of the coating. Processing innovations will focus on aqueous coating development including such techniques as spray coating, screen-printing, and dip coating. In addition, materials that form scales other than silica will be evaluated. Candidate materials will be exposed in facilities at ORNL and will be characterized to identify the most promising materials for specific applications.

Slurry Coating Development

This program has been investigating several approaches to improving the environmental stability of SiC. One approach that is being taken is to coat the surface of a hexaloy SiC substrate using low cost, slurry based coatings. There are numerous slurry-based approaches including dip coating, screen-printing, spin coating, spray coating, and vacuum coating. All processes have indicative advantages and challenges, and these are summarized in Table 1. As a result, two coating methods were selected for evaluation; a near term, materials evaluation approach, screen-printing, and a long term, system

Table 1

Technique	Advantages	Issues
Dip Coating*	Inexpensive. Conducive to 3D structures.	Thickness variation as a function of dip direction.
Screen Printing*	Controlled coating thicknesses and densities	Difficult to coat 3D structures.
Spin coating	Thin coating.	Difficult to coat 3D structures.
Spray Coating*	Inexpensive. Conducive to 3D structures.	Thickness variation. Line of sight.
Vacuum Infiltration	Can coat internal or weave type structures.	Viscosity of slurry/depth of slurry penetration.

evaluation approach, dip coating. Screen-printing was selected such that the candidate material systems could be quickly "screened" for efficacy while minimizing processing set-up times and parameters. Once the material issues are evaluated, development of a dip coating system will be initiated to demonstrate processing feasibility. The candidate material system, mullite, was selected based on thermal expansion match to SiC and relative corrosion resistance to fossil environments.

Coatings of Washington Mills mullite were prepared using the screen-printing process. Screen-printed coatings of mullite were densified on to the surface of SiC substrates using traditional air sintering techniques. The resulting coatings varied in thickness from 9 microns to 150 microns depending upon processing conditions. The importance of the effect of processing on the resulting microstructure and ultimately the effectiveness of the coating is illustrated in Fig. 1. The edge views shown in Figs. 1A and B are of sintered coatings that were applied using screen-printing and spray coating, respectively. The screen-printed coating is thin (approximately 10 microns) and dense whereas the sprayed coating is much thicker (approximately 25 microns) to provide closed porosity.

A SiC sample with a coating of approximately 150 microns thick was tested at 1204°C for 500 hours in 100% humidity (Fig. 2). Upon completion of the test, there was little evidence of the mullite coating in the central path of the gas stream. Some mullite remained at the sample edges. In the central areas, silica was found underneath a mixed layer of mullite grains in an alumino-silicate matrix. The oxidation was comparable to an uncoated surface. As a result, processing conditions are being adapted to increase the density of the coating (increasing the solids content of the ink), to densify in non-oxidizing conditions to minimize any oxygen present in the boundary layer, and to add dopants such as alumina to the mullite to tie up any residual silica that may be present.

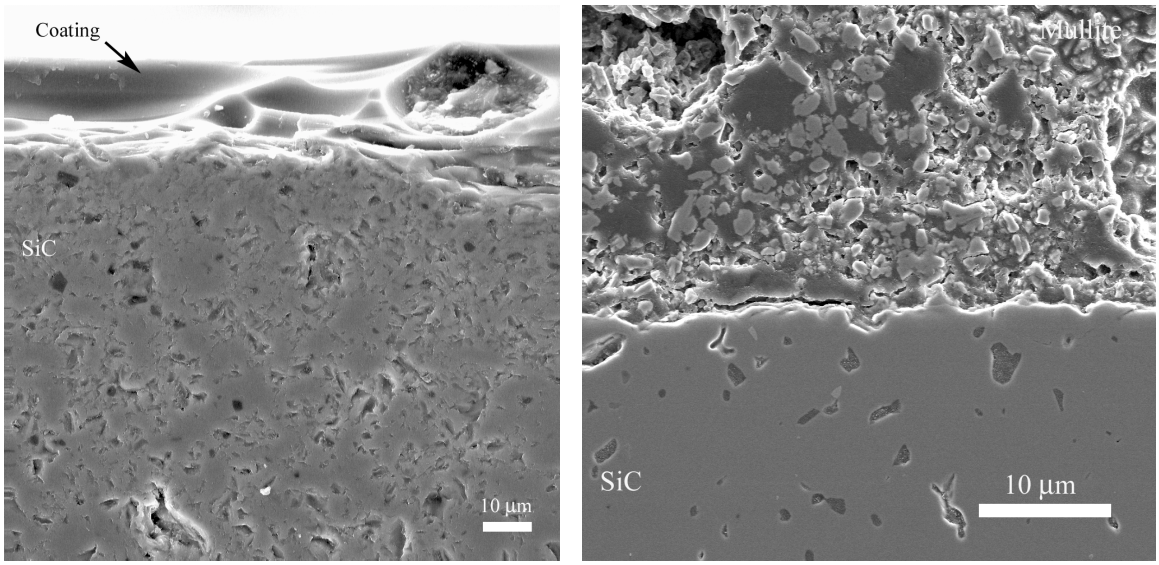

Fig. 1. (A) Mullite deposited by screen printing. Sintered at 1600°C in air for 2 hours. (B) Mullite deposited by spraying. Sintered at 1600°C in air for 2 hours.

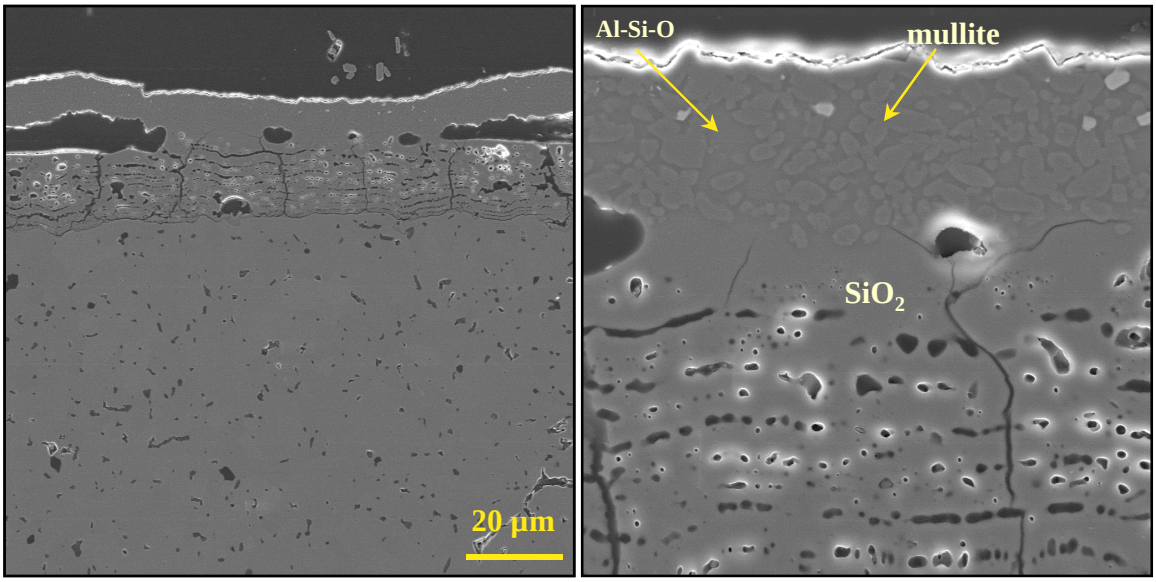

Fig. 2. Polished cross section of mullite coating on SASiC after 500 hours exposure at 1204°C, 100% H_2O.

Surface Alloy Development Feasibility Study One challenge in the densification of a slurry coating is the prevention of silica formation at the coating – substrate interface. Oxygen will diffuse to the substrate during the sintering process until densification is complete. Even if steps are taken to limit the oxygen diffusion during this densification process, the formation of a silica layer at the coating – substrate interface can still occur if the coating does not completely prevent oxygen transport. Thus, the development of a sacrificial coating that oxidizes and/or diffuses via a heat treatment or in-situ to form a volatility barrier have been proposed to address this concern. Thus, the concept of looking at the use of a

thin metallic precursor layer as a route to form a self-graded oxide surface layers that can act as volatility barriers to protect against aggressive species that would degrade a silica layer was proposed. In this approach, the metal layer would completely convert to ceramic by an oxidation pretreatment.

For a feasibility evaluation, the authors proposed using four of the well characterized alumina-forming intermetallic systems, yttrium doped chrome aluminide (Cr_2AlY), hafnium doped nickel aluminide (NiAlHf), chromium/yttrium doped nickel aluminide (NiCrAlY), and chrominum/yttrium doped iron aluminide (FeCrAlY). These compositions were selected with a range of CTE, high temperature strength properties in the metal layer, and base metal component chemistries in order to explore what the key issues are regarding the conversion of the metal layer to ceramic and the formation of a dense, adherent oxide after oxidation pretreatment. It is anticipated that the oxide layer formed will be a duplex layer with an outer layer of alumina and an inner layer consisting of a graded oxide layer of the base metal of the aluminide, Si and Al, as depicted in Figs. 3 and 4.

In order to determine if the concept of using thin metallic precursors was feasible, an initial experiment using another high coefficient of thermal expansion material, TiCrAlY, was utilized. It was surmised that if this material would survive excessive thermal cycling in laboratory air without spalling off the substrate, then the other materials selected would also be feasible. Feng Huang and Mark L. Weaver of the University of Alabama, Tuscaloosa sputtered a 2–3 micron coating of Ti-51Al-12Cr on to a SASiC substrate. The substrate was then exposed to ten, 100 hour cycles to 1100°C in laboratory air. Excellent adherence was seen as no spallation occurred. As shown in Fig. 4, the alumina layer that formed at the surface was not continuous. In spite of that, it was determined that the concept of sacrificial metallic layers was worth more investigation.

Thus, the University of Alabama sputtered NiAlHf, Cr_2AlY, NiCrAlY, and FeCrAlY on to Hexaloy SASiC substrates. The resulting substrates were exposed to 1150°C in flowing oxygen for 0.5 hour to convert the coating to alpha alumina prior to stability testing. The resulting microstructures of the SASiC substrates exposed at 1150°C are shown in Figs 5 through 8. All of the coatings were adherent in spite of the thermal expansion coefficient mismatch from the starting materials. However, the full conversion to alpha alumina was not seen. Raman spectroscopy showed evidence of transient aluminas in all of the preheat-treated samples. The contribution of the coating and its interaction with the substrate can be noted in the different alumina morphologies produced after pretreatment as shown in Figs. 5 through 8. Both the NiAl(Hf) and NiCrAlY coatings showed needle like morphology with some overall porosity. The Cr_2AlY and FeCrAlY had a more spherical morphology as expected with alpha alumina, but the overall density of the coating was still poor. The substrates were subsequently exposed to 72 hours at 1000°C in 100% humidity, and analysis is currently being completed. It is anticipated that the results should reflect that off a non-protective (non-dense) coating.

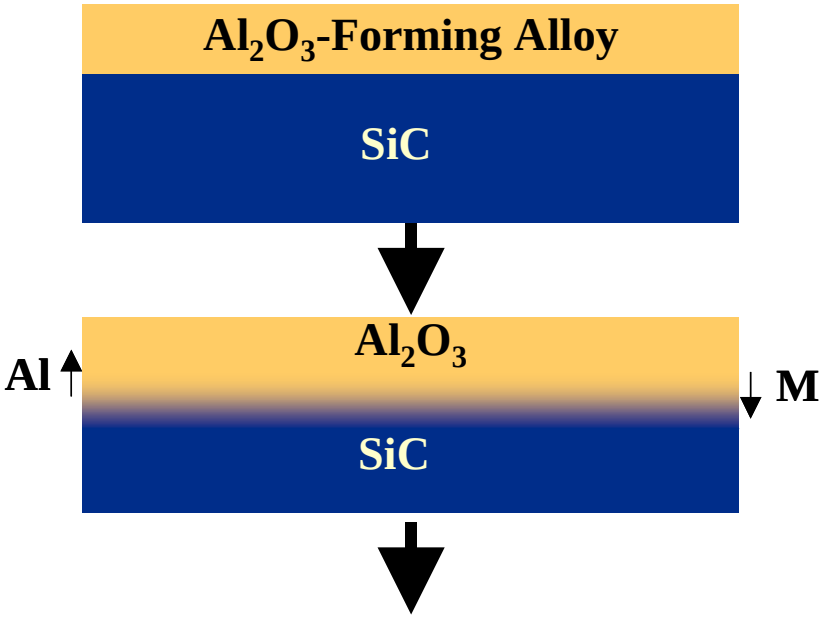

Fig. 3. Schematic of a sacrificial self-grading alumina-forming precursor.

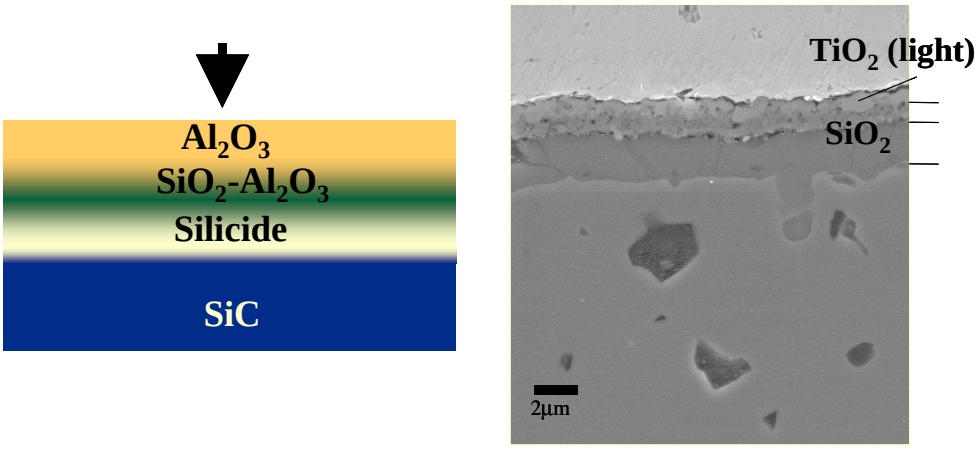

Fig. 4.Exposure of 3 mm sputtered Ti-51Al-12Cr on SiC showed excellent adherence after ten, 100 hour cycles to 1100°C in laboratory air. No spallation occurred.

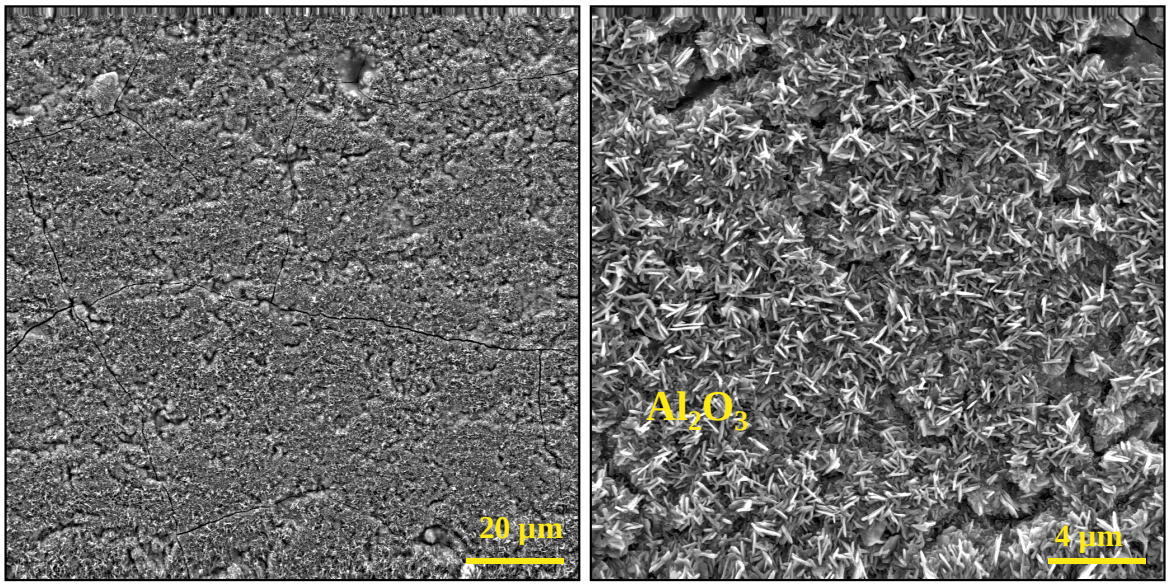

Fig. 5. Surface feature of NiAl(Hf) coating on SASiC after 1150°C, 30 minute heat treatment.

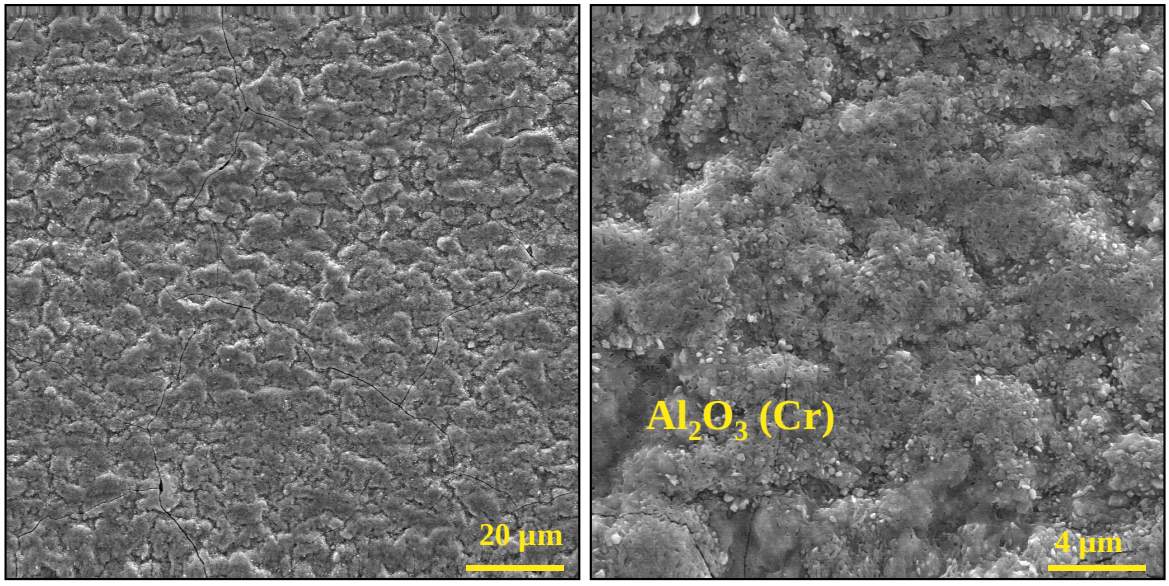

Fig. 6. Surface feature of Cr_2(Al)Y coating on SASiC after 1150°C, 30 minute heat treatment.

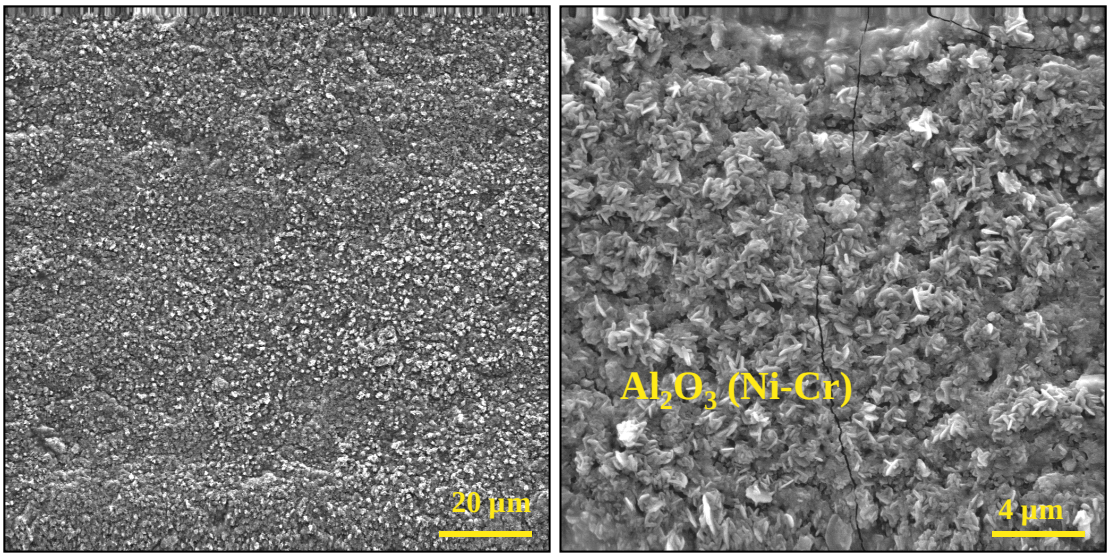

Fig. 7. Surface feature of NiCrAlY coating on SASiC after 1150°C, 30 minute heat treatment.

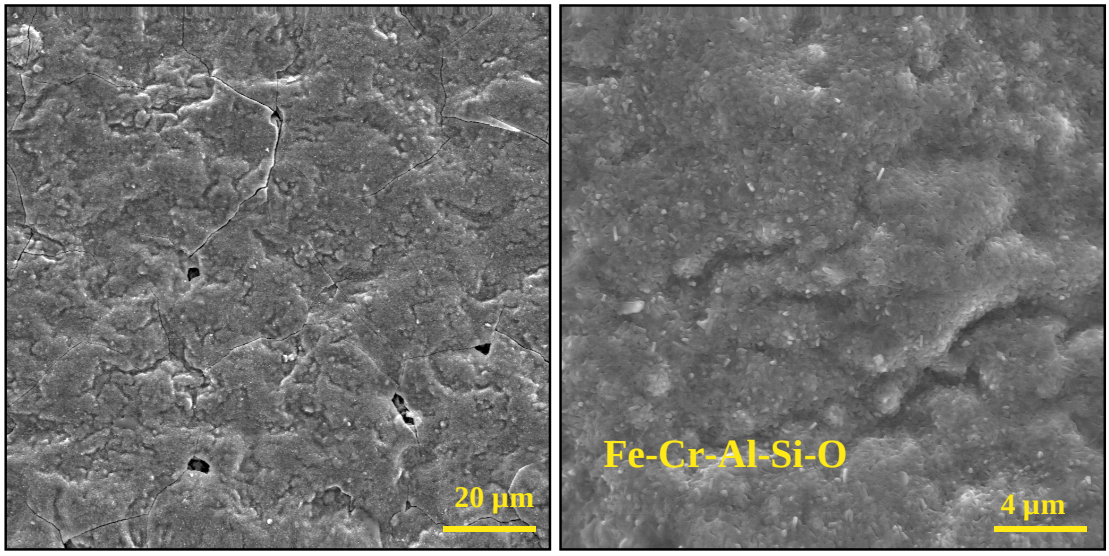

Fig. 8. Surface feature of FeCrAlY coating on SASiC after 1150°C, 30 minute heat treatment.

SUMMARY

Two approaches were taken to address the development of novel, protective coatings for SiC ceramics for use in harsh fossil environments. The first approach utilized a low cost aqueous based slurry method. Screen-printed mullite coatings on SASiC substrates were tested at 1204°C for 500 hours in 100% water environment and demonstrated the feasibility of this process. The second approach that was proposed was a sacrificial coating that oxidizes via a heat treatment to form a volatility barrier. The feasibility of the concept was demonstrated using a thin metallic precursor layer. Four alumina-forming alloys were chosen and were tested first at 1150°C for 30 minutes in flowing oxygen and subsequently at 1000°C for 72 hours in 100% water environment.

CHEMICALLY VAPOR DEPOSITED YSZ FOR THERMAL & ENVIRONMENTAL BARRIER COATINGS

T. M. Besmann
Oak Ridge National Laboratory

V. Varanasi and T. J. Anderson
University of Florida

T. L. Starr and W. Xu
University of Louisville

INTRODUCTION

Thermal barrier coatings, or TBC's, are excellent materials for improving the performance, longevity, and overall costs of gas turbine engine (GTE's) lifetimes (Haynes 1997). These ceramic coatings, made of yttria-stabilized zirconia (YSZ), improve GTE lifetimes by reducing the turbine blade temperature and preventing turbine blade failure (Haynes 1997). A schematic of the TBC system is shown in Fig. 1.

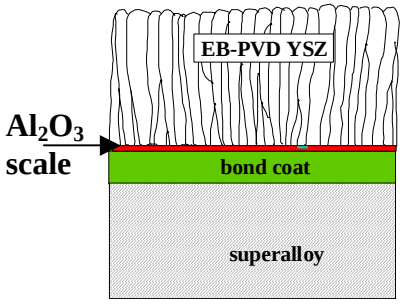

Fig. 1. Schematic of TBC.
(After J. A. Haynes)

The nickel- or cobalt-superalloy turbine blade is protected by three coating layers: an oxidation-resistant aluminum-rich bond coat, a thermally-insulating YSZ top coat, and an α-alumina scale interface (Haynes 1997). The aluminum-rich bond coat is an alloy of MCrAlY (M= Ni or Co), and is coated onto the blade by plasma spraying (Haynes 1997). The YSZ top coat is typically zirconia (ZrO_2) stabilized by six- to eight-weight percent (3.5- to 5.5-mole percent) yttria (Y_2O_3), and is currently deposited onto the bond coat by electron-beam, physical vapor deposition (EB-PVD) (Haynes 1997).

There are several advantages to using a YSZ top coat for the superalloy blade. The decrease in blade temperature of as much as 167°C improves the blade lifetime by three- to four-fold. This top coat can even improve fuel consumption by more than one percent. In addition, less air-cooling will be required, thus increasing the GTE thermal efficiency and reliability (Haynes 1997).

There are two methods by which YSZ is fabricated: (1) plasma spraying and (2) EB-PVD (Haynes 1997). Upon thermal cycling, plasma sprayed YSZ tends to promote a rough top coat-scale interface. This rough coating has a strong tendency to spall due to inadequate thermal expansion match between the YSZ and the alumina. The EB-PVD YSZ has a columnar microstructure which can allow grains to separate to accommodate substrate expansion, and a much smoother top coat-scale interface. Since this EB-PVD coating has a desirable columnar microstructure, there tends to be less of a thermal mismatch issue

between the YSZ top coat and the underlying bond coat and scale interface. Since the EB-PVD technique allows for reduced thermal match mismatch stess and improved chemical adhesion between the top coat and scale interface, this technique is preferred over plasma spraying (Haynes 1997).

EB-PVD, however, is very costly. An alternative is metallorganic chemical vapor deposition (MOCVD) of the YSZ top coat. This is potentially a much cheaper technique, in which transport and kinetic control can help to fabricate tailored YSZ coatings. The goal is to obtain the 100 to 250 μm YSZ coatings, with a similar microstructure to that of EBPVD, but at a much lower cost. In addition, the technique can allow coating of surfaces that are unavailable to EB-PVD and can produce a uniform seal-coat on top of an EB-PVD layer.

EXPERIMENTAL DESIGN

The MOCVD experimental design is based on several factors. First, low cost and effective precursor. Second, a controlled oxygen source. Third, a substrate that simulates the scale interface or blade material. Finally, a flow system and reactor design that is gas-diffusion deposition rate-limited.

For the zirconium and yttrium metal sources, $Zr(tmhd)_4$ and $Y(tmhd)_3$ were chosen due to their adequate closeness in vapor pressure, their high thermal stability (up to 500°C), their cost, and their success as a precursor for YSZ thin films and $YBa_2Cu_3O_7$ superconductors. The oxygen source was chosen to be pure O_2 and the reactions are as follows:

$$Zr(tmhd)_4(g) + xsO_2(g) \rightarrow ZrO_2(s) + \text{waste organics} \quad (1)$$

$$Y(tmhd)_3(g) + xsO_2(g) \rightarrow Y_2O_3(s) + \text{waste organics} \quad (2)$$

To complement this choice of precursors and oxygen source, a stagnation flow design was employed because it allows the determination of the rate-limiting processes and promotes efficient deposition. Stagnation flow offers design flexibility by controlling residence time, prevents pre-reaction of metallorganic precursors, provides for high deposition rates, and promotes deposition uniformity. Furthermore, stagnation flow allows growth rates to be gas-diffusion limited as opposed to surface-reaction/kinetics limited.

In a stagnation flow reactor the gas mixture with a laminar flow profile approaches a gas-distributing nozzle in a cylindrical flow tube reactor [Fig. 2(A)]. The gas-distribution nozzle "breaks up" the laminar flow profile of the gas stream (B) which enters the region above the substrate (C). In this region, the velocity, temperature, and reactant concentration gradients of the forced-convective gas stream are independent of the substrate diameter. As the gases approach the substrate, heterogeneous reactions occur on the substrate to form the coating (D). The coating thickness is independent of the substrate diameter and grows in the axial direction. Moreover, the coating growth rate depends solely on the gas flow.

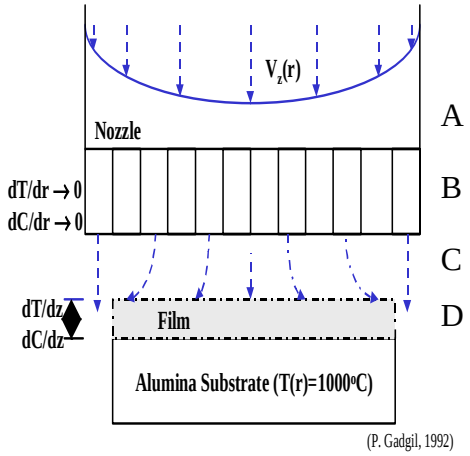

Fig. 2. Schematic of stagnation-pont flow reactor. *(After P. N. Gadgil)*

A reactor and flow system have been developed for the deposition of YSZ (Fig. 3). The precursors were dissolved in tetrahydrofuran (THF) and continuously injected through a check valve into the reaction chamber by a syringe pump. To ensure quick evaporation of the precursor and solvent, the precursor solution was fed to an ultrasonic nozzle. The axygen carrier gas was fed through heated gas lines and into the stainless steel injector. The gas streams mix and flow through the injector (maintained at 200°C by a heating jacket of silicone oil) toward the substrate. The substrate (inductively heated by a radio frequency coil heating a Mar-M247 susceptor) was maintained at 900°C for the set of experiments described in this report. Waste gases were trapped in an isopropanol-dry ice bath. The deposition time was typically one hour.

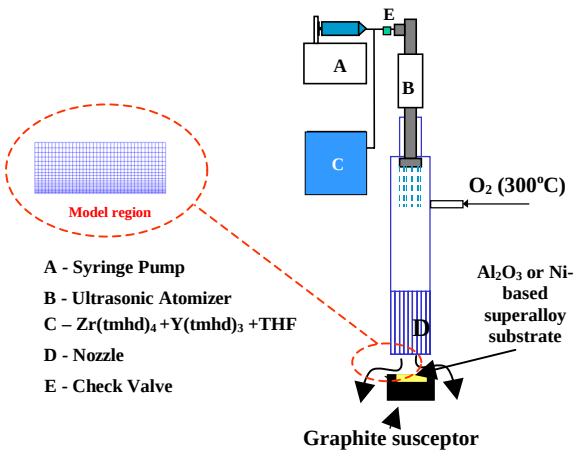

Fig. 3. Flow schematic of MOCVD reactor.

RESULTS AND DISCUSSION

X-ray diffraction (Cu K-α, θ-2θ) revealed that the deposition of 8 wt % YSZ (tetragonal) was successful on the superalloy (Fig. 4) and alumina. Scanning electron microscopy (Hitachi S800) showed the coatings were 3 to 4 μm thick on the alumina (Fig. 5) and 4 to 5 μm thick on the superalloy (Fig. 6).

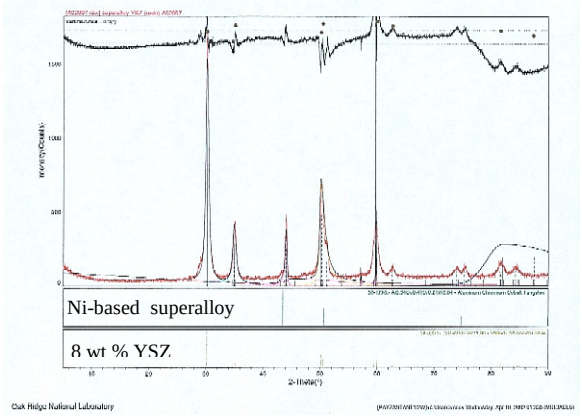

Fig. 4. Results of XRD.

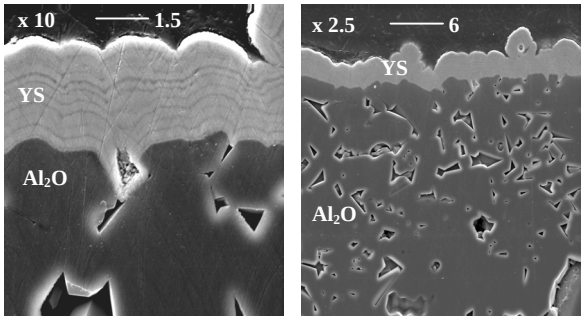

Fig. 5. Micrograph of YSZ on alumina.

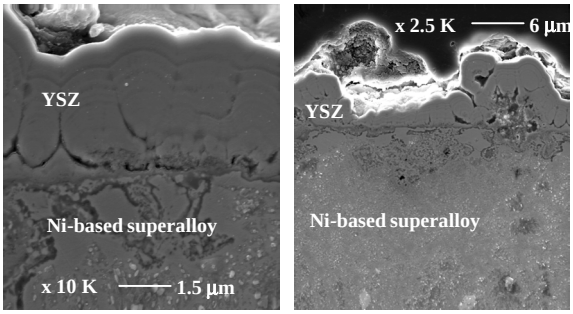

Fig. 6. Micrograph of YSZ on the superalloy.

Using these experimental conditions, detailed modeling predicted deposition rate and uniformity shown in Fig. 7. On one hand, there is moderately good agreement between experimental deposition rates and modeled deposition rates (12 to 13 µm/h). On the other hand, there was some variation in the coverage of the coating technique. Experimentally, the coating is uniform with only a 0 to 15% difference in thickness between the edges and the middle of the substrate whereas modeling predicted a 2 to 5% difference.

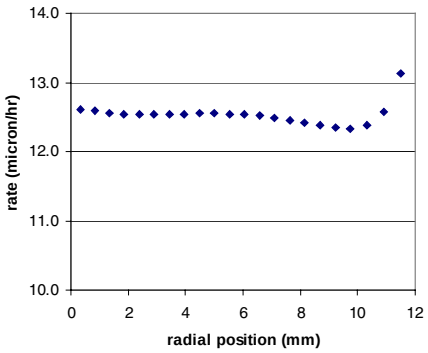

Fig. 7. Modeled results of experimental conditions. Conditions: Ts = 960°C, P = 18 torr, 0.87 ml/min THF soln. with X(tmhd) at 0.04 g/ml, Y/(Y+Zr)=0.165, 100 sccm O_2. (*After T. L. Star*)

FUTURE WORK

While successful, these preliminary results indicate that more work is needed to optimize the precursor delivery system so as to obtain better control of the rate of precursor

flow to the substrate. A critical next step in the effort is to develop an understanding of how deposition parameters can control microstructure and can deposit columnar structures. A kinetics parametric study will allow improvement in the parallel modeling effort, and this has a high priority.

SUMMARY

The need to reduce the cost of TBC fabrication is necessary for the commercialization of these coatings for gas turbine engines. MOCVD offers a cost effective, non-"line-of-sight", uniform deposition technique that can either replace or supplement EB-PVD coatings. A stagnation flow reactor was used to successfully deposit YSZ on alumina and a nickel-based superalloy. Results of XRD and SEM show that YSZ coatings were successfully obtained with a thickness of 3 to 4 μm on alumina and 4 to 5 μm on the superalloy for a one hour deposition time. Future efforts will require refining the precursor delivery system and obtaining an understanding of the microstructure-deposition parameter relationship and the kinetics of deposition.

REFERENCES

Gadgil, P. N. "Single Wafer Processing in Stagnation Point Flow CVD Reactor: Prospects, Constraints and Reactor Design." *Journal of Electronic Materials*, Volume 22, Number 2: 1992.

Haynes, J. A. *Oxidation and Degeneration of Thermal Barrier Coating System*. University of Alabama at Birmingham. Birmingham, Alabama: 1997.

Matsuno, S., F. Uchikawa, and S. Utsunomiya. "Etalorganic Chemical Vapor Deposition Using a Single Solution Source for High J_C $Y_1Ba_2Cu_3O_{7-X}$ Superconducting Films." *Applied Physics Letters*. Volume 60, Number 19, pp. 2427–2429: 1992.

Jiming Zhang, Robin A. Gardiner, Peter S. Kirlin, Robert W. Boerstler, and John Steinbeck. "Single liquid source plasma-enhanced metalorganic chemical vapor deposition of high-quality $YBa_2Cu_3O_{7-x}$ thin films". *Applied Physics Letters:* Volume 61, Number 24, 1992.

Starr, T. L. ibid. 2002

MULTI-PHASE Cr-BASED ALLOYS FOR AGGRESSIVE HIGH TEMPERATURE ENVIRONMENTS

M. P. Brady, C. T. Liu, P. F. Tortorelli,* J. H. Zhu, L. R. Walker,
J. L. Wright, and C. A. Carmichael
Oak Ridge National Laboratory
***Tennessee Technological University**

INTRODUCTION

The objective of this work is to develop and characterize a new family of Cr alloys strengthened with intermetallic second phases for structural use in aggressive corrosion environments at 900 to 1300°C. The potential advantages of Cr are high melting point, moderate density, and good high-temperature corrosion resistance in many environments. However, these are negated by inadequate high-temperature strength, ambient-temperature brittleness, and susceptibility to environmental embrittlement at elevated-temperatures by nitrogen penetration. The developmental alloys consist of a Cr solid solution matrix reinforced with the intermetallic Cr_2Ta Laves phase as a dispersed second-phase particle or of lamellar Cr solid solution-Cr_2Ta eutectic structures [1–4]. Substantial progress has been made in developing attractive high-temperature tensile strength, creep resistance, and oxidation/hot corrosion resistance through control of alloy composition and microstructural features [1,3]. For most potential components/applications, it is desirable to have a minimum room-temperature fracture toughness of at least 15–20 MPa√m. However, efforts to improve room-temperature toughness by microalloying the Cr matrix phase and microstructure control have not been successful, with the best alloys exhibiting only modest ambient-temperature fracture toughness of 12–14 MPa√m.

Two approaches for improved fracture toughness at room temperature have been investigated: (1) ductilization of unalloyed Cr by the addition of MgO [5–7] and (2) macroalloying to improve the fracture toughness of the Cr matrix phase in Cr-Cr_2Ta alloys [8]. Tensile elongations in excess of 10% were achieved by extruded MgO-dispersed Cr alloys at room temperature. However, these alloys exhibit relatively low yield strengths (30 ksi range) and efforts to increase strength by Cr_2Ta precipitates without sacrificing the gains made in room-temperature ductility have not been successful. The MgO-dispersed Cr alloys were also found to exhibit excellent corrosion resistance in alkali molten salts, which makes them of great interest for application in high-temperature black liquor gasifiers and kraft recovery boilers [9], for which high strength is not a key issue for many components. Development efforts devoted to Cr-MgO alloys were successfully spun off during FY 2002 into a new project under the Office of Industrial Technologies Forest Products Program specifically targeted to these application.

Recent efforts devoted to macroalloying additions have succeeded in significantly improving the room-temperature fracture toughness of the Cr-Cr_2Ta family of alloys by the addition of significant amounts of transition metal(s), referred to as X due to patent considerations [8]. During this year, the development effort has been focused on the effect of X additions on the microstructure and properties of Cr-Cr_2Ta alloys.

DISCUSSION OF CURRENT ACTIVITIES

Experimental

Subsized chevron-notched three-point bend samples approximately $3 \times 4 \times 25$ mm were used to evaluate fracture toughness at room temperature. Fracture toughness values obtained by this technique should be considered semiquantitative; details are provided in reference 10. The samples were prepared to a 600 grit surface finish and then notched using a low speed diamond saw. The crosshead speed was 0.6mm/min. A modulus of 250 GPa was estimated. Tensile properties were evaluated at 1000°C in air (5 minute heat up) using sheet tensile samples approximately 0.6–0.7 mm thick with a gage length of 12.7 mm. The samples were prepared to a surface finish of 600 grit and a crosshead speed of 2.54mm/minute was used (strain rate of 3.33×10^{-3}/s). Isothermal oxidation behavior was evaluated at 1100°C in air by thermogravimetric analysis (TGA) using 12 mm $\times$ 12 mm $\times$ 1 mm coupons prepped to a 600 grit finish. Cyclic oxidation was evaluated at 1100°C in air for eleven, 100 h cycles (1100 h total exposure).

Microstructure

Analysis of a series of Cr-Ta-X base alloys by electron probe microanalysis (EPMA) indicated that additions of X preferentially partition to the Cr_2Ta Laves phase (1.4:1 where 1 represents the overall bulk X content in the alloy) resulting in X depletion in the Cr matrix phase (0.85:1). The eutectic composition was, however, strongly affected. The eutectic composition of the Cr-Cr_2Ta base alloys without the X element contains 9.8 at.% Ta, but is shifted to lower concentrations of Ta (several at.%) with increasing levels of X additions. A typical eutectic structure is shown in Fig. 1.

Mechanical Properties

The shift in eutectic composition had a profound effect on the mechanical properties of these multi-phase alloys at room and elevated temperatures, with the best toughness values, in the range of 18.5 to 21 MPa.$m^{1/2}$, obtained with eutectic structures. The eutectic composition with lower levels of Ta (higher

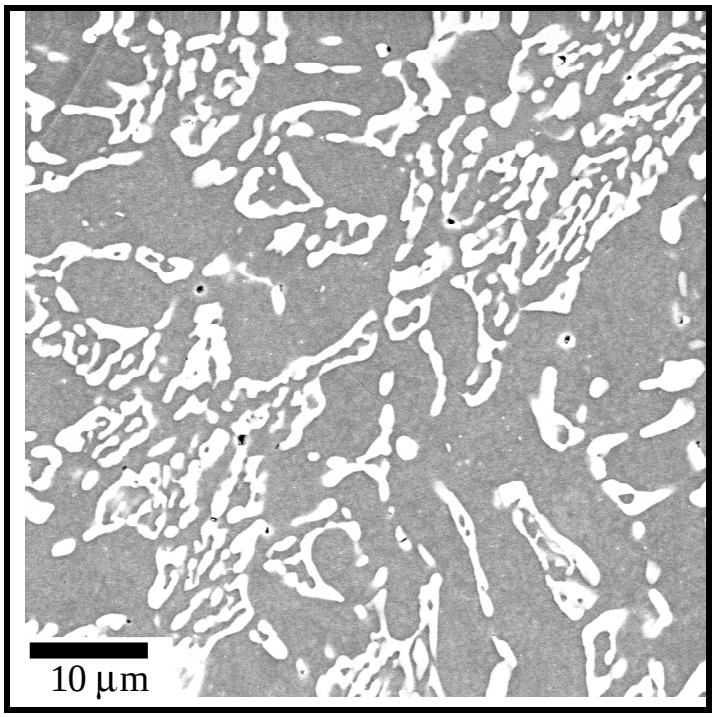

Fig. 1. Scanning electron microscopy (SEM) image showing the typical eutectic structure in a X-modified Cr-Cr_2Ta base alloy. The light phase is based on the Cr_2Ta Laves phase and the dark matrix is the Cr solid solution phase.

Table 1. Room-temperature fracture toughness

Alloy Designation	X (at.%) A<B<C	Ta (at.%)	Room-Temperature Fracture Toughness ($MPam^{1/2}$)
CN 175	Level A	5.0	12.9
CN 176	Level A	5.5	14.7
CN 177	Level A	6.0	14.4
CN 183	Level A	6.6	17.8
CN 185	Level A	6.8*	18.5
CN 182	Level A	7.0	17.5
CN 188	Level B	6.3*	21.0
CN 178	Level C	5.0	18.5
CN 179	Level C	5.5	20.0
CN 181	Level C	5.7*	20.3
CN 180	Level C	6.0	18.6

*Near eutectic composition.

levels of X) was generally tougher, yielding a fracture toughness >20 MPa.$m^{1/2}$ at room temperature (Table 1). However, the shift to the lower Ta eutectic compositions also weakened the alloy at high temperatures (Table 2). For instance, the reduction of Ta in the eutectic composition in the range of 6.8 to 5.7 at.% Ta resulted in a decrease of the tensile yield strength from 400 to 240 MPa at 1000°C. The room-temperature fracture toughness values obtained by X additions, with appropriate levels of Ta to yield the eutectic structure, meet the targeted goals of this program and are considered sufficient for handling and installation of components in low-impact applications. Current efforts are devoted to enhancement of the high-temperature strength by minor alloying additions.

Table 2. Tensile properties at 1000°C (Ta level adjust to yield eutectic structure)

Alloy Designation	X (at.%), Ta (at.%) A<B<C	Tensile Yield Strength ksi (MPa)	Ultimate Tensile Strength ksi (MPa)	Elongation (%)
CN 185	Level A, 6.8	57.7 (398)	69.3 (477)	2.8
CN 188	Level B, 6.3	51.8 (357)	56.7 (391)	4.4
CN 181	Level C, 5.7	34.8 (240)	41.2 (284)	18.2

High-Temperature Oxidation and Corrosion Behavior

The first generation of Cr-Cr_2Ta base alloys showed good resistance to air oxidation in the 900–1100°C temperature range, comparable to the better commercially available Cr_2O_3-forming alloys. Further, these alloys have exhibited some promising resistance in molten alkali salts (950–1000°C), coal ash deposits (950°C), and coal slag (up to 1300°C) [2,9]. Preliminary evaluation and characterization suggests that alloying of Cr-Cr_2Ta alloys with X additions does not significantly degrade air oxidation resistance and that the mechanism of oxidation is similar to the previously developed alloys.

Thermogravimetric data at 1100°C in air for a series of alloys based on a baseline Cr-Ta-X alloy, CN 179 (described in Table 1, also contains additions of 3Si and 0.2La at.%), showed similar (slightly higher) kinetics to Cr-8Ta-5Mo-3Si-0.1La at.%, an optimized Cr-Cr_2Ta alloy (Fig. 2). Alloy compositions corresponding to the Cr matrix phase composition (CN 179 Matrix) and Laves phase dispersion (CN 179 Laves) also exhibited similar oxidation kinetics (Fig. 2). An alloy CN 179 coupon (with less than optimum levels of Si and La additions) was also subjected to eleven, 100 h cycles at 1100°C in air (1100 cumulative hours at 1100°C). Although some spallation was evident, total coupon weight change was only on the order of 10 mg/cm2, indicative of a reasonable degree of oxidation resistance.

Preliminary evaluation of the oxidized CN 179 and related alloy coupons suggested that X additions significantly reduced the extent of embrittling Cr_2N subscale formation in the Cr matrix phase. A high level of X additions was, however, found to significantly degrade molten alkali salt resistance (100 h immersion screening in molten smelt at 950–1000°C [2,9]), presumably due to the resultant lower levels

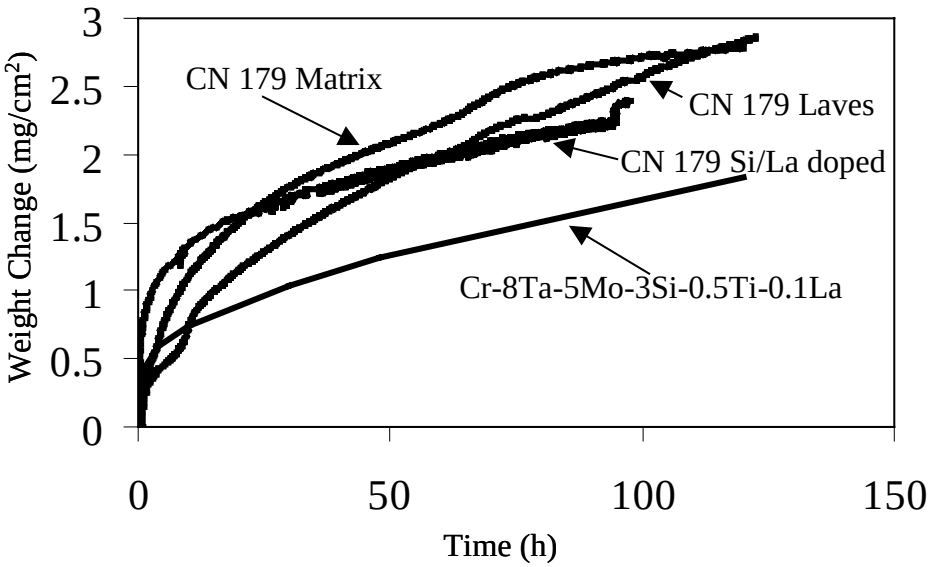

Fig. 2. TGA data at 1100°C in air.

of Cr and/or Ta in the alloy. Further characterization and study of these effects are planned in order to optimize oxidation resistance, hot corrosion resistance, and mechanical properties.

Interestingly, initial attempts to further improve oxidation resistance of the Cr-Ta-X alloys by Al additions resulted in the formation of a continuous Al_2O_3 scale at 1100°C in air, rather than the Cr_2O_3 base scale typically formed on these alloys (Fig. 3). Alumina scales exhibit lower oxidation kinetics than Cr_2O_3 scales and are much less prone to volatility related losses at elevated temperatures, particularly in water vapor containing environments. Both of these factors would effectively extend the upper temperature air oxidation limit of this family of alloys and/or reduce/eliminate the need for a protective coating. Full characterization of the microstructure of this alloy and an initial assessment of mechanical properties are planned.

REFERENCES

1. M. P. Brady, J. H. Zhu, C. T. Liu, P. F. Tortorelli, L. R. Walker, C. G. McKamey, J. L. Wright, C. A. Carmichael, D. J. Larson, M. K. Miller, and W. D. Porter, *Materials at High Temperatures*, vol. 16, no. 4, pp. 189–193 (1999).
2. M. P. Brady, C. T. Liu, J. R. Keiser, P. F. Tortorelli, V. K. Sikka, E. Lara-Curzio, C. A. Walls, C. G. Westmoreland, C. A. Carmichael, J. L. Wright, J. D. Vought, M. Howell, H. Longmire, K. L. Crowley, and M. L. Weaver, in Proceedings of the Fourteenth Annual Conference on Fossil Energy Materials, Knoxville, TN, April 24–26, 2000, R.R. Judkins, Compiler, ORNL TM-2000/249, paper 5.5 (2000).

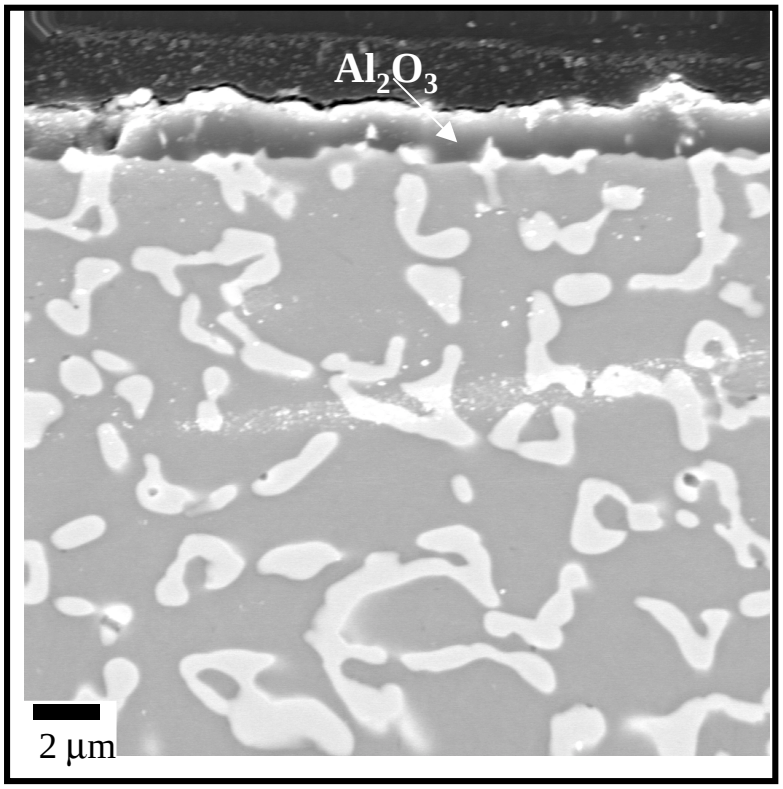

Fig. 3. SEM cross-section micrograph of an Al-modified Cr-Ta-X base alloy after 24 h oxidation at 1100°C in air. The dark phase is the Cr solid solution matrix phase and the light phase is based on the Cr_2Ta Laves phase.

3. C. T. Liu, J. H. Zhu, M. P. Brady, C. G. McKamey, and L. M. Pike, *Intermetallics*, 8, 9-11, pp. 1119–1129 (2000).
4. M. P. Brady, J. H. Zhu, C. T. Liu, P. F. Tortorelli, and L. R. Walker, *Intermetallics*, 8, 9-11, pp. 1111–1118 (2000).
5. D. M. Scruggs, 'Ductile Chromium Composition," U.S. Patent 3, 175, 279 (Mar. 30, 1965).
6. D. M. Scruggs, L. H. Van Vlack, and W. M. Spurgeon, *J. Amer. Ceram. Soc.*, 51, 9, pp. 473–481 (1968).
7. M. P. Brady, I. M. Anderson, M. L. Weaver, H. M. Meyer, L. R. Walker, M. K. Miller, D. J. Larson, I. G. Wright ,V. K. Sikka, A. Rar, G. M. Pharr, J. R. Keiser, and C. A. Walls, "On the Mechanism of Nitrogen Impurity Management in the Room-Temperature Ductilization of Cr by MgO Additions," submitted to Acta Materialia.

8. M. P. Brady, C. T. Liu, I. M. Anderson, P. F. Tortorelli, J. H. Zhu, I. G. Wright, V. K. Sikka, C. A. Walls, L. R. Walker, S. B. Waters, J. L. Wright, and C. A. Carmichael, "Multi-Phase Cr-Based Alloys for Aggressive High Temperature Environments," *Proceedings of the Fifteenth Annual Conference on Fossil Energy Materials*, Knoxville, TN, April 30–May 2, 2001, R.R. Judkins, Compiler (2001).
9. R. A. Peascoe, J. R. Keiser, C. R. Hubbard, and M. P. Brady, "Performance of Selected Materials in Molten Alkali Salts," in *Proceedings of the 10th International Symposium on Corrosion in the Pulp and Paper Industry*, Valtion Teknillinen Tutkimuskeskus (VTT), Espoo, Finland, pp. 189–200 (2001).
10. J. H. Schneibel, C. A. Carmichael, E. D. Specht, and R. Subramanian, *Intermetallics*, 5, p. 61 (1997).

ACKNOWLEDGEMENTS

This research was sponsored by the U.S. Department of Energy, Fossil Energy Advanced Research Materials (ARM) Program. Oak Ridge National Laboratory is managed by U.T.-Battelle, LLC for the U.S. Department of Energy.

OXIDE DISPERSION-STRENGTHENED ALLOY DEVELOPMENT

I. G. Wright, C. G. McKamey, and B. A. Pint
Oak Ridge National Laboratory

INTRODUCTION

This is not a new alloy development program, per se, but rather the intent is to provide the materials support information needed for the successful introduction and use of ODS alloy tubes in the extreme conditions envisioned in advanced fossil-fuelled combustion of conversion systems. The topics of interest are associated with differences between ODS alloys and the widely-used high-temperature alloys, where the peculiar properties of ODS alloys must be addressed in their application and use to ensure that their potential benefits are fully realized. The current focus is on needs identified in the on-going Vision 21 program to improve the properties of ODS-FeCrAl alloy MA956 for use in very high-temperature heat exchangers. Figure 1 provides a visualization of the reason for the continued interest in ODS alloys. Data generated by Starr and Tariq[(1)] to represent the average creep rupture strength of high-temperature alloys (for which creep is controlled by dislocation climb) are plotted as a function of temperature, together with data for the maximum theoretical creep rupture strength of these alloy obtained from considerations of the thermal stability of the strengthening precipitates (carbides, nitrides, etc.). Literature data for the creep rupture strength (in the longitudinal/extrusion direction) of ODS-FeCrAl and ODS-NiCr alloys are plotted for comparison to illustrate that these represent a separate class of alloys with unmatched creep strength. The data in Fig. 1 should be viewed with some caution, however, since the ODS data are for 10 kh (no published data for 100 kh were found), and so the 100 kh curves would expected to be somewhat lower stress levels; nevertheless, they are still expected to be greater than the projected theoretical maximum curve shown for conventional alloys. One of the peculiarities of ODS alloys is that the creep strength in the longitudinal direction typically is higher than that in the transverse (hoop) direction by a factor of 2 or more. Also indicated in Fig. 1 is the transverse/hoop strength level required (using the Birks[(2)] criterion that hoop stress $\approx 1.89 \times$ internal pressure) in tubes operating under typical ultra-supercritical steam conditions, and as an indirectly-fired heat exchanger in an open-cycle gas turbine system with a pressure ratio up to 40:1. Clearly, these requirements are at or beyond the capabilities of conventional alloys.

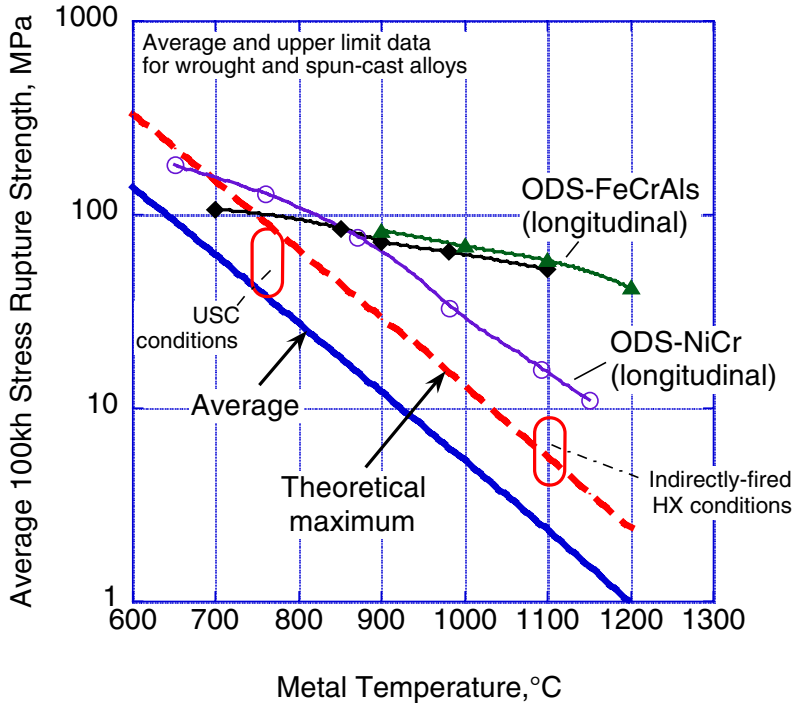

Fig. 1. Comparison of current and theoretical maximum stress rupture strengths of available wrought and spun-cast alloys (after Starr and Tariq, 2002) with properties of ODS alloys.

DISCUSSION OF CURRENT ACTIVITIES

Joining

The critical dependence of the creep strength of ODS alloys on microstructure translates to a need to preserve the grain shape, orientation, and the distribution of the dispersed oxide particles through a joint. Most conventional and several novel joining routes have been investigated over the years for joining ODS alloys, including:

1. Fusion welding: which typically leads to agglomeration of the dispersoid, and recrystallization of the microstructure.
2. Laser welding: which minimizes the size of the fusion zone, and has found application in some structures.[3]
3. Explosive bonding: was successfully demonstrated in short-term runs of an ODS heat exchanger in the COST-501 program.[4] A 'harp' design was used the avoid problems of bending the 4m-long ODS-FeCrAl alloys tubes, the ends of which were bonded to thick sections of a conventional high-temperature alloy, which then were welded conventionally to the headers. The arrangement of these joints is shown schematically in Fig. 2. Potential longer-term problems with such joints are

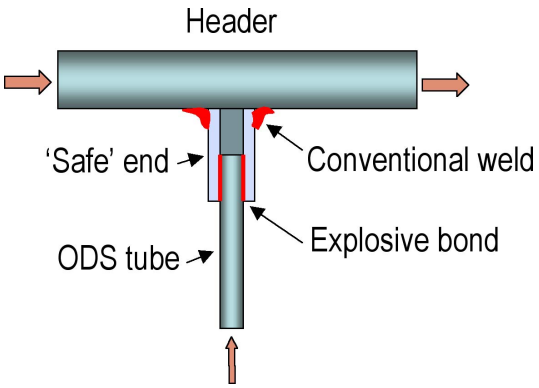

Fig. 2. Schematic diagram of ODS tube-to-header joint used in heat exchanger in COST-501 program.

interdiffusion with the conventional alloy 'safe ends' and the consequent effects on the strength of both alloys.

4. Friction welding: results in distortion of the ODS alloy microstructure in the vicinity of the joint; an example of the microstructure of a friction-welded joint in ODS-Fe_3Al is shown in Fig. 3. Tests earlier in this program[5] indicated that such joints retained < 50% of the stress rupture strength (longitudinal) of the parent ODS alloy.

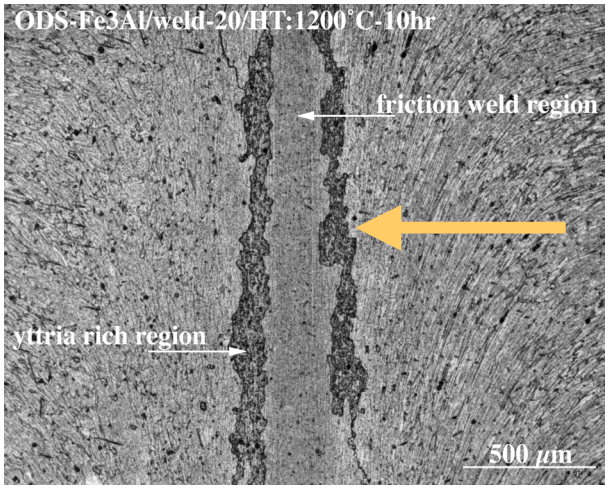

Fig. 3. Cross section of a friction-welded joint ODS-Fe3Al after in recrystallization (longitudinal direction shown by large arrow).

5. Diffusion bonding: transient liquid-phase bonding (TLP) was successfully demonstrated for an ODS-Ni-Cr alloy in the U.S. Department of Energy's High Performance Power Systems (HiPPS) program.[6] A novel joint design using corner blocks made from the same ODS alloy allowed the heat

exchanger to be fabricated from straight tubes, as illustrated in Fig. 4. The alloy for which this bonding procedure was developed forms a chromia scale; the ODS-FeCrAl alloys of current interest form alumina scales, which are significantly more stable and tenacious, and so pose a more difficult challenge.

6. Pulsed magnetic welding apparently was used successfully on ODS alloy MA760 (Fe-13Cr-based) in studies for the Liquid Metal Fast Breeder Reactor program,[7] the report also contains a comment that an ODS-FeCrAl (MA956) also was successfully joined by this technique, but no details nor reference were give. Further, the report contained no information about bond strength.
7. Mechanical joints such as threading and seal brazing may be practical if the heat exchanger is designed to accommodate such an approach. The bayonet-type heat exchanger under consideration in the COST 522 program,[8] and shown schematically in Fig. 5, is an example of such a design.
8. Arc-assisted diffusion bonding is being developed in a Small Business Innovative Research program by MER Corp. of Tucson, Arizona. Apparently, a feature of this approach is that any alumina film formed along the interface to be joined is removed by local arcing.

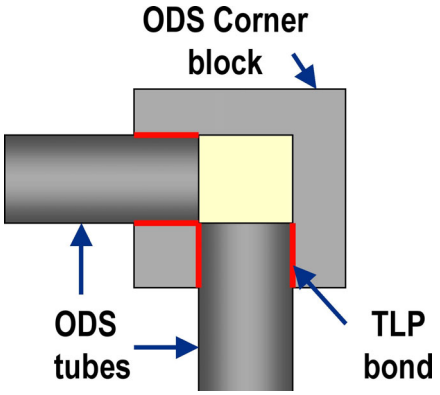

Fig. 4. Schematic diagram of corner block assembly approach used to join ODS tubes in heat exchanger in HiPPS program.

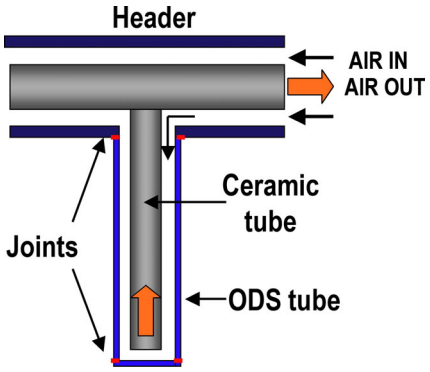

Fig. 5. Schematic diagram of ODS tube-to-header joint used in heat exchanger design proposed in the COST-522 program.

There are efforts in place in the Special Metals-Vision 21 program[9] to examine approaches 3 through 6, and the European COST 522 program has addressed approach 7 including the development brazes. One of the goals of this program is to ensure that information is available on all possible joining routes for ODS alloys, so that where possible, samples are obtained for characterization. Figure 6 shows metallographic cross sections of a joint made by MER Corp. in a rod of unrecrystallized ODS-Fe_3Al. The appearance of the joint was very clean with possibly a few small pores, and there appeared to be little if

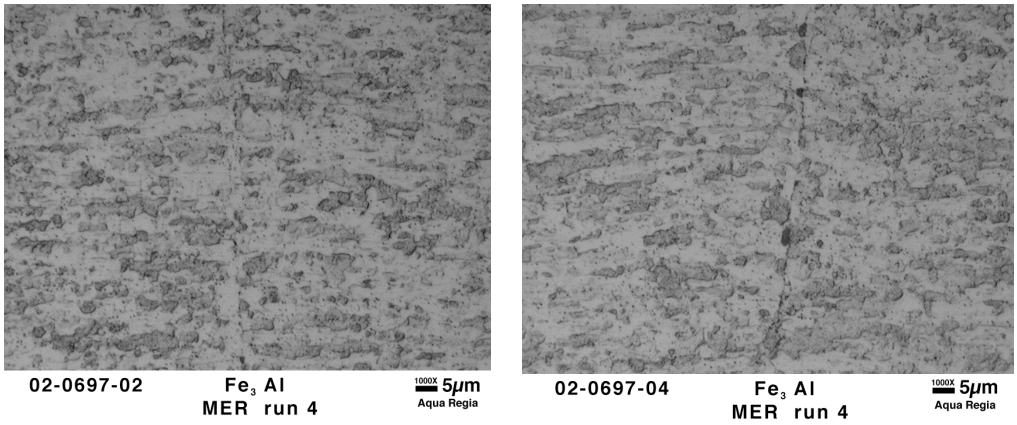

Fig. 6. Joint in unrecrystallized ODS-Fe_3Al produced by arc-assisted diffusion bonding (MER Corp.).

any distortion of the alloy microstructure. The microstructure following a recrystallization treatment (2 h at 1250°C) in a muffle furnace in air confirmed that there was not distortion of the microstructure, and also indicated that both halves of the joint recrystallized independently, with no grains growing across the joint. The higher magnification views suggested what appeared to be either very localized deformation at the joint, or the growth of some porosity, which has yet to be properly identified. The creep strength of this bond before recrystallization is indicated in Fig. 7 and was, in fact, less than that of the friction-welded bond shown in Fig. 3, retaining 33 percent of the parent metal (longitudinal) creep rupture strength. After the recrystallization treatment, the bond strength was reduced further.

Mode of Failure

Although ODS alloys exhibit exceptional high-temperature creep strength, their mode of failure is quite different from that on conventional high-temperature alloys, hence the impetus for the development of the 'creep threshold' curve shown in Fig. 8. When loaded above the threshold stress, the alloy exhibits creep and sudden failure with very little warning. Creep tests were conducted at or above the threshold stress using specimens of ODS-Fe_3Al and the ODS-FeCrAl alloy MA956, with extensometer readings taken every 10 seconds in order to detect signs of impending failure. The intent was to stop specimens at different points in their creep life to characterize the type and extent of microstructural changes, and so understand the reason for the mode of failure. Even at this rate of data gathering, there was no obvious warning of failure. Instead, nominally identical specimens were run for increasing times up to just before failure, and retrieved for microstructural analysis by transmission electron microscopy. Two examples are shown in Fig. 9; the obvious difference is the dense mass of dislocations in the specimen approaching failure, compared to that from earlier in the creep exposure. Clearly the dislocations are pinned very successfully by the dispersed oxide particles, which is the basis for the excellent creep strength, but this

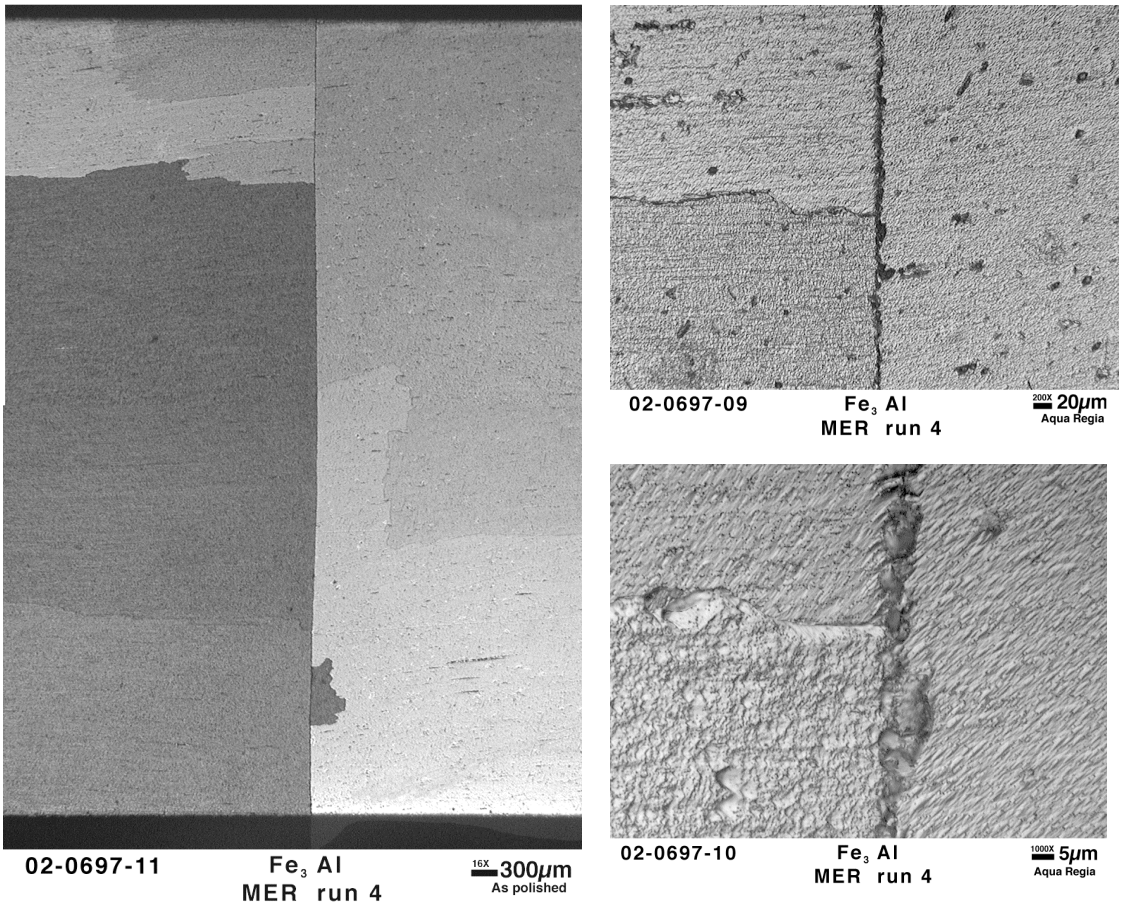

Fig. 7. Microstructure of joint produced by arc-assisted diffusion bonding in ODS-Fe_3Al after recrystallization.

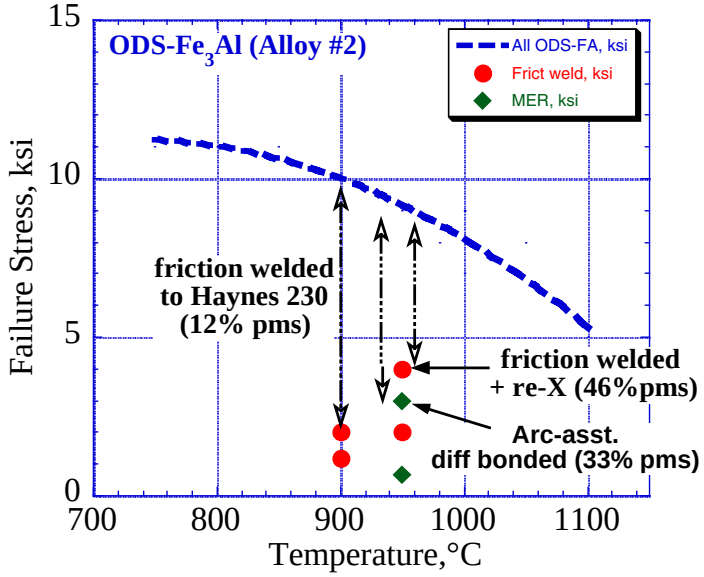

Fig. 8. Creep 'threshold' curve for comparison of strength of joints.

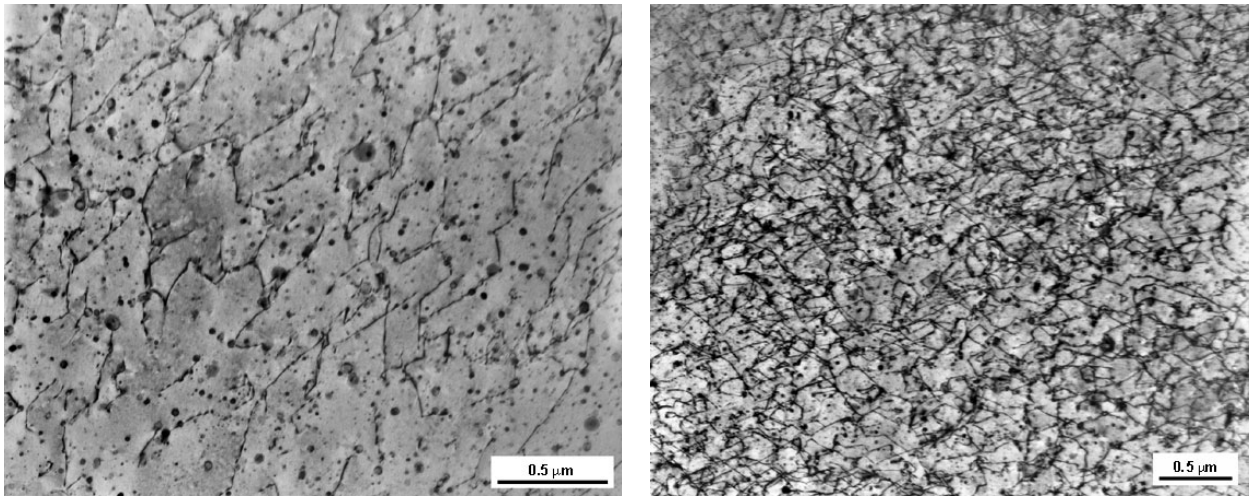

(a) **(b)**

Fig. 9. Transmission electron micrographs showing microstructure of ODS-FeCrAl after (a) 'steady-state' creep; and (b) immediately before failure in creep.

very pinning—the failure of the dislocation to climb and the alloy to creep, results in the inexorable build up of dislocations, which results in a microstructure that is increasingly unable to deform, i.e., it becomes brittle.

Optimization of Alloy Microstructure

Available routes to modify the microstructure of ODS alloys to improve creep strength in the transverse/hoop direction, which is required for tubes (see Fig. 1), have been examined. The processing route used by Dour Metal for its ODS-FeCrAl alloy (ODM751) gave an 'onion skin' structure with pancake-shaped grains that overlapped each other, with heavily serrated grain boundaries,[(10)] and so would be expected to result in a greater similarity in transverse and longitudinal properties. While there is no available documentation of the process steps involved, it is suspected that control of post-consolidation recrystallization was exerted through the introduction of specific nucleation sites (addition of additional inert particles near the end of the milling phase), and the application of a controlled stress before recrystallization. In a recently-concluded Brite-Euram program,[(11)] 'flow forming' of consolidated ODS-FeCrAl tubes was used to introduce a spiral grain structure after recrystallization. This approach appears to have been successful, although the inability to run the process at a sufficiently high metal temperature resulted in some defects in the finished tubes.

Observations of the influence of the strain introduced (or the redistribution of impurities that may act as nucleation sites) during friction welding of butt joints on the orientation of the recrystallization path in ODS-Fe_3Al (see Fig. 3) suggested a similar approach to that used in the Brite-Euram program. The microstructure of a rod of ODS-Fe_3Al was distorted by the application of torsion, after which the alloy

was recrystallized by a simple furnace anneal. Although the extent of torsional displacement possible with available equipment was relatively small (some 30°), as shown in Fig. 10 it appears that some modification of the recrystallization path was effected. In order to influence the transverse creep strength, however, significantly more distortion would be required; while this approach may be impractical with tubes, other routes such consolidation of the ODS powder by spiral extrusion may be possible.

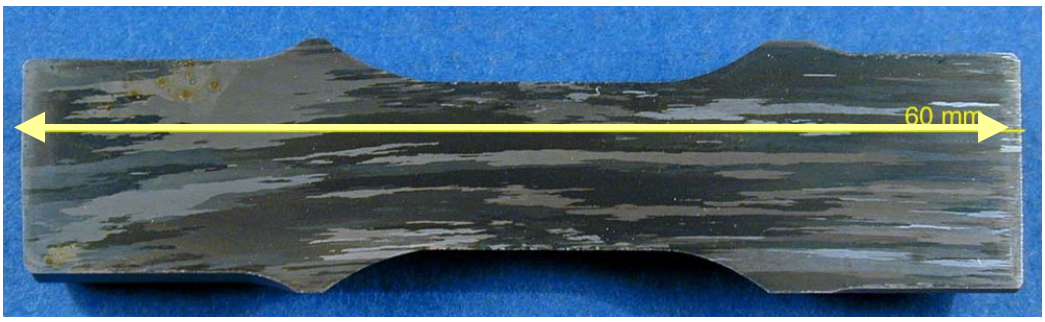

Fig. 10. Etched surface of a 60 mm-long torsion bar of ODS-Fe_3Al etched to show the macrostructure after recrystallization.

In an attempt to exert more control over the recrystallization behavior of ODS alloys, uniformly-thick bars of as-consolidated ODS-Fe_3Al were supported on a quartz plate and heated by a moving, precision high-intensity heat source, essentially performing a zone anneal. In an attempt to determine the conditions necessary to establish and maintain a narrow zone of alloy at a suitable recrystallization temperature (≈1300°C), specimens were placed with one end in the beam and, after the heating conditions were established, the beam was moved along the surface at a accelerating speed. The macrostructures resulting from one pass of the beam are shown in Fig. 11 for four different beam intensities (620, 640, 670, and 700 amps). At 620 amps, the lamp was translated at 15 mm/s or the first 25 mm, then at 10 mm/s for the next 25 mm, and finally at 12 mm/s for the final 25 mm of specimen length. Some melting of the sample edges occurred at the initial translation speed of 15 mm/s, but when the speed was reduced to 10 mm/s recrystallization was initiated; however, increasing the speed to 12 mm/s resulted in a sufficient drop in the bulk temperature that recrystallization stopped. At 640 amps using the same translation steps, nucleation occurred at 15 mm/s and persisted when the translation speed was reduced from 15 to 10 mm/s, but recrystallization again stopped when he speed was increased from 10 to 12 mm/s. Minimal melting of the sample occurred. At 670 amps using translation steps of 14, 10, and 12 mm/s, respectively, uniformly-wide, straight grains were nucleated over the distance 10 to 35 mm from the start, but then abruptly stopped; some melting of the alloy edges also accompanied the recrystallization. At 700 amps and translation speed steps of 15, 10, and 12 mm/s, respectively, significant melted initiated within 10 mm of the start position, and persisted some 62 mm along the specimen. Recrystallization occurred

Fig. 11. Etched surfaces of bars of ODS-Fe_3Al after recrystallization in a moving heat source.

only in this same region. Obviously this approach has merit, but thetime at temperature is critical, and must be well defined and controlled.

Oxidation-Limited Service Lifetimes

In a continuing effort to develop a reliable methodology for predicting the oxidation-limited service lifetime of alumina scale-forming ODS alloys, the goal is to have the capability to predict lifetime from a knowledge of alloy oxidation characteristics and the exposure temperature. This involves not only determining the temperature-dependence of the kinetics in each phase of oxidation from long-term exposures, but also understanding the criteria for transition from stage to stage and processes that signify the end of protective oxidation behavior. For the ODS-FeCrAl alloys final breakdown usually initiates at a specimen edge or corner, so that recent efforts have been aimed at examining the effect of component shape on oxidation lifetime. The input needed for the modeling include the oxidation rate constants for the main identifiably-distinct stages of oxidation, as well as the oxide thickness at which transition between stages occurs, and the minimum aluminum level at the alloy surface at which breakdown initiates. Complicating factors are the fact that scale spallation occurs, and that a gradient develops in the

alloy solute (Al) from the metal-oxide interface to the center of the specimen, whereas the initial model assumed that the surface Al level was the same as the bulk level. Figure 12 shows the locations in which failure occurred in specimens of ODS-FeCrAl alloy MA956 after exposure in air at 1250°C. The shapes and sizes were chosen to allow comparisons to be made of the effect of surface area to volume ratio, as well as shape, as indicated in Table 1, where *d* is the maximum distance from the center of mass as defined in Fig. 13.

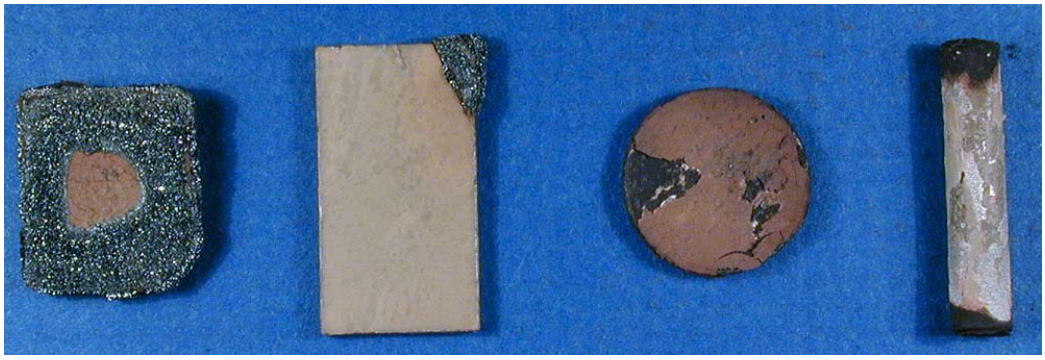

Fig. 12. Location of oxidation failure initiation site for different specimen shapes; ODS-FeCrAl MA956 oxidized in air at 1250°C.

Table 1. Dimensions of Different Specimen Shapes

Shape	*t*, mm	*l*, mm	*w*, mm	*A*, mm^2	*V*, mm^3	*V*/*A*, mm	*d*, mm	Life, h 1250°C
Disc	1.6	15	—	353	280	0.79	7.5	2,300
P_1*	1.6	14	12.5	435	280	0.64	9.4	2,100
P_2*	1.6	23	12.5	686	450	0.66	13.1	1,400
Cyl	—	23	5	375	401	1.07	?	2,500

*parallelepipeds

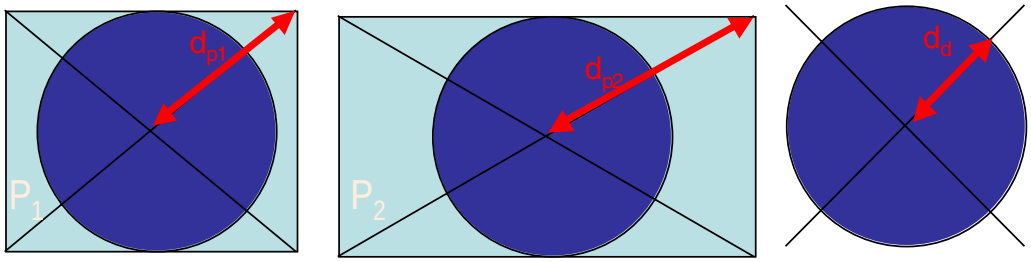

Parallelepiped P_1 **Parallelepiped P_2** **Disc**

Fig. 13. Definition of *d*, the maximum distance from the center of mass, for different specimen shapes.

As shown in Fig. 14, the form of the oxidation kinetics was essentially the same for the parallelepiped and disc-shaped specimens, whereas the cylinder exhibited noticeably more scale spallation. At the high oxidation temperature used, the Al concentration profile in this alloy is essentially flat, so that the notion that, for a given surface area-to-volume ratio, the shape with a point furthest from the center of mass will be first to reach the critical Al level, seems reasonable. There is also the complicating factor that stresses in the scale are maximum at specimen corners and edges, so that failure initiation at the furthest corner is expected.

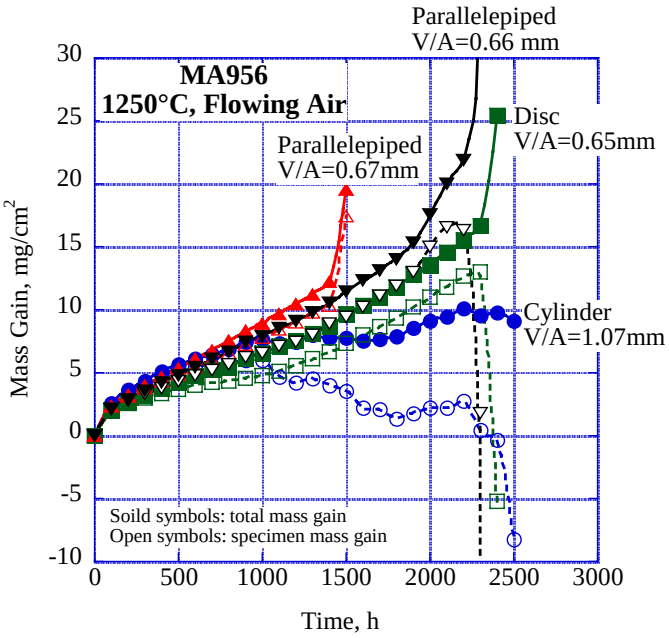

Fig. 14. Oxidation kinetics at 1250°C in air for different specimen shapes of Alloy MA956.

The observed and calculated lifetimes for this alloy at 1250 and 1300°C in air are shown in Fig. 15 as a function of specimen thickness and of surface area-to-volume ratio for disc-shaped specimens. Curiously, the lifetime is slightly over-predicted when calculated as a function of specimen thickness, and slightly under-predicted when calculated as a function of shape factor.

Long-term corrosion data are being generated in air over a range of temperatures for all available ferritic ODS alloys as well as FeCrAlY alloys, to provide input for the predictive model development. In addition, exposures in coal-fired systems, as well as in steam will provide data with which to compare the laboratory results.

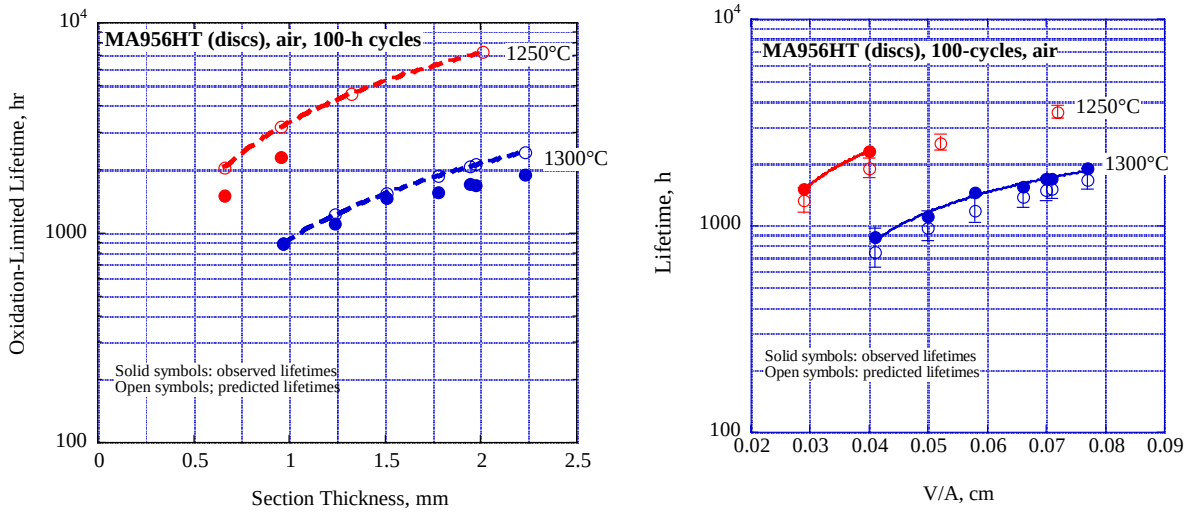

Fig. 15. Calculated oxidation-limited lifetimes for Alloy MA956 at 1250 and 1300°C in air.

REFERENCES

1. F. Starr and S. Tariq, European Technology Development Ltd, Ashtead, Surrey; private communication, 2002.
2. N. Birks and C. A. Smith, "Factors in the selection of advanced alloys for advanced heat exchangers," presented at *Intl. Conference on Materials Issues in Heat Exchangers and Boilers*, Inst. of Materials (1997).
3. C. Brown, E. Verghese, D. Sporer, and R. Sellors, "PM2000 honeycomb structures," paper No. 98-GT-565, presented at the 43rd ASME Gas Turbine Conference, Stockholm, Sweden (1998).
4. F. Starr, A. R. White, and B. Kazimierzak, in *Materials for Advanced Power Engineering 1994*, D. Coutsouradis, et al., eds. (Kluwer Academic Publishers, 1994) pp. 1393–1412.
5. I. G. Wright, C. G. McKamey, and B. A. Pint, "ODS alloys for high-temperature applications," *Proc. 14th Annual Conference on Fossil Energy Materials*, Knoxville, Tennessee, April 2000.
6. N. S. Bornstein and D. J. Seery, "Progress in using ODS alloy in the HITAF air heater," Materials & Components, 136, 10–11 (1998).
7. M. L. Hamilton, et al., "Fabrication technological development of the ODS alloy MA957 for fast breeder applications," Report No. PNNL-13168 on DOE Contract No. DE-AC06-76RLO 1830 (2000).
8. F. Olsson, S. A. Svensson, and R. Duncan, "Externally-Fired Gas Turbine Cycles with High-Temperature Heat Exchangers Utilizing Fe-Based Alloy Tubing," pp. 139–153 in *Proceedings of the 15th International Plansee Seminar*, G. Kneringer, P. Rodhammer, and H. Wildner, eds., Plansee Holding AG, Reutte (2001).

9. M. A. Harper, “Development of ODS heat exchanger tubing,” quarterly technical reports on DOE program No. DE-FC26-00NT40970 (2002).
10. D. M. Jaeger and A. R. Jones, “The development of grain shape in iron-based ODS alloys,” in *Materials for Advanced Power Engineering 1994*, Part II, D. Coutsouradis et al., eds. (Kluwer Academic Publishers, 1994) pp. 1515–1522.
11. Y. L. Chen, A. R. Jones, and U. Miller, “Hoop creep resistance of flow-formed ferritic oxide dispersion-strengthened alloy tubes,” submitted to J. Mater. Sci. (2002).

Mo-Si-B ALLOY DEVELOPMENT

J. H. Schneibel
Oak Ridge National Laboratory

INTRODUCTION

Nickel-base superalloys have outstanding oxidation and mechanical properties at elevated temperatures, but their service temperatures are inherently limited to temperatures around 1000˚C. In order to increase the thermodynamic efficiency of Fossil Energy systems, materials capable of much higher temperatures are needed. One approach, pioneered in Japan, focuses on precious metal based superalloys [1]. While these superalloys have simple fcc-based crystal structures, which allow significant plastic deformation, a heavy price is paid in terms of mass density and cost. An alternative approach is based on oxidation resistant intermetallic compounds which have lower densities and are less costly, but which are inherently brittle. In particular, silicide intermetallics, which can have outstanding oxidation resistance, are being considered. A prime example is $MoSi_2$ that is widely used in heating elements for resistance furnaces. Its good oxidation resistance is due to the formation of a protective silica glass scale. However, $MoSi_2$ is very brittle with a room temperature fracture toughness on the order of 3 MPa $m^{1/2}$ [2]. Also, it becomes very weak at high temperatures [2]. If the Si concentration is reduced below that of $MoSi_2$, phases such as Mo_5Si_3, Mo_3Si, and α-Mo (Mo solid solution) form. These phases will have a lower oxidation resistance, but they may potentially impart greater fracture toughness, particularly in the case of α-Mo. Two main alloy systems have been examined to date. In the first one, which was pioneered by Akinc and collaborators [3], intermetallic alloys consisting of Mo_5Si_3, the T2 phase Mo_5SiB_2, and the A15 phase Mo_3Si were investigated. These types of alloys are indicated in the schematic ternary phase diagram in Fig. 1. They exhibit excellent oxidation resistance at elevated temperatures (e.g., 1300°C). The boron additions are crucial for providing the observed oxidation resistance [4,5], as already hinted at in an early study of the ternary Mo-Si-B phase diagram by Nowotny et al. [6]. In the second system, which was pioneered by Berczik et al. [7,8], alloys consisting of α-Mo, Mo_3Si, and T2 were investigated. While these alloys are not as oxidation resistant as Mo_5Si_3-T2-Mo_3Si alloys, they contain a ductile phase, α-Mo. Depending on its volume fraction and distribution, the α-Mo can improve the room and high temperature fracture toughness significantly. The fracture toughness will increase with increasing α-Mo volume fraction and, for a given α-Mo volume fraction, will be higher if the α-Mo forms as a continuous matrix instead of individual particles [9]. Clearly, then, the optimization of Mo-Si-B alloys requires a trade-off between fracture toughness on the one hand, and oxidation resistance on the other.

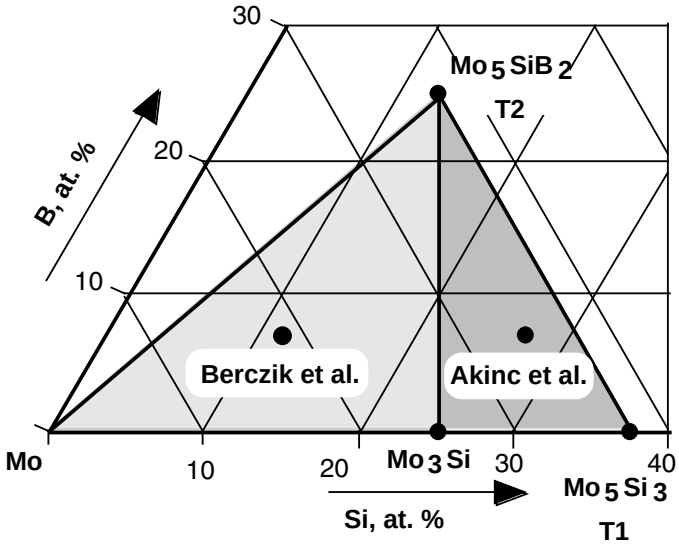

Fig. 1. Schematic illustration of the Mo-rich section of the ternary Mo-Si-B phase diagram.

Another issue is the creep resistance of these types of alloys. Akinc et al. have already shown that Mo_5Si_3-based alloys exhibit excellent creep resistance [3]. Mo_3Si, $(Cr,Mo)_3Si$, and the T2 phase are all very strong at elevated temperatures [10–12]. Since it can be safely assumed that the creep strength of α-Mo is lower than that of Mo_3Si and T2, the creep strength of Mo-Mo_3Si-T2 alloys is likely to depend on the α-Mo volume fraction. It will also depend sensitively on the microstructural morphology—if the α-Mo is distributed as a continuous matrix or "binder" phase instead of isolated particles, the creep strength will be low. In addition, as commonly observed in creep, the grain or phase size will play an important factor—generally, the creep strength tends to increase with increasing grain or phase size. The competing requirements for optimum oxidation resistance, fracture toughness, and creep strength are schematically shown in Fig. 2. Using the Mo-Si-B system we will illustrate the issues raised in Fig. 2. It should also be noted that several aspects of Mo-Si-B alloys are also being examined within the Department of Energy/Basic Energy Sciences Synthesis & Processing Center on "Design and Synthesis of Ultrahigh-Temperature Intermetallics." For example, the significant thermal expansion anisotropy of Mo_5Si_3, which gives rise to profuse microcracking during processing, has now been understood based on first-principles calculations [13]. Based on these calculations alloying additions for Mo_5Si_3 have been found which reduce the ratio of the thermal expansions in the *c*- and *a*-directions from 2 to 1.2 [14].

EXPERIMENTAL

The alloys in this work were prepared by arc-melting of elemental starting materials in a partial pressure of argon (70 kPa) on a water-cooled copper hearth. The purity of the starting materials Mo, Si and B was 99.95, 99.99, and 99.5 wt%, respectively. Unless stated otherwise, alloy compositions will from now on be

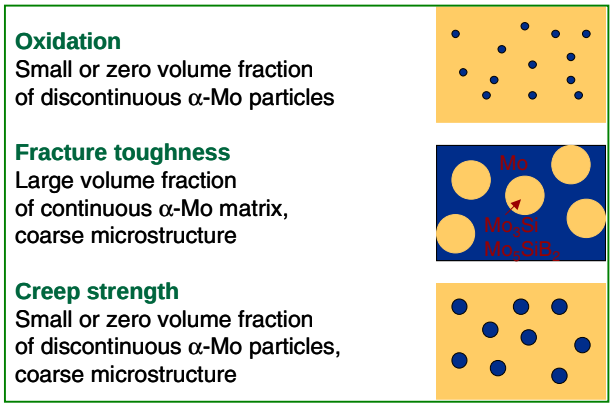

Fig. 2. Schematic illustration of the phase volume fractions and microstructures needed to satisfy competing requirements.

stated in at. %. The alloys were re-melted several times in order to improve their homogeneity. Sometimes the alloys were allowed to solidify in elongated water-cooled Cu molds, in other cases they were drop-cast into cylindrical water-cooled copper molds with diameters of 12.5 or 25 mm. After casting, the alloys were usually annealed for 24 hours at 1600°C in vacuum at a pressure of approximately 10^{-4} Pa. Several as-cast alloys were crushed into powders with sizes ranging from 20 to 230 µm. They were mixed with various amounts of Mo powder (2–8 µm) and consolidated either by hot isostatic pressing in sealed Nb cans or by uniaxial hot-pressing in a graphite hot press. In a novel approach to be described in more detail in the experimental section, the surface of Mo-Si-B particles (which were obtained by crushing castings into powder) was "coated" with a thin (10 µm) layer of Mo by removing Si via vacuum annealing

Microstructural examination was carried out by optical microscopy as well as scanning electron microscopy (SEM). Metallography specimens were prepared by grinding, mechanical polishing, and etching in Murakami's etch. The phases were identified by a combination of energy dispersive spectroscopy (EDS) in an SEM, by wavelength-dispersive spectroscopy (microprobe), and powder x-ray diffraction.

In order to assess the oxidation resistance of the Mo-Si-B alloys, screening tests were carried out. Small coupons (typically $10 \times 10 \times 1$ mm) were weighed and annealed for 1 day in an air furnace at 1300°C such that all their surfaces were oxidized. Their oxidation resistance was determined by dividing their weight change after annealing by their surface area.

Fracture toughness values were estimated from the energy dissipation during controlled crack growth of chevron-notched specimens [15].

Compression specimens with a diameter of 3 mm and a height of 6 mm were electro-discharge machined. Their creep strengths were evaluated from constant displacement rate tests in flowing argon at temperatures ranging from 1200 to 1400°C in an Instron testing machine equipped with a $MoSi_2$ furnace.

RESULTS AND DISCUSSION

Oxidation Resistance

Figure 3 illustrates the influence of the microstructure on the oxidation resistance. The alloy on the left was processed by mixing Mo-20Si-10B (at. %) powder particles (obtained by crushing a casting with that composition) with Mo powder. The nominal composition after mixing was Mo-16.8Si-8.4B (at. %). The Mo occurred in the form of large, elongated particles. The alloy on the right had the same nominal composition, but it was consolidated directly from powder obtained from a Mo-16.8Si-8.4B casting, without adding any Mo powder. Since the α-Mo in this alloy is present in the form of small particles, the oxidation resistance of this alloy is much better than that of the one on the left, see Fig. 3.

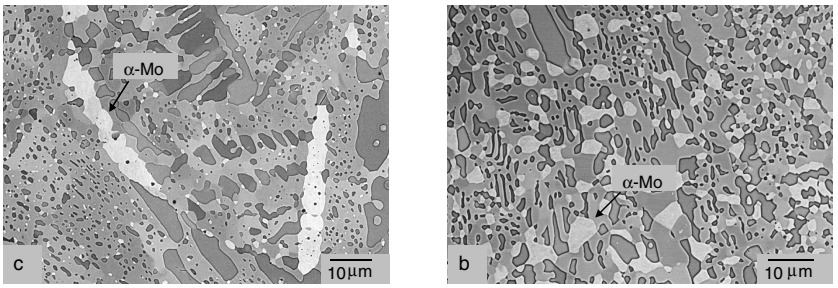

Weight loss 220 g/cm² (1day/1300C/air)

Weight loss 5.7 mg/cm² (1day/1300C/air)

Fig. 3. The oxidation resistance depends sensitively on the microstructure.

Fracture Toughness

For a given volume fraction of a toughening phase, the fracture toughness is greatest when this phase is distributed continuously, acting as a "binder" for brittle silicide particles, similar to the microstructure of WC-Co [9]. Melting and casting, or powder-metallurgical processing starting with Mo-Si-B castings cannot deliver such microstructures, and a new technique had therefore to be developed. The Mo-Si system is unique in the sense that, depending on the oxygen partial pressure, either Mo or Si can be removed from its surfaces. During oxidation in air, Mo is removed as MoO_3, the surfaces are enriched in Si, and a protective SiO_2 scale develops. During annealing in vacuum, silicon instead of Mo is oxidized. Because of the low partial pressure of oxygen, SiO forms instead of SiO_2. SiO is volatile and is removed. As a consequence, the surface becomes a Mo solid solution. This approach proved to be very useful to effectively "coat" Mo-Si-B powder particles with a thin (10 μm) film of α-Mo. The reactions occurring during the annealing, as well as a cross-section through an annealed powder particle, are shown in Fig. 4.

"Coating" of silicide powders with Mo

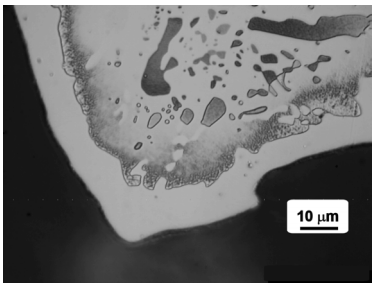

Mo-20Si-10B powder particle after 16 h at 1600°C in vacuum

Fig. 4. Formation of a thin α-Mo layer on a Mo-20Si-10B particle during annealing in vacuum.

$$Mo_3Si + 1/2O_2 \rightarrow SiO\uparrow + 3\ Mo$$
$$Mo_5SiB_2 + 1/2\ O_2 \rightarrow SiO\uparrow + 2\ Mo_2B + Mo$$

The kinetics of the reaction follows a power law—the thickness of the α-Mo layer grows proportional to time$^{1/2}$. This is not surprising since the removal of the silicon involves diffusion of Si through the α-Mo layer to the surface where it is removed as SiO. Since the α-Mo layer increases progressively in thickness, the rate at which the Si is removed slows down with time.

Figure 5 shows the microstructure of silicide material processed in this manner. An α-Mo layer was produced on Mo-20Si-10B powder particles which were then consolidated by hot isostatic pressing in a Nb can at 1600˚C for 2 h at a pressure of 30 ksi. The nominal composition of the consolidated alloy was Mo-15Si-10B. As shown in Fig. 5, the room temperature fracture toughness of this material is quite high, namely, 14 MPa m$^{1/2}$, as measured with flexure tests carried out with chevron-notched specimens [15]. This value is higher than that of a cast and annealed alloy (Mo-12Si-8.5B) with a higher α-Mo volume fraction of approximately 40%, which has a fracture toughness of 9.5 MPa m$^{1/2}$ (determined by the same technique). The reasons for the high fracture toughness of the PM material are two-fold. First, the α-Mo is distributed continuously and a propagating crack can therefore not avoid it by going around it. Second, the microstructural size of the α-Mo ligaments is large and this also enhances the fracture toughness.

CREEP STRENGTH

Slow high-temperature compression tests with a constant crosshead displacement rate were carried out in flowing argon. The initial strain rate was 1×10^{-5} s^{-1}. A quasi-steady state flow stress (steady-state creep strength) was typically reached after a plastic strain of about 2%. Sometimes a gradual load drop occurred after a strain of a few percent. The creep strength was estimated as the engineering stress for a plastic strain of 2%. Alloys based on Mo-12Si-8.5B in which the Mo was partially replaced by W or Nb were cast and annealed (24 h/1600˚C/Vacuum). The alloying additions did not change the scale and morphology of the microstructure significantly. However, with tungsten, a small amount of a Mo_5Si_3-based phase is observed.

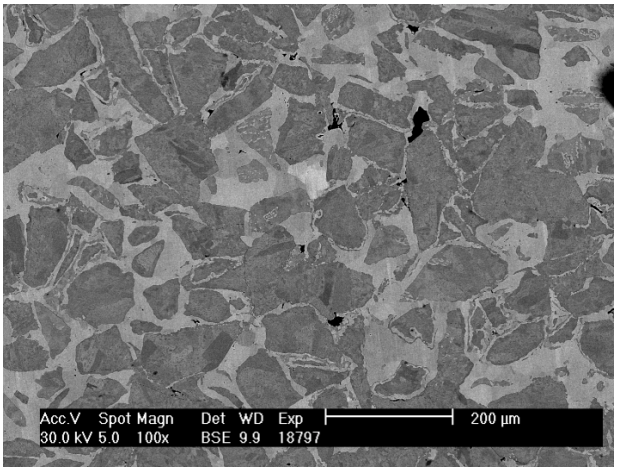

Fig. 5. The microstructure of hot isostatically pressed silicide with the nominal composition Mo-15Si-10B illustrating the continuous nature of the α-Mo matrix (bright contrast).

Table 1 shows electron microprobe data for the partitioning of the W or Nb in the different phases. Tungsten partitions primarily to the α-Mo. Consistent with its atomic size (which is almost identical to that of Mo) and its relative low solubility in the Mo_3Si and Mo_5SiB_2 phases, W does not improve the creep strength significantly (Fig. 6). Niobium, on the other hand, which partitions strongly to all phases and has a much larger atomic size than Mo, causes substantial solid solution strengthening.

Figure 7 illustrates the pronounced influence of the morphology and scale of the microstructure on the creep strength. As a base line, the creep strength of cast and annealed Mo-12Si-8.5B is indicated. When the α–Mo in Mo-16.8Si-8.4B is fine and discontinuous (see right-hand side of Fig. 3), the creep strength at 1400˚C is poor. This is consistent with the fine microstructure and the abundance of high-diffusivity paths for mass transport, such as grain and interface boundaries. At "lower" temperatures the strength of this alloy is high—presumably Hall-Petch strengthening, characteristic of fine-grained microstructures at lower temperatures, occurs. An alloy with the same nominal composition, but a much coarser microstructure is much stronger in creep (see also the microstructure on the left-hand side of Fig. 3).

Table 1. Composition of the phases in Mo-19.5W-12Si-8.5B and Mo-19.5Nb-12Si-8.5B

Note that the B concentrations tend to be overestimated.

Specimen	Phase	Mo	Nb	W	Si	B
Mo-19.5Nb-12Si-8.5B	α-Mo	82.1	15.7		2.2	
	Mo_3Si	59.6	17.2		23.2	
	Mo_5SiB_2	35.2	21.0		11.5	32.2
Mo-19.5W-12Si-8.5B	α-Mo	60.9		33.1	0.4	5.6
	Mo_3Si	69.7		4.5	23.7	2.1
	Mo_5SiB_2	39.0		8.7	9.1	43.3
	Mo_5Si_3	57.1		3.9	35.7	3.3

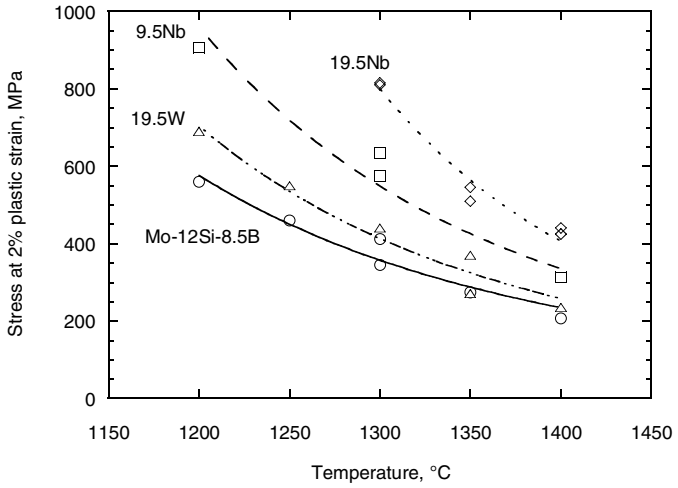

Fig. 6. Creep strength of cast and annealed molybdenum silicides.

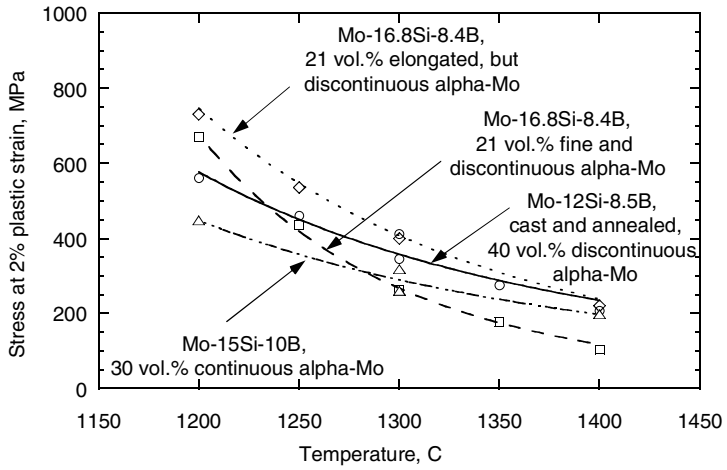

Fig. 7. Creep strength of Mo-Si-B alloys with different α-Mo volume fractions, size scales, and morphologies. The creep strength of cast and annealed Mo-12Si-8.5B is indicated for reference.

CONCLUSIONS

Boron-containing silicides with compositions in the Mo-Mo_3Si-Mo_5SiB_2 three-phase field can be quite resistant to oxidation. When the volume fraction and the continuity of the α-Mo solid solution phase is reduced, the oxidation resistance increases. However, at the same time the room temperature fracture toughness decreases. This is no surprise since both Mo_3Si and Mo_5SiB_2 are brittle phases. For a given α-Mo volume fraction, the room temperature fracture can be dramatically improved by making the α-Mo a continuous "binder" phase instead of small, isolated particles. The creep strength can be dramatically improved by solid solution alloying. Again, for a given α-Mo volume fraction, the control of the

microstructural scale and morphology is of critical importance. The compositional and microstructural design of Mo-Si-B alloys involves a trade-off between the simultaneous demands for adequate oxidation resistance, fracture toughness and creep strength. While the Mo-Si-B system is unique in the sense that it can deliver solutions to each of these demands, further work is needed to optimize both composition and microstructure such that all three requirements are satisfied at the same time.

ACKNOWLEDGMENTS

This work was sponsored by the Office of Fossil Energy, Advanced Research Materials (ARM) Program, U.S. Department of Energy, under contract DE-AC05-00OR22725 with Oak Ridge National Laboratory managed by UT-Battelle, LLC. Technical discussions with, and the help of, D. S. Easton and C. A. Carmichael are greatly appreciated. Likewise, the help of M. J. Kramer in discovering the Si-removal effect, the advise of M. P. Brady on the removal of Si as SiO, and the review of the manuscript by J. A. Horton are gratefully acknowledged.

REFERENCES

1. Y. Yamabe-Mitarai, “High-temperature strength of Ir-based refractory superalloys,” Mat. Res. Soc. Symp. Proc. Vol. 646, J. H. Schneibel et al., eds., pp. N3.6.1–3.6.12.
2. A. K. Vasudévan and J. Petrovic, “A comparative overview of molybdenum silicide composites,” Mater. Sci. and Engng. A155 (1992) 1–17.
3. M. K. Meyer, M. J. Kramer, and M. Akinca [sic], “Compressive creep behavior of Mo_5Si_3 with the addition of boron,” Intermetallics 4 (1996) 273–281.
4. M. Akinc, M. K. Meyer, M. J. Kramer, A. J. Thom, J. J. Huebsch, and B. Cook, “Boron-doped molybdenum silicides for structural applications,” Intermetallics A261 (1999) 16–23.
5. M. K. Meyer, A. J. Thom, and M. Akinc, “Oxide scale formation and isothermal oxidation behavior of Mo-Si-B intermetallics at 600–1000°C,” Intermetallics 7 (1999) 153–162.
6. H. Nowotny, E. Kimakopoulou, and H. Kudielka, Mh. Chem. 88 (1957) 180–192.
7. D. M. Berczik, United States Patent 5,595,616 (1997), “Method for enhancing the oxidation resistance of a molybdenum alloy, and a method of making a molybdenum alloy.”
8. D. M. Berczik, United States Patent 5,693,156 (1997), “Oxidation Resistant Molybdenum Alloys.”
9. R. Raj and L. R. Thompson, “Design of the microstructural scale for optimum toughening in metallic composites,” Acta Metall. Mater. 42 (1994) 4135–4142.
10. I. Rosales and J. H. Schneibel, “Stoichiometry and mechanical properties of Mo_3Si,” Intermetallics 8 (2000) 885–889.

11. S. V. Raj, J. D. Whittenberger, B. Zeumer, and G. Sauthoff, “Elevated temperature deformation of Cr_3Si alloyed with Mo,” Intermetallics 7 (1999) 743–755.
12. R. D. Field, D. J. Thoma, J. C. Cooley, F. Chu, C. L. Fu, M. H. Yoo, W. L. Hults, and C. M. Cady, “Dislocations in Mo_5SiB_2 T2 Phase,” Intermetallics 9 (2001) 863–868.
13. C. L. Fu, X. Wang, Y. Y. Ye, and K. M. Ho, “Phase stability, bonding mechanism, and elastic constants of Mo_5Si_3 by first-principles calculation,” Intermetallics, 7 (1999) 179–184.
14. J. H. Schneibel, C. J. Rawn, T. R. Watkins, and E. A. Payzant, “Thermal expansion anisotropy of ternary molybdenum silicides based on Mo_5Si_3,” Phys. Rev. B 65 (2002) 134112.
15. J. H. Schneibel, M. J. Kramer, Ö. Ünal, and R. N. Wright, “Processing and mechanical properties of a molybdenum silicide with the composition Mo-12Si-8.5B (at. %),” Intermetallics 9 (2001) 25–31.

INVESTIGATION OF ADVANCED ALLOYS FOR HEAT RECOVERY SYSTEMS

R. W. Swindeman, M. L. Santella, and P. J. Maziasz
Oak Ridge National Laboratory

INTRODUCTION

The objective of the research on advanced alloys is to provide databases and design criteria that will assist contractors in selecting optimum alloys for construction of components needed to contain process streams in advanced heat recovery systems. Typical components include steam line piping and superheater tubing for ultracritical steam cycles (600 to 815°C), heat exchanger tubing for advanced steam systems (650 to 870°C), foil materials for recuperators on advanced turbine systems (700 to 750°C), heat exchanger tubing for pulsed combustors (650 to 950°C), and tubesheets, plenums, and liners for hot gas cleanup systems (850 to 1000°C). The near term objective is to gather data that will permit the consideration of advanced steels for applications to 900°C in oxidizing environments or to 870°C slightly sulfidizing environments. Studies include the collection of data that will permit the consideration of third-generation advanced ferritic steels for service to 650°C, Ni-Co-Cr-Al alloys for service to 950°C, and oxide dispersion strengthened (ODS) alloys in aggressive environments to 1000°C.

Background

In the United States, new power generation needs are being met by the use of co-generation and the installation of medium-size gas turbines. Research in the fossil power industry is largely focused on condition assessment and life extension of aging components. Research related to inspection, damage assessment, and repair is actively supported by fossil power and petrochemical industries (1). In both industries, replacement of components with “new” and “advanced” materials is sometimes required, and research on the performance of the advanced materials for such components is in progress. Development of advanced materials for the fossil power industry has largely performed in Japan under sponsorship of the Electric Power Research Institute (2,3). Alloys such as tungsten-vanadium-modified 2 ¼%Cr (T23), 9%Cr (T92), and 12%Cr (T122) steels have reached ASME Code status and are being used to replace T11, T22, and austenitic stainless steels such as 304H and 321H. These advanced ferritic steels are candidates for the construction of piping systems, headers, and tubing for steam service to 600°C and higher, but more research is needed before the complex metallurgical constitution of the alloys is fully understood and their reliability for long-time service can be guaranteed. Advanced austenitic stainless steels for service above 600°C include niobium-modified 310 stainless steel (HR3C), a titanium-modified 20Cr-25Ni-Nb stainless steel (NF709), and copper-modified stainless steel (super 304 and SAVES 25).

Of these steels, HR3C has attained Code status as 310HCbN and a copper-modified stainless steel is in the Code- approval process. The steels are intended for superheater tubing, and the code-approved allowable stresses are generally limited to 732°C. The database for some of these stainless steels (NF 709, SAVES 25, and 310TAN) extends to 900°C but the poor oxidation resistance of the stainless steels limits their use. Similar to the advanced ferritic steels, there is much to be learned about the behavior of the complex austenitic steels in high-temperature environments. For service above 732°C, alloys containing over 30% nickel, such as HR 120 and alloy 230, have been developed. Also, there is renewed interest in cobalt-containing alloys, such as alloy 617 and Inconel 740.

Advanced Martensitic Steels

Issues have arisen in regard to the usage of the advanced ferritic steels in high-temperature service. Recently, concerns were raised about the welding procedures for the advanced martensitic steels. To avoid hydrogen cracking, a pre-heat of 204°C or higher is required for these alloys. Pre-heat temperatures may be close to the martensite finish temperature for steels such as Grade 91, hence some of the austenite produced in the welding heat cycle could remain untransformed. It would save energy if fabricators could proceed to the post weld heat treatment (PWHT) without cooling below 204°C, but there is concern that austenite retained in the weldment at 204°C would produce fresh martensite after the PWHT. Further, filler metals used for welding Gr91 are permitted to contain up to 1% Nickel. Nickel and manganese are known to lower the critical temperature where martensite or tempered martensite begins to transform to austenite (Ac1 temperature) on heating. If the PWHT is above this temperature, some of the austenite during PWHT could produce fresh martensite or softer ferrite upon cooling slowly. The influence of untempered martensite on the high-temperature performance Gr91 is unknown. To assist in the resolution of the issue, weldments of Grade 91 are being examined (4). Collaboration with industrial includes the Babcock and Wilcox Company and the Stoody Company. The (Ni+Mn) compositions being investigated are provided in Table 1 and include a range of (Ni+Mn) from 0.43 to 1.89. The Ac1 at 0.43% (Ni+Mn) is estimated to be around 830°C which is well above the typical PWHT range of 760 to 780°C. The Ac1 at 1.89 (Ni+Mn), however, is estimated to be 740°C. This temperature below the typical PWHT and near the minimum PWHT permitted for Gr91, namely 732°C. Hence, fresh martensite could form by virtue of retained austenite at the pre-heat temperature or from austenite that formed as a result to the PWHT above the Ac1.

Creep rupture testing was started on samples of a submerged arc weldment (SAW) containing high (Ni+Mn). Temperatures were at 550, 600, and 650°C with emphasis on 600°C. Samples were tested after

Table 1. (Ni+Mn) content of Grade 91 materials under investigation

Material	Wt % (Ni+Mn)	Estimated Ac1 (°C)
Base 2	0.55	830
Base 3	0.53	830
SA weld	1.41	775
FCA weld 1	1.42	775
FCA weld 2	1.38	775
FCA weld 3	0.43	830
FCA weld 4	1.89	740

SA = submerged arc weld in 50-mm plate;
FCA= flux core arc weld in 25-mm plate.

exposure to PHWT temperatures of 740 and 780°C. These temperatures represent the extremes for the PWHT temperature. Testing to 10,000 hours indicated that specimens containing fresh martensite (hold pre-heat at 204°C) had lower creep rates and lower rupture ductilities than specimens with fully tempered martensite (drop pre-heat to room temperature). In all cases, weld metal was stronger than base metal.

Flux core arc welds (FCAW) were produced. One had low (Ni+Mn) and the other high (Ni+Mn). The low (Ni+Mn) weld had a martensite finish temperature at or above the preheat temperature (204°C). The initial creep rupture testing indicated that holding or dropping preheat made no difference in creep after a PWHT of 4 hours at 760°C. The high (Ni+Mn) weld metal had a martensite finish temperature below the preheat temperature. Here, the specimens from the hold pre-heat had lower creep rates than the specimens from the drop pre-heat weld after a PWHT of 4 hours at 760°C. These results are being considered by the Electric Power Research Institute in developing industry guidelines for joining advanced martensitic steels.

Efforts continued to examine the long time stability of martensitic steels (5,6). Working with the Babcock & Wilcox Company, Gr91 specimens exposed to service conditions were evaluated in comparison to samples from laboratory aging exposures. Exposure times in service ranged to 155,000 hours, while the laboratory exposures ranged to 75,000 hours. Also, some specimens were removed from creep testing after times as long as 100,000 hours. Generally, it was observed that service exposures produced metallurgical conditions similar to thermal aging and low-stress creep. The coarsening of the substructure resulting in softening. Generally, the rupture life decreased and creep rate increased for a given post exposure condition. However, the ability to accelerate the damage rate and relate the properties observed in short-time test to long time performance has not yet been demonstrated.

New martensitic steels are being developed for advanced steam cycle applications. High nitrogen 12%Cr show exceptional strength (7), and studies of their creep resistance are just beginning. Sheet and bar products have been produced of a cobalt bearing 12%Cr steel have 0.16% nitrogen. This steel will be

subjected to a variety of heat treatments including austempering to bring our stable vanadium nitride particles.

Advanced Austenitic Stainless Steels

Creep testing was started on Inconel 740 supplied by Special Metals. Material that was solution annealed at 1050°C was found to be weak relative to expectations. Re-annealed at 1200°C was performed and testing resumed.

REFERENCES

(1) EPRI/DOE Conference on Advances in Life Assessment and Optimization of Fossil Power Plants, Sheraton World Resort, Orlando, Florida, March 11–13, 2002.

(2) R. Viswanathan and W. T. Bakker, "Materials for Ultra Supercritical Fossil Power Plants- Boiler Materials: Part I," J. Materials Engineering and Performance, Vol. 10, February, 2001, pp. 81–95.

(3) F. Masuyama, "History of Power Plants and Progress in Heat Resistant Steels," *ISIJ International*, Vol. 41 (2001) No. 6, pp. 612–625.

(4) M. L. Santella, R. W. Swindeman, R. W. Reed, and J. M. Tanzosh, "Martensitic Transformation, Microsegregation, and Creep Strength of 9Cr-1Mo-V Weld Metal," paper presented at the 6th *International Conference on Trends in Welding Research*, Callaway Gardens, Pine Mountain, Georgia, April 16, 2002.

(5) R. W. Swindeman, P. J. Maziasz, M. L. Santella, and G. M. Ludka, "Investigation of Advanced Alloys for Heat Recovery Systems," paper presented at the *16th Annual Conference on Fossil Energy Materials*, Wyndham Baltimore Inner Harbor, Baltimore, Maryland, April 23, 2002.

(6) R. W. Swindeman, P. J. Maziasz, I. G. Wright, and J. Tanzosh, "Damage Assessment of Grade 91 Specimens Removed from Long Time Creep Tests," paper presented at the EPRI/DOE conference on *Advances in Life Assessment and Optimization of Fossil Power Plants*, Sheraton World Resort, Orlando Florida, March 12, 2002.

(7) A. Gocmen, P. Ernst, and P. Holmes, "Principles of Alloy Design in High Nitrogen 12% Chromium Steels," *Materials Science Forum*, Vols. 318-320, 1999, pp. 215–226.

DEFINING FAILURE CRITERIA FOR EXTENDED LIFETIME METALLIC COATINGS

B. A. Pint, Y. Zhang,[†] P. F. Tortorelli, J. A. Haynes, and I. G. Wright
Oak Ridge National Laboratory
[†]Center for Manufacturing Research
Tennessee Technological University

INTRODUCTION

Aluminide coatings have been studied for many years because of their excellent corrosion resistance in oxidizing, sulfidizing, carburizing and water-containing environments.1-5 They are of particular interest for improving the corrosion resistance of Fe-base alloys to achieve higher operating temperatures in fossil energy systems where sulfur and water vapor can cause severe oxidation problems.1,5-12 One of the factors that inhibits their application is a lack of sufficient data about their potential benefits in terms of lifetime and applicable environments. In order to address that issue, model coatings are being fabricated at ORNL for corrosion testing and diffusion studies in order to develop a comprehensive lifetime evaluation approach for aluminide coatings. One ferritic (Fe-9Cr-1Mo) and one austenitic alloy (304L) have been selected as substrate materials for study. An important issue in developing a lifetime model is defining the coating failure criteria. As the Al in the coating is consumed by corrosion or back-diffusion in the substrate, there will be a critical Al content, below which the coating is no longer effective in protecting the underlying substrate. In order to help define these limits in various environments and as a function of temperature, model alloys have been cast with Al contents from 10-20% Al (all chemical compositions are given in atom percent) and Cr contents up to 10%. Testing of these alloys will help simulate coating performance as the coating becomes depleted in Al. Another factor that could reduce coating lifetime is the thermal expansion mismatch between Fe3Al and the substrate.5 This difference could cause cracking or deformation that could reduce coating life. Corrosion testing using thermal cycling is of particular interest because of this potential problem.

Initial work used relatively thin (50-60μm) coatings produced by chemical vapor deposition (CVD) that performed well in cyclic testing at 800°C in a simulated exhaust gas environment (air with 10vol.% water vapor), but poorly in a sulfidizing environment.5 However, application temperatures for these substrate alloys are likely to be lower such that subsequent testing was conducted at 700°C. Because of the poor performance of the thin coatings in sulfidizing environments, thicker coatings with higher Al contents were produced using a higher Al activity CVD process. Initial results are presented on the oxidation performance of these coatings. Thicker coatings also are now being annealed at 500°-800°C for up to 10,000h to determine diffusion rate constants.

EXPERIMENTAL PROCEDURE

The substrates used in this study were Fe-9Cr-1Mo and 304L (Fe-18Cr-9Ni nominally) to represent the performance of ferritic and austenitic alloys, respectively. The laboratory-scale CVD reactor and coating process have been described elsewhere.[5] The CVD process was selected for controlled laboratory studies and should produce coatings similar to a well-controlled, above-pack process that could be used commercially. In order to increase the coating thickness and Al content in the CVD process, the standard exposure was increased from 6h at 900°C to 4h at 1050°C and the Al activity was increased by including Cr-Al alloy pieces in the reactor during deposition.[13]

For comparison in the oxidation testing, model alloys with Al contents of 11-22% and Cr contents of 0-10% were cast using induction melting and a water-cooled copper mold. The alloys were annealed for 4h at 1300°C and were polished to a 0.3μm finish prior to oxidation testing. All oxidation coupons and coated specimens were cleaned in acetone and alcohol prior to oxidation.

Previous work[5] reported oxidation results at 800°C. The current work focuses on 700°C as a more realistic application temperature for the substrate alloys. Cyclic oxidation testing in air with 10±0.5vol.%H_2O was conducted in an automated test rig with a cycle consisting of 1h at temperature and 10min cooling at room temperature. Both ends of the vertical reaction tube were closed and the water vapor was controlled in the carrier gas by a water injection system described elsewhere.[10] Before and after exposure, selected specimens were examined by light microscopy, field emission gun, scanning electron microscopy (SEM) equipped with energy dispersive x-ray analysis (EDXA), x-ray diffraction (XRD), and electron probe microanalysis (EPMA) using wavelength dispersive x-ray analysis. The surface product of cross-sectioned specimens was protected by Cu-plating the specimen prior to mounting in epoxy.

RESULTS AND DISCUSSION

AS-DEPOSITED COATING CHARACTERIZATION

Figure 1 shows an example of a coating made by a high Al activity process. It is almost an order of magnitude thicker than the coatings made by the low activity CVD process.[5] Also, the outer, high-Al content layer has increased in thickness from 3-5μm to 50-60μm. For comparison, the EPMA profiles for the two types of coatings are shown in Figure 2. The high Al activity coatings also have a significantly higher Al content. Using XRD, the outer layer may be β-FeAl. However, with the small volume of material, it is difficult to differentiate this phase from Fe_3Al. One issue with the thicker coatings is the presence of cracks at the coating-substrate interface, arrows in Figure 1. These cracks were particularly severe for the coatings on 304L causing through-thickness cracking in some cases and delamination of the coating. These cracks may be a result of the thermal expansion mismatch between substrate and coating.[5] The cracking problem was alleviated by using a post-deposition anneal in the CVD reactor for 2h at 1150°C.[13]

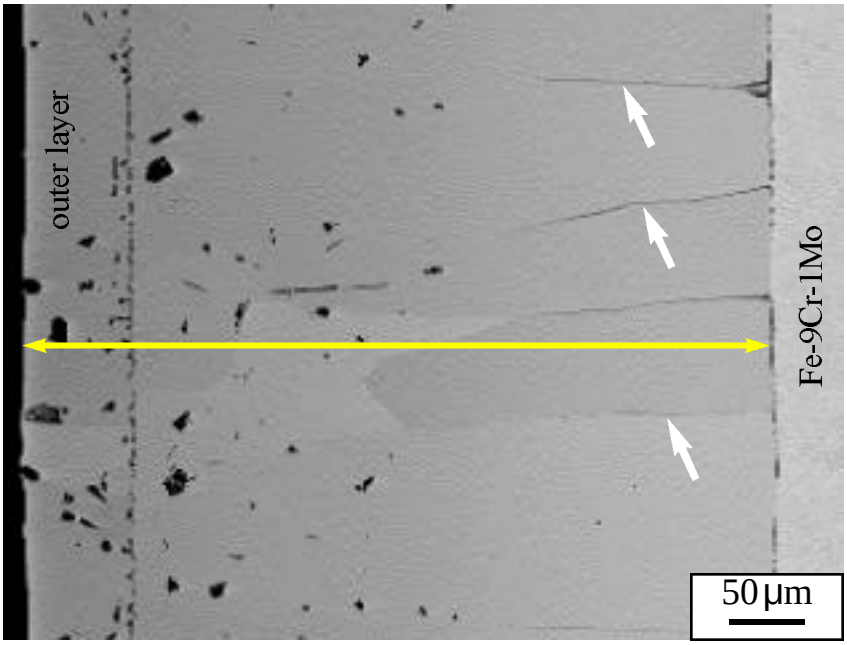

Figure 1. EPMA back-scattered electron image of the as-deposited high Al activity CVD aluminide coating on Fe-9Cr-1Mo. The white arrows show cracks in the coating.

CYCLIC OXIDATION RESULTS

The low activity Al coatings were evaluated at 700°C along with uncoated Fe-9Cr-1Mo and 304L specimens. Previous work showed severe degradation of the uncoated substrates at 800°C and a similar accelerated attack was observed at 700°C, Figure 3. The uncoated Fe-9Cr-1Mo specimen showed a high mass gain due to Fe-rich oxide formation while the uncoated 304L specimen showed mass losses due to

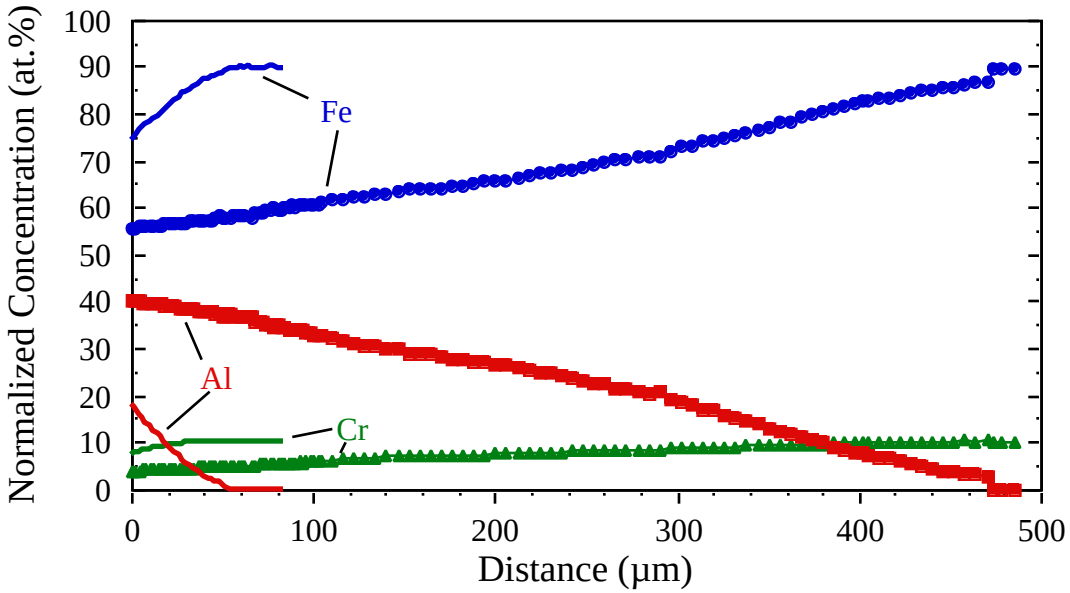

Figure 2. Fe, Al and Cr profiles in the as-deposited coatings on Fe-9Cr-1Mo using EPMA. The lines show the low activity coating and the symbols the new, high Al activity coating.

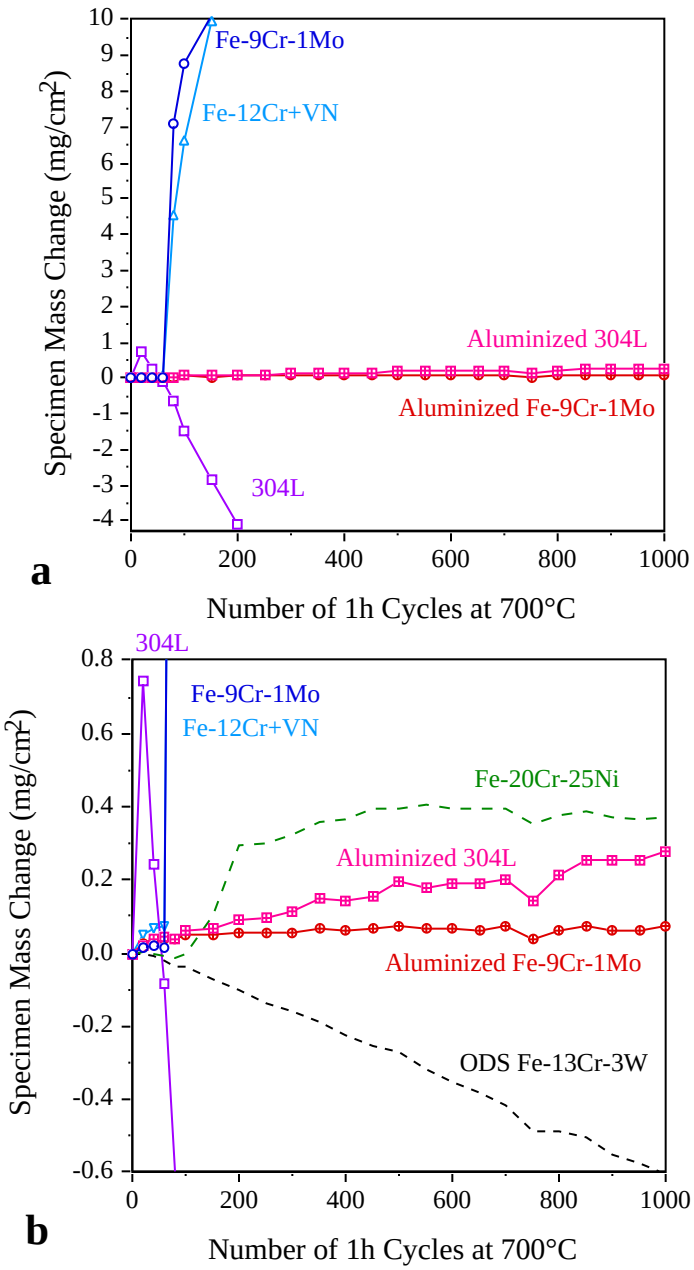

Figure 3. Specimen mass changes during 1h cycles at 700°C in air+10%H_2O. Coated specimens were made using the low Al activity CVD process.

spallation of Fe-rich oxide. Both exposures were stopped after 200, 1h cycles. This behavior would not be expected in dry, oxidizing environments but has been observed in numerous other studies containing steam or water vapor.[6-12] In contrast, the aluminized specimens of each substrate type showed only small mass gains after 1000 cycles. This improvement is attributed to the lower volatility of an external alumina scale compared to the Cr-rich scale formed on the uncoated substrates.[14] No negative effect of thermal cycling was observed in this test, however, the thin Al-rich layer in these coatings may not have generated sufficient strain to cause cracking or other associated failure during testing. Such effects could occur with a thicker coating.

For comparison, a Fe-12Cr with VN (manufactured by ABB Alstrom) was included in the test and showed similar behavior as the Fe-9Cr-1Mo specimen, Figure 3a. It also was removed after 200 cycles. A NF709 (Fe-20Cr-25Ni) specimen showed better behavior with low mass changes after 1000 cycles due to its higher Ni and Cr contents compared to 304L. (Recent work has shown that both higher Ni and Cr contents improve the performance of stainless steels in wet air.[15]) A similar low mass change was noted for an oxide dispersion strengthened (ODS) Fe-13Cr-3W specimen. The small, steady mass loss is associated with the evaporation of $CrO_2(OH)_2$.[9] This ODS alloy performs well despite its low Cr content because of its fine subgrain structure which allows for rapid, short-circuit Cr diffusion in the substrate.[16]

Similar exposures with water vapor are being conducted on specimens coated with the high Al activity process. The specimens have completed 850, 1h cycles and show very similar performance as the thinner coatings with no signs of coating degradation, Figure 4. Any thermal expansion mismatch problem should be exacerbated by the higher Al content, thicker coating and high cycle frequency but no problem has been observed yet. This suggests that the thermal expansion mismatch may not be an important factor.

POST-TEST COATING EVALUATION

Post-test characterization of the coated and uncoated specimens tested at 700°C in wet air has been completed. Figure 5 contrasts the thick, Fe-rich oxide formed on uncoated Fe-9Cr-1Mo after 200, 1h cycles with the thin alumina scale formed after 1000, 1h cycles at 700°C. The scale on the uncoated substrate consists of two layers, with the inner layer containing some Cr. The coated specimen appears very similar to the as-deposited condition with a thin Al-rich outer layer and some Al-rich particles near the coating-substrate interface, Figure 5b. However, the EPMA profile shows that the coating has a much

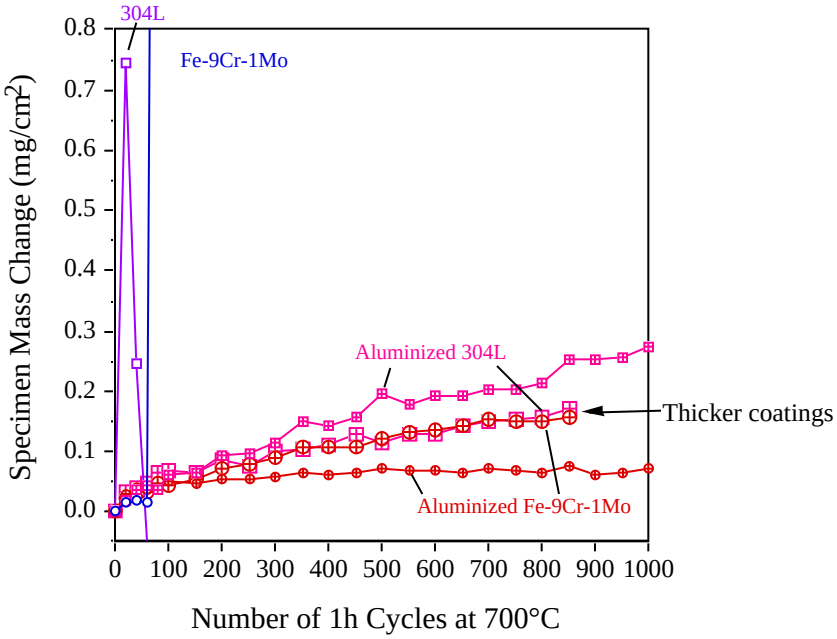

Figure 4. Specimen mass changes during 1h cycles at 700°C in air+10%H_2O. Resulted are shown for specimens coated with both the high and low Al activity processes.

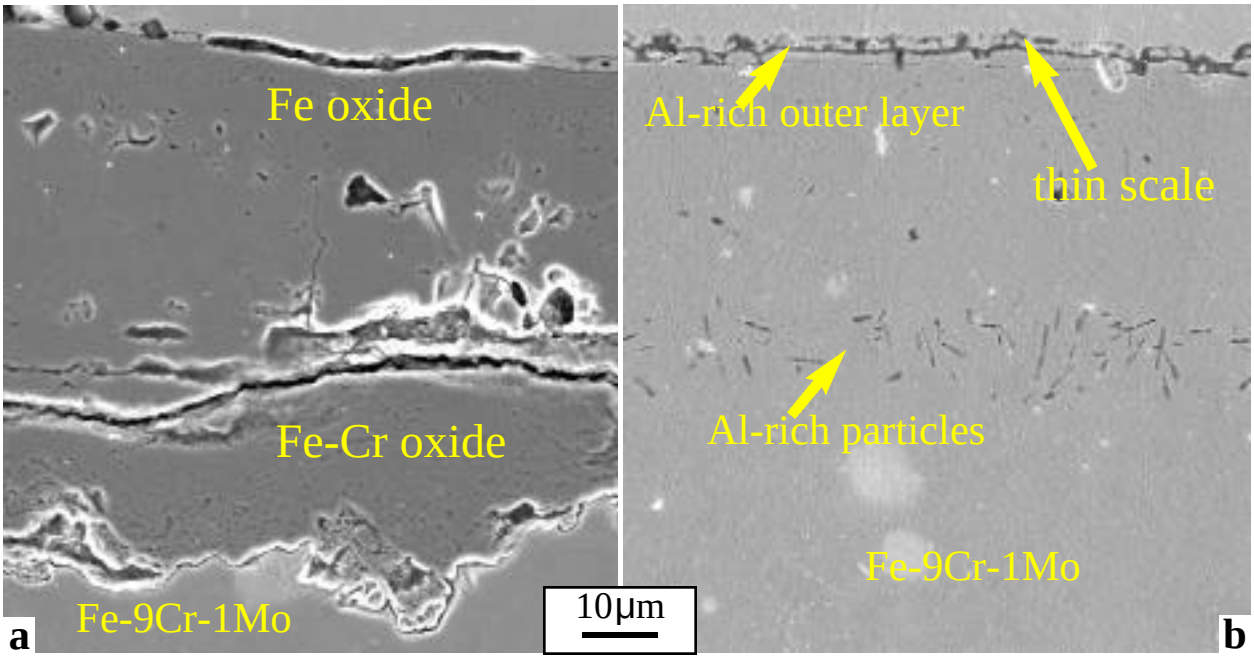

Figure 5. (a) uncoated Fe-9Cr-1Mo substrate after 200, 1h cycles and (b) low Al activity aluminized Fe-9Cr-1Mo substrate after 1000, 1h cycles at 700°C.

lower Al content after the 1000h exposure, Figure 6. There is still a high Al content in the outer layer, but the Al content rapidly decreased in the inner layer. The spikes in the Al profile are due to the Al-rich particles.

Characterization of the uncoated and coated 304L specimens showed similar results. The uncoated 304L specimen showed a thick oxide after 200 cycles at 700°C, Figure 7a, indicating that the measured mass

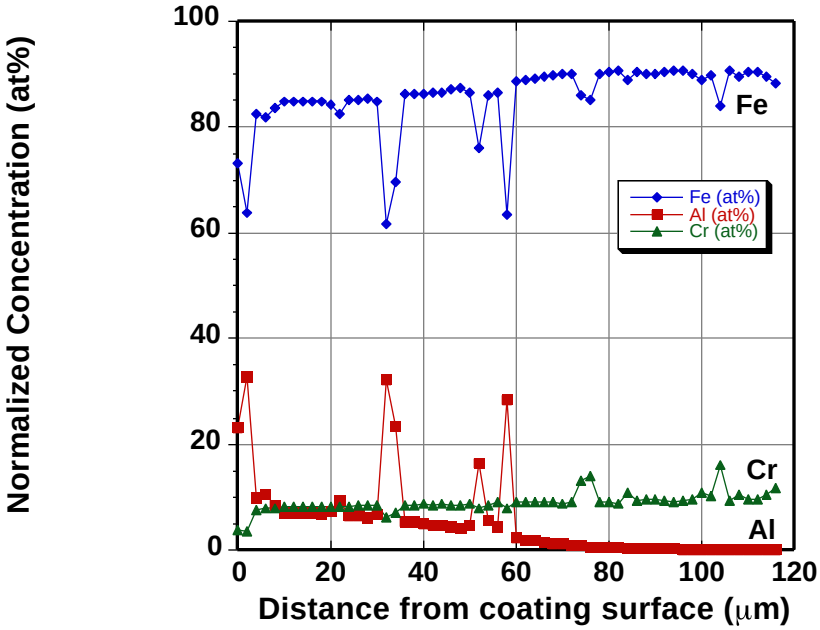

Figure 6. Fe, Al and Cr profiles in the low Al activity coating on Fe-9Cr-1Mo after 1000, 1h cycles at 700°C in air+10%H_2O using EPMA.

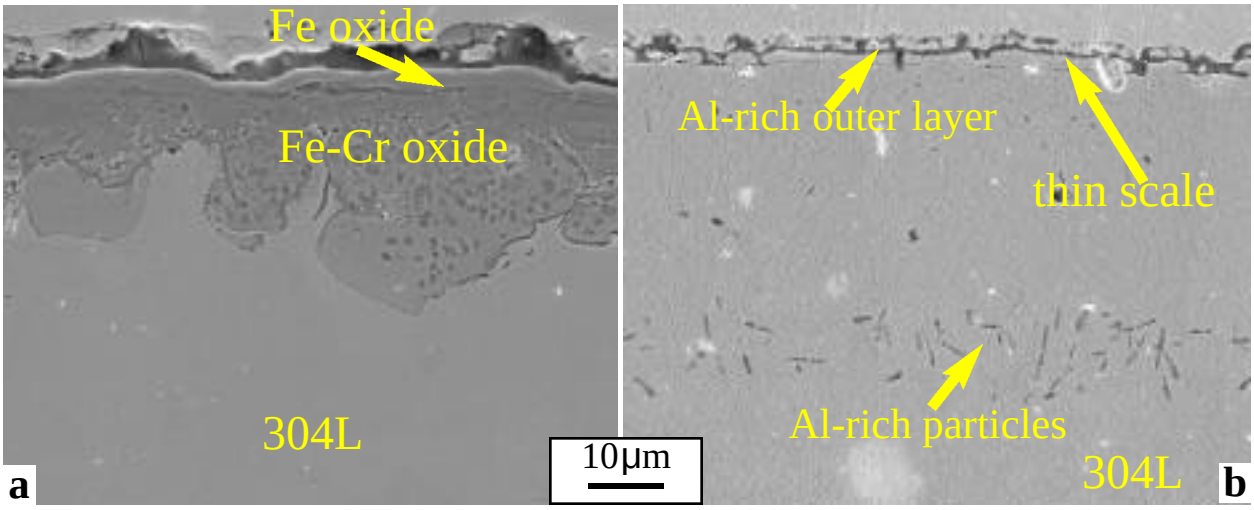

Figure 7. (a) uncoated 304L substrate after 200, 1h cycles and (b) low Al activity aluminized 304L substrate after 1000, 1h cycles.

loss was due to the spallation of the thick oxide. The aluminized 304L specimen showed a thin, protective oxide scale and an Al-rich outer layer and Al-rich particles near the coating-substrate interface. An EPMA profile of the coating, Figure 8, showed that the Al content of the coating had dropped to even lower levels than that observed on the Fe-9Cr-1Mo substrate. Below the Al-rich outer layer, the Al content was ≤5%.

FAILURE CRITERIA

The results for the thin coatings in air plus water vapor demonstrate that even low Al contents can significantly improve the oxidation behavior of ferritic and austenitic alloys at 700°C. However, the same

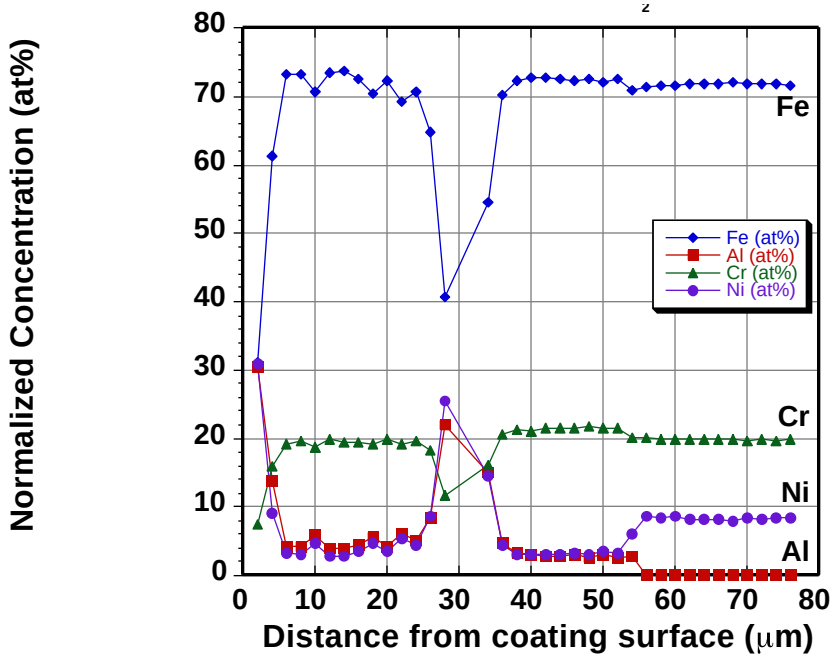

Figure 8. Fe, Al Cr and Ni profiles in the low Al activity coating on 304L after 1000, 1h cycles at 700°C in air+10%H_2O using EPMA.

was not true for sulfidation testing at 800°C, where the thin coatings performed poorly after the first cycle.[5] This raises the general question of how to define the minimum Al content required for coatings as a function of application temperature and environment. Results for sulfidation testing of coatings and cast Fe-Al both appear to indicate that ≈20%Al is needed for protective behavior.[5,17] This was an important factor in examining the higher Al activity coatings, which showed excellent performance with the Fe-9Cr-1Mo substrate during 5, 20h cycles at 800°C in H_2-H_2S-H_2O-Ar ($P_{S_2}=10^{-6}$atm; $P_{O_2}=10^{-22}$atm). The minimum Al content required for sulfidation protection is needed to model the coating lifetime. During exposure, the coating will lose Al from reaction product formation and back-diffusion into the substrate. When the Al content of the coating drops below this minimum value, the coating will no longer be protective. However, the sulfidation test was performed in a severe environment and a lower Al content may be sufficient with a lower sulfur content or lower temperature exposure. The performance of the thin coatings at 700° and 800°C demonstrate that lower Al contents are sufficient in wet air, but because no coating failures have been observed, it is not possible to define the critical Al content for this environment from these results.

In an attempt to define the failure criteria in wet air at 700°C, cast alloys were exposed in 1h cycles. Alloys with 13-22%Al and 500ppma Hf were exposed to this environment. (The Hf was added in order to improve scale adhesion[18] so that these alloys could be tested at temperatures up to 1200°C for other applications.) Compositions with less than 20%Al showed high mass gains upon initial exposure, Figure 9a. At longer times, the increase in mass was negligible, Figure 9b. In cross-section, the scales formed on the lower Al content alloys consisted of an outer iron oxide layer and an inner, Fe-Al oxide. The amount of Fe-rich oxide decreased with increasing Al content in the alloy, Figure 10. If the thick, Fe-rich oxide were to form on a coated specimen, the coating would be largely consumed. Thus, from these results it appeared that 20% Al was necessary for both sulfidizing and oxidizing environments. However, the profiles in Figure 2 show that the coating also contains a significant Cr content and this addition is

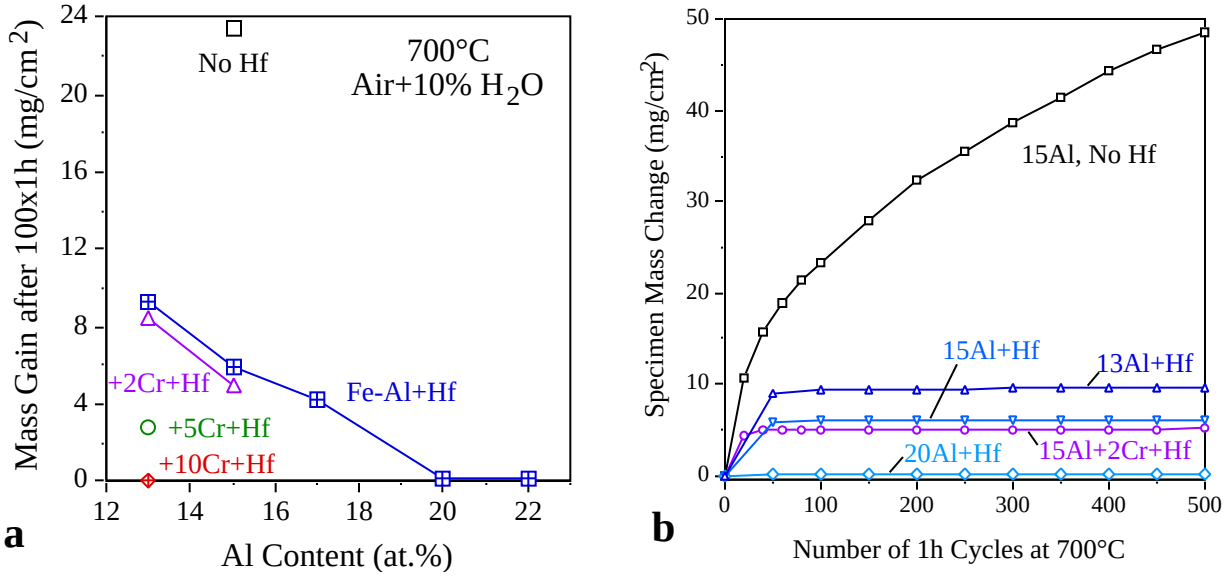

Figure 9. Mass gains for cast Fe-Al alloys after exposure in 1h cycles at 700°C in air + 10 vol.%H_2O. (a) summary of mass gains after 100 cycles and (b) mass change during 500 cycles for selected materials.

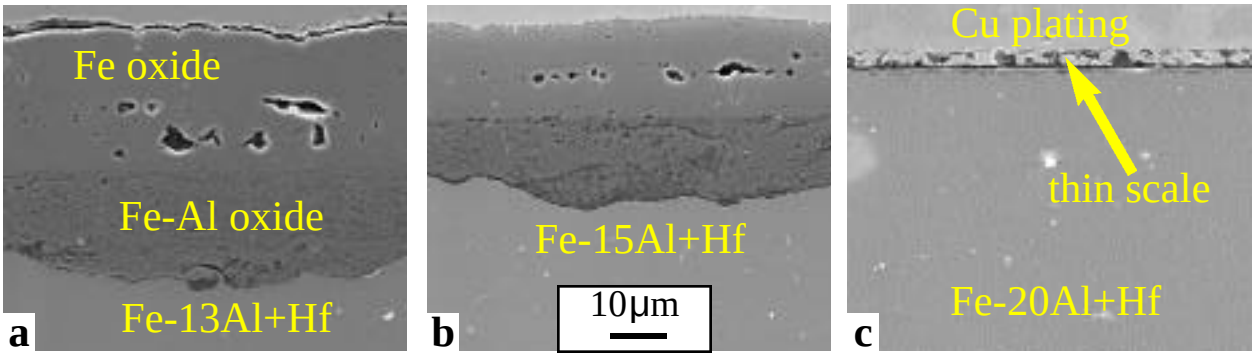

Figure 10. Polished cross-section after 800, 1 h cycles at 700°C in wet air, (a) Fe-13Al+Hf (b) Fe-15Al+Hf and (c) Fe-20Al+Hf.

expected to improve the oxidation resistance by a third element effect.[19] Cast alloys with 13-15%Al, 2-10%Cr and 500ppma Hf also were exposed in wet air at 700°C and the Cr addition had a significant beneficial effect, particularly when 10%Cr was added; an alloy with only 13%Al performed as well as the Fe-20%Al+Hf specimen. Thus, when substantial Cr is present in the coating, as is the case for the coatings on Fe-9Cr-1Mo and 304L, the critical Al content appears to be less than 13%Al. More work with lower Al content alloys is needed to specify the critical Al content in this environment. Based on these results for cast alloys it is not surprising that even the thin coatings perform well.

The addition of Hf was thought to play little role at this low temperature. However, when a Hf-free, Fe-15Al cast specimen was tested in wet air at 700°C, it performed significantly worse than Hf-doped Fe-15Al, Figure 9. Rather than showing an initial high mass gain followed by little mass change, the Hf-free material showed continuous, significant mass gain up to 500 cycles, suggesting that Hf may have a beneficial, but not yet explained, role at this temperature. This results also suggested that incorporating Hf into the coating might have a beneficial effect even for low temperature applications.

SUMMARY

In order to develop a comprehensive lifetime model for aluminide coatings on Fe-base alloys, model coatings are being made by a laboratory CVD process for diffusion and corrosion studies. Specimens made by a higher Al activity CVD process are being tested as coatings made by a low Al activity did not have sufficient Al to provide sulfidation resistance. After exposure for 1000, 1h cycles in air plus 10% water vapor at 700°C, the low Al activity coatings on Fe-9Cr-1Mo and 304L showed a protective alumina scale but low Al levels remained in the coating. For developing a coating lifetime model, the corrosion and diffusion testing will provide rates of Al consumption as a function of temperature. The remaining missing information is the critical Al content below which the coating is no longer protective. Results to date indicate that this value needs to be determined by considering the temperature, environment and both the Al and Cr contents in the coating. No thermal expansion problems have been observed during cyclic testing however, during deposition of the thick coatings, an in situ anneal was needed to ameliorate crack formation.

ACKNOWLEDGMENTS

The authors would like to thank K. Cooley, M. Howell, L. D. Chitwood and H. Longmire at ORNL for assistance with the experimental work and D. F. Wilson and C. G. McKamey at ORNLfor their comments on the manuscript. This research was sponsored by the U.S. Department of Energy, Fossil Energy Advanced Materials Research Program under contract DE-AC05-00OR22725 with UT-Battelle, LLC.

REFERENCES

1. P. F. Tortorelli and K. Natesan, *Mater. Sci. Eng*., A258 (1998) 115.
2. P. F. Tortorelli, J. H. DeVan, G. M. Goodwin, M. Howell in: *Elevated Temperature Coatings: Science and Technology I*, Eds. N. B. Dahorte, J. M. Hampikian, J. J. Stiglich; TMS, Warrendale, PA, 1995, p.203.
3. F. D. Geib and R. A. Rapp, *Oxid. Met.*, 40 (1993) 213.
4. M. Zheng and R. A. Rapp, *Oxid. Met.*, 49 (1998) 19.
5. B. A. Pint, Y. Zhang, P. F. Tortorelli, J. A. Haynes and I. G. Wright, *Mater. High Temp.*, 18 (2001) 185.
6. G. C. Wood, I. G. Wright, T. Hodgkiess, D. P. Whittle, *Werk. Korr*., 21 (1970) 900.
7. J. Shen, L. Zhou and T. Li, *Oxid. Met.*, 48 (1997) 347.
8. H. Nickel, Y. Wouters, M. Thiele and W. J. Quadakkers, *Fresenius J. Anal Chem.*, 361 (1998) 540.
9. H. Asteman, J.-E. Svensson, M. Norell and L.-G. Johansson, *Oxid. Met.*, 54 (2000) 11.
10. B. A. Pint and J. M. Rakowski, NACE Paper 00-259, Houston, TX, presented at NACE Corrosion 2000, Orlando, FL, March 2000.
11. V. Lepingle, G. Louis, D. Petelot, B. Lefebvre and J. C. Vaillant, *Mater. Sci. Forum*, 369-372 (2001) 239.
12. S. Henry, A. Galerie and L. Antoni, *Mater. Sci. Forum*, 369-372 (2001) 353.
13. Y. Zhang and B. A. Pint, in Proc. Sixteenth Annual Conf. Fossil Energy Materials, R. R. Judkins (comp.), U. S. Department of Energy, 2002, in press.
14. E. J. Opila and N. S. Jacobson, in *Fundamental Aspects of High Temperature Corrosion*, D. A. Shores, R. A. Rapp, and P. Y. Hou, Eds., Proc. Vol.96-26, Electrochemical Society, Pennington, NJ, 1996, p.344.
15. R. Peraldi and B. A. Pint, submitted to Mater. High Temp., 2002.
16. Zs. Tökei, K. Hennesen, H. Viefhaus and H. J. Grabke, *Mater. Sci. Technol.*, 16 (2000) 1129.
17. J. H. DeVan and P. F. Tortorelli, *Corr. Sci.*, 35 (1993) 1065.
18. B. A. Pint, K. L. More, P. F. Tortorelli, W. D. Porter and I. G. Wright, *Mater. Sci. Forum*, 369-372 (2001) 411.
19. F. H. Stott, G. C. Wood and J. Stringer, *Oxid. Met.*, 44 (1995) 113.

CONCEPTS FOR SMART PROTECTIVE HIGH-TEMPERATURE COATINGS

P. F. Tortorelli, M. P. Brady, I. G. Wright, and B. A. Pint
Oak Ridge National Laboratory

INTRODUCTION

Environmental resistance is a critical material barrier to the operation of fossil energy systems with the improved energy efficiencies and environmental performance described by the goals of the Vision 21 concept of the Office of Fossil Energy. All fossil fuel-derived processes contain reactive species and high-temperature degradation arising from reactions of solids with gases and condensible products often limits performance or materials lifetimes such that efficiency, emission, and/or economic targets or requirements are not realized. Therefore, historically, the development of materials for fossil-fuel combustion and conversion systems has been closely linked to corrosion studies of alloys and ceramics in appropriate environments so as to identify reaction or degradation mechanisms and develop and/or select materials that offer improved performance. This project is somewhat different from such studies in that it focuses on the feasibility of new routes to controlling the critical chemical and mechanical phenomena that collectively form the basis for environmental protection in relevant fossil environments by exploring compositional and microstructural manipulations and cooperative phenomena that have not necessarily been examined in any detail to date. This can hopefully lead to concepts for "smart" coatings or materials that have the ability to sense and respond appropriately to a particular set or series of environmental conditions in order to provide high-temperature corrosion protection.

DISCUSSION OF CURRENT ACTIVITIES

This project is new in FY02 and the first concepts being explored involve silicides, as there is some evidence that such materials have enhanced resistance in oxidizing/sulfidizing and sulfidizing environments and in air/oxygen at very high temperatures. In this regard, molybdenum silicides may prove to be of particular interest. Molybdenum is known to sulfidize fairly slowly[1] and there has been recent progress in developing Mo-Si-B systems with improved oxidation resistance at high temperatures.[2,3] This project builds on previous work that evaluated certain aspects of the multiphase nature (composition, morphology) of the molybdenum-rich Mo-Si-B system (Fig. 1) on protective oxide formation.[4] The initial emphasis of this project is on the roles of dispersed reservoirs of α-Mo and Si-enriched phases in determining sulfidation and oxidation resistance.

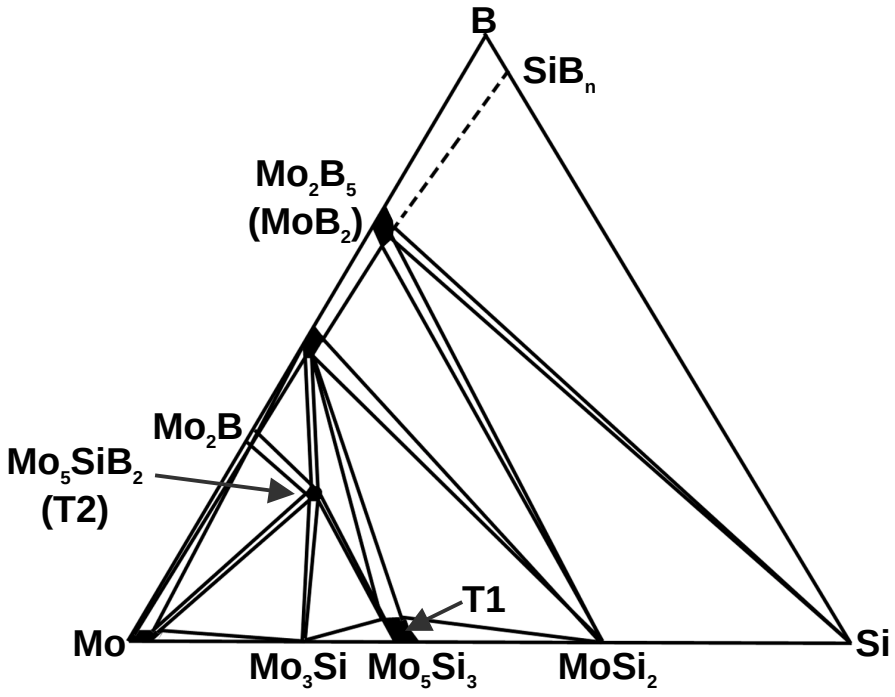

Fig. 1. A schematic Mo-Si-B phase diagram based on Nowotny et al., 1957.

Automated cyclic oxidation exposures were conducted on Mo-Si-B alloys in dry, flowing O_2 at 1200°C using a cycle consisting of 60 min at temperature and 10 min out of the furnace. Specimens were attached to alumina rods with Pt-Rh wires and mass changes were measured after 1, 5, 20, 40, 60, 80, and 100 cycles and then every 100 cycles using a Mettler model AG245 balance. The resulting gravimetric data are shown in Fig. 2. Note that the specimens containing α-Mo showed a substantial mass loss for the first thermal cycle, but that, subsequently, only modest changes in specimen weight were measured. Indeed, after the first cycle, the rates of mass change of the two Mo-Mo_5SiB_2-Mo_3Si specimens were equivalent to and less than those measured for the T1- Mo_5SiB_2-Mo_3Si coupons and not much different than that of the $MoSi_2$-containing alloy. Such observations suggest a multistage mechanism in which the α-Mo is rapidly removed by formation of volatile MoO_3 and the resulting near-surface enrichment in silicon and boron facilitate the formation of a protective borosilicate or silica layer that grows laterally to seal the remaining Mo-rich areas of the alloy from the environment. This type of process qualitatively resembles what happens in carbon-containing SiC composites under oxidizing conditions at high tmepratures[5,6] and suggests that the oxidation behavior of this multiphase system can possibly be controlled through microstructural manipulation. If so, oxidation resistance can be maximized by finely dispersing not only the most active phase (a-Mo), but also the one that can act as a source for Si (the most

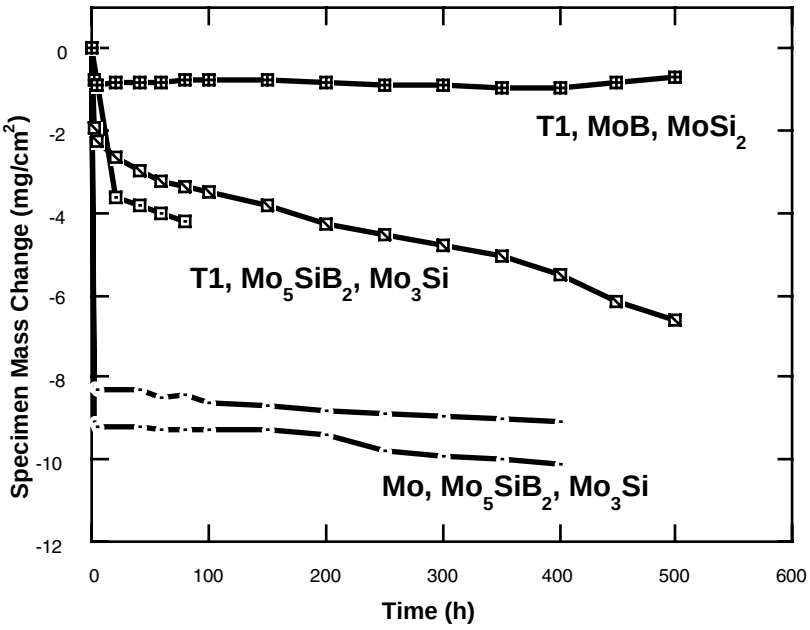

Fig. 2. Specimen mass change of Mo-Si-B alloys as a function of time at 1200°C for 1-h thermal cycles.

Si-rich component).[7] In this regard, Schneibel has recently shown that a Mo-Mo_5SiB_2-Mo_3Si alloy with a fine-scale microstructure had significantly better isothermal oxidation resistance than a similar composition with a coarse phase dispersion.[8] Near-term future work will focus on the effects of phase and composition manipulations in the Mo-Si-B system on isothermal and cyclic oxidation and sulfidation susceptibilities in order to gauge the possibilities of developing such alloys as smart protective coatings.

REFERENCES

1. S. Mrowec, *Oxid. Met*., 44 (1995) 177–209.
2. M. K. Meyer and M. Akinc, *J. Am. Ceram. Soc*., 79 (1996) 938–44.
3. M. K. Meyer, A. J. Thom, and M. Akinc, *Intermetallics*, 7 (1999) 153–62.
4. P. F. Tortorelli, B. A. Pint, K. L. More, A. J. Thom, and M. Akinc, "The Influence of Boron and Silicon in Improving the Oxidation Resistance of Mo_5Si_3," *ORNL Fossil Energy Program Annual Report for April 2000 to March 2001*, Oak Ridge National Laboratory report ORNL/TM-2001/89, R.R. Judkins and P.T. Carlson (comp.), July 2001, www.ornl.gov/fossil/Newsltr/01Annual.PDF.
5. L. Filipuzzi and R. Naslain, *J. Am. Ceram. Soc.*, 77 (1994) 467–74.
6. F. Lamouroux, R. Naslain, and J-M. Jouin, *J. Am. Ceram. Soc.,* 77 (1994) 2058–68.
7. G. Wang, B. Gleeson, and D. L. Douglass, *Oxid. Met*., 35 (1991) 333–48.

8. J. Schneibel, “Mo-Si-B Alloy Development,” *Proc. 16th Annual Conf. on Fossil Energy Materials*, U.S. Dept. of Energy, April 2002, www.netl.doe.gov/publications/proceedings/02/materials.

DURABILITY AND RELIABILITY OF SOLID OXIDE FUEL CELL MATERIALS AND COMPONENTS

Edgar Lara-Curzio and M. Radovic
Oak Ridge National Laboratory

INTRODUCTION

Fuel Cells generate electricity through an electrochemical process in which the energy stored in a fuel is converted directly into electricity. Fuel cells consist of an electrolyte material, which is sandwiched in between two electrodes (a porous anode and a cathode). The input fuel is catalytically reacted (electrons removed from the fuel elements) when it passes over the anode and the resulting ions flow through the electrolyte toward the oppositely charged electrode. The electrons, which cannot pass through the electrolyte, flow through an external circuit to serve an electric load. At the cathode, ions combine to create by-products, and depending on the input fuel and electrolyte, different chemical reactions will occur.

Solid Oxide Fuel Cells (SOFC) use a ceramic, solid-phase electrolyte. To achieve adequate ionic conductivity in ceramic electrolytes, the system must operate at high temperatures, which leads to higher efficiency but also results in higher rates of material degradation. Although fuel cells have been around since the 1830's and have been used successfully in the space program, their potential future use in distributed power applications will require demonstration of reliable operation for periods of time that will be measured in tens of thousand of hours. As design methodologies emerge for SOFCs, designers need to consider the innate features of the ceramic materials that will be incorporated in their designs. To minimize ohmic losses, most SOFC designs are based on the use of electrolytes that are tens of microns thick, at which point the electrolyte cannot longer be self-supporting. Manufacturing techniques therefore involve the engineering of multilayer anode/electrolyte/cathode assemblies to provide the required support.

The Solid State Energy Conversion Alliance (SECA) was formed to accelerate the commercial readiness of solid-oxide fuel cell systems in the 3 kW–10 kW size range. The SECA Core Technology Program was established to support the industrial teams participating in the SECA Program in a number of areas that include the prediction of reliability and durability of SOFCs. Predictions of service life and reliability of SOFCs will require a fundamental understanding of the initiation and progression of damage in the various materials and components as a function of material microstructure, processing and fabrication, residual stresses, and service history.

The scope of this project is to identify the mechanisms responsible for the failure and durability of materials and components for SOFCs and using that information, develop a probabilistic-based life-prediction analysis. Such analysis will address the stochastic nature of the strength of ceramic materials, the defects and mechanisms that are life limiting, their evolution during service life, and their interaction with environmental and other effects.

SUMMARY OF ACTIVITES

An important element of the methodology that will be developed to predict the durability and reliability of SOFC materials and components is a thorough understanding of the relationships among the microstructure and the distribution of defects in the material, and its mechanical properties. Defects can be inherent to the material's microstructure or can be introduced during manufacturing, processing and assembly. Mechanical properties of interest include: elastic constants, strength and fracture toughness. Because most SOFC systems are based on the use of flat, layered structures, the structural integrity of the components will be controlled by the in-plane biaxial strength of the material. During this period, a test fixture was designed to determine the in-plane biaxial strength of flat, plate-like components according to ASTM C 1499 "Standard Test Method for Monotonic Equibiaxial Flexural Strength of Advanced Ceramics at Ambient Temperature." This standard test method covers the determination of the equibiaxial strength of advanced ceramics at ambient temperature under monotonic uniaxial loading using a concentric ring configuration. Figure 1 shows a picture of the fixture that was designed and fabricated, using aluminum oxide, to determine the in-plane biaxial strength of SOFC components by using the concentric ring configuration. Because of its construction using ceramic materials, the test fixture can be used for testing materials at temperatures as high as 1400°C. Figure 2 shows a schematic of the loading configuration for this test.

Fig. 1. Picture of high-temperature fixture for the determination of in-plane equibiaxial strength.

This fixture was designed using a modular approach to allow also for the evaluation of fracture toughness by the double-torsion test (Fig. 3). Figure 4 is a schematic of the double-torsion test configuration. The popularity of this technique stems from a number of reasons. For example, the magnitude of the stress intensity factor in the specimen is independent of crack length. This feature allows crack

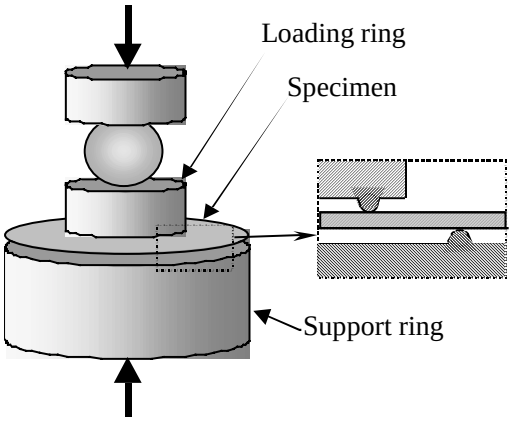

Fig. 2. Schematic of ring-on-ring configuration for the determination of in-plane equibiaxial strength.

Fig. 3. Picture of high-temperature fixture for the determination of fracture toughness by double-torsion.

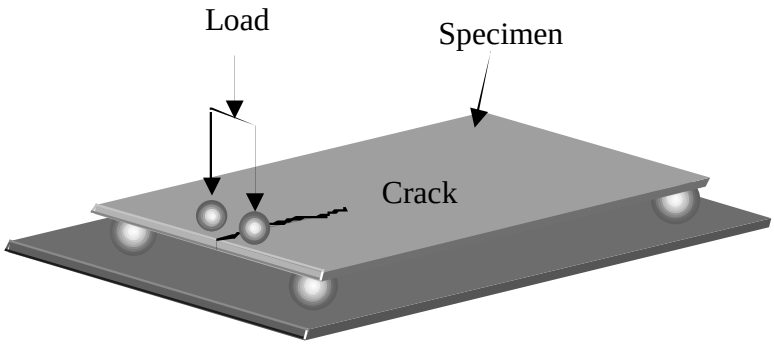

Fig. 4. Schematic of double-torsion test for determination of fracture toughness.

growth data to be obtained on opaque specimens, and the relatively simple configuration can be extended for testing at elevated temperature and hostile environments.

In-plane biaxial strength tests will be complemented by non-destructive evaluation using infrared imaging. We have found that infrared imaging is a powerful tool for identifying defects (i.e., voids, delamination) in SOFC materials and components. Furthermore, this technique will be very useful in the future when the long-term behavior of SOFC materials will be investigated and the monitoring of growth and propagation of defects becomes necessary to support the development of life-prediction methodologies. Figure 5 shows a schematic of the test configuration used for infrared imaging while Fig. 6

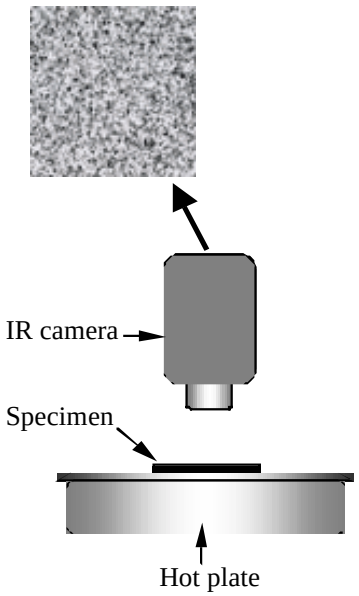

Fig. 5. Schematic of experimental set-up for infrared imaging of SOFC materials.

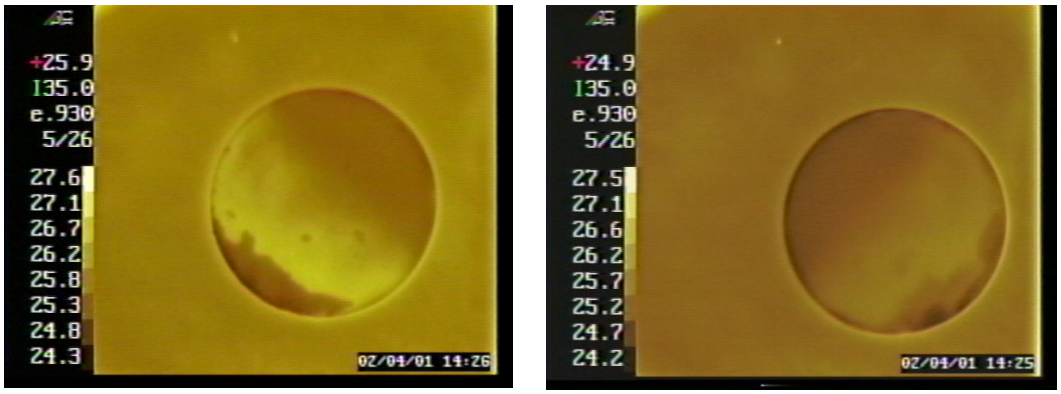

(a) **(b)**

Fig. 6. Infrared image obtained for multilayer yttria-stabilized zirconia specimen. (a) top. (b) bottom. Bright areas indicate regions of delamination.

shows infrared images obtained for a multilayer yttria-stabilized zirconia specimen.[1] In these images, bright areas correspond to regions where delamination has occurred because the heat conductivity of air is lower than that of the material.

During next year, these techniques will be employed to characterize the mechanical properties and behavior of SOFC materials in support of SECA industrial teams.

[1] Samples provided by T. Armstrong, ORNL.

REFERENCE

B. J. Pletka, E. R. Fuller, and B. G. Koepke, “An Evaluation of Double-Torsion Testing- Experimental,” Fracture mechanics Applied to Brittle Materials, ASTM STP 678, S. W. Freiman, Ed., American Society for Testing and Materials, 1979 pp. 19–37.

ECONOMICAL THERMAL PROCESSING OF SOLID OXIDE MEMBRANE MATERIALS

T. R. Armstrong, B. L. Armstrong, T. J. Huxford, D. C. Harper, C. A. Walls, and C. A. Blue
Oak Ridge National Laboratory

INTRODUCTION

Substantial progress has been made in the development of an innovative rapid thermal processing method for manufacturing solid oxide membrane components. Previous work has shown that conventional furnace sintering of a tape cast, nickel oxide (NiO) precursor material, which had been screen-printed with a thin yittrium stabilized zirconia (YSZ) coating (<9 um), can reliably produce thin dense films of YSZ electrolyte on a NiO porous anode support. In the present work, a new processing method has been developed using a focused plasma-arc-lamp IR heating source to sinter specimens, instead of a conventional furnace. The objective of this approach is to reduce the furnace processing time from 36 hours to less than 20 hours, while producing thin dense films of YSZ electrolyte on a NiO porous anode support. Experimental results indicate that by taking advantage of the high power density and precise control capability of the plasma-arc-lamp to heat only the sample without having to also heat a furnace mass, will allow more rapid heating profiles. Preliminary results, using samples identical to those used to develop the furnace sintering profiles, have resulted in virtually identical results with respect to the microstructure of the membranes. Processing times have been shortened to one hour and have the potential to be further reduced to minutes. The production of samples that have consistent flatness is currently being developed.

EXPERIMENTAL PROCEDURE

A unique thermal processing facility at the Oak Ridge National Laboratory, Fig. 1, has been used to investigate the feasibility of developing rapid heating methods for manufacturing solid oxide membrane components. The 300 kW plasma-arc-lamp used in this facility, Fig. 2, is capable of focusing a beam of incoherent light, 0.2 to 1.4 microns, on an area as small as 10 cm^2 at a power density of 3500 W/cm^2. At these power density levels the lamp provides a capability to initiate melting in any substance in fractions of a second. The utility of this facility is not just limited to the high power and high power density capability of the 300kW plasma-arc-lamp. Precise control of the lamp is essential for practical industrial processing applications. In this regard, note in Fig. 2 that the plasma lamp is coupled to a robotic manipulator. This robot has, state-of-the-art, 6-axis capability and provides the lamp capability to scan complex surfaces, with a prescribed heat flux. Other facility attributes allow the arc lamp to be configured with a variety of different reflectors, two of which are

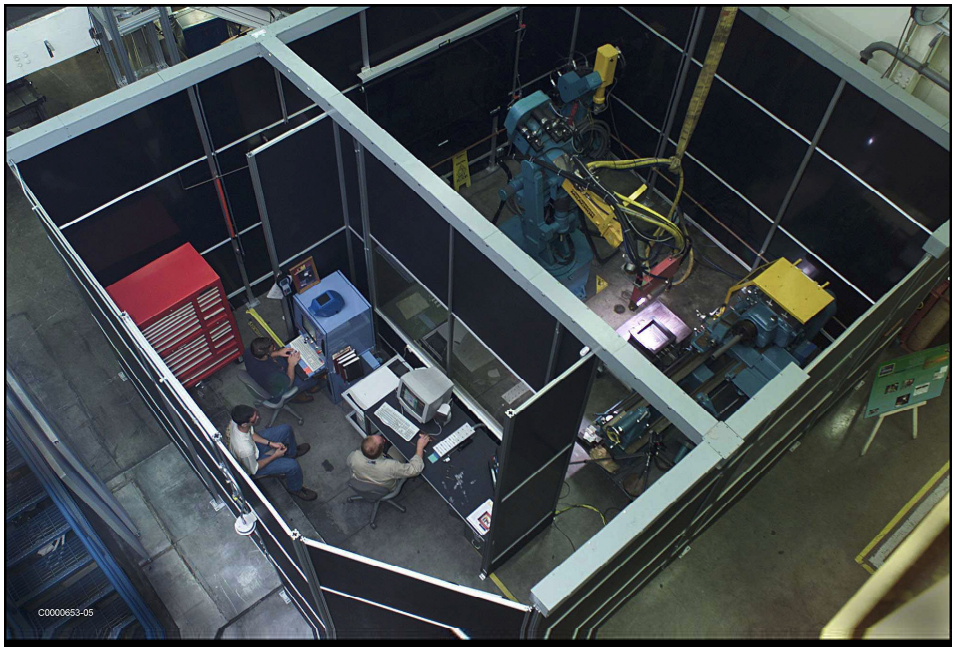

Fig. 1. The Plasma-Arc-Lamp Processing Facility at the Oak Ridge National Laboratory.

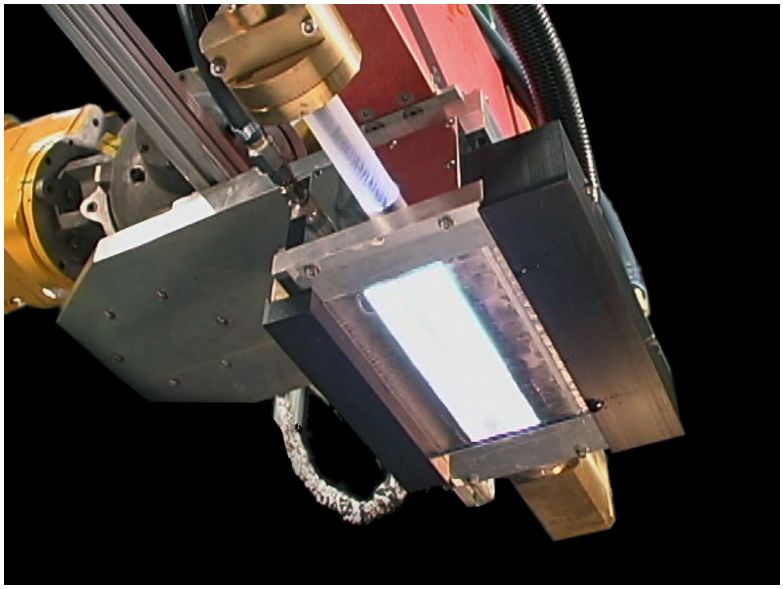

Fig. 2. A view looking into the exit aperture of the 300 kW plasma-arc-lamp installed in the ORNL test facility.

shown schematically in Fig. 3. Other reflectors are available at our Plasma Arc Lamp Facility that provide focused, rectangular beam profiles measuring: 3 cm by 20 cm and 3 cm by 35 cm, which produce power densities of 1200 W/cm^2 and 600 W/cm^2, respectively. A uniform irradiance reflector shown in Fig. 3 (right) will provide a uniform heat flux over a 20 cm by 20 cm area at 200 W/cm^2.

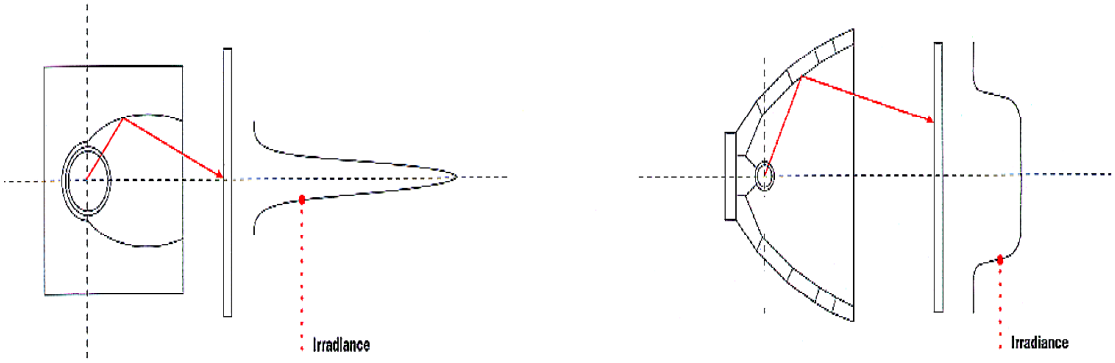

Fig. 3. Typical Plasma-Arc-Lamp reflector configurations.

Control of the lamp power output is essential for the thin film processing applications described in this paper. In this regard, the lamp is capable of continuously varying power levels, accurate to within 0.1%, in either a pulsed or DC mode. Power levels are PC controlled and can be precisely incremented in 0.001sec intervals from idle to full power.

Shown schematically in Fig. 4, are the basic electrical/mechanical attributes of the arc lamp that allow very rapid and precise modulation of the power output. Our arc lamp source is configured as a simple quartz tube, 4 cm ID, into which a mixture of deionized water and argon are injected (Fig. 4). The mixture is injected tangentially into the quartz tube's interior at one end of the tube. The resultant helical flow down the length of the tube produces a thin film of water against the tube wall, which effectively cools it. The argon gas flows in a similar fashion down the core of the tube and provides the medium into which a high-pressure plasma arc can be formed for passing up to 1200 A. These sources are able to operate continuously for up to 1000 hours. Power output is continuously variable from near 1 kW to full power and requires only 0.001 sec. to ramp up or be extinguished.

Other ancillary equipment that is useful for IR lamp processing includes: (1) a variety of processing boxes that are available for the heating of specimens in different atmospheres when using the plasma arc lamp (Fig. 5), (2) on-line video cameras for monitoring and recording of experiments, and (3) PC-based data acquisition and control is available in the facility to record and control: temperature, heat flux, lamp head position/kinematics parameters and lamp electrical operating characteristics.

Initial experiments were carried out on solid oxide fuel cell membranes consisting of a 10 mm yttria stabilized electrolyte (YSZ) supported on a 1 mm thick NiO/YSZ anode. Anode substrates were prepared by tape casting. The resulting dried tape was laminated together to produce a substrate of desired thickness (1 mm) and cut to size by a hot knife (i.e., 25.4 mm diameter disc or 25.4 mm square wafer). The YSZ coating was applied to the anode by screen printing using a proprietary binder developed at ORNL. The coated substrates were then bisque fired for 2 hours at 1000°C in air.

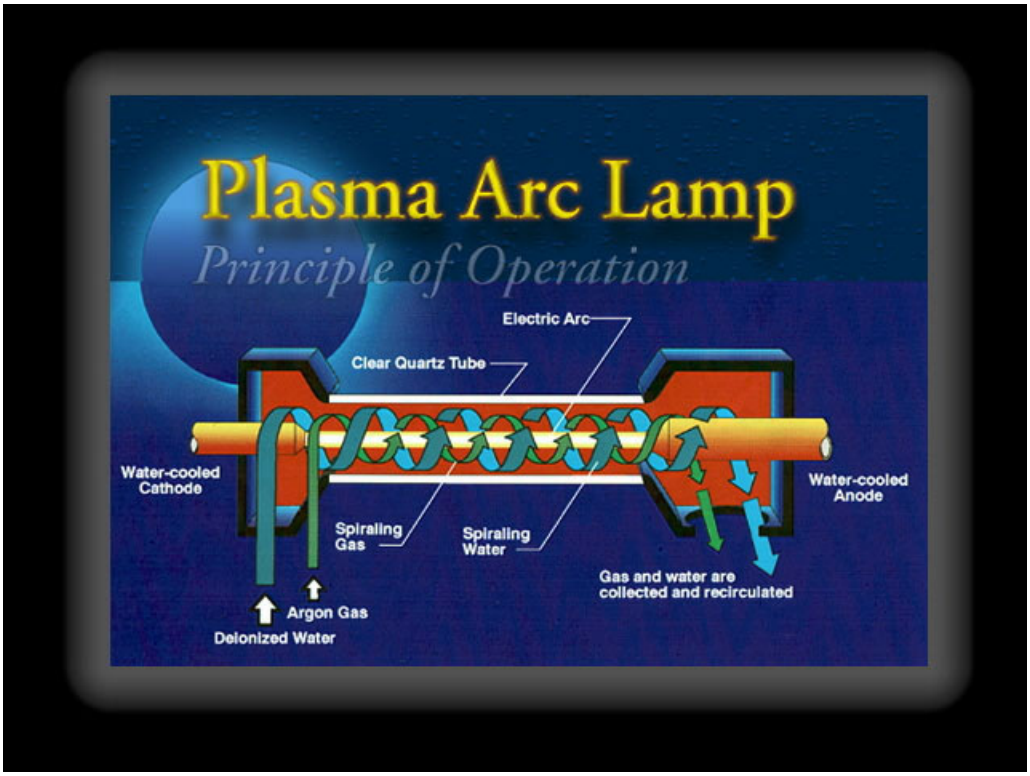

Fig. 4. Plasma-arc-lamp operating principal schematic.

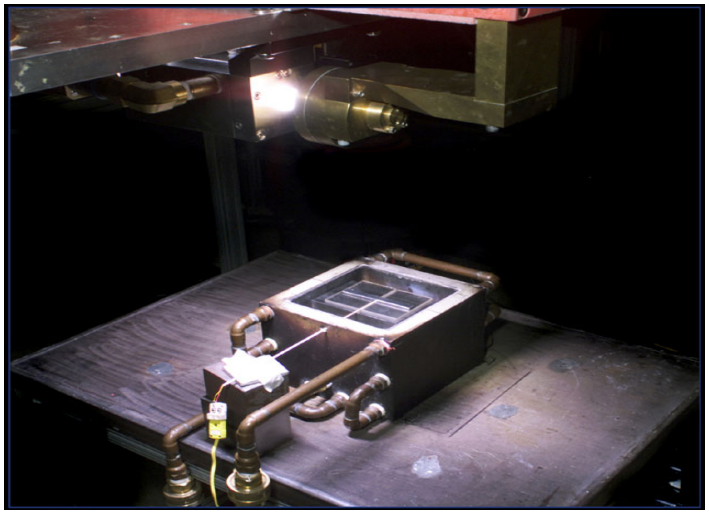

Fig. 5. Water-cooled chamber processing chamber used to provide vacuum or special gaseous atmospheres during processing by plasma-arc-lamp. Specimen chamber has a Quartz cover that is transparent to the lamp IR beam.

INFRARED PROCESSING

Initial considerations that motivated the study of high density infrared (HDI) solid oxide fuel cell membranes was the drive to considerably reduce the sintering time to reduce cost and increase productivity. The current solid state sintering process can be simply described as requiring a slow and uniformly heated source (i.e., furnace) that increases the sample temperature at an average rate of 4°C/min to 1400°C. The samples are held at 1400°C for two hours and slowly cooled to room temperature at the 0.33°C/sec rate. Other details of the process involved selectively covering the samples with inert covers to eliminate thermally induced distortions. This process nominally required 48 hours and would constitute the most significant cost in the manufacture of commercial components.

Other research at the HDI processing facility at the ORNL has been successful in processing coatings with dissimilar thermal properties. In many ways, HDI processing is similar to laser flash heating technology in that very high power heat fluxes can be precisely applied to surfaces. HDI, however, can illuminate substantially more surface area at comparable flux densities and does not result in convective mixing.

A basic strategy of HDI processing in brittle materials is to gently and very precisely preheat the substrate/coating system to a temperature close to where the desired processing outcome of melting or sintering will occur. Once this point has been reached, the application of a small increment in heat flux of the correct duration is all that is needed to produce the desired outcome. This can often be accomplished much more quickly with HDI, compared to a furnace, as the components are directly heated with a uniform surface heat flux. In addition, by having very precise control of the heat flux intensity and duration, it is often possible to optimize a heating cycle with respect to minimizing mechanical stresses due to: temperature gradients, sintering or other phase and material property changes. In the discussion below, two initial attempts for HDI processing of the YSZ/NiO system are described even though they were largely unsuccessful. Their inclusion however, may be of interest as the techniques used demonstrate the processing flexibility possible with the infrared lamp and led to a third process that was very successful for obtaining membranes with the desired microstructure.

The first attempt to process samples were placed on a quartz plate, which was supported by a steel block and preheated with the HDI source set at low power (10 to 300 W/cm^2) by scanning across the sample surface at approximately 10 mm/sec. Following a series of preheating scans, the lamp power was increased, 700 to 1200 W/cm^2, and the samples again scanned at rates ranging from 5 to greater than 20 mm/sec. In these runs, no sample was produced that did not experience severe mechanical damage. Selected samples fragments were analyzed by both optical and electron microscopy to evaluate microstructural development. Dense, but fractured YSZ coatings were

observed on some samples. As a result of this first series of experiments, it became obvious that a less severe thermal cycling approach would be required. In addition, better diagnostics would be required in order to observe the densification process of the screen-printed YSZ coating.

In the second series of experiments, a number of samples (Fig. 6) were prepared. These samples had a type S thermocouple attached to the backside of each of the samples. The thermocouple weld bead was milled to a flat surface in order to mate with the anode substrate and attached with a ceramic adhesive. These samples were run with the HDI lamp in a fixed position with the sample positioned at the 1cm wide focal point of the lamp. An additional visual diagnostic was included in the new set-up by a shuttered video camera. The camera was able view the samples with a 50X telephoto lens at full lamp power and provided real time feed back on the condition of the sample during processing.

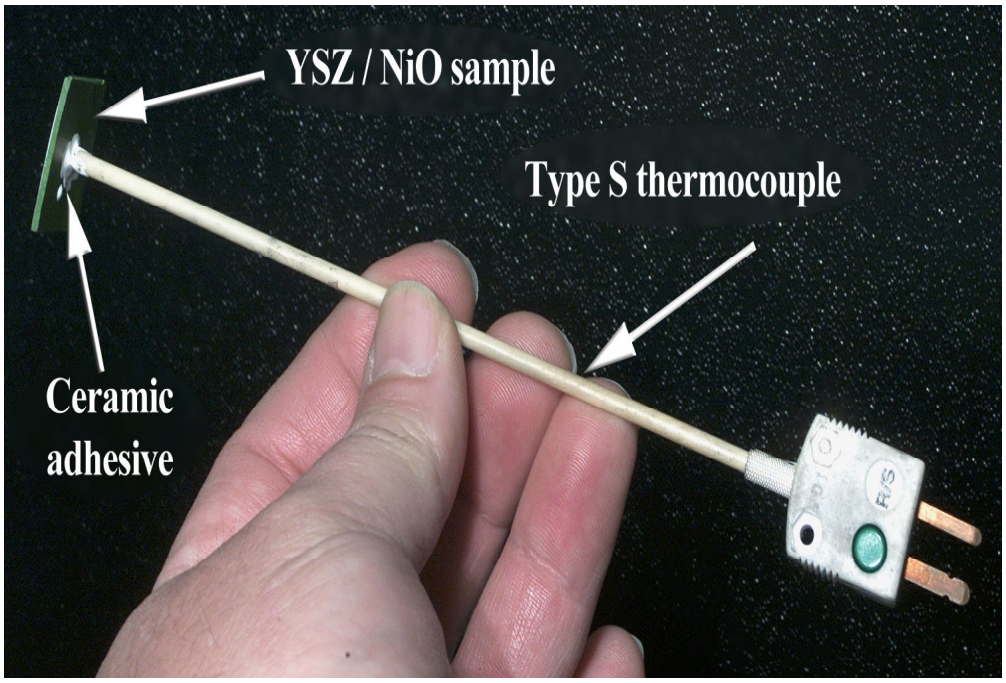

Fig. 6. Type S thermocouple attached to backside of a YSZ/NiO processing sample.

Experiments that were carried out with this series of samples were focused on determining the lamp power and rear face sample temperature that coincided with densification of the YSZ coating. Because the focused beam width was 1.0 cm wide at the surface of the 2.5 cm wide sample, we were able to visually observe a range of sample responses due to the temperature gradients that were present in the sample. A plot of the temperature as a function of power is shown in Fig. 7.

For the sample that was processed to the profile shown in Fig. 7, three distinct material responses were observed in the sample: (1) the center of the hot surface over sintered (this region was distinctly

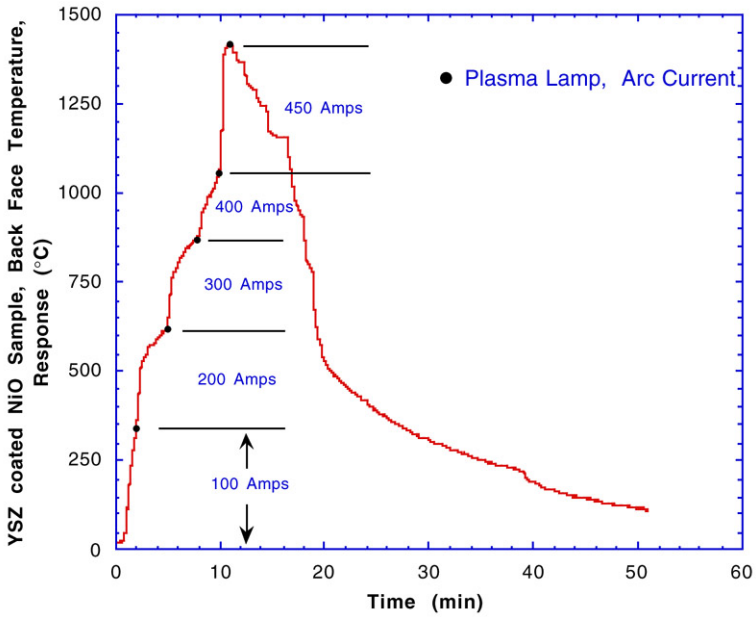

Fig. 7. Rear face temp. Response, YSZ/NiO 1cm wafer, at the focus of the HDI lamp.

black in color indicative of melting of the NiO), (2) in a 0.5 cm band around the central spot, the YSZ densified (become transparent), and (3) In a third region around the periphery of the sample, a narrow band of the YSZ remained as the original the screen-printed coating before processing. During the course of the processing run, each of the different regions were clearly visible on the real-time video monitor.

After a series of runs as described above, a new processing strategy was formulated. The main features of this new approach resulted in the elimination of the thermocouple as a necessary diagnostic tool in favor of the real-time video monitor. The effectiveness of the ceramic adhesive in insulating the backside of the sample resulted in the setting of samples on an aluminum oxide setter. This allowed concurrent heating of the sample from both sides as the base heated up in the HDI beam. Also observed in the earlier sample runs were severe mechanical deformations of the sample that occurred coincident with the sintering interval of the process. This deformation was virtually eliminated by covering the sample with a 3 mm thick sapphire disc.

After updating the process as described above, new samples were run with the lamp positioned in the divergent region of the HDI beam which provided uniform heating of the complete sample. Fig. 8 shows the before and after processing appearance of the YSZ/NiO sample clearly showing the transition to the transparent YSZ coating and the sintering shrinkage.

The heating profile used to produce the results shown in Fig. 8 is shown in Fig. 9. The sample was placed on an aluminum oxide wafer and covered with a 3 mm thick 10 mm diameter sapphire

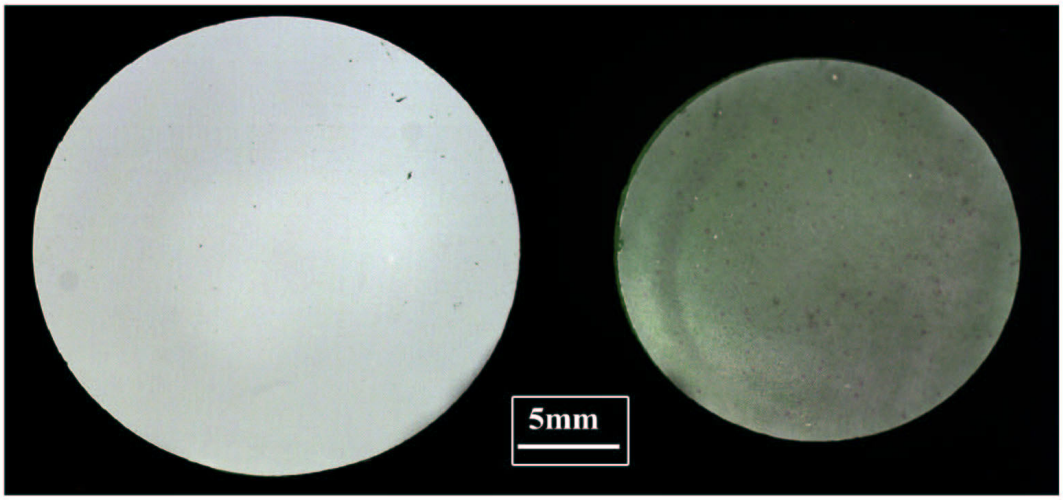

Fig. 8. YSZ/NiO sample, before and after HDI processing

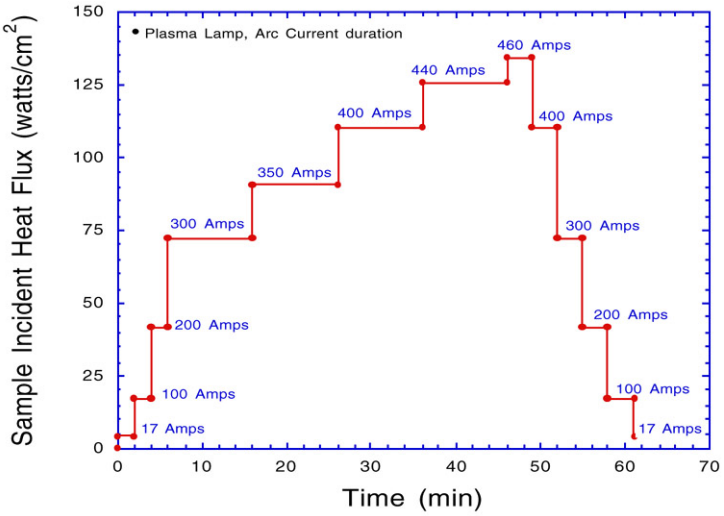

Fig. 9. HDI, arc current profile and resultant sample heat used to sinter the sample shown in Fig. 8.

cover during process. The sapphire cover helped to keep sample flat during the process. The aluminum oxide wafer provided an insulating boundary on the rear face of the sample and the wafer edges also absorbed radiation from the HDI beam. These factors provided a more uniform heating of the sample with respect to its thickness, which in-turn decreased the temperature gradient through the sample and therefore the thermally induced bending stresses.

Other interesting features of the process described above are shown in Fig. 10 as a sequence of still photographs taken from the processing run videotape. In the upper left photo, the sample is 35 minutes into the processing sequence and was slowly heated with an incremental heat flux from

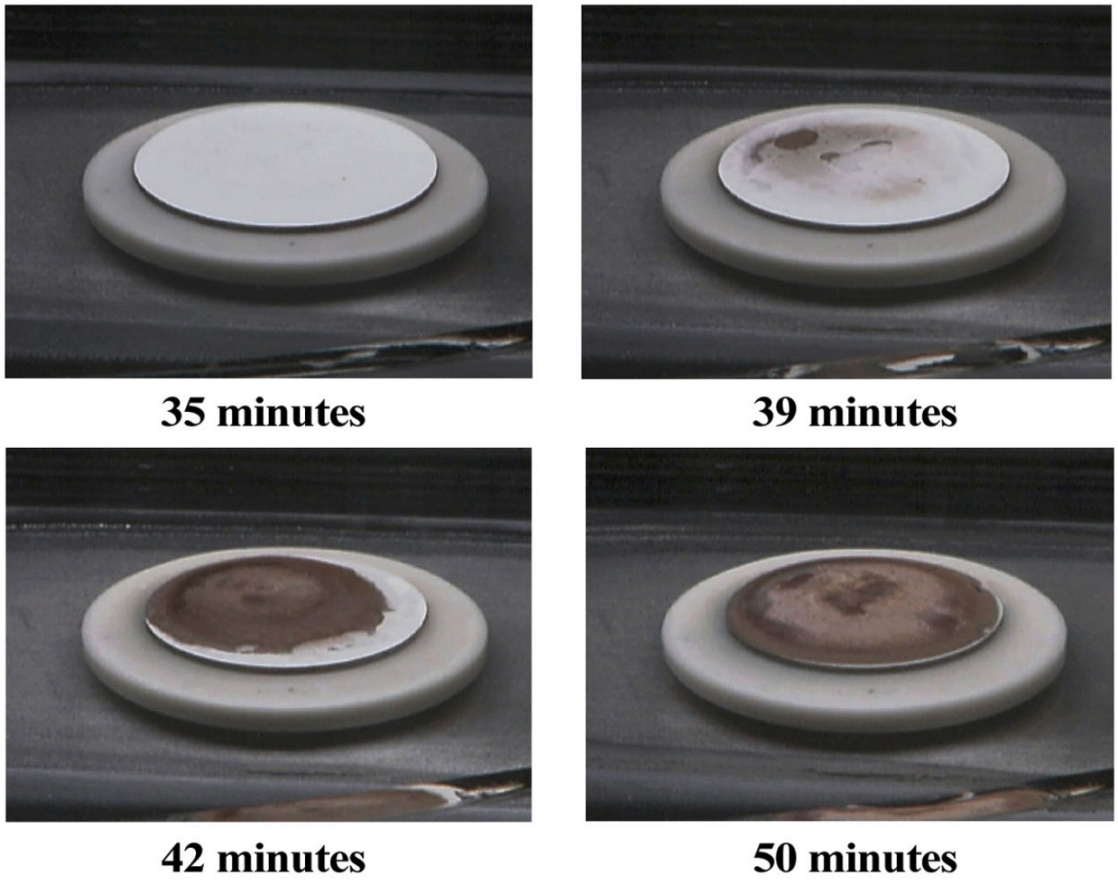

Fig. 10. Densification sequence of the YSZ/NiO sample when by the heat flux profile indicated in Fig. 9

5 W/cm^2 to 110 W/cm^2 . Note that the sample is still flat and virtually unchanged from its room temperature appearance. In the next photo, taken at 39 minutes, the sample has been at 125 W/cm^2 for three minutes and the early stages of YSZ coating densification are apparent. In the last two photos taken at 42 and 50 minutes respectively, the sample has completed densification after the last heat flux increase to 135 W/cm^2 at 39 minutes and is already cooling down.

CONCLUSIONS

A new processing method has been developed using a focused plasma-arc-lamp IR heating source to sinter solid oxide fuel cell membranes. The new IR technique is able to reduce conventional furnace processing time of 36 hours to 18 hours. The new method is able produce equivalent samples with thin dense film of YSZ electrolyte on a NiO porous anode support. Further development of the HDI processing technique for this application may lead to a better understanding of methods to optimize both the conventional furnace sintering process as well the HDI process.

BARIUM CERATE–BASED MATERIALS FOR HYDROGEN SEPARATION MEMBRANES

R. D. Carneim, P. F. Becher, C-H. Hsueh, and T. R. Armstrong
Oak Ridge National Laboratory

1. INTRODUCTION

1.1 Chemical Stability Issues in Barium Cerate–Based Proton Conductors

It is well known that many barium-containing phases decompose into $BaCO_3$ and other phases (generally oxides, hydroxides, or carbonates, depending on the other elements present in the phase and the environment) in the presence of CO_2 in a certain temperature range. Perovskite barium cerate phases are no exception. Shima and Haile studied the effect of A-site cation stoichiometry on, among other things, the stability of doped and undoped $BaCeO_3$ compositions. It was noted that samples with Ba excess reacted with atmospheric CO_2, while stoichiometric and Ba-deficient compositions did not. It was further discovered that undoped $BaCeO_3$ could not accommodate any Ba deficiency (CeO_2 would precipitate), though the doped material could; however, a large Ba deficiency resulted in a significant decrease in total conductivity.

Another technique for improving the chemical stability of this class of materials is using additional dopants. For example, $BaZrO_3$ is extremely resistant to decomposition in CO_2-containing environments. Even acceptor-doped compositions are more stable than undoped barium cerate. Since $BaZrO_3$ and $BaCeO_3$ easily form solid solutions, it is possible to replace any desired fraction of the Ce in $BaCeO_3$ with Zr. Ryu and Haile found that Zr_{Ce} substitution did indeed improve the stability of doped and undoped $BaCeO_3$; however, at the expense of conductivity.

In this study, both approaches—A-site stoichiometry and doping—are examined. High-temperature x-ray diffraction in flowing CO_2 was used to detect the presence of $BaCO_3$ in powder sample of various compositions. Initially, the effect of A-site stoichiometry ≤ 1 was examined to determine the composition to be used for the majority of this work (i.e., synthesis, processing, and characterization). The effect of additional dopants was then studied to determine their effect on chemical stability.

1.2 Synthesis

The use of combustion synthesis (CS) [i.e., glycine nitrate process (GNP)] is an attractive powder synthesis technique due to its potential for producing high-purity nanocrystalline powders with excellent compositional homogeneity and low energy-input requirements. In this process, glycine is used as a fuel that can be encouraged to react with (burn) metal nitrates. If the fuel and oxidizer are intimately mixed, such a burn is self-sustaining requiring only a small amount of heat to ignite the mass. Theoretically, the reaction products of a stoichiometric fuel–oxidizer mixture are CO_2, H_2O, and N_2 gasses, and fine

agglomerated particles of the desired oxide composition. (Non-stoichiometric burns are not considered in this work; however, such mixtures would produce CO and/or NO_x, and produce a different reaction temperature and rate relative to the stoichiometric case.) In practice, however, lab scale reactions do not proceed perfectly resulting in noxious gasses, fuel residue, and multi-phase product (individual metal oxides, carbonates, hydroxides, even nitrates). The scaled up version commercialized by Praxair uses spray drying to dehydrate a sucrose (fuel)/metal nitrate mixture which passes from the spray drier directly into a combustion chamber for conversion into a metal oxide. The resulting powders must often be calcined to remove residual organic material and to produce the desired phase. High-temperature calcination of combustion-synthesized powders negates, at least partially, some of the advantages CS is known for: The powder may become contaminated by impurities in the calcination environment, and it will almost definitely be coarsened. Another purpose for high-temperature calcination is to coarsen the powder to make it more compatible with most fabrication processes.

With the objective of producing a powder by CS that can be used as burned (i.e., formed and sintered with minimal [or no] additional powder preparation steps), the GNP was studied in detail to determine the process parameters that produce the most useful powder. It stands to reason that the character of the powder is greatly affected by the nature of the combustion reaction: the higher the reaction temperature, the cleaner the reaction and more likely a single-phase powder will be produced. A high-velocity (explosive) reaction would result in a well-dispersed smoke-like powder, most of which would be lost to the exhaust. A slow but high-temperature reaction may produce hard (partially sintered) aggregates. There are several ways to modify the reaction including changing the burn stoichiometry and changing the initial and/or ambient temperature. The method of adjusting the reaction used in this work is changing the chemistry. By using different fuels and oxidizers the reaction can be significantly altered without producing toxic gasses or requiring environmental controls. The fuels studied are glycine, urea, carbohydrazide, and oxalic dihydrazide. The oxidizer type was changed by using different salts as the metal source. Three different combinations were used: metal nitrate sources for all three cations, substituting barium nitrite ($Ba[NO_2]_2$) as the barium source—which slightly decreases the amount of reactants relative to the all-nitrate case, and substituting cerium (IV) ammonium nitrate ($[NH_4]_2Ce[NO_3]_6$) as the cerium source—which significantly increases the amount of reactants.

As a comparison, the fundamentally different synthesis method of homogeneous coprecipitation (CP) was examined. Homogeneous coprecipitation also has the potential for producing homogeneous nanocrystalline powders. With this process, however, a high-temperature calcination step is unavoidable. A commercially synthesized powder procured from Praxiar Specialty Materials was also examined.

2. SYNTHESIS

2.1 Composition Selection

Based on available literature data and the non-sensitivity of the composition, $BaCe_{0.80}Y_{0.20}O_{3-\delta}$ was chosen for this study. Yttrium-doped barium cerate has one of the highest conductivities of oxide materials, and a relatively wide usable temperature range (Fig. 1). As a reference a 1 kg lot of powder was obtained from Praxair with this composition. Since many barium-containing compounds tend to decompose into $BaCO_3$ and other oxides (in this case, $Ce_{1-x}Y_xO_{2-x/2}$) at moderately high temperatures in the presence of CO_2, the final composition chosen for this study was the slightly barium-deficient composition $Ba_{0.98}Ce_{0.80}Y_{0.20}O_{3-\delta}$ (BCY88) in order to improve its stability under these conditions (Sect. 3).

2.2 Stock Solution Preparation

In preparation for both synthesis processes, the metal sources with variable (i.e., not precisely known) water contents were dissolved in deionized water, filtered, and the resulting solutions characterized. Cerium (III) nitrate ($Ce[NO_3]_3 \bullet xH_2O$, source) and yttrium nitrate ($Y[NO_3]_3 \bullet xH_2O$, source) solutions were prepared for this reason. Barium nitrate ($Ba[NO_3]_2 \bullet H_2O$, source) was also prepared in this manner due to its low and slow solubility, and a barium nitrite solution was prepared mainly to allow filtering prior to use (barium carbonate was found on dissolving the solid). Cerium (IV) ammonium nitrate was used in powder form. The solutions were characterized by gravimetric analysis of the oxide after calcination or by complexometric titration with ethylendiaminetetraacetic acid disodium salt (EDTA•2Na). Solutions were prepared to have metal ion concentrations of approximately 1 mol·kg or greater, with the exception of $Ba[NO_3]_2$ which has a much lower solubility than the other materials. This process allows precise compositional control during the preparation of the precursor solutions for CS and CP which is required for multi-cation mixed metal oxides.

2.3 Combustion Synthesis I—Solid Intermediate

2.3.1 Solid-Intermediate Combustion Synthesis

Initially, all twelve precursor compositions were tested under “best-case-scenario” conditions as a screening process to eliminate poorly-behaved metal source–fuel combinations. The twelve compositions were the three combinations of metal sources, each of which were used with each of the four fuels (Table 1). Appropriate masses to produce 15 grams of BCY88 of each component were combined in a beaker (glass) and stirred in the manner outlined in Table Mixing. After all components were completely dissolved, the solution was heated, with continued agitation, to allow water to evaporate. Prior to the solution becoming an unwieldy sticky mass in the bottom of the beaker, the material was transferred to a

Table 1. Compositions and Characteristics of Materials Prepared Using Solid-Intermediate GNP-CS

Ba Source	Ce Source	Fuel	Drying and Product Characteristics	T_{ig}/°C	Burn Characteristics	Sintered Density/ g·cm^{-3}
Nitrate	Nitrate	glycine	hard, hygroscopic, colorless glassy	322	self-sustaining, moderate speed, fluffy product	3.99
Nitrate	Nitrate	urea			results in low-density flakes; color differences	
Nitrate	Nitrate	carbazide	hard, hygroscopic, pink glassy	322	vigorous reaction, not self-sustaining; many fine ejected particles	
Nitrate	Nitrate	oxalic dihydrazide	chalky, bright yellow	312	vigorous reaction; moderate speed; appears self-sustaining; no shape change (product contained)	4.31
Nitrate	Amm. Nitrate	glycine	brownish, gooey	302	self-sustaining, moderate speed, fluffy product	4.18
Nitrate	Amm. Nitrate	urea	yellow, pasty		results in flakes (higher density than 2); color differences; some char	1.99
Nitrate	Amm. Nitrate	carbazide		338	vigorous but slow reaction, not self-sustaining; many fine ejected particles	
Nitrate	Amm. Nitrate	oxalic dihydrazide	chalky, bright yellow	312	vigorous reaction; slower than 4; appears self-sustaining; no shape change (product contained)	4.53
Nitrite	Nitrate	glycine	light brown, glassy	332	ignition delay with larger pieces, low speed; fluffy product (though less so than 1)	2.98
Nitrite	Nitrate	urea	light brown, pasty		results in flakes (higher density than 6); color differences	
Nitrite	Nitrate	carbazide	dirty pink, glassy	270	rapid burn, not self-sustaining; color differences; nice powder	
Nitrite	Nitrate	oxalic dihydrazide	bright yellow, low-density, chalky	338	long ignition delay; not self-sustaining; nice powder and yield	3.74

flat glass plate with its surface temperature controlled at approximately 150°C on a hot plate and dried to completion. [An earlier cursory test determined that the ignition temperature of most of these compositions was higher than 300°C. The surface temperature was frequently checked (type K thermocouple surface temperature probe) to ensure 150°C was not exceeded.] During this final drying stage, the material was manually agitated with a metal spatula. The dried precursors were placed in unsealed glass sample jars that were placed in a desiccator with calcium sulfate (DriRite) desiccant.

The bulk of the samples were then reacted to produce powder for testing. Each composition was reacted by placing pieces of it under a metal crucible on a metal pan on a hot plate at above 400°C—well above the ignition temperature (T_{ig}) of the compositions that ignite. The crucible was in place to prevent the material from wandering during burning and to contain as much product as possible. The materials that did not ignite were reacted by placing them in a furnace at 500°C for 10 min in an alumina sagger. These powders were then analyzed by x-ray diffraction (XRD) for phase determination. The as-burned

powders were also pressed into pellets (≈1 g powder pressed uniaxially at 70 MPa in a 12.7 mm diameter cylindrical steel die) and sintered for 600 min at 1450°C, 1550°C, and 1650°C in air (heating at 5°C·min^{-1}, cooling at 10°C·min^{-1}). Densities were determined of the intact sintered pellets by the Archimedes method in ethanol. X-ray diffraction was also performed on the sintered pellets to determine the final phase.

2.4 Combustion Synthesis II—Conventional GNP-Type

Based on the characteristics of the initial twelve samples, four compositions were selected for further testing. Precursor solutions were prepared as above to produce approximately 50 g of powder. These compositions were then burned as in conventional GNP-CS: rather than drying the solutions, each composition is taken in 50 mL to 200 mL batches, poured into a 4 L stainless steel beaker and heated on a hot plate at its maximum setting until the solution dried sufficiently and ignited. A 100 mesh stainless steel sieve covered the beaker to contain the product. The resulting powders were collected and sieved (using a second 100 mesh stainless steel sieve). Powders produced in this manner required some sort of heat treatment to remove residual organic material from incomplete combustion. These powders were divided into thirds and each portion calcined at a different temperature. The powder was placed in an alumina sagger and placed in a hot furnace for 20 min. The calcination temperatures were 600°C, to burn off the residual organics without affecting the phase composition of the powder, 1000°C, to partially react the powder to produce a specific mixture of phases, and 1200°C, to completely transform the powder to single-phase BCY88. Phase identification was performed on the calcined powders with XRD, and pellets were pressed, sintered, and analyzed as above (except pressing pressure was 105 MPa).

2.5 Homogenous Coprecipitation

Powders were produced by drop-wise adding the appropriate metal nitrate solution to the heated and agitated ammonium oxalate ($[NH_4]_2C_2O_4$) solution, then washing, drying, and calcining the precipitate. The metal nitrate solution was prepared by mixing the appropriate amounts of the Ba-, Ce-, and Y-nitrate stock solutions and diluting the result with deionized water to the desired concentration. For example, to produce 500 mL of solution with a metal ion concentration of 0.1 mol·L^{-1}, the appropriate amounts of the stock solutions were used to produce 25 mmol BCY88 and this mixture diluted to a total volume of 500 mL. Ammonium oxalate solutions were prepared by dissolving the $(NH_4)_2C_2O_4$•H_2O powder in the appropriate amount of deionized water with heat and agitation. For example, the $(NH_4)_2C_2O_4$ solution used with the above metal nitrate solution was a 0.1 mol·L^{-1} solution with an total oxalate ion to metal ion ratio of 3; 0.15 mol of $(NH_4)_2C_2O_4$•H_2O was dissolved in heated deionized water to make 1.5 L of

solution. Metal nitrate solutions, at room temperature, were added drop-wise—but rapidly—to $(NH_4)_2C_2O_4$ solutions at 70°C.

After the metal nitrate solution was consumed, the heat was turned off and the mixture allowed to cool to room temperature overnight with continued stirring. Stirring was then discontinued and the precipitate allowed to settle. After 20 min to 60 min, the liquid was poured off and deionized water added to wash the precipitate. The new mixture was stirred for a few minutes and then allowed to settle again. This washing procedure was repeated four or more times. After the final wash cycle, the precipitate was transferred into a glass pan (Pyrex™) and completely dried in a drying oven at 50°C to 100°C. After producing the first such composition, high-temperature XRD (HTXRD) was performed on the precipitate to determine the necessary calcination temperature. Diffraction patterns were obtained from room temperature to 1300°C at 100°C intervals. Based on the HTXRD results, calcination of the precipitates was performed by placing the precipitate, in an alumina sagger, into a furnace at 1100°C for 30 min.

3. POWDER CHARACTERIZATION AND SINTERING

Initially, powders were pressed into pellets and sintered with a minimum of intermediate processing to determined the synthesis parameters that would produce a powder with the simplest processing requirements. Powders resulting from solid-intermediate combustion synthesis were processed as-burned, powders from conventional GNP-CS were calcined at three different temperatures as described above, and powders from coprecipitation were used after the 1100°C calcination step.

Based on the initial experiments using solid-intermediate combustion synthesis, four compositions clearly produced superior sintered pellets; those using either all standard nitrate metal sources or $(NH_4)_2Ce(NO_3)_6$ with $Ba(NO_3)_2$ and $Y(NO_3)_3$, and either glycine or ODH as the fuel (Fig. 2). Table 1 also lists reaction characteristics as observed and sintered pellet densities (1550°C for 10 h). Powders were then produced using these parameters with the conventional GNP-CS process. Though this process was expected to not produce as high quality a powder as the solid-intermediate version, it has the advantage—at the laboratory scale—of demanding significantly less painstaking preparation and having fewer safety concerns. The best results (sintered samples) were obtained using standard nitrate metal sources and ODH or glycine fuel (Fig. 3). The choice of fuel had a significant effect on the behavior of the process and character of the powder. The ODH-fueled powder was more compact and easier to handle than the glycine-fueled powder, and resulted in a better sintered pellet. Using glycine as the fuel resulted in a very loose, low-density powder; however, due to the greater solubility of glycine, preparation for, and execution of the combustion process was more straightforward. Powders produced by coprecipitation also produced acceptable sintered pellets. Though this powder was also fairly dense (similar to the ODH-fueled combustion synthesized powder), it had a paste-like consistency which resulted in poor flowability.

Figure 2 also shows the results of sintering powders synthesized using $Ba(NO_2)_2$ and/or urea and carbazide. Those samples prepared with urea did not densify, though most of these pellets remained intact. This is in contrast to the pellets prepared with the carbazide-fueled powders, which densified somewhat but developed different phases in the interior and exterior regions of the pellets and eventually disintegrated with time at ambient conditions.

Those samples prepared with $Ba(NO_2)_2$ as the barium source followed this pattern; it was eliminated due to inferior densification of even the glycine- and ODH-fueled compositions. Further study may be warranted to determine the fundamental causes of the poor behavior of powders prepared with these fuels and barium source.

Some particle size and size distribution measurements have been done to determine the fundamental powder characteristics responsible for the some of the differences in behavior. Further data in this area is currently being collected, as well as specific surface area measurements. From the currently available data (Figs. 4 and 5) it is possible to make a few qualitative conclusions. First of all, there is no significant difference (i.e., order of magnitude) in the median particle sizes of the various powders examined (the four conventional GNP-CS–produced powders and the CP-produced powder). From the micrographs, it is clear that the glycine-fueled powder is composed of particles which have a porous, web-like morphology; the ODH-fueled powder has particles composed of a relatively dense arrangement of nanometer-scale primary particles; and the coprecipitated powder is composed of large, brick-shaped agglomerates (a relic of the oxalate crystallization process) with an intermediate density.

3.1 Stability in CO_2

3.1.1 BCY88 Compositions

A series of $Ba_xCe_{0.80}Y_{0.20}O_{3-\delta}$ powders was synthesized with x = 0.90, 0.95, 0.98, and 1.00 (BCY08, BCY58, BCY88, and BCY108, respectively) to study the effect of A-site deficiency on the stability of this composition in CO_2. These powders were produced by the traditional GNP-CS method using yttrium nitrate, cerium ammonium nitrate, and barium acetate as the cation sources and glycine as the fuel. Each of the powders was characterized using high-temperature XRD (HTXRD, instrument) in 101.3 kPa (1 atm) flowing CO_2 as follows. A sample of the powder was placed on the platinum-rhodium heater strip of the instrument and the sample chamber sealed. The temperature was raised to 1200°C in air or flowing helium and held for 20 min. An XRD scan under these conditions confirmed the sample was single-phase perovskite. At this point the gas in the sample chamber was switched to flowing CO_2. The following steps were then repeated until no perovskite phase remained: hold for 5 min, perform XRD scan, lower temperature by 50°C (Fig. 6).

Results of this study are shown in Fig. 7. Note that the temperature was controlled at even 50°C increments by a thermocouple welded to the opposite side of the heater strip, but a more accurate measure of the sample temperature for each scan was determined by optical pyrometry. In the stoichiometric case (BCY108), $BaCO_3$ peaks are apparent in the scan at ≈1120°C. The barium-deficient compositions, however, do not form $BaCO_3$ until ≤1060°C. This measurable difference, though modest, indicated that a barium-deficiency could be accommodated and improved the stability of the phase. Since no significant difference was noted between the three barium deficient compositions, the highest barium-content composition, BCY88, was chosen as the focus of this study. The reduction in A-site occupancy is sufficient to reduce the possibility of decomposition and small enough that it should not significantly affect electrical properties.

3.1.2 Effect of Zr, Mg, and V Additions

The substitution or addition of these cations into the basic $BaCeO_3$ composition was examined in an effort to improve stability and/or ease processing requirements. Ryu and Haile studied the effect of partially substituting Zr for Ce in undoped and Gd- and Nd-doped $BaCeO_3$. It was found that a large amount of Zr substitution in doped samples (0.20 to 0.40 of the B-site depending on the acceptor dopant species) resulted in the composition being nearly completely immune to $BaCO_3$ formation. Unfortunately, conductivity decreased by as much as an order of magnitude with Zr addition relative to the doped, Zr-free compositions. The current study attempted to combine the stability-enhancing effects of partial Zr_{Ce} substitution and using a Ba-deficient composition to improve the stability in CO_2-containing environments with a lower Zr content than the previous study; thereby avoiding the dramatic conductivity reduction. Both undoped and Y-doped compositions were investigated.

Samples were prepared by the conventional GNP-CS process and characterized by HTXRD in flowing CO_2 as described above. Higher initial temperatures for the analysis were required as $BaCO_3$ formed in some of these compositions at temperatures ≥1200°C. Figure 8 shows the results for the Zr-containing samples: $Ba_{0.98}Ce_{0.85}Zr_{0.15}O_{3-\delta}$ and $Ba_{0.98}Ce_{0.95}Zr_{0.05}O_{3-\delta}$ (BCZ885 and BCZ895, respectively). Of the undoped samples, the two lower Zr-content compositions contained $BaCO_3$ at temperatures as high as ≈1300°C. The final sample (BCZ885), however, was considerably more stable, remaining single-phase perovskite throughout the entire temperature range tested (down to ≈750°C). The standard Y doping was added to the stable BCZ885 composition resulting in the following behavior: This composition is single-phase perovskite at ≥900°C. This is a significant improvement over the corresponding Zr-free composition (BCY88); however it is not as good as the compositions reported by Ryu and Haile, and the effect of this amount of Zr in this composition on conductivity has not been determined. All Mg-doped

compositions ($Ba_{0.98}Ce_{0.85}Mg_{0.15}O_{3-\delta}$ and $Ba_{0.98}Ce_{0.95}Mg_{0.05}O_{3-\delta}$ [BCM885 and BCM895]) and the Mg- and V-doped composition ($Ba_{0.98}Ce_{0.82}Mg_{0.15}V_{0.03}O_{3-\delta}$ [BCMV8/15/3]) contained $BaCO_3$ at temperatures up to ≈1350°C.

4. CONCLUSIONS

4.1 Synthesis

The synthesis study is nearly complete, though more powder will be synthesized as needed for further characterization. It was determined that several synthesis routes are available depending on the processing or product requirements. Conventional GNP-CS using glycine as the fuel is the most straightforward and forgiving synthesis method; however, the resulting powder has an extremely low density and is therefore more difficult to store and process than other options. With slightly more effort, this process utilizing ODH as the fuel is attractive: the resulting powder is easier to work with, though precursor preparation requires more time and energy (the precursor solution must be heated). The best quality powder appears to have been produced using the solid-intermediate precursor combustion synthesis method with ODH as the fuel. The advantages of this method are better homogeneity and more complete combustion. However, precursor preparation and processing requires care and much time. These problems might be alleviated by integrating the drying and combustion stages into a one-step, two-zone spray pyrolysis process which should, conceivably produce better results even than those obtained with the laboratory-scale process used in this work.

4.2 Properties

Significant work will still be done in the area of powder characterization and sintered part properties. As mentioned above, detailed powder characterization is currently in progress. Finally, several sintered test specimens will be prepared for determination of conductivity and hydrogen permeation, and further stability and sintering studies described below.

4.3 Chemical Stability

Significant work has been done in determining the stability of this class of materials in powder form at high temperatures in a pure CO_2 environment. It was known that the presence of barium in compounds often results in decomposition into a $BaCO_3$ and other phases. It was found that a slight barium deficiency in the composition inhibited this process and this was exploited. Further results showed that significant substitution of Zr for Ce resulted in a sizable improvement in stability. This effect may warrant future study.

The characterization done thus far has been under "worst-case-scenario" conditions: a high surface area powder was subjected to pure, flowing CO_2. In actual application, the material is a dense body subjected to conditions with a lower partial pressure of CO_2. Further stability studies of this material will be done under more representative conditions including behavior in an H_2O environment.

4.4 Constrained Sintering

The final major section of this study involves the constrained sintering of this material. Specifically, producing a thin, dense membrane of BCY88 on a thick, porous support of the same material. A model and analytical procedure by Hsueh is available for modeling the stress distribution in this type of geometry that takes into account the sintering of both the film and the substrate. Experimental techniques for determining the elastic and viscous properties of the materials being modeled during sintering are, to a great extent, established. The uniaxial viscosity of the sintering body can be determined with a minimum of experimental runs utilizing a cyclic loading technique during isotheral sintering in a dilatometer. This is based on a method suggested by Cai et al. during constant heating rate sintering and has been successfully applied to the isothermal case. The most promising method for determining the elastic tensor as a function of density during sintering is resonant ultrasound spectroscopy (RUS). With this technique, a disk-shaped sample is supported by three ultrasonic transducers and inserted into the hot zone of a furnace. Resonance spectra can be obtained at various times during the sintering cycle, which can be used to determine the relevant elastic constants (isotropic symmetry is assumed for polycrystalline ceramics). This technique has produced useful information for test samples at room temperature. However, this technique is sensitive to various parameters, particularly the precise sample size and shape. Irregularities that are initially present or emerge during sintering can cause resonant peak shifts, extinction, and/or splitting which complicate the analysis.

5. BIBLIOGRAPHY

P. Z. Cai, D. J. Green, and G. L. Messing, *J. Am. Ceram. Soc.*, **80,** 1940 (1997).

P. Z. Cai, G. L. Messing, and D. J. Green, *J. Am. Ceram. Soc.*, **80,** 445 (1997).

F. Chen, P. Wang, et al., *J. Mater. Chem.*, **7,** 1533 (1997).

C. H. Hsueh, *Scrip. Metall.*, **19,** 1213 (1985).

K. Katahira, Y. Kohchi, T. Shimura, and H. Iwahara, *Solid State Ionics*, **138,** 91 (2000).

T. Norby, *Solid State Ionics*, **125,** 1 (1999).

K. J. Ryu and S. M. Haile, *Solid State Ionics*, **125,** 355 (1999).

D. Shima and S. M. Haile, *Solid State Ionics*, **97,** 443 (1997).

K. Takeuchi, C.-K. Loong, et al., *Solid State Ionics*, **138,** 63 (2000).

APPLICATION OF BARRIER MEMBRANE TECHNOLOGY TO CATALYTIC CRACKER RECYCLE GAS HYDROGEN SEPARATIONS

L. D. Trowbridge
Oak Ridge National Laboratory

INTRODUCTION

In FY2000, ORNL's Chemical Technology Division constructed a test bed for lab-scale evaluation of inorganic membranes designed to separate hydrogen from hydrogen/hydrocarbon gas streams. In FY2001, a 6-month extension of this activity was funded under the Ultra-Clean Fuels program. The inorganic membranes to be tested are those developed under a different portion of the Fossil Energy Program by the Inorganic Membrane Technology Laboratory (IMTL) located at East Tennessee Technology Park (ETTP) in Oak Ridge, TN. ORNL's experimental role is to test IMTL's membranes using flammable gas mixtures, first using surrogate binary gas mixtures (e.g., $H_2 + CH_4$ or $H_2 + C_2H_6$) but later using gas mixtures generated by a lab-scale catalytic cracker to be obtained from Phillips Petroleum.

The gas membranes to be tested take the form of tubes. The test bed is intended to hold one short section of such a tube. Full scale application will involve many longer, parallel tubes. The goal of this work is to determine the capability of specialized inorganic membranes for separating hydrogen from hydrocarbon streams. Realistic gas separation measurements will yield separations that incorporate a number of inherent inefficiencies that can be fairly well characterized and predicted from gas transport measurements. To be able to predict performance under conditions other than the specific ones examined experimentally, it is necessary to make the appropriate measurements allowing one to factor out these known, predictable inefficiencies so as to reveal the inherent ideal separation efficiency of the membrane.

Gas separation efficiency is generally interpreted by the equation:

$$(\alpha - 1) = E_p\, E_m\, E_c\, E_b\, (\alpha^* - 1)$$

In this equation, α is the actual separation factor, a function of the concentrations of the components in the two product streams:

$$\alpha = [\, Y / (1 - Y)\,] / [\, X / (1 - X)\,]$$

where Y is the mole fraction of the desired component flowing out the enriched stream and X is the mole fraction of that component flowing out the depleted stream. E_p is the back pressure correction factor (the ratio of the pressure drop across the membrane to the high-side pressure). E_m is the mixing efficiency, a function of the flow and composition-dependent gas transport parameters, such as the diffusivity and viscosity of the gases. E_c is the cut correction factor, a function of the fraction of the gas which transits the membrane. These factors can be calculated from measurable experimental parameters following the formulations presented in Ebel (1972) and Hogland (1979).

Two variables in the above equation which have not been mentioned are E_b, the membrane (i.e., barrier) efficiency, and α^*, the ideal separation factor. Separation relying purely on the relative velocity of gas molecules, so-called Knudsen flow (from whence the term “Knudsen membrane” derives), has an α^* equal to the ratio of the average molecular velocities. A design variation on this is the “molecular sieve” membrane, which hash pores sufficiently small that it relies on both the molecular velocities plus the effect of different molecular sizes to improve separation of light, small molecules over larger, heavy ones. If the pore size distribution is known, the ideal separation factor for this type membrane can also be estimated. For these two membrane designs, α^* can be readily calculated, leaving E_b as the ultimate parameter to be determined from the experiment. A third design strategy, the “surface flow” membrane, involves transport via surface condensation, surface diffusion, and re-evaporation of the more condensable component. Its ideal separation factor is not as well defined, and the experimental parameters to be determined are the combined factor “E_b (α^* - 1)”.

The IMTL-designed and manufactured membranes, though by no means identical to those used in the gaseous diffusion uranium enrichment plants, are descended from those types of membranes. As such, these membranes are at present considered classified materials, so lab security is a consideration. Security modifications to the laboratory were completed and the security plan for the work prepared and approved. The experiments discussed in this report were conducted under these security arrangements. It should be said that though each particular inorganic membrane design and application is initially considered as being potentially classified, when there is sufficient interest for commercialization, a review can be undertaken to determine if the application can be considered unclassified. This has been successfully done for a number of applications. The process is, however, sufficiently time-consuming that it is not appropriate to do it during the R&D stage of application development.

EXPERIMENTAL APPARATUS

The experimental system, largely constructed in FY 2000, was completed, tested, and utilized for separation measurements on an IMTL Knudsen membrane in FY 2001. A simplified schematic of the experimental system is shown in Fig. 1.

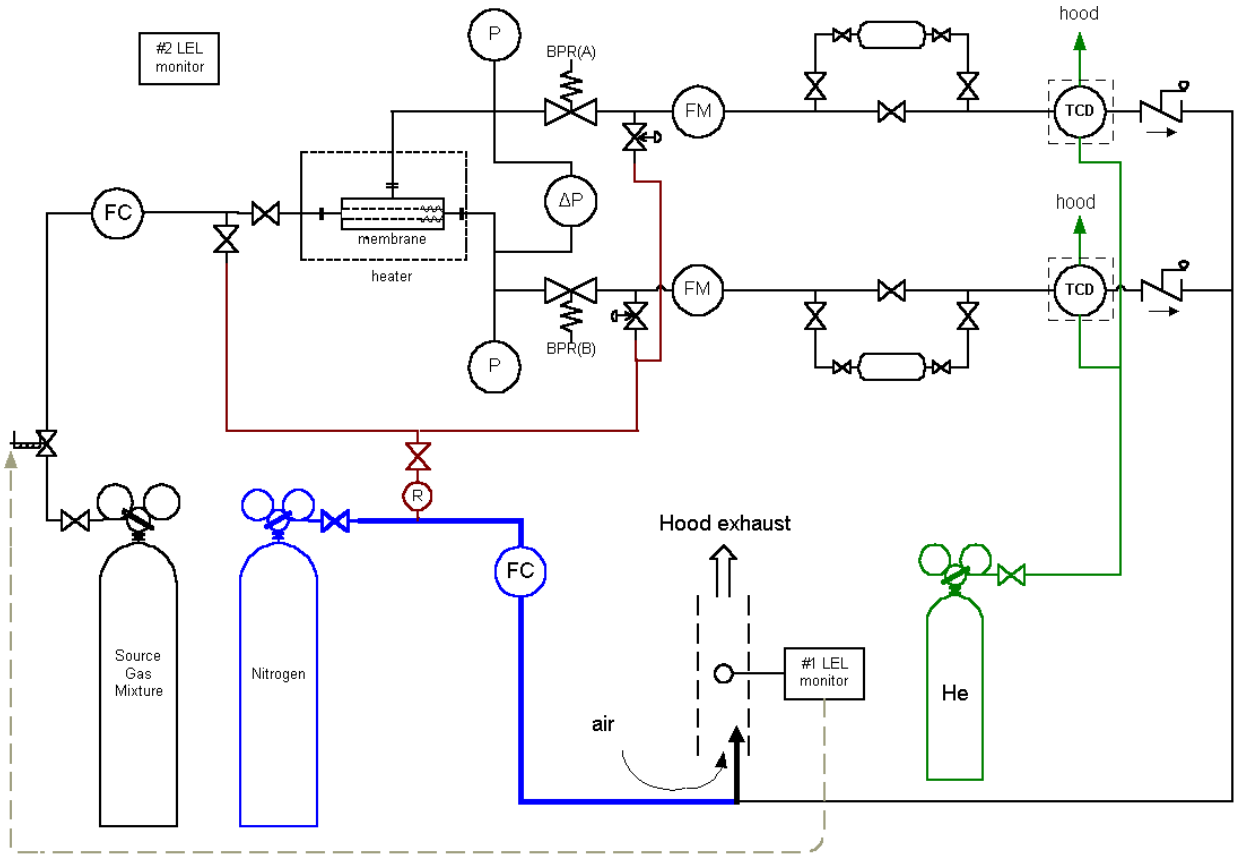

Fig. 1. Schematic of membrane test apparatus showing major operational elements only.

The system at present utilizes pre-mixed binary gas mixtures for the gas inlet supply. The gases are separated in a single pass through the membrane. Figure 2 shows a photograph of a membrane holder mounted in its temperature-controlled oven. Pressure is monitored in each stream (P) as is the pressure difference between the two separated stream (ΔP). Pressure is controlled in each stream by back-pressure regulators (BPR). The total flow in the system is controlled upstream of the membrane by a flow controller (FC) and measured downstream in each stream by flow meters (FM). Each stream (or a side-stream thereof) passes through a thermal conductivity detector (TCD) to determine composition. Downstream of the TCDs, the two streams are mixed and then diluted below the lower flammability limit

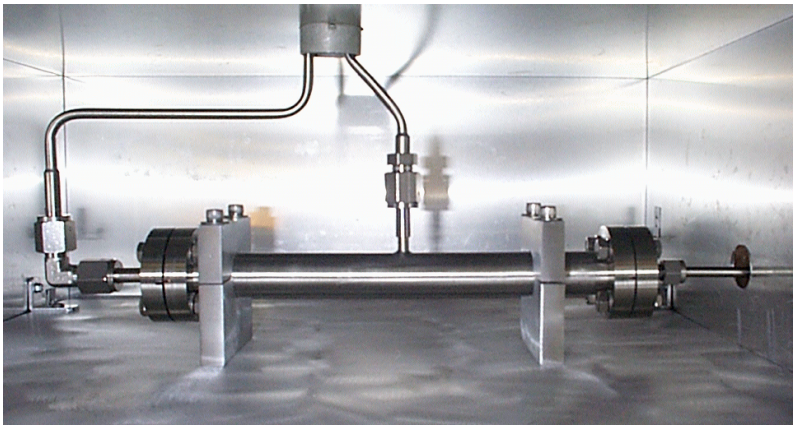

Fig. 2. Membrane holder mounted in oven.

with a controlled flow of nitrogen. The mix is then exhausted to the laboratory hood. Flows, pressures, temperatures and concentrations are measured and recorded by an on-line data acquisition system. As a more definitive back-up to the composition measurements made by the TCDs, samples can also be taken for analysis by gas chromatography.

The primary control on the flammability of the gases is the dilution of the exhaust stream to below its flammability limit. Control on the degree of dilution is set by the flow controllers (FC) on the source gas stream and the nitrogen stream. To verify that the gas is indeed below the flammability limit, an LEL (lower explosion limit) device monitors the exhaust stream continuously. A second LEL device monitors the general atmosphere in the vicinity of the apparatus. Safety approvals for operating this system have been obtained.

For the experiments reported here, a single inorganic membrane tube of proprietary composition was used. This was a Knudsen membrane provided by IMTL (designation 1226678-1-1).

A typical experiment consists of the following steps:

a. The temperature of the oven in which the membrane holder resides is set to and allowed to stabilize at the desired temperature.
b. The TCDs are allowed to warm up, then are calibrated using the gas mixture to be separated and also the pure components.
c. A flow of diluent N_2 is established which will keep the system effluent below the LEL for the mixture at the maximum mixture flow contemplated.
d. An open path is set up from the inlet through the membrane and through the two TCDs.

e. Target conditions are selected (inlet mixture flow, low-side P, high-side P); the appropriate control elements (inlet flow-controller and the two back-pressure regulators) are set to achieve these conditions.
f. TCD outputs are tracked on the data acquisition system computer. When the concentrations in both the high- and low-pressure sides of the membrane have stabilized, the outcome of the experiment is recorded.

At this point, new target conditions can be selected and the process iterates through (e) and (f). Data for all measured parameters (temperatures, pressures, flows, LEL indication in exhaust, TCD output) is continuously recorded by the data acquisition computer; this data is post-processed to calculate separation factors and separation efficiency.

PROGRESS

The Knudsen membrane previously mentioned was installed in the system in July 2001. Initial shakedown experiments were conducted on two non-flammable gas mixtures (He/Ar and He/CO_2). Following that, experiments were run on three flammable mixtures (H_2/CH_4 , H_2/C_2H_6, and H_2/C_3H_8). In all cases the gases consisted of 75% by volume of the light component (He or H_2) and 25% of the heavy component. Experiments spanned the low-pressure range accessible to the apparatus (low side pressure from atmospheric pressure to 100 psia). The hardware (pressure sensors and back pressure regulator range) allow a low-to-high-side pressure difference of up to 100 psid, but the permeability of this particular membrane was sufficiently high that the low-side flowmeter would be over-ranged under such conditions, so practical pressure differences were less than this.

For each gas, experiments were run at three or four temperatures between room temperature and just under 200°C. A given series of experiments would yield 1 to 3 dozen separation points at average pressures (defined as the average of the high- and low-side membrane pressure) ranging from just over 1 atmosphere absolute to about 8 atmospheres absolute. The cut (the fraction of gas transiting the membrane) ranged from a low to high fraction. Total flows ranged from ~ 200 std cc/min to 1700 std cc/min. Separation factors were calculated from the concentrations observed by the two TCDs. These were then corrected for the known effects previously alluded to (cut, back pressure and mixing) and a membrane efficiency was calculated. The general trend in membrane separation efficiencies is depicted in Fig. 3, which summarizes the H_2/C_2H_6 experiments. At lower average pressure, the efficiency is

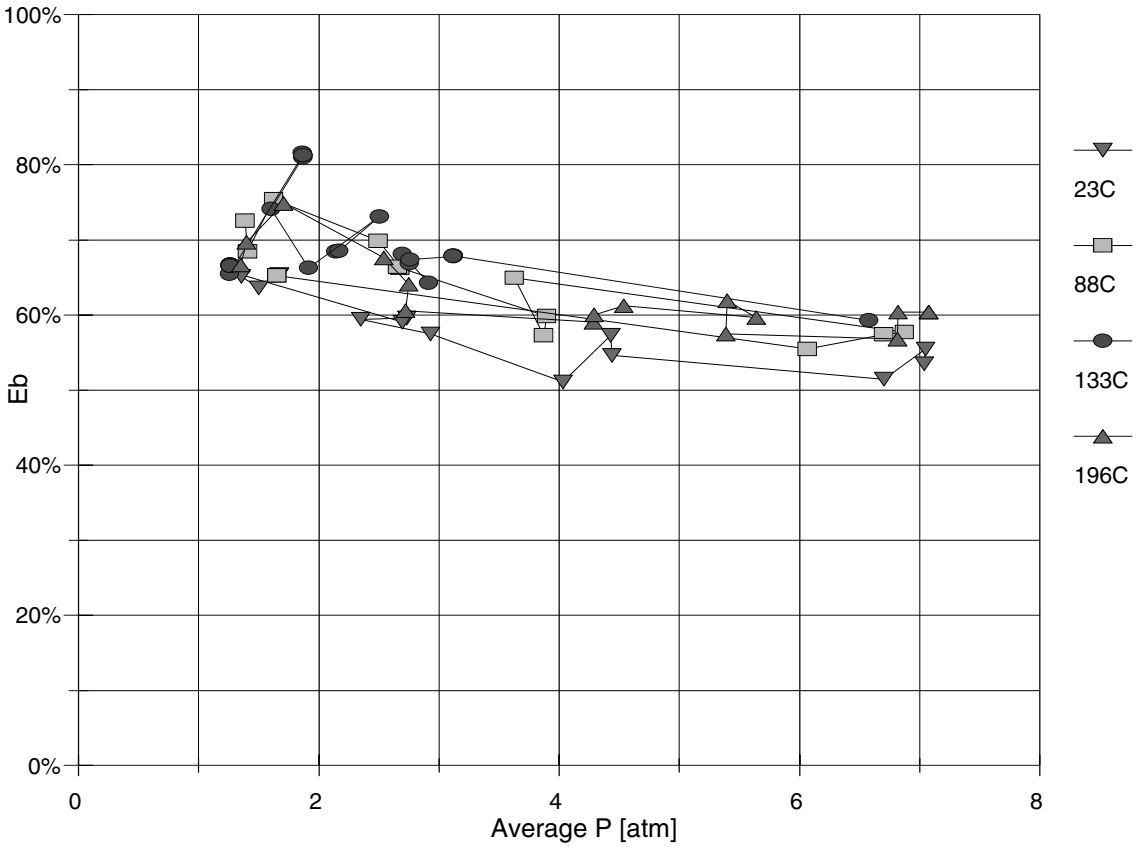

Fig. 3. 75% H_2 + 25% C_2H_6 separation at 23 to 196°C for an IMTL Knudsen membrane.

The separation results are expressed as separation efficiency, E_b. The observed separation factor is corrected for back pressure, cut, and mixing efficiency, then ratioed to the expected ideal (Kundsen) separation factor, per:

$$(\alpha - 1) = (\alpha^* - 1)\, E_p\, E_c\, E_m\, E_b$$

higher that at higher average pressure, where one would expect a greater fraction of the flow to be in the non-separative viscous flow regime. There is a suggestion that higher temperature may lead to better separation efficiency, but experimental scatter do not make this conclusion a firm one for this system.

Table 1 summarizes the separation efficiencies for the systems and temperatures examined at low (average P ~ 1.5atm absolute) and high (average P ~ 7 atm absolute) pressures. In the H_2/C_3H_8 system and the He/CO_2 system, lower separation at room temperature as compared to elevated temperature is

Table 1: Experimental average separation membrane efficiency E_b, expressed in percent; statistically are reproducible to about +/- 5%. <P> is the average of the membrane high- and low-side pressures

	<P> = T / C	Low P ~1.5 atm	High P ~7 atm
He/Ar	**23**	85	70
	93	85	70
	130	—	—
	196	85	70
He/CO_2	**24**	80	57
	93	85	67
	130	—	—
	196	83	70
H_2/CH_4	**23**	78	63
	93	85	70
	130	85	70
	183	85	70
H_2/C_2H_6	**24**	75	55
	88	75	57
	133	75	60
	196	75	55
H_2/C_3H_8	**24**	52	40
	90	60	50
	133	63	52
	190	65	52

more evident. These two mixtures have the most condensable heavy components of the mixtures examined. Likely the onset of significant surface flow is responsible for this behavior.

CONCLUSIONS

Work on the Knudsen membrane has been carried out largely to develop experimental methods and to demonstrate that this apparatus and approach is capable of determining separation efficiency with reasonable accuracy in the range of physical conditions of interest. For the relatively low separation factors that a Knudsen membrane affords, this has been accomplished and thus there should be no difficulty studying membranes with higher separation factors. Smaller pore-size membranes, some

designed to enhance surface flow of heavier components and others to take advantage of molecular sieving, are being developed by IMTL and should be available for testing in the near future.

REFERENCES

R. A. Ebel and L. P. Pasquier, “Design of a Gaseous Diffusion Stage,” NUCLEAR ENGINEERING - PART XXIII, AIChE Symposium Series, 123(68) p 107, (1972)

R. L. Hoglund, J. Schacter, and E. von Halle, “Diffusion Separation Methods,” ENCYCLOPEDIA OF CHEMICAL TECHNOLOGY, vol 7, 3rd Edition, J. C. Wiley and Sons, (1979).

CHARACTERIZATION OF FIELD-EXPOSED IRON ALUMINIDE HOT GAS FILTERS

C. G. McKamey, P. F. Tortorelli, E. Lara-Curzio, and R. R. Judkins
Oak Ridge National Laboratory

D. McCleary
Global Energy Inc.

J. Sawyer
Pall Process Equipment Development

INTRODUCTION

The use of a power turbine fired with gas produced from coal will require some form of gas cleaning in order to protect turbine and downstream components from degradation by erosion, corrosion, or deposition. Hot-gas filtration is one form of cleaning that offers the ability to remove particles from the gases produced by gasification processes without having to substantially cool and, possibly, reheat them before their introduction into the turbine. This technology depends critically on materials durability and reliability, which have been the subject of study for a number of years [see, for example, Refs. 1–4].

Materials used in hot-gas filters are required to withstand prolonged exposure to corrosive, high-temperature gaseous environments, as well as to condensable vapors and solid species, some of which may have the potential for localized interaction with the filter material after extended times. The gas streams may be purely oxidizing (such as those produced by pressurized fluidized bed combustors, PFBCs) or relatively reducing, in which the sulfur species are principally in the form of H_2S, as in the case of the product gas from integrated gasification combined cycle (IGCC) processes or from carbonizers. Degradation of metallic filter elements has been observed under oxidizing, sulfidizing, and/or carburizing conditions and acts as a driving force for the development of ceramic hot-gas filters, particularly for the higher temperatures associated with advanced gasification and combustion designs. However, iron aluminides can also be considered for such applications because they offer reliability advantages over ceramic filters and typically have good to exceptional high-temperature corrosion resistance in a variety of sulfur-bearing environments relevant to coal-derived energy production systems [5–10].

Metallurgical and mechanical evaluations of dense and porous Fe_3Al-based alloys exposed in test beds that simulate environments associated with IGCCs and PFBCs have been conducted [4,11]. Experiments with as-fabricated porous iron-aluminide filter materials showed good high-temperature corrosion resistance in air, air + SO_2, and H_2S-containing environments. Preoxidation improved the

corrosion resistance. The hoop strength of the filters was not significantly affected by the preoxidation treatment or by 100-h exposures in air or air+SO_2 at 800 and 900°C. The purpose of the current study was to extend such evaluations to iron-aluminide filters that have been exposed in an actual gasification plant.

EXPERIMENTAL PROCEDURES

Sintered metal filter elements of iron aluminide have been used for hot-gas cleaning at Global Energy Inc.'s Wabash River (Indiana) gasification plant. These cylindrical (~60 mm outer diameter) elements were fabricated by Pall Corporation (Cortland, NY) from water-atomized alloy powder produced by Ametek, Inc. (Eighty-Four, PA). The composition of the powder was nominally Fe-28 at. % Al-2% Cr-0.1% Zr (FAS-Zr). Several pieces of FAS-Zr elements were supplied by Global Energy, Inc. to Oak Ridge National Laboratory after use in the Wabash River Plant's clean-up system. In other cases, o-ring specimens (nominal inner diameter of 56 mm, wall thickness of 2 mm, and width of approximately 12.7 mm) were cut from as-fabricated Pall elements, inserted into the filter system at Wabash River for various lengths of operating time, and then returned to ORNL for evaluation. (The general exposure conditions are listed in Table 1.) The elements from which the specimens were cut were usually fabricated of FAS-Zr, but in a few cases, o-rings of an FAL alloy composition (Fe-28 at.% Al-5% Cr-0.1% Zr) were exposed. During these exposures, the filter materials were exposed to gas produced by combustion of either coal or petcoke at temperatures estimated to be in the range of 450–500°C (see Table 1). Note that, in the case of the o-rings, specimens were either placed directly in the filter vessel (dirty-gas side) or in the plenum that routes the filtered gas from the element bundles (clean-gas side).

Evaluation of filter materials included mechanical testing of o-rings by internal pressurization to determine tangential (hoop) stress-strain behavior. The o-rings tested in this manner were from the specimens exposed as such (see above) or were cut from the pieces of actual filter elements received from the Wabash River plant. The internal pressurization tests were conducted in ambient air either by subjecting an elastomeric insert (for as-fabricated filter samples) to axial compression at a constant displacement rate of 2 mm/min or by use of a positive radial-displacement wedge mechanism (for the field-exposed filter samples). After mechanical testing, the fracture surfaces were examined using

Table 1. Fe-Al filter material exposed at the Wabash River Plant

Filter Design	Pre-oxidation Temp.(°C)	Exposure time (h)	Exposure details[d]	Results of microstructural analyses	Fracture Strength (kN)
IA-187 IA-188 IA-191 IA-141	As fabricated As fabricated 800 1000	None None None None		40–50% porous; oxide particles on pore surfaces; oxide coating on surfaces of 0.5-3 µm thickness; ligaments averaged 6-10µm	2.0
DC-20[a]	800	574	Vessel	Light surface deposits, some regions of non-uniform porosity	2.0
DC-36[a]	800	1565	Vessel	Non-uniform porosity, pores may be blocked	1.6
DC-88[a]	800	2185	Vessel, 250 h petcoke	Fe-S outer layers, blocking gas flow	1.4
IA-188[b]	As fabricated	1628	Clean	Filter blocked by Fe-S throughout inner 2/3 of filter	
IA-187[b]	As fabricated	2237	Clean, 100 h petcoke	Filter blocked throughout, thicker deposit on inner surface	1.1
IA-187[b]	As fabricated	3865	Clean, 100 h petcoke	Completely full of Fe-S, thick layers on both sides, filter blocked	
DC-207	800	1988	Clean, all petcoke	No surface deposits, large Fe-S layers blocking gas flow, medium interior corrosion	2.2
IA-191[b]	800	2237	Clean, 100 h petcoke	No deposit, some Fe-S, filter OK	2.2
DC-205[b]	800	4335	Clean, last ~3000–3500 h petcoke	OK, no deposit, some Fe-S throughout	2.2
IA-141[b]	1000	2237	Clean, 100 h petcoke	Lots of Fe-S throughout, scattered open pores, may still be filtering	
IA-141[b]	1000	3865	Clean, 100 h petcoke	Completely full of Fe-S, thick layers on both sides	
DC-208[b]	800 (blue)	1988	Clean, all petcoke	Light deposit, light corrosion, pores open	2.3
DC-211[b]	800 (blue)	1988	Dirty, all petcoke	Heavy deposit, light corrosion, pores open	2.2
DC-209[b]	800 (gray)	1988	Clean, all petcoke	Medium deposit, heavy corrosion, pores blocked	0.9
DC-210[b]	800 (gray)	1988	Dirty, all petcoke	Heavy deposit, significant corrosion, filter may be blocked	1.5
DC-192[b]	800 (FAL)[c]	2347	Clean, 1000–1500 h petcoke	Light-to-medium surface deposits, light corrosion, pores open	1.5
DC-193[b]	800 (FAL)[c]	6212	Clean, 1000–1500 h petcoke	Light-to-medium surface deposits, light corrosion, pores open	2.2
DC-195[b]	800 (FAL)[c]	2347	Dirty, 1000–1500 h petcoke	Medium-to-heavy surface deposits, light corrosion, pores open	1.4
DC-206[b]	800 (FAL)[c]	4335	Dirty, last ~3000–3500 h petcoke	Heavy deposit, light corrosion, pores open	2.0

[a]Specimen from filter element.
[b]Specimen was o-ring cut from filter element.
[c]FAL composition = Fe-28at.%Al-5at.%Cr.
[d]Clean = clean-gas side; dirty = dirty-gas side.

scanning electron microscopy (SEM) and pieces were cut from the o-rings for microstructural analysis using optical and SEM, energy dispersive x-ray spectroscopy (EDS), electron microprobe, and Auger electron spectroscopy.

RESULTS

As-Fabricated Filter Materials

The as-fabricated filter materials were 40–50% porous with sintered ligaments that ranged between 1 and 30 µm in thickness with an average of approximately 9 µm. There were numerous oxide particles on pore surfaces (Fig. 1) and at the boundaries of agglomerated powder particles [11]. Qualitative analysis by EDS showed that these particles were most likely alumina and zirconia. These oxides form during the water atomization process and most likely coarsened during subsequent processing. After preoxidation at 800–1000°C, the original oxide particles were still clearly evident and a thin protective alumina scale had formed on the metal surfaces. (Pall typically preoxidizes the iron-aluminide filter elements.) Depth profiling by Auger electron spectroscopy showed that the alumina scale formed by preoxidation at 800°C averaged approximately 2 µm in thickness, but could vary between 0.5 and 3 µm. Filters with oxide layers in this thickness range are gray in color. In addition to several of these, a filter element with various shades of blue was also used to provide o-ring specimens for exposure at the Wabash River Plant. This coloration would indicate a thinner alumina film was formed during preoxidation and, indeed, Auger analysis determined that the oxide coating on the pore surfaces of the blue filter was approximately 0.2 µm. An as-fabricated filter without preoxidation was similarly analyzed and was found to have an alumina layer that was no more than several hundredths of a micron thick.

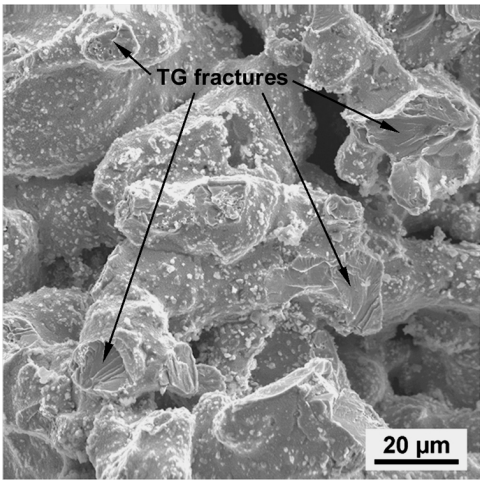

Fig. 1. SEM micrograph of as-fabricated FAS-Zr filter material (IA-187) showing transgranular failure through fully sintered material and oxide particles on powder surfaces.

Determination of the room-temperature tangential stress-tangential strain curves using the rubber-insert-internal pressurization approach showed that the porous iron aluminides had reasonable strengths [11]. The average fracture strength for o-rings cut from two as-fabricated filter elements (IA-187, IA-188, three specimens each) was approximately 2 kN (see Table 1). Microscopy of the ruptured o-rings showed transgranular failure through the fully sintered ligaments and that the fracture surfaces

were free of oxide particles (Fig. 1). As such, the fracture surfaces were typical of the ductile failures observed for fully dense iron aluminide and, when allowance is made for the reduced load-bearing area, the measured strengths appear to be consistent with those for similar dense alloys [6]. Preoxidation at 800°C for 7 h had no influence on the hoop strength of the FAS-Zr filter material [11]. Limited data for filters preoxidized at 1000°C showed a slightly higher hoop strength, which, may indicate that some amount of densification occurred during preoxidation at that temperature.

Specimens from Exposed Filter Elements

Two different samples of the DC-20 filter, exposed for 574 h in the filter vessel at the Wabash River plant, were examined (see Table 1). The porosity in this filter was non-uniform, with the sample in Fig. 2a showing normal porosity, while the sample in Fig. 2b had less porosity over the inner half of the filter. A light deposit containing S, As, Ge, Si, Cu, Sb, C, Zn, Ca, K, P was observed on the outer surface (that is, the gas inlet side of the filter wall) of both samples. Very little deposit was present on the inner (gas outlet) surface.

The DC-36 filter saw the same exposure conditions as the DC-20 filter, but for a longer length of time (1565 h). The porosity in this filter was non-uniform, with the inner one-third of the filter having much less porosity than normal (like that shown for DC-20 in Fig. 2b). The outer surface of the filter (top in Fig. 2b) contained a light-to-medium deposit consisting of As, Ge, S, Si, and O, while the inner surface had a very light deposit of mostly S and C. Pore surfaces in the interior of the filter were covered with an Al-O product approximately 2 μm thick. Corrosion was not substantial.

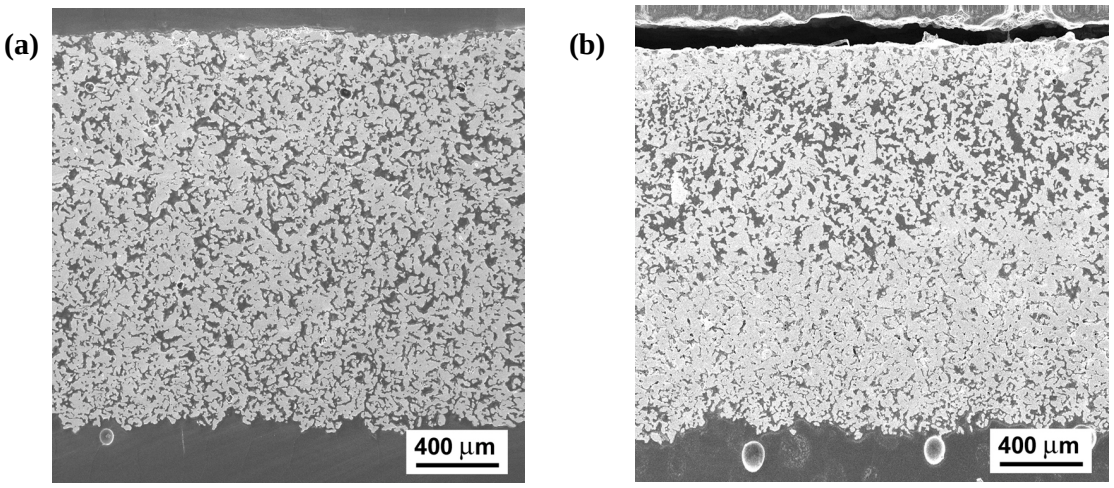

Fig. 2. Microstructures of two different samples of filter DC-20 exposed 1565 h in the Wabash River Plant: (a) showing normal porosity and (b) showing low inner surface porosity. Outer surface (gas inlet side) of filter is at top, inner surface (gas outlet) at bottom.

Filter element DC-88 was exposed in the vessel at Wabash River for 2185 h. As shown in Fig. 3, microstructural examination indicated that many of the pores in approximately the outer 750 µm of the filter (top in Fig. 3), as well as approximately 300 µm from the inner surface, were almost completely filled. In addition, layers of corrosion products approximately 100 and 50 µm thick were observed on the outer and inner surfaces, respectively. These layers appeared to be growing outward from the filter, since the wall thickness after exposure was about 200 µm greater than before exposure. The fracture strength of this filter element, along with that of DC-36 above, was slightly less than that of the DC-20 and as-fabricated filters (see Table 1).

The microstructure and composition of the DC-88 filter element after exposure was characterized using an electron microprobe. Figure 4 shows that the occluded filter region near the outer surface was composed of basically two phases: Al-O (see Figs. 4c,f) and Fe-S (see Figs. 4b,e). The layer that formed outward from the surface was Fe-S [12]. No areas of Fe_3Al were detected in this 750-µm region near the outer surface, indicating that the entire original Fe-Al-Cr matrix in this area had been consumed by corrosion. The Cr in the original filter material appears to have been incorporated predominantly into the Al-O phase (see Fig. 4d). Microprobe analysis showed that the Fe-S layer on the surface also contained many other elements and particles filtered from the gas

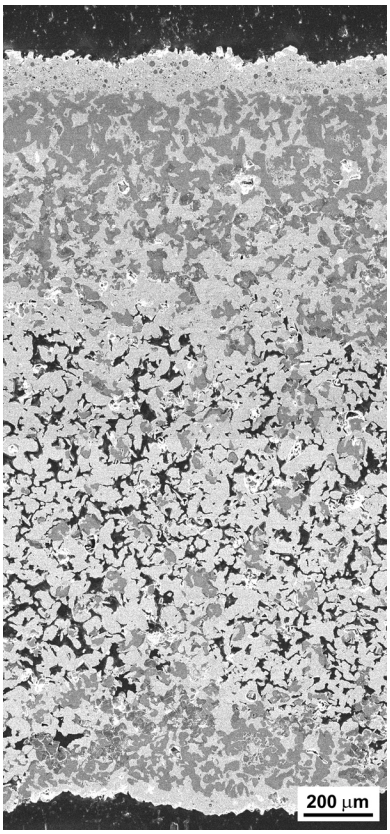

Fig. 3. Microstructure of filter DC-88 exposed for 2185 h in the Wabash River Plant.

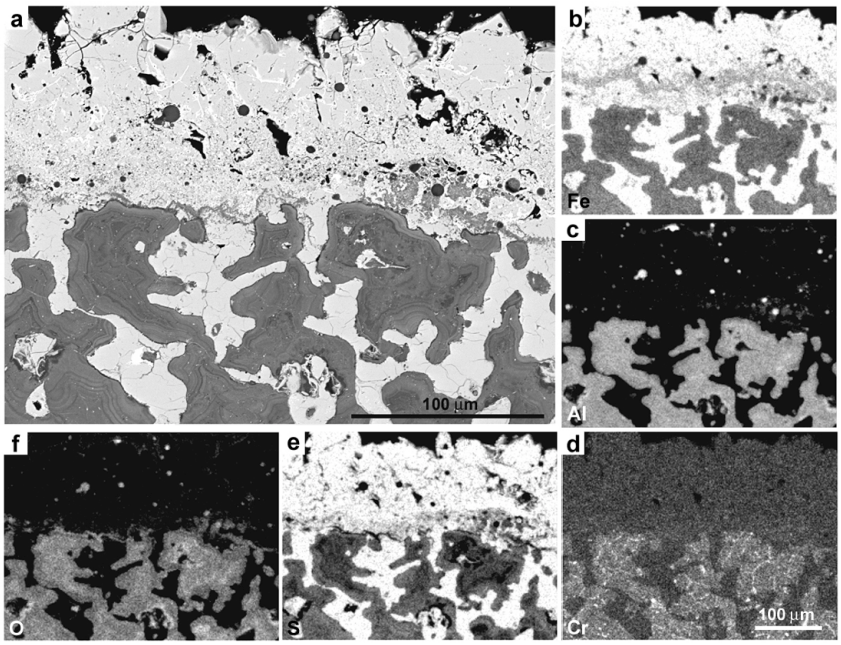

Fig. 4. Backscattered electron image (a) and x-ray maps for (b) Fe, (c) Al, (d) Cr, (e) S, and (f) O in the outer region of filter DC-88.

stream, including oxides of Al and Si, as well as Ni, Zn, Ca, K, Ge, As, and Sb. The occluded region of the inner surface (that is, the outlet side of the filter wall) was also composed of Fe-S and Al-O, with a surface layer of Fe-S. The layer also contained a significant amount of As and some Ni, but few, if any, of the other elements that were observed on the outer surface. In the transition regions of the filter, between the completely occluded regions and the porous original matrix still present toward the center of the filter, some of the Fe-Al-Cr matrix phase was detected along with the Fe-S and Al-O phases. Figure 5 shows a backscattered electron image of such a region. The x-ray scan across the three phases revealed the light and medium contrast phases to be Fe-Al-Cr and Fe-S, respectively. The composition for the Fe-Al-Cr phase is approximately the same as the original filter material, (i.e., Fe-28Al-2Cr), while the composition of the Fe-S phase indicates that it is most likely FeS. A spike in the Al and O levels and a decrease in the Fe level at the interface between these two phases indicate that an Al_2O_3 coating is still present on the surface of the Fe-Al-Cr particle. The dark phase is a complex oxide containing Fe, Al, S, and Cr. The layered structure of that phase shown in Fig. 5. It is believed to be an intermediate phase between the Fe-Al-Cr matrix and the FeS/Al-O structure present nearer the outer and inner surfaces of the filter.

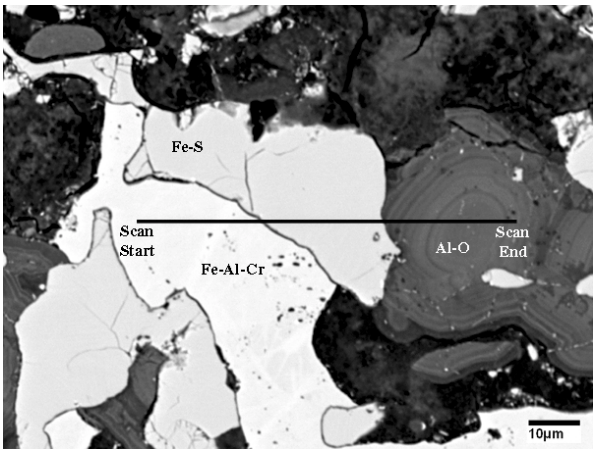

Fig. 5. Backscattered electron micrograph showing the three different phases observed in filter DC-88 exposed for 2185 h. Line shows location of x-ray scan across the phases.

Specimens Exposed as O-rings

As described in the Experimental Procedures section, o-ring specimens were cut from as-fabricated filter elements and then exposed on the clean- or dirty-gas side of the Wabash River Plant's filtration system. Three o-rings were exposed on the clean-gas side of the filter system without preoxidation: IA-188 for 1628 h, IA-187 for 2237 h and another o-ring of IA-187 for 3865 h. Figure 6 compares the microstructures of these three filter o-rings after exposure. All three o-rings appeared to be blocked with reaction products, with only a small percentage of the pores open toward the outer and inner surfaces of the filter exposed for 1628 h. Higher magnification of the center areas of these filters shows the presence of three main phases (the three levels of contrast in Fig. 7), with the lighter contrast phase (the Fe-Al

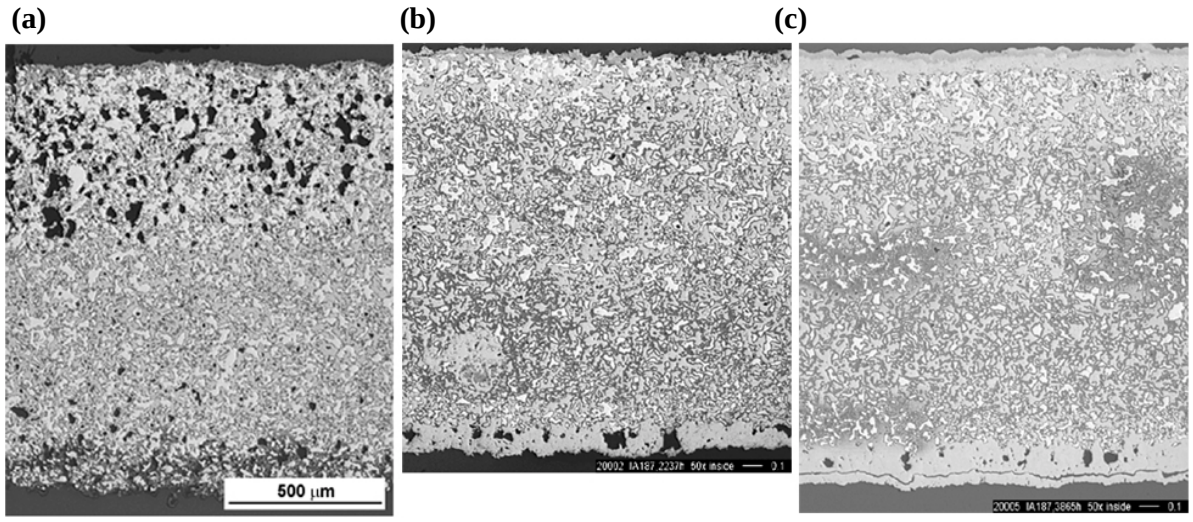

Fig. 6. Optical micrographs showing the microstructures of as-fabricated Fe-Al filters (a) IA-188 after 1628 h, (b) IA-187 after 2237 h, and (c) IA-187 after 3865 h of exposure on the clean-gas side of the Wabash River Plant.

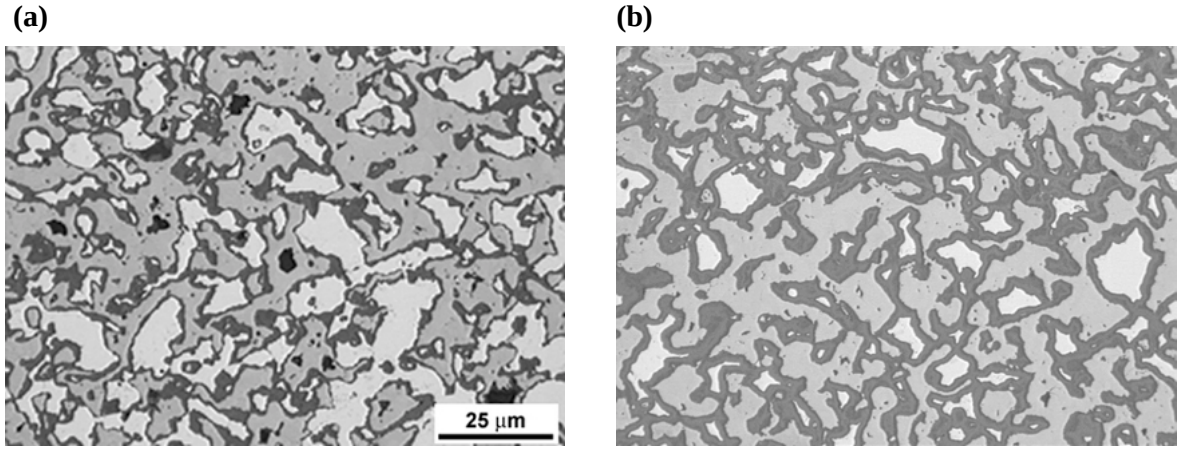

Fig. 7. High magnification optical micrographs showing the microstructures of as-fabricated Fe-Al filters (a) IA-188 after 1628 h and (b) IA-187 after 3865 h of exposure on the clean-gas side of the Wabash River Plant.

matrix) gradually disappearing with time. Analysis of these three phases using EDS showed that, with continued exposure, the Fe-Al matrix was gradually being converted into Al-O and Fe-S products. This and other analyses suggest that the iron diffuses outward to fill the pores with Fe-S. The results of internal pressurization tests of o-rings from the IA-187 filter exposed for 2237 h showed that the strength was reduced by approximately half in comparison to the as-fabricated filters (see Table 1).

O-rings from filter elements that had been preoxidized for 7 h at 800°C were exposed on the clean-gas side of the filter system (see Table 1): DC-207 for 1988 h, IA-191 for 2237 h, and DC-205 for 4335 h.

The o-rings exposed for 2237 and 4335 h were in very good condition, with no surface deposits, no reduction in strength, and only minor Fe-S formation throughout the filter. Their microstructures were similar to that observed for the typical unexposed filter (as in Fig. 2a). However gas flow in the DC-207 o-ring which had been exposed for only 1988 h was completely blocked by the formation of almost solid bands of corrosion products on the outside and inside surfaces (see Fig. 8). High magnification SEM (Fig. 8b) and EDS (Fig. 8c) indicated again that the Fe-Al matrix was being converted into Fe-S and Al-O products. The corrosion products formed throughout the filter and Fig. 9 shows the Fe-S growing inside the pores in the center of the filter wall. However, the filter appeared to be blocked by the solid bands of corrosion products on the outer and inner surfaces.

As part of the study of preoxidation conditions, two o-rings (from filter IA-141) that were preoxidized at 1000°C were exposed for 2237 and 3865 h on the clean-gas side of the plant's filtration system. The microstructures of the o-rings exposed for 2237 and 3865 h were similar to those shown in Fig. 6a,b. Both o-rings appeared to be blocked to the flow of gas although the one exposed for 2237 h still had a noticeable number of unblocked pores. Each had layers of Fe-S on both surfaces, the thickness of which approached 100 µm. High magnification SEM showed an increase in corrosion products and a decrease in the amount of Fe-Al matrix with increasing exposure time, as was shown for the as-fabricated filters in Fig. 7.

As described above, a filter element with a thinner preformed oxide layer on pore surfaces was used to provide o-ring specimens for exposure at the Wabash River plant. After plant exposure for 1988 h, the o-rings cut from the blue filter (o-rings DC-208 and -211 in Table 1) contained only small amounts of corrosion product regardless of location on the clean- or dirty-gas side and their microstructures were similar to that of the as-fabricated filter shown in Fig. 2a.

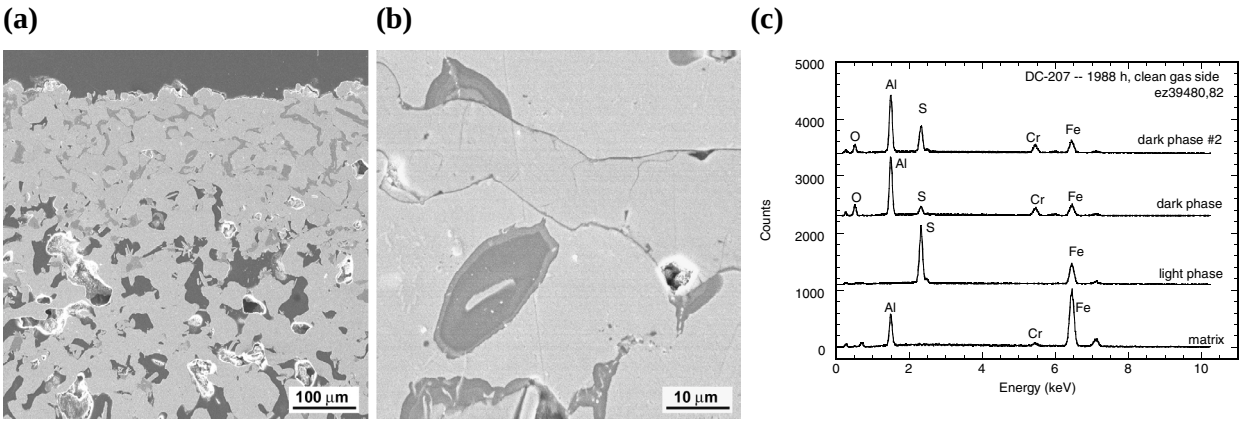

Fig. 8. Low- (a) and high-magnification (b) SEM micrographs and (c) EDS spectra for phases present in DC-207 exposed for 1988 h on the clean-gas side.

In contrast, o-rings from the gray preoxidized filters exposed at the same time for the same length of time (o-rings DC-209, -210 in Table 1) were almost completely blocked by the formation of Fe-S and Al-O (see Fig. 10). The presence of such a large amount of the more brittle corrosion products resulted in significantly reduced fracture strengths for the gray o-ring specimens (0.9–1.5 kN, see Table 1).

Four FAL o-rings were included in the various exposures at the Wabash River Plant and the results are listed at the end of Table 1. All the exposed FAL o-rings, whether exposed for 6212 h on the clean-gas side or for 4335 h on the dirty-gas side, exhibited minimal amounts of corrosion products. As expected, the surface deposits on the o-rings exposed on the dirty-gas side were much thicker than on the o-rings exposed on the clean-gas side, but this thicker surface deposit did not affect the appearance, strength (see Table 1), or filtering capacity of the FAL o-rings.

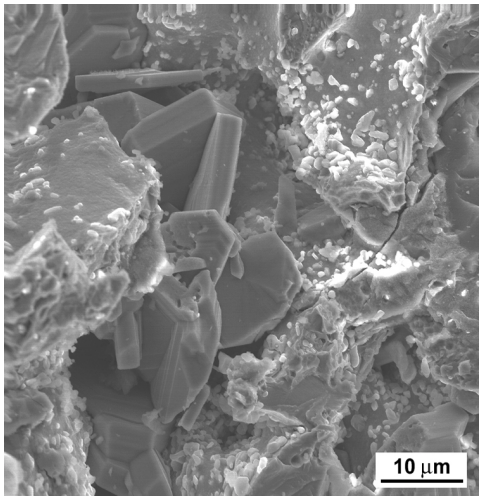

Fig. 9. Iron-sulfur particles forming inside pores in the interior of o-ring DC-207 exposed for 1988 h on the clean-gas side.

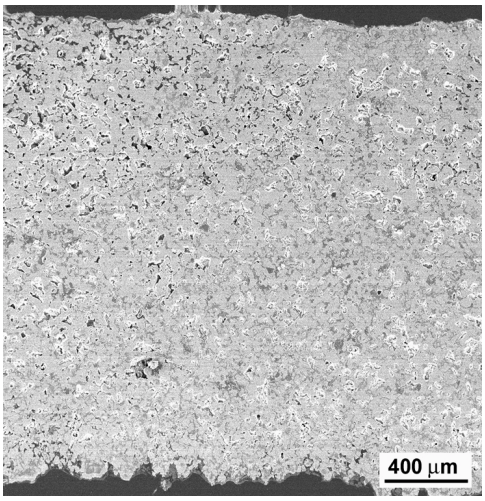

Fig. 10. SEM micrograph showing blocked pores in o-ring DC-209 (from gray filter) after exposure for 1988 h on the clean-gas side.

Strength Measurements

Examination of the strength data reported in Table 1 indicates an inverse correlation between the amount of sulfidation observed and the fracture stress of the o-ring during loading by internal pressurization. The hoop-strength data, albeit limited, when combined with the microstructural analyses, qualitatively indicate that the iron-aluminide filters maintain approximately their original strength as long as Fe-S formation has not occluded more than approximately 50% of the pores.

DISCUSSION

Evaluation of specimens from plant exposures is complicated by variations in operating conditions from one run to another. Both coal and petcoke (higher sulfur content) were used as fuel during the

exposure sequences and the temperature was not necessarily the same in each run (probably ranged from 450 to 550°C). In addition, many of the longer exposure times were made up of as many as three different campaigns between which the specimens were exposed to unknown lengths of downtime and any corrosion associated with such [10,12,13]. Nevertheless, this work has yielded some important information about the nature of corrosion of iron aluminides in an operating gasification plant.

Iron aluminide alloys rely on a thin alumina scale for protection against corrosive environments at high temperatures. For this application, filter elements are normally preoxidized at temperatures much higher than the gasification filtration unit to assure that a protective alumina film forms. This scale has been observed on preoxidized elements (see above and Ref. 11). In this work, o-ring specimens cut from filters that were not preoxidized and from an element preoxidized at 1000°C were found to be fairly heavily corroded after as little as 1628 h of exposure (see results for IA-141, -187, and -188 in Table 1 and Figs. 6–8). In contrast, with one exception (DC-207), the o–rings preoxidized at 800°C were still not filled with corrosion products after 4335 h (see results for IA-191, DC-205, -207 in Table 1 and Fig. 9). Even in the case of DC-207, corrosion wasn't as severe as in the absence of preoxidation; its fracture strength (which generally tended to decrease with increasing corrosion—see Table 1) was equal to the starting material. These results show the importance of the formation of a continuous alumina layer in assuring corrosion resistance during operation of the gasifier and reinforce the need for appropriate preoxidation in this regard. Preoxidation at 1000°C was not as effective as that done at 800°C. In another study [14], the 1000°C preoxidation treatment was found to result in an alumina layer on the filter that was locally disrupted by large zirconia particles and not uniformly continuous and thin. Because of this (and Al depletion concerns – see below), it would not be expected to be as protective as the one formed by preoxidation at 800°C [14].

Corrosion failure in these filter materials appeared to be associated with the formation of Fe-S inside the pores of the filter. However, as described above, Al-O products were always observed in conjunction with the sulfides. This can be interpreted as a type of breakaway oxidation (sulfidation) in which aluminum is locally depleted by growth of alumina so that, after some point, if the protective scale is breached, iron sulfides form relatively rapidly. The thinness of the ligaments of the filters (average diameter of 9 μm) magnifies the importance of aluminum depletion/breakaway as the degradation mode because there is a relatively small volume of this element available to form the protective alumina [15]. This suggested mechanism may explain the better performance of the blue filter materials vis-à-vis the gray ones; Auger analyses have shown a thinner aluminum oxide film on the blue material (see above), thereby indicating a greater starting residual aluminum content in the alloy at the time of exposure. The

higher aluminum content will increase the time to sulfidation (breakaway). In the same way, the amount of residual aluminum in the filter material preoxidized at 1000°C could be less than what is found in the specimens preoxidized at 800°C and may explain the greater corrosion susceptibility of the former.

The comparison of results from the specimens placed on the dirty- and clean-gas sides, respectively, of the filtration system at the Wabash River gasification plant provides important supporting information regarding the corrosion failure mechanism. As expected, deposits were heavier for those specimens exposed on the dirty-gas side (see Table 1). However, the extent of corrosion (formation of Fe-S, see above) did not depend on specimen placement. This observation is consistent with the sulfidation degradation mode described above and indicates that the corrosion mechanism is associated with gaseous sulfur and oxygen species rather than the char per se.

As described in the Results section, the FAL (Fe-28% Al-5% Cr-0.1%Zr) o-rings were not substantially degraded after exposure for up to 6212 h on the clean-gas side and up to 4335 h on the dirty-gas side of the filtration system—only a relatively small amount of Fe-S was observed. In contrast, after approximately 2000 h, Fe-S was already starting to form in filter o-rings made from FAS-Zr powder. Higher chromium concentrations in Fe_3Al-based alloys degrade sulfidation resistance at higher temperatures [5,7], but may play a beneficial role in this lower temperature gasification plant environment by promoting alumina formation or improving corrosion resistance at ambient temperatures during downtime [16]. Effects of downtime corrosion can significantly negatively affect subsequent elevated temperature sulfidation [12,13] and, as mentioned above, may have played a role in the present case for those specimens that saw more than one run cycle during plant exposure.

SUMMARY AND CONCLUSIONS

Because of their good to excellent high-temperature corrosion resistance in sulfur-bearing environments, iron aluminide alloys are being evaluated as a potential material of construction for metallic filters to be used to clean fossil-fuel-derived gases prior to their introduction into gas turbines. Over 20 iron-aluminide filter-element or o-ring specimens have been characterized after exposure at the Wabash River Plant for times of approximately 400 to 6200 h. Several variables appear to be important to the length of service of these filters, including the preoxidation conditions during fabrication of the filter, time and temperature of exposure, and composition of the iron aluminide. The general mode of corrosion failure involves the formation of iron sulfide that grows into and occludes the pores, resulting in blockage of the filter and reduction in mechanical strength. This process appears to be accelerated at longer exposure times, possibly due to the depletion of aluminum from the filter alloy matrix and the resulting

breakdown of the protective alumina layer. A comparison of o–rings exposed on the clean- and dirty-gas side of the unit showed similar corrosion rates and indicated that the heavier surface deposits produced during exposure on the dirty-gas side does not affect the corrosion process.

The Fe-Al filters tended not to experience much degradation when (somewhat) optimal preoxidation was included as part of the fabrication process. Several filter specimens showed good resistance to 6212 h. The limited hoop-strength data generated to date have shown that iron-aluminide filters maintain their original strength as long as Fe-S formation has not occluded more than approximately 50% of the pores.

ACKNOWLEDGMENTS

Research at Oak Ridge National Laboratory is sponsored by the Office of Fossil Energy, Advanced Research Materials Program, U.S. Department of Energy under Contract DE-AC05-00OR22725 with UT-Battelle, LLC.

REFERENCES

1. M. A. Alvin, *Mater. at High Temp*. 14 (1997) 285–94.
2. J. E. Oakey, *Mater. High Temp*. 14 (1997) 301–11.
3. N. R. Quick and L. D. Weber, *Proc. Second International Conf. on Heat Resistant Materials*, ASM Intern., Materials Park, OH (1995) 663–71.
4. P. F. Tortorelli, C. G. McKamey, E. Lara-Curzio, and R. R. Judkins, *Proc. International Gas Turbine and Aeroengine Congress & Exhibition*, ASME Intern., New York (1999), paper 99-GT-268.
5. J. H. DeVan, *Oxidation of High-Temperature Intermetallics*, The Mineral, Materials, and Metals Society, Warrendale, PA (1989) 107–115.
6. C. G. McKamey, J. H. DeVan, P. F. Tortorelli, and V. K. Sikka, *J. Mater. Res*. 6 (1991) 1779–1805.
7. J. H. DeVan and P. F. Tortorelli, *Mater. High Temp*. 11 (1993) 30–35.
8. P. F. Tortorelli and J. H. DeVan, *Oxidation and Corrosion of Intermetallic Alloys*, Purdue University, West Lafayette, IN (1996) 267–331.
9. J. L. Blough and W. W. Seitz, *Proc. of Eleventh Annual Conference on Fossil Energy Materials*, Oak Ridge National Laboratory, Oak Ridge, TN (1997) 357–366.
10. W. T. Bakker, *Corrosion/98*, NACE Intern., Houston, TX (1998) paper number 185.

11. P. F. Tortorelli, E. Lara-Curzio, C. G.. McKamey, B. A. Pint, I. G. Wright, and R. R. Judkins, *Proc. Advanced Coal-Based Power and Environmental Systems*, U. S. Department of Energy (1998) paper PB7.
12. W. T. Bakker and J. Stringer, *Mater. High Temp*. 14 (1997) 35–42.
13. S. R. J. Saunders, D. D. Gohil, and S. Osgerby, *Mater. High Temp*. 14 (1997) 167–73.
14. B. A. Pint, B. A., Oak Ridge National Laboratory, Oak Ridge, TN, unpublished results, 2000.
15. W. J. Quadakkers and K. Bongartz, *Werkst. Korros*. 45 (1994) 232–38.
16. R. A. Buchanan, J. G. Kim, R. E. Ricker, and L. A. Heldt, *Oxidation and Corrosion of Intermetallic Alloys*, Purdue University, West Lafayette, IN (1996) 351–419.

ESTIMATION OF CARBON CREDITS IN CARBON DIOXIDE SEQUESTRATION ACTIVITIES

K. T. Klasson and B. H. Davison
Oak Ridge National Laboratory

INTRODUCTION

The approach for the activity, Estimation of Carbon Credits in Carbon Dioxide Sequestration Activities, will be based on the proposed approaches for forest systems. The desired result is a general methodology for evaluation of other sequestration options, which may result in temporary or permanent carbon fixation. The scope will be to develop the model in a series of small focus group meetings.

A process that involves sequestration of carbon, either from the atmospheric carbon dioxide (or other carbon-based greenhouse gas) or from the stack gases of a plant, should be evaluated on the same basis so that it can be compared to other sequestration options. As an example, we are providing the following discussion of some of the variables that may be evaluated:

1. ***Net Mass of Carbon Sequestered:*** It is important to have accurate estimates for the mass of carbon sequestered. For example, if a pond is used for heavy algae growth on atmospheric carbon dioxide, it is necessary to estimate any amount of methane that may be formed and emitted from the pond during anaerobic digestion in the sediments. Also, if substantial amount of lime is used to control the pH, it may be appropriate to assign a carbon equivalent corresponding to the amount of carbon dioxide (or other carbon) emitted during the production of the lime. To address these issues it is important to draw distinct boundaries and account for all the carbon flows.

2. ***Duration of Carbon Sequestration:*** It is intuitive that a long sequestration period is advantageous. However should it be expected that any sequestration activity should pass a threshold duration (e.g., 100 years) before being considered? Or, should the carbon sequestration activity receive full credit the year it is effective, and later receive a debit when possibly the carbon is released? The latter approach corresponds to some of the accounting strategies that are discussed in support of the Kyoto protocol. However, it does not allow for a priori comparison when two alternative activities are considered for the sequestration. If the time factor is important, several approaches may be taken - the threshold method is one, a linear relationship between the credit assigned and the duration sequestered is a second method. A third and fourth method may be to consider progressive approaches to bring incentives for longer- or shorter-term sequestration activities. It is possible that a threshold sequestration time (e.g., 100 years) is common among all methods after which full credit is

given. When discussing time it is also important to realize that the sequestration and the emissions may be spread out over time and that a life-cycle approach for the activity is used. For example, if the algae pond is used for several decades before it is harvested and the algae converted into bio-fuels, the activity has sequestered a net amount of carbon each year, but it is being released all at once. It is probably appropriate to take into account that some of the carbon was sequestered for a long time, but other portions were not. An attractive method to approach the time factor may be to define the Time Value of Carbon (analogous to the time value of money) and to use present-value-type calculations to bring all carbon flows to a single time.

3. ***Energy Use for Carbon Sequestration:*** The use of easily distributed energy (e.g., electricity) during the sequestration or maintenance of the stored carbon may be important to consider. This is energy that most likely resulted in carbon dioxide emissions during its generation. Thus, the energy can be converted into carbon equivalence and taken into account in the same fashion that other carbon flows are considered with respect of time. The use of waste energy that cannot be distributed (e.g., geothermal heat or process plant waste heat) should be considered "carbon neutral."

4. ***Land Use for Carbon Sequestration:*** If the sequestration activity will occupy a significant amount of land and if that land is a sink for carbon this has to be taken into account.

5. ***Others:*** Cost, regulatory issues, environmental impact, and social impact fall into this category. These are items very important for any undertaking and should be considered. However, it is in some cases very subjective and they should be kept separate from the carbon metrics evaluation. They each have strong merit and should be addressed but it may be appropriate to abstain from assigning any value to these factors. Cost represents a separate factor that can be evaluated through standard cost estimation methods. Costs will be part of this work if data are available. For example, if the cost for an algae pond has been estimated, it will be noted, but it will not be part of the carbon metrics.

In order to investigate if the above factors are appropriate to consider when a carbon sequestration activity is being evaluated, several focus group meetings will be held with others who are working on carbon credit trading and carbon credits for Land Use Change and Forestry. Both ORNL internal and external focus group meetings will be held. This will make sure that the initial approach taken gains support and understanding.

PRESENTATIONS AND PUBLICATIONS

Klasson, K. T., R. M. Counce, and B. H. Davison, "Development of a General Methodology for Evaluation of Carbon Sequestration Activities" in meeting proceedings from the 223rd American Chemical Society National Meeting in Orlando, FL, 2002.

Klasson, K. T., R. M. Counce, and B. H. Davison, "Evaluation of a Carbon Dioxide Separation Activity Based on Absorption from Flue Gas Streams: A White Paper," Oak Ridge National Laboratory, Oak Ridge, TN 37831, 2002.

Klasson, K. T. and B. H. Davison, "Full-Cycle Carbon Emissions (FCCE) Factors from Resource Use in Carbon Sequestration Activities: A White Paper," Oak Ridge National Laboratory, Oak Ridge, TN 37831, 2001.

Klasson, K. T. and B. H. Davison, "Evaluation of a Carbon Dioxide Sequestration Activity Based on Production of Carbon-rich Fertilizers: A White Paper," Oak Ridge National Laboratory, Oak Ridge, TN 37831, 2001.

Klasson, K. T. and B. H. Davison, "A General Methodology for Evaluation of Carbon Dioxide Sequestration Activities," submitted to *Technology* (as part of the International Dixy Lee Ray Symposium), 2001.

Klasson, K. T. and B. H. Davison, "Estimation of Carbon Credits in Carbon Dioxide Sequestration Activities: A White Paper," Oak Ridge National Laboratory, Oak Ridge, TN 37831, 2000.

Klasson, K. T., R. M. Counce, and B. H. Davison, "Development of a General Methodology for Evaluation of Carbon Sequestration Activities" presented at the 223rd American Chemical Society National Meeting in Orlando, FL (April 2002).

Klasson, K. T. and B. H. Davison, "A General Methodology for Evaluation of Carbon Dioxide Sequestration Activities," presented at the Twelfth Symposium on Separation Science and Technology for Energy Applications, Gatlinburg, TN (October 2001).

Klasson, K. T. and B. H. Davison, “Estimation of Carbon Credits in Carbon Dioxide Sequestration Activities,” presented at the First National Conference on Carbon Sequestration, Washington, DC (May 2001).

Klasson, K. T. and B. H. Davison, “A General Methodology for Evaluation of Carbon Dioxide Sequestration Activities,” presented at the 23rd Symposium on Biotechnology for Fuels and Chemicals, Breckenridge, CO (May 2001).

Klasson, K. T. and B. H. Davison, “Chemical Engineering and Carbon Dioxide Sequestration Strategies,” presented to Knoxville-Oak Ridge Section of American Institute of Chemical Engineers, Knoxville, TN (March 2001).

Klasson, K. T. and B. H. Davison, “Estimation of Carbon Credits in CO_2 Sequestration Activities,” presented at the 22nd Symposium on Biotechnology for Fuels and Chemicals, Gatlinburg, TN (May 2000).

Klasson, K. T., “A General Methodology for Evaluation of Carbon Dioxide Sequestration Activities,” presented at University of Arkansas, Fayetteville, AR (January 2001).

Klasson, K. T. and B. H. Davison, “Estimation of Carbon Credits in CO_2 Sequestration Activities,” presented to a forum at National Energy Technology Laboratory, Morgantown, WV (November 2000).

Klasson, K. T. and B. H. Davison, “Estimation of Carbon Credits in CO_2 Sequestration Activities,” presented as a technical seminar at Oak Ridge National Laboratory, Oak Ridge TN (August 2000).

APPLICATION OF NATURAL AND INTRODUCED TRACERS FOR OPTIMIZING VALUE-ADDED SEQUESTRATION TECHNOLOGIES

D.R. Cole and G.R. Moline
Oak Ridge National Laboratory
(Collaborators: J. G. Blencoe, J. Horita, S. Fisher, and C. Thorton)

INTRODUCTION

This project is one element (Task B.3) of an interdisciplinary public-private partnership, GEO-SEQ, that was established to develop and deliver the enabling technology and information needed to accelerate application of safe and cost-effective methods for geologic sequestration of carbon dioxide. Team members include researchers from LBNL, LLNL, Stanford University, the Texas Bureau of Economic Geology and the Alberta Research Council. The overall goal of the ORNL effort is to provide methods to interrogate the subsurface that will allow direct improvement of CO_2 sequestration during EOR, ECBM, EGR, or use of brine formations. This will be accomplished by utilizing the power of natural (isotopic) and applied gas tracers to decipher the fate and transport of CO_2 injected into the subsurface as well as other relevant processes. These methods have the potential to provide near-real-time information on process optimization. The resulting data will be used also to calibrate and validate the predictive models used for (a) estimating CO_2 residence time, reservoir storage capacity, and storage mechanisms, (b) testing injection scenarios for process optimization, and (c) assessing the potential leakage of CO_2 from the reservoir. This activity is being conducted in concert with the geophysical and inverse-modeling methods described in Tasks B.1 and B. 2 and will provide a means for calibrating the transport model and as an aid to interpreting the time-series geophysical data. This work directly addresses a key objective of the overall GEO-SEQ project: to increase confidence in and the safety of geologic sequestration by identifying and demonstrating cost effective and innovative monitoring technologies to track migration of carbon dioxide and its reaction products in geologic formations.

RESULTS: NATURAL ISOTOPE TRACERS

Naturally-occurring elements, such as the stable isotopes of the light elements (O, H, C, S, N), noble gases and their isotopes (He, Ne, Ar, Kr, Xe), and radioactive isotopes (e.g., tritium, ^{14}C, ^{36}Cl, ^{125}I, ^{129}I, ^{131}I), have been used extensively to determine the sources of fluid and gas species and their mechanisms of migration, assess the extent of fluid/rock interactions, and quantify the residence times of fluids in the subsurface. These naturally occurring constituents and their isotopic compositions have the advantage of being readily available in most systems. In particular, by accounting for how $^{13}C/^{12}C$ and $^{18}O/^{16}O$ ratios in CO_2 vary during the injection process, we can (a) understand complex natural geochemical processes

involving CO_2 in the subsurface, and (b) assess and monitor quantitatively both short- and long-term consequences of subsurface CO_2 injection and sequestration, and possible leakage from the system.

Isotope Partitioning Studies

Carbon and oxygen isotope partitioning experiments in static systems have been conducted at temperatures of 35 and 50°C to complement previously reported 20°C results. CO_2 of known C and O isotope composition was reacted with various geological materials and the isotopic difference between free CO_2 and CO_2 adsorbed onto the solids was measured. As with our 20°C studies, both C and O isotope values of the free CO_2 are always enriched in the heavier isotope (^{13}C or ^{18}O) relative to CO_2 adsorbed onto mineral surfaces. For crystalline phases such as quartz, calcite and montmorillonite, the magnitude of this partitioning decreases with increasing temperature as a rate of a only a few per mil per 15°C increase in temperature. Isotopic behavior determined for the Lost Hills core was opposite to that observed in the crystalline solids. The magnitude of both C and O partitioning increased at a rate of several per mil per 15°C increase in temperature for all four core samples tested. Similar behavior was also observed for the one Lost Hills oil sample also investigated. These results have two implications for the monitoring of CO_2 during injection testing. First, the temperature dependence of the adsorption process can be ignored for CO_2 interaction with crystalline host lithologies, but not in cases where hydrocarbons are present. Second, the difference in the direction of enrichment between hydrocarbon bearing and non-hydrocarbon bearing host rocks as a function of temperature might afford a possible further means to determine what horizons the CO_2 interacted with.

Carbon and oxygen isotope partitioning experiments in static systems have also been conducted at a temperature of 20°C as a function of CO_2 pressure which was varied from less than 0.01 bar to 0.1 bar. As with our previous studies, both C and O isotope values of the free CO_2 are always enriched in the heavier isotope (^{13}C or ^{18}O) relative to CO_2 adsorbed onto mineral surfaces. The overall magnitude of the partitioning was generally consistent with what we have reported previously—i.e., the carbon isotope difference between free CO_2 and sorbed CO_2 increased in order from quartz to calcite to Lost Hills core to montmorillonite, and from quartz to calcite to montmorillonite to Lost Hills core for oxygen. The effect of pressure increase is much less pronounced compared to the magnitude we observed for the temperature effect. For crystalline phases such as quartz, calcite and montmorillonite, the magnitude of the carbon and oxygen isotope partitioning increased at a rate of only about 0.1 and 0.2 per mil per 20 mbar increase in PCO_2, respectively. Isotopic partitioning between CO_2 and the Lost Hills core was somewhat greater wherein we observed an increase in carbon isotope partitioning of between 0.2 and 0.3 per mil per 20 mbar increase in PCO_2. The change in oxygen was roughly a factor of two greater than carbon for the

Lost Hill samples. There is a tendency for the partitioning to reach steady state as pressure approaches 0.1 bar, probably signifying attainment of CO_2 saturation on the mineral surfaces.

Gas Sorption Studies

Detailed measurements were carried out on the surface areas and pore sizes of solids used in our adsorption isotope studies using a newly acquired Quantachrome surface area analyzer. The sorption gas used in all cases was N_2. Five samples were examined: quartz, calcite, montmorillonite, Lost Hills core 4, and Argonne premium coal sample Pocahantus #3. The average measured specific surface areas in m^2/gm are 0.1233, 0.7129, 8.965, 1.418 and 1.304, respectively. The ranges in micro-pore size were also determined from sorption/desorption isotherms. These ranges (in angstroms) for quartz, calcite, montmorillonite, Lost Hills and coal, respectively, are: 6–40 (average ~12), 15–50 (average ~25), 5–8 (average –6), 12–100 (average ~30), and 5–20 (average ~10). Macro-pore sizes estimated for the Lost Hill core and coal are on the order of several thousand angstroms in diameter. These data are needed to assess the behavior of CO_2 adsorption and its subsequent isotope partitioning during interaction with the solids.

As a prelude to CO_2 adsorption-desorption measurements on our geological materials (e.g., quartz, calcite, montmorillonite, etc.), we obtained a suite of carbon materials that have been used previously in CO_2 sorption studies. These include amorphous carbon, graphite, and charcoal. The purpose of this exercise was to test and calibrate our surface area/pore size analyzer for CO_2 gas. Our previous experience has only been with the use of either N_2 or Kr as adsorbing species. All three carbon materials exhibit similar sorption isotherm behavior when recast on a per-unit-area-basis. Measurements were conducted at two temperatures: 0 and 20°C, the latter being more appropriate for subsurface conditions. The isotherms indicate two distinct regions of coverage that are separated by a wide plateau; this plateau appears broader at 0°C. The adsorption at very low pressures (<0.01 torr) is compatible with high-energy adsorption on one array of carbon atoms occupying the prism faces. Additional adsorption at higher pressures then occurs on sites of lesser energy in the more abundant basal planes. The charcoal sample exhibited more of the basal-plane sorption behavior than the other carbon materials tested.

CO_2 adsorption-desorption isotherms were measured at 20°C for montmorillonite using the Quantachrome Autosorb I surface area analyzer. A comparison with previous measurements on N_2 adsorption-desorption indicate that CO_2 adsorbs far less than N_2 as expected because of its great molecular diameter. At a total pressure of one atmosphere, N_2 covers the montmorillonite surface at a concentration of roughly 0.26 mmoles/m^2 whereas CO_2 concentration reaches only 0.0076 mmoles/m^2, a difference of nearly 1.5 orders of magnitude. Both gases exhibit concave upwards adsorption trends for plots of moles/m^2 (y-axis) plotted versus log pressure (x-axis), with N_2 displaying a much flatter initial

trend indicative of adsorption on prismatic crystal faces. Overall, however, adsorption for both gases is dominated by the basal plane surfaces of the clay.

Isotope and Gas Chemistry at the Lost Hills, CA, CO_2 Injection Site

Gas chromatograph combustion isotope ratio mass spectrometry (GC-C-IRMS) was used to characterize the isotopic and gas chemistry of gases from the Chevron Lost Hills, CA, system (Fig. 1). Carbon and oxygen isotopes were measured in the injection CO_2 (sampled 8/11/00), CO_2 from pre-injection "reservoir" gases (wells 11-8D, 12-8D, and 12-7 sampled 8/11/00), and the return CO_2 sampled in wells 11-8D (sampled 1/4/01; 12/20/01), 12-8D (sampled 12/6/00; 12/20/01), 12-7 (sampled 12/6/00; 12/20/01), 11-7B (sampled 12/20/01), 11-9J (sampled 12/20/01), and 12-8C (sampled 12/20/01). Carbon isotopes have also been measured in C_1–C_6 hydrocarbon gases. The initial injection CO_2 had a $\delta^{13}C$ (PDB) value of –30.1 ‰ and a $\delta^{18}O$ (VSMOW) value of –1.12 ‰. Gases sampled prior to injection were dominated by CH_4 with lesser amounts of CO_2 and subordinate amounts of C_2–C_6. The $\delta^{13}C$ (PDB) values for CH_4 in pre-injection and all return gases were very similar, ranging from –36 to –42 ‰, with an average of –40.4‰ (± 1.5‰ 1 σ).

The $\delta^{13}C$ (PDB) values for pre-injection CO_2 ranged from 15.6 to 18.5 ‰ whereas the return CO_2 gases from the first sampling effort (12/6/00 and 1/4/01) exhibited a narrow range of values, -27.5 to

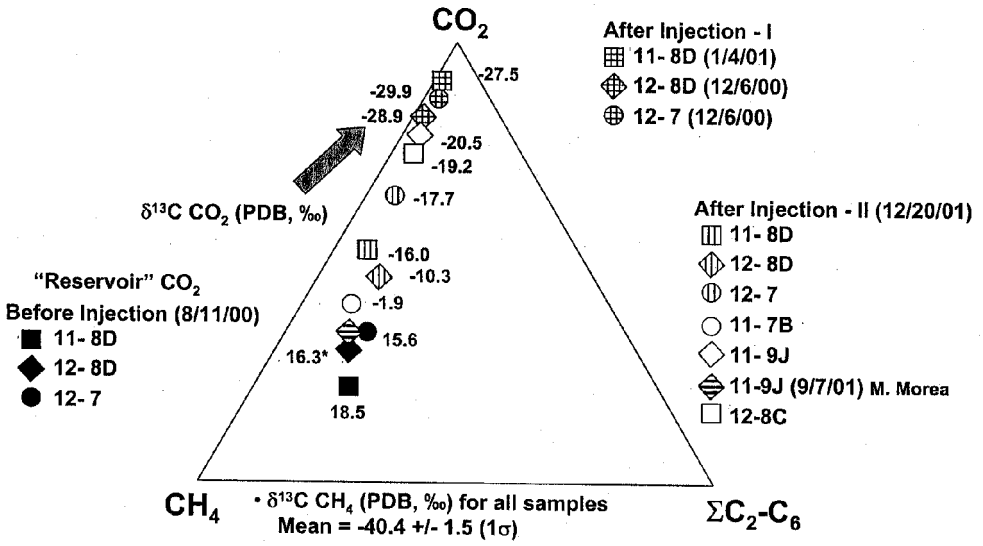

Fig. 1. Summary of chemistry and carbon isotope compositions for gases sampled at Lost Hills.

–29.9 ‰. Chemically, return gases from this first sampling effort were very rich in CO_2 and clearly have carbon isotope values very close to the injection CO_2. Interestingly, the percentages of injection CO_2 estimated from the isotopic data (using –30.1 ‰ as the injectate end member and 16.8 as the average "reservoir" gas end member) do not agree exactly with similar estimates based on gas chemistry (see Fig. 1). In all cases for this first sampling effort, the isotopic mixing model over-estimates the amount of injectate CO_2 compared to the gas chemistry model by 6 to 14 %. Assuming that the gas chemistry is a better measure of mixing, this means the isotopic values are somewhat more negative (by a few per mil) than simple binary mixing would predict. Pathways that might explain this include (1) loss of CO_2 to an aqueous phase, and/or (2) oxidation of hydrocarbons (CH_4, oil) to CO_2 either inorganically or microbially. The minor differences in predicted mixing percentages based on the isotope and chemical models indicate that these exchange mechanisms made only a minor contribution to the overall carbon isotope budget in the Lost Hills gases immediately after the first main CO_2 injection episode (terminated due to sanding).

This is not true, however, for the gases sampled from all wells on 12/20/01 (see Fig. 1). Gas chemistries indicate that the amount of injectate CO_2 was less dominant than the previous sampling at the end of 2000. The data show a clear trend on the ternary plot of CO_2-CH4-Σ C_2-C_6 where samples collected on 12/20/01 fall on a line connecting the "reservoir" gases with gases collected at the end of 2000. Gases with the most amount of injectate CO_2 include 11-9J, 12-8C and 12-7 with $\delta^{13}C$ values of –20.5, -19.2 and –17.7 ‰, respectively. The remaining wells (11-8D, 12-8D, and 11-7B) have $\delta^{13}C$ values of –16, -10.3 and –1.9 ‰, respectively. Use of the same kinds of simple isotopic and chemical mixing models for these results indicates that the isotopic model over-estimates the percentage of injectate CO_2 by between 8 and 20%. CO_2 injected since the sanding problem of 12/00 was carried out as two distinct pulses, one lasting from March to early May, 2001 and a second lasting from September to November, 2001 (personal comm., Mike Morea, Chevron). Interspersed between these two CO_2 injection pulses was a period of water injection, which was also continued after the last CO_2 pulse in December of 2001. The isotopic and chemical data indicate that this complex injection did not lead to a greater influx of CO_2 to the return wells, and in fact seems to indicate that the CO_2 may have had sufficient time to interact more extensively with water and/or hydrocarbons in the reservoir.

The $\delta^{18}O$ compositions of the pre-injection CO_2 ranged from about 16 to 24 ‰ (average ~20.9‰), whereas the return CO_2 gases from the first sampling effort were somewhat more enriched, ranging from approximately 29 to 34 ‰. Since these samples are dominated by injectate CO_2 (78–90%), this constitutes nearly a ~30 ‰ increase in $\delta^{18}O$ from the injection value of –1.1 ‰. Simple mixing of an isotopically light injectate and the heavy "reservoir" CO_2 cannot explain the even heavier $\delta^{18}O$ values measured in the three return wells. It is likely that the enrichment in ^{18}O is due to kinetically fast exchange of CO_2 with water encountered during migration. The oxygen isotope fractionation between

CO_2 and water is ~37 ‰ at 45°C (a reasonable estimate of the subsurface reservoir temperature), so applying this number to the oxygen values measured for the return CO_2 yields $\delta^{18}O$ values for water of between –3 and –7 ‰. These values are generally consistent with numbers reported for ground waters in this part of CA. The interaction of CO_2 with the water in the reservoir is also consistent with the carbon isotope data that suggest possible loss of CO_2 to the aqueous phase as one mechanism to produce isotopic values somewhat more negative than the chemical mixing models predict.

Modeling Isotope Exchange During CO_2-Fluid-Solid Interactions

Model mass-balance isotope reaction calculations were conducted to assess the magnitude of both C and O isotope change in CO_2 as it reacts with calcite and water (see Fig. 2). The calculations assume reaction in a closed system where CO_2 is allowed to react simultaneously with a HCO_3^--brine and calcite. Equilibrium isotope fractionation is assumed in all calculations carried out for both 20° and 100°C. Results of these calculations are shown in Fig. 2 where $\delta^{13}C$ (on the PDB scale) are plotted against the $\delta^{18}O$ (on the SMOW) of CO_2. The initial CO_2 has been given values of 32 per mil and –36 per mil for O and C, respectively. The isotopic change in C and O are calculated for different scenarios where CO_2 is reacted with calcite and H_2O of varying initial composition. In all cases, the C isotope values of CO_2 increase because we allow it to react with calcite having a single initial enriched value (0 per mil). We see that depending on whether the initial calcite and brine are enriched or slightly depleted in ^{18}O, the CO_2 isotopic trajectories can be quite different–i.e., one with increasing ^{18}O (trajectories moving to the upper right) versus those that decrease (trajectories moving to the upper left). Magnitudes of change along any given trajectory are controlled by initial isotopic compositions, temperature and the ratio of CO_2 to

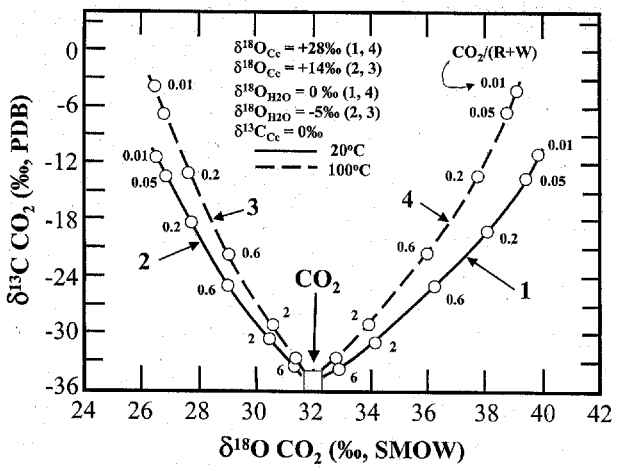

Fig. 2. Example results of mass-balance isotope-reaction modeling.

calcite + brine, examples of which are shown as open circles with their respective CO_2/calcite+H_2O oxygen and carbon mole ratios. These preliminary calculations indicate that by coupling the experimental partitioning data with measurements from real field tests, simple models may contribute to our understanding of how CO_2 migrates and what it encounters in the subsurface.

RESULTS: APPLIED GAS TRACERS

Tracer studies have become an important technique for *in situ* subsurface characterization, allowing detailed interrogation of complex systems, which have components moving, mixing, and reacting. Simultaneous injection of multiple tracers at different concentrations and frequencies can lead to a maximum retrieval of information on subsurface conditions relevant to the fate and transport of CO_2. This approach has been used successfully to isolate and in many cases quantify specific processes affecting transport, including: diffusion into low permeability materials, sorption, partitioning into non-aqueous phase liquids, partitioning into trapped gas phases, and biodegradation.

Design and Construction of a Flow System

We have selected a design for a flow-through column apparatus that will allow us to test the relative interactions of the gas tracers with a variety of reservoir materials and under a range of pressure and temperature conditions appropriate for proposed injection scenarios (Fig. 3). The apparatus was designed after the slim-tube equipment used by Dugstad et al. (1992, *Appl. Radiat. Isot.*, vol.43 [4], pp. 527–535), but has numerous improvements and increased capabilities. The system, currently nearing completion, is comprised of several features: (a) carrier gas and He reservoirs, (b) brine reservoir, (c) tracer gas injection volume, (d) gas homogenization reservoirs, (e) brine flow line, (f) sample loop, and (g) gas chromatograph. The design will allow for injection of brine and/or hydrocarbons to test tracer response at variable saturation over a range of temperatures (up to ~80°C) and pressures (up to ~300 bars) appropriate for proposed injection scenarios. It incorporates the capability for He-porosimitry, thus enabling porosity determinations. The flow columns can be easily replaced for series experiments with different substrates, and the column diameter and length can be easily varied. Currently, the sample coil is 20 feet long and is filled with Ottawa sand (20–30 mesh). Multiple flow paths have been incorporated into the design, allowing a second gas reservoir to be prepared for injection while the first is flowing. This will permit continuous injection of a given tracer mix or pulsed injections of different mixtures without disturbing the overall flow through the column.

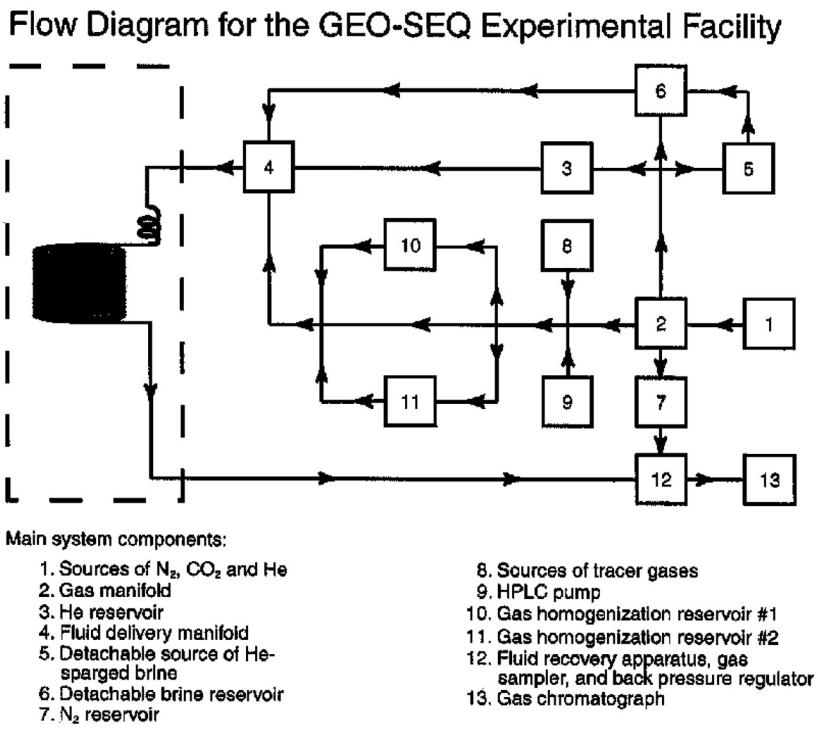

Fig. 3. Schematic drawing showing components of the flow column apparatus.

Development of gas tracer analytical protocols

On the analytical front, an effort has been underway to simultaneously detection 7 different co-injected tracers by gas chromatograph/electron capture detection (GC/ECD) analysis (see examples in Fig. 4): SF_6, perfluoromethylcyclopentane (PMCP), perfluoromethylcyclohexane (PMCH), and four different isomers of perfluorotrimethylcyclohexane (PTCH). Two other perfluorocarbon tracers (PFT) will also be experimentally tested: perfluorodimethylcyclobutane (PDCB), and perfluorodimethyl-cyclohexane (PDCH). Other researchers have used packed columns, molecular sieve columns, and capillary columns for chromatographic separation of PFTs and SF_6. After testing several GC columns and analysis protocols in order to obtain the optimal separation of the tracer peaks, we have chosen an $AlOH_2$ megabore capillary column and a temperature program that ramps from 120°C to 150°C. The advantage of capillary columns is sharper peaks and smaller retention times. Use of a megabore column (0.53-mm diameter) allows injection volumes of up to 5 ml, thus enhancing detection of low concentrations. Because of the high detection sensitivity of these gas tracers, small variations in analytical procedure, leakage, or increased background concentrations can result in large analytical errors. Some researchers have noted difficulty in reproducibility, with standard errors on the order of 20%. We have developed methods that significantly reduce the total standard error. Using these methods we conducted numerous

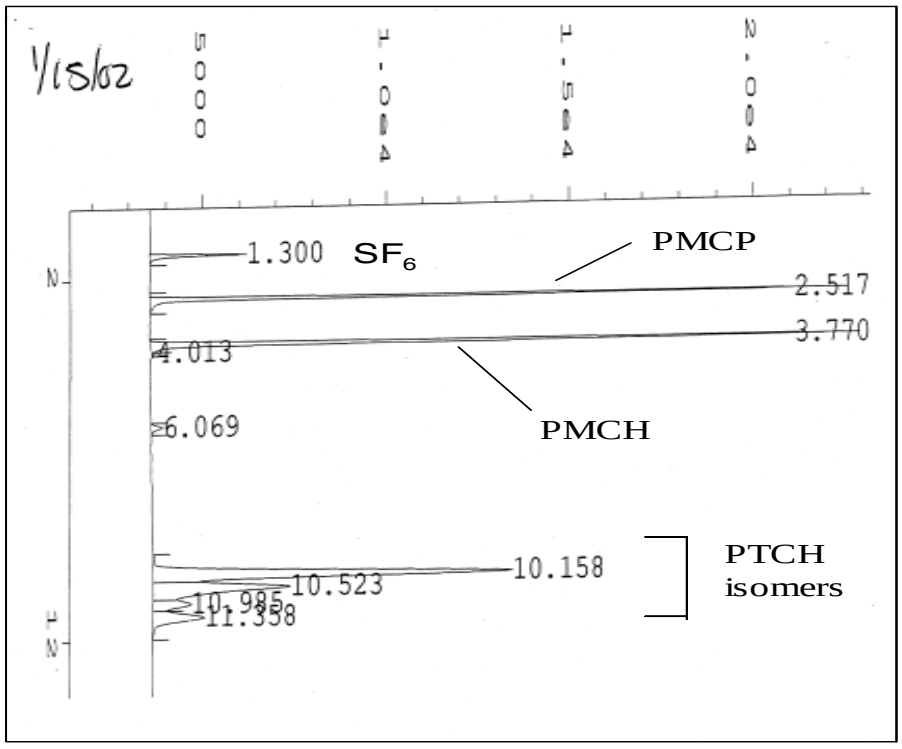

Fig. 4. Example gas chromatogram showing effective tracer separation and sharp peaks.

tests where 2–3 PFTs were co-injected leading to very stable concentration ratios of the tracers with standard errors on the order of 1%. This is important because it is changes in the concentration ratio of the co-injected tracers that we wish to resolve.

PRESENTATIONS AND PUBLICATIONS

Blencoe, J. G., Cole, D. R., Horita, J., and Moline, G. R. (2001). Experimental geochemical studies relevant to carbon sequestration. Proceedings of 1st National Conference on Carbon Sequestration, May 15–17, Washington, DC, 14 p.

Cole, D. R., Horita, J., and Riciputi, L. R. (2001). Fundamental studies of stable isotope exchange in systems relevant to energy utilization. 11th Annual V. M. Goldschmidt Conf., Hot Springs, VA, May 20–24, 2001.

Horita, J., Blencoe, J. G., and Cole, D. R. (2001). Fundamental geochemical research on long-term carbon sequestration in subsurface environments. AAPG Annual mtg., Denver, June 3–6, 2001.

*Cole, D. R. and Chakraborty, S. (2001). Rates and mechanisms of isotope exchange. In Stable Isotope Geochemistry, J. W. Valley and D. R. Cole, editors, Rev. in Mineralogy and Geochemistry, Vol. 43, 83–223.

*Chacko T, Cole D. R., and Horita, J. (2001). Equilibrium oxygen, hydrogen and carbon isotope fractionation factors applicable to geological systems. In Valley, J. W., and Cole, D. R. (eds.) Stable Isotope Chemistry, Rev in Mineralogy and Geochemistry, Vol. 43, 1–81.

*Valley, J. W. and Cole, D. R. [Editors] (2001). Stable Isotope Geochemistry. Reviews in Mineralogy and Geochemistry, Vol. 43, p. 662.

(*Partial funding also from the Geosciences Program, Office of Basic Energy Sciences.)

ENHANCING CARBON SEQUESTRATION AND RECLAMATION OF DEGRADED LANDS WITH FOSSIL-FUEL COMBUSTION BYPRODUCTS

Anthony V. Palumbo,[1] James E. Amonette,[2] J. Zhou,[1] F. Blaine Mettting,[2] W. Lee Daniels,[3] Kathryn Haering,[3] and Rattan Lal[4]

[1]Oak Ridge National Laboratory; [2]Pacific Northwest National Laboratory; [3]Virginia Tech; [4]Ohio State University

INTRODUCTION

This project examines the potential use of lands that have been disturbed by mining, highway construction, or poor management practices for terrestrial carbon sequestration. The approach includes examination of the effects of amendments with solid byproducts from fossil-fuel combustion, paper production, and biological waste-treatment facilities for enhancing carbon sequestration. The primary goal is to identify and quantify the key factors leading to successful C sequestration and reclamation of degraded lands and to communicate this information in the form of guidelines or other formats to the community. A scientific evaluation of existing field sites where amendments have been applied provides the basis for the guidelines. Results from the available literature are combined with additional new measurements of properties at these sites including (1) the extent and nature of the sequestered C, (2) microbial communities and their influence on greenhouse-gas emissions, and (3) redox, alkalinity, toxic metals, and key soil physical properties. Long-term field studies will also be designed and site(s) recommended for the demonstration and further optimization of this approach. Specific tasks focus on the accumulation of carbon in soil over time (including carbon sequestered in deep soil horizons) and the impact of environmental conditions on the rate of accumulation, assaying for populations of denitrifying bacteria that can effect emissions of greenhouse gases, comparing the results to DOE/CSiTE measurements, and evaluating management practices to optimize this sequestration strategy. Technology transfer workshops are employed to engage industry and create working partnerships. Project results will be summarized in a set of optimum site-management practices and practical guidelines which include policy and technical considerations.

BACKGROUND

The concern for the potential global change consequences of increasing atmospheric CO_2 has necessitated the development of mechanisms to reduce or stabilize atmospheric CO_2. During the next several decades, a program focused on terrestrial sequestration processes can make a significant contribution to abating the increase, and easing the transition to other renewable energy sources. Within this context, the restoration of degraded soils represents an opportunity to couple carbon sequestration with the utilization of fossil fuel and energy byproducts and other waste material (e.g., sludge, biosolids, mulch) while achieving ecological and aesthetic benefits for society in improved soil quality, biodiversity, and ecosystem services.

The goal of this project is to study the use of fossil fuel byproducts to foster carbon sequestration in degraded lands. This has the triple benefits of carbon storage, byproduct utilization and land reclamation. This research will be conducted in conjunction with the DOE Center for Research on Enhancing Carbon Sequestration in Terrestrial Ecosystems (CSiTE), which will allow DOE to leverage existing CSiTE activities by expanding its research and partnerships to degraded lands and the use of fossil energy by-products to stimulate carbon sequestration in those terrestrial ecosystems.

The potential of energy byproducts such as fly ash as soil amendments to enhance C sequestration in degraded lands can be most fully realized if these inorganic byproducts are applied in conjunction with organic amendments, including both mulch from biomass productivity, as well as process waste materials such as biosolids, and pulp and sludge from paper production. These organic amendments can have beneficial effects that complement and extend those of the inorganic flyash material, including:

- Organic matter can improve soil structure and moisture retention capacity of soil by sorbing to mineral surfaces and creating a more reactive network for water, air, and nutrient interactions in the soil and contributing additional pH buffering capacity.
- Organic matter can contribute directly and indirectly to soil fertility by releasing nutrient elements within the organic structure and acting as a metal-ion buffer in soil to make micronutrients available to plants.
- Organic matter can stabilize toxic metals in soil, thereby reducing their migration to groundwater and reducing their uptake and toxic effects in plants. Soil organic matter has been demonstrated to bind a variety of metals that are sometimes present in flyash and FGD byproducts, such as Zn, Ni, Pb, Cd, Cu, and B.

GOALS AND TECHNICAL APPROACH

The **goals of this project** encompass both scientific and technology transfer components:

Scientific Goal: Identify optimal selection and delivery strategies to maximize the contribution of amendments to carbon sequestration.

Technology Transfer Goal: Foster interactions between the scientific and user communities to maximize the application of new knowledge and approaches for enhancing terrestrial C sequestration through optimal utilization of fossil energy by-products and management of degraded lands.

Our **research strategy** to achieve the Scientific Goal of optimizing C sequestration has three parts.

1. *Evaluate Existing Experimental Sites:* Because of the diversity and extent of previous amendment studies and the long times needed to determine success or failure from a C-sequestration perspective, we are evaluating a number of existing sites where flyash and biosolids amendments have already been applied. These experimental sites were selected to represent different levels of amendments, different types of fly ash (alkaline and acid), and different ages since treatment. Data obtained from these experimental manipulations were not originally designed to explore the potential for C-sequestration, and we are supplementing existing information with additional measurements of key parameters such as the depth distribution and amounts and types of organic and inorganic C present, emission of greenhouse gases, and changes in nitrogen cycling microbial communities. This new information is being correlated with amendment treatment parameters and other soil properties to identify the most favorable (and detrimental) combinations of soils, fossil-fuel combustion byproducts, and management practices.
2. *Conduct Laboratory Experiments to Identify Key Amendment Types and Potential Management Strategies:* A limited set of laboratory experiments to assess the relative impacts of different environmental conditions such as wetting and drying cycles, oxidizing and reducing conditions, and specific amendments that enhance the accumulation of C by soils will be conducted. Experiments with model compounds and simple mineral amendments, as well as with degraded soils amended with coal combustion byproducts and other industrial sources of organic C will be performed. In addition we will examine the potential for release of other greenhouse gases as a result of the amendments in greenhouse scale studies. This work will focus on nitrous oxide

emissions as a result of nitrogen input via the amendments. The results of these bench-scale experiments will guide the design of field-scale experiments and help ensure their success.

3. *Design Field Experiments to Test and Demonstrate C Sequestration:* The third part of our strategy will be to design a limited set of experiments at one or two sites that focus on the deep incorporation of specific amendments (fly ash and FGD products, in combination with other sources of organic C such as biosolids, pulp and paper byproducts) to enhance sequestration of C. The(se) site(s) would be selected to represent typical degraded lands (e.g., mine reclamation sites, degraded agricultural lands) near existing coal combustion plants where transportation costs associated with application of coal-combustion byproducts and other amendments would be minimized. The results of this research would not be known for several years and would require support beyond the current proposed work to be fully successful.

Our strategy to achieve the *Technology Transfer* goal is currently focused on communication and is expanding to policy studies

1. *Communication*: The Regional Partnerships in Terrestrial Carbon Sequestration Workshop conference was sponsored by the U.S. Department of Energy and National Energy Technology Laboratory (NETL) along with The DOE Consortium for Research on Enhancing Carbon Sequestration in Terrestrial Ecosystems (CSiTE) on November 6-7, 2001 at the Radisson Plaza-Hotel in Lexington, KY. The purpose of the workshop was to bring the coal and utility industries together with, government, academia ,and other organizations to discuss offsetting carbon dioxide emissions by storing carbon in the vegetation and soils of degraded lands. The workshop format was hands-on, including breakout discussions, presentations, panel discussions, and a poster session. The workshop was an outgrowth of research being conducted by Oak Ridge and Pacific Northwest National Laboratories and their university research partners. This research will result in a set of practical site management guidelines for maximizing carbon sequestration on degraded lands and also designed to get stakeholder input in designing these guidelines. Presentations from the meeting and summaries of the breakout sessions can be found at: http://www.netl.doe.gov/publications/proceedings/01/carbon seq terr/cseq-terr01.html.
2 *Policy Studies:* The potential effectiveness and efficacy of combining carbon sequestration and mine land reclamation has yet to be assessed from ecological, economic, social, and institutional perspectives. This approach seeks to undertake a portion of this assessment, by focusing on economic, social, and institutional issues that must be addressed for the technical information to

be effectively applied. We envision a three-fold approach: (a) assessing the current situation in light of existing regulations and the values, goals, and positions taken by parties typically engaged in mine reclamation policy- and decision making; (b) developing realistic scenarios to analyze the potential for carbon sequestration on reclaimed land; and (c) proposing realistic mechanisms for promoting carbon sequestration on reclaimed land in ways that are likely to comply with regulations and have the potential to be acceptable (or, not highly objectionable) to involved constituency groups.

TECHNICAL PROGRESS

Depth Distribution of Soil Carbon

Samples were taken from sites in the east including West Virginia and Virginia (Lee Daniels) and from sites in the Midwest including several sites in Ohio (Rattan and Lal). Samples were analyzed at Va. Tech, Ohio State, and ORNL.

In the east, the mine soils sampled ranged in age from 19 years in the Controlled Placement (CP) experiment to 10 years old in the Powell River Sludge experiment (Areas PL and D). All mine soils described had well-developed horizonation with clear A horizons and moderately well developed transitional AC horizons. The AC horizons in several of the CP pedons contained moderate structure and could possibly warrant description as weak B horizons (Bw).

In the CP experiment, soils receiving high amounts of either biosolids or sawdust contained A horizons that were darker than the control soils, and/or contained AC horizons with “browner” coloration. Higher soil organic carbon was noted with biosolid treatments (Fig. 1), in addition only the control and the low biosolid treatments increased in % carbon over time in the A horizon. The wetter soil described in area D also exhibited distinct redoximorphic features due to what appears to be aquic soil conditions. Rooting was generally common to a depth of 35 to 50 cm in most soils observed, but was limited by densic (Cd) layers in

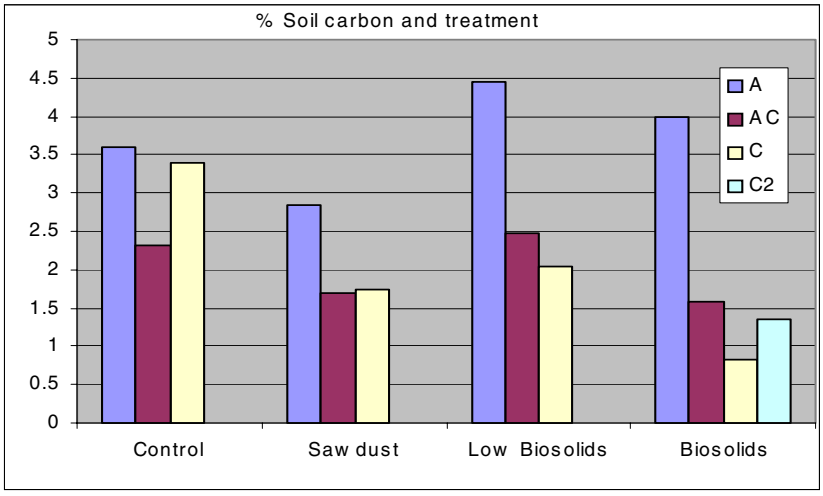

Fig. 1. CP (controlled placement) for organic amendments –19 years post treatment.

several pedons. When compared with earlier soil descriptions from these same experimental areas, the mine soils observed are clearly progressing down a pedogenic pathway of continued darkening of the AC horizon and overall strengthening of structure grade in their A horizons. As expected, these mine soils are very rocky, ranging from 40 to 80% coarse fragments in all horizons described. The fine earth fraction (<2 mm) is also relatively coarse with a sandy loam texture.

Powell River Biosolids (PRS) Project

Mine soil C levels in the PL experimental plots did not show a long-term effect of biosolids treatment on C levels in the surface soils (A horizon); however, deeper treated soil layers (AC horizon) do appear to be higher in organic C. The AC horizon was also considerably deeper and darker in color than that observed in the control treatment, possibly resulting in the development of deeper soil horizons due to the downward mobility of C. Localized soil wetness regime did not appear to lead to higher rates of C sequestration and retention in the pair of mine soils sampled in section D. However, the Cd horizon of the "wet" soil did appear to contain significantly more C to greater depths than the dry soil (Fig. 2).

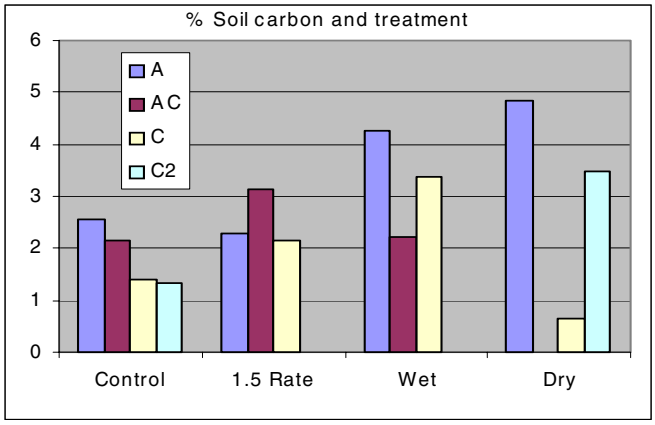

Fig. 2. PL and D areas 10 years post sludge treatment.

Controlled Overburden Placement (CP) Project

Soil organic matter levels in the CP experiment mine soils sampled show a clear effect of the 1982 treatment applications of biosolids. However, the soils receiving sawdust do not appear to differ in soil C levels from the untreated controls (Fig. 1). The data also reconfirm (via high apparent C levels in the C horizons) that Walkley-Black estimation of organic matter in these mine soils is subject to positive errors due to Fe and Mn oxidation.

Biosolid and FGD Amendments on Mine Soil in Ohio

The impact of mine soil reclamation on soil organic carbon and microbial biomass carbon content were assessed at a site near Dover, in eastern Ohio. There were three treatments: topsoil application, topsoil with FGD, topsoil with FGD and biosolids (manure). Soil samples were obtained seven year after

the application of reclamation treatments. Both total and microbial biomass carbon were greater in the manure plus FGD treatments. A high microbial biomass carbon content is an indication of improvement in soil quality leading to increase in agronomic productivity and environment moderation (filtration of water and biodegradation of pollutants).

Soil samples were also obtained from three additional reclaimed sites in south eastern Ohio. These sites are being analyzed for physical and chemical properties, such as bulk density and aggregation.

Microbial Analysis

Application of Fungal Ribosomal Analysis

Our preliminary studies of reclaimed mine sites and control plots have illustrated the relatively low diversity of the fugal community in surface soils. A total of 22 DNA samples extracted (Hurt, Qiu, et al. 2001) from soils were amplified using primers for 18S and 26S ribosomal RNA (rRNA) (Borneman and Hartin 2000). An initial diversity assessment was made using terminal restriction fragment analysis (TRF) with the PCR products. The PCR products were labeled with fluorescent primers and digested with four base cutter (e.g., HhaI, DpnII, MspI, and HaeIII). These digested products were run on a 3700 DNA analyzer for the fragment analysis. In this set, of 22 samples analyzed by RLFP, we found that there were relatively few fragments in the samples (Palumbo and Yang, unpubl. Data). We found (Fig. 3) that the number of fragments per sample (2–10) was significantly lower than has been seen from soil samples when bacteria targeted (e.g., Liu, Marsh et al. 1997). Our results showing relatively low diversity when compared to the bacterial community were also consistent with those of Borneman and Hartin (Borneman and Hartin 2000) who found only a total of 10 clones in two soil samples.

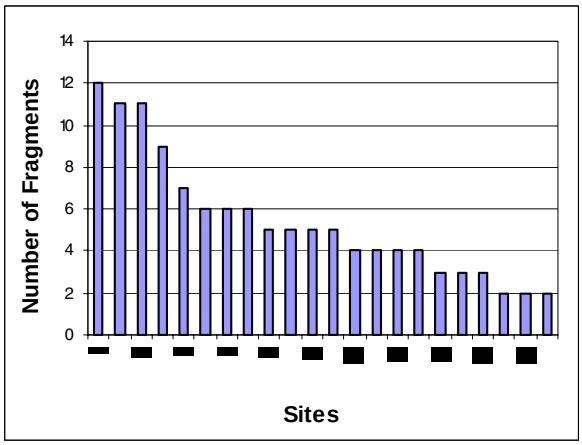

Fig. 3. Number of fragments in a sample at each site. Site data is ordered from the highest to lowest number of fragments.

The low diversity of the fungal community is also evident when comparing among samples (Fig. 4). Many of the fragments were found in multiple samples with the 2 most common samples found in more than 40% of the samples. In the Borneman and Hartin (Borneman and Hartin 2000) study 60% of the clones were in found in common between the two soils. Again this is in contrast to bacterial communities when finding any common genomic signatures among samples is unusual.

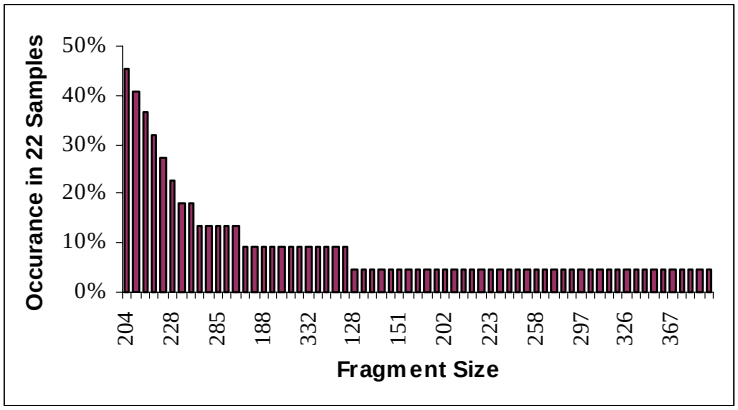

Fig. 4. Frequency of occurrence of specific fragments in the 22 samples. Representative fragment sizes are listed on the x axis.

Functional Analysis

In addition to phylogenetic data we are obtaining information about significant carbon cycling enzymes and metabolic processes. A total of 20 samples showed products using PCR amplification with primers designed for lignase. We cloned the PCR products from 8 samples and have stared sequencing of the products. Additional genes will be targeted including those for tyrosinase (a fungal phenol oxidase) that is being used in other tasks on the project. Extracted DNA will also be hybridized in a microarray format to give information on the diversity and quantity of enzymes that are involved in aerobic metabolism, denitrification, iron reduction, sulfate reduction, and methanogenesis.

Application of Innovative Carbon and Nitrogen Analysis Methods

The need for rapid analysis of both the soil quantity and quality is an essential part of determining the techniques of choice for measuring SOC. We have been testing the application of new methods for carbon analysis to mine soils. We are evaluating laser-induced breakdown spectroscopy (LIBS) in the determination of the total concentration of carbon and nitrogen in soils The primary focus to date has been on the variability associated with the technique when applied to mine soils. In the future, we will also examine electrochemical–surface enhanced Raman spectroscopy (Electro-SERS). There is potential for the LIBS method to become field instrument that can be used for in situ, real time monitoring of total carbon and nitrogen in soil.

Laboratory Assessment of Potential Amendment Technologies

Enhancement of organic C levels in degraded lands requires that the equilibrium between humic material formation and degradation processes be shifted substantially in the direction of formation. Our understanding of the specific chemistry involved suggests that the rate-limiting step of the "humification" reaction involves oxidative polymerization of phenolic compounds with other humic monomers such as benzoic and amino acids to form humates. This step is catalyzed by tyrosinase and related phenol-oxidase enzymes produced naturally by fungi. The focus of this portion of the project, then, has been to determine the optimal conditions under which this process occurs and to identify possible co-catalysts that either are already present in coal combustion byproducts (CCBs) or can be made more effective by judicious amendments with CCBs.

Preliminary work conducted as part of the CSiTE project demonstrated a synergetic effect of Mn oxides and, to a lesser extent, Fe oxides on the rate of the enzymatic humification reaction. These minerals are found in some CCBs, notably fly and bottom ashes, and thus offer some potential for use of these materials as amendments. A number of questions, however, remain as to the optimal conditions under which to apply these amendments, and our work in this portion of the project has focused on resolving these issues. In particular, we wished to separate the contributions of wetting and drying cycles from those associated with oxidizing and reducing cycles. Both types of cycles, as well as freezing and thawing cycles, occur in most temperature-zone surface soils, and to some extent can be controlled by site management (e.g., control of drainage, addition of reducing CCBs, etc.). In addition, physical properties such as porosity, the lengths of the individual cycles, and the numbers of cycles for a given amount of monomer added, are being studied.

We designed and constructed a test system that would allow us to vary the moisture content and oxygen content of soils independently while the humification reaction was occurring. We decided to tackle the problem in two stages. First we selected a set of model mineral phases including quartz, smectite (common clay mineral), Fe-coated smectite, Mn oxide, and a porous synthetic silica (Davisil). Various combinations of these materials were taken through one of three different treatment regimes: (1) "natural analog," involving wetting and drying under stagnant conditions and diffusive contact with air; (Fig. 5). (2) wetting and drying under strictly oxidizing conditions maintained by flowing air through the samples, and (3) oxidizing and reducing under continuously moist conditions. Three different treatment

Fig. 5. Natural analog samples, 35% RH, in fume hood.

cycles (i.e., wet/dry, or oxidizing/reducing) were also examined during the 8-week study including 1 treatment cycle with 2 weeks in the first part of the treatment regime (e.g., wet) and 6 weeks in the second part (e.g., dry), 2 treatment cycles consisting of two-weeks in each part of the treatment regime, and 4 treatment cycles in which each part of the regime lasted one week.

Based upon preliminary results, physical parameters such as microporosity are very important. Bentonite clay was effective when wetting/drying cycles occur, but was less effective under constantly wet conditions. With low C (>0.5%) additions, more wet/dry cycles yield better retention (Fig. 6), with higher C additions, no improvement with cycling was seen.

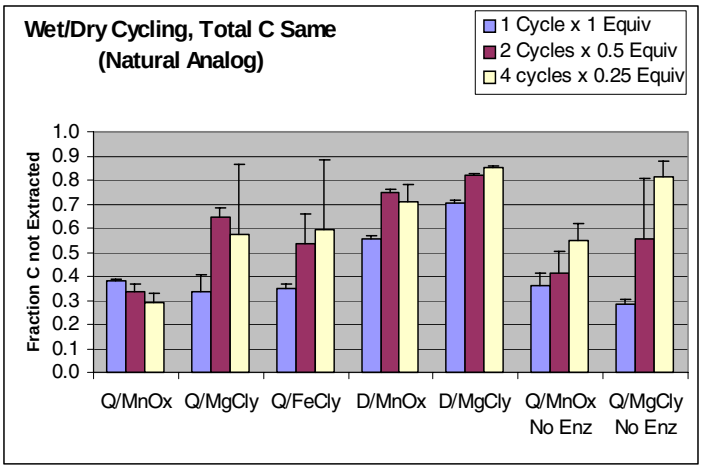

Fig. 6. Initial results: C "retention" assumes no loss to CO_2.

In the second stage of the experiment, the set of materials to be investigated will focus on CCBs and organic wastes (e.g., sawdust) in contact with a low-C soil from a degraded land site (Wise County, WV). The experimental plan calls for experiments with combinations of flyash/bottom ash or FGD sludge with sawdust in the presence of the low-C soil and will directly test the enhancing ability of these amendments under the optimal treatment regime(s) identified during the first stage. Some limited experimentation with Mn fertilization will also be performed.

REFERENCES

Borneman, J. and R. J. Hartin (2000). "PCR primers that amplify fungal rRNA genes from environmental samples." *Applied and Environmental Microbiology* **66**(10): 4356–4360.

Hurt, R. A., X. Y. Qiu, et al. (2001). "Simultaneous recovery of RNA and DNA from soils and sediments." *Applied and Environmental Microbiology* **67**(10): 4495–4503.

Liu, W. T., T. L. Marsh, et al. (1997). "Characterization of microbial diversity by determining terminal restriction fragment length polymorphisms of genes encoding 16S rRNA." *Applied and Environmental Microbiology* **63**(11): 4516–4522.

BIOMINERALIZATION FOR CARBON SEQUESTRATION

T. J. Phelps, R. J. Lauf, and Y. Roh
Oak Ridge National Laboratory

INTRODUCTION

The purpose of this research is to develop an understanding of the mechanisms by which iron-reducing and carbonate-precipitating microorganisms sequester carbon dioxide into solid carbonate mineral phases and to use this knowledge to design biological processes to capture carbon dioxide from fossil fuel plants while stabilizing fly ash wastes. This research will develop a scenario by which fly ash is stabilized into carbonate solid conglomerates that could potentially be useful as fill materials. We envision an open system, whereby ash collection ponds would be colonized with calcareous microorganisms capable of producing calcite, aragonite, and iron carbonates such as siderite. These carbonates would be formed in situ, at the surface by photosynthetic algae, and at depth by anaerobic carbonate producing bacteria. Results to date demonstrate that iron-reducing bacteria indeed convert CO_2 into sparingly soluble carbonate minerals such as calcite and siderite using metal containing fly ash and lime. Biological carbonate mineral formation using fly ash and lime materials indicated that bacteria may complement the capture of carbon dioxide from fossil fuel plants while potentially stabilizing fly ash wastes and bind the fly ash into solid materials. In essence, the proposed research adds a depth factor on the previous concepts of algal ponding. First, it would remove carbon from the atmosphere and immobilize it into a stable mineral phase. Second, it could turn waste ash into a product. Third, it could at the very least stabilize the ash to reduce the leaching of metals into the environment. Fourth, the process could be combined with a waste treatment strategy in which the carbonate forming microbes would use waste products from agriculture or food processing to supply energy for microbial growth. This would constitute energy plexing by combining multiple diverse waste streams into new products.

The proposed concept of ponds for the precipitation of low quality aggregates is an early example of energy-plexing; combining known diverse energy processes into a close-proximity constructive product line. We envision an energy-plex gaining advantage from alkaline ecosystems based on the algal ponds of the Great Salt Lake (GSL) during its low period of the 1970's. While the surface of the lake was algal rich there was complex biogeochemical processing occurring in the waters, facilitating the production of carbonate-rich deposits. We propose adding the carbonate precipitating aspects of high ionic strength microbial cultures with biogeochemically robust anaerobic microorganisms that precipitate carbonates in the water and sediments.

GOALS AND EXPERIMENTAL APPROACH

The objective of this research is to examine biogeochemically facilitated carbon sequestration processes using metal-rich fly ash in the presence of different atmospheres (N_2, N_2-CO_2, and H_2-CO_2) as well as in HCO_3^- buffered media (30–210 mM). Biological conversion of CO_2 into sparingly soluble carbonate minerals such as calcite ($CaCO_3$) and siderite ($FeCO_3$) has been studied using Fe(III)-reducing bacteria in conjunction with metal containing fly ash and lime. This coal utilization research will develop a scenario by which fly ash is stabilized into carbonate solid conglomerates that could potentially be useful as fill materials.

Psychrotolerant (NV-1, W3-7-1), mesophlic (BrY), and thermophilic (TOR-39, C1) Fe(III)-reducing bacteria were used to examine biogeochemical processes such as dissolution and mineralization using fly ash in the presence of N_2, N_2-CO_2, and H_2-CO_2 headspace gases, as well as in HCO_3^- buffered media (30–210 mM). In this study, we examined the microbial formation of carbonate minerals using thermophilic (*Thermoanaerobacter ethanolicus,* TOR-39) (Liu et al., 1997), mesophilic (*Shewanella alga,* BrY) (Rossello-Mora et al., 1994), and psychrotolerant (*Shewanella alga,* PV-4*; Shewanella pealeana,* W3-7-1) (Stapleton et al., 2002) bacteria (Table 1).

Table 1. Microbial isolates chosen for current and ongoing investigations at ORNL

Organisms	Source	Incubation temperature	Electron donors used for growth
TOR-39	Subsurface sediments	45–75°C, Thermophile	Glucose, Lactate, Formate
C1	Subsurface sediments	45–75°C, Thermophile	Glucose, Lactate, Pyruvate, H_2, Formate
BrY	Estuary sediments	25°C, Mesophile	Lactate, H_2, Formate
W3-6-1	Oceanic sediments	0–37°C, Psychrotolerant	Lactate, H_2, Formate
PV-4	Sea water near hydrothermal vent	0–37°C, Psychrotolerant	Lactate, H_2, Formate

Culture media contained the following ingredients (g/L): 2.5 $NaHCO_3$, 0.08 $CaCl_2 \cdot 2H_2O$, 1.0 NH_4Cl, 0.2 $MgCl_2 \cdot 6H_2O$, 10.0 NaCl, 7.2 HEPES, 1.0 resazurin (0.01%), 0.5 yeast extract, 10 ml of Oak Ridge National Laboratory (ORNL) trace minerals, and 1 ml ORNL vitamin solutions (Phelps et al., 1989). No reducing agents were added to media. Table 2 shows the Fe- and Ca-rich fly ashes and lime chosen for biologically facilitated precipitation of carbonate minerals for carbon sequestration. These Fe- and Ca-rich fly ashes were selected based on mineralogical and chemical characterization from several sources.

Table 2. Fly ash and lime currently investigated at ORNL

Material	pH	SiO_2	Al_2O_3	Fe_2O_3	CaO	MgO	Mineralogy
ORNL Steam Plant Ash, Oak Ridge, TN	7.7	34.4	19.1	15.2	1.8	0.4	Mullite ($Al_6Si_3O_{15}$), Quartz (SiO_2)
TVA Bull Run Ash, Oak Ridge, TN	6.4	48.1	24.4	8.4	1.6	0.9	Mullite ($Al_6Si_3O_{15}$), Quartz (SiO_2)
TVA Johnsonville Ash, Chattanooga, TN	8.4	44.9	20.9	24.7	2.5	1.1	Mullite ($Al_6Si_3O_{15}$), Maghemite (Fe_2O_3), Quartz (SiO_2)
Springerville Ash, Joseph city, AZ	11.4	45.9	19.1	2.9	15.0	0.9	Mullite ($Al_6Si_3O_{15}$), Portlandite [$Ca(OH)_2$], Quartz (SiO_2)
ORNL Inhouse Lime	11.7	8.9	1.5	0.7	44.8	22.9	Calcite ($CaCO_3$), Quartz (SiO_2)

The Fe(III)-reducing bacteria (Table 1) and metal-rich fly ashes (Table 2) were used to examine microbially facilitated precipitation and mineral formation in the presence of N_2, N_2-CO_2 (80% N_2-20% CO_2), and H_2-CO_2 (80% H_2/20% CO_2) headspace. Effect of bicarbonate buffer concentration (30–210 mM) on microbially facilitated precipitation and biomineralization with metal-rich fly ash was also examined using those Fe(III)-reducing bacteria. The pH of the medium with metal-rich fly was ash adjusted from 6.5 to 9.5. Hydrogen (100% or 80% H_2/20% CO_2), glucose (10 mM), or lactate (10 mM) served as an electron donor (Table 1).

Experiments were performed at 25°C for psychrotolerant cultures (W3-7-1, PV-4) and for the mesophilic culture (BrY), and at 60–65°C for the thermophilic culture (TOR-39, C1). Experiments were terminated after 30 days of incubation for the psychrotolerant and mesophilic bacteria and after 21 days for the thermophilic bacteria.

RESULTS AND CURRENT ACTIVITIES

Solution chemistry: Measurements of Eh and pH values were plotted (Fig. 1) on Eh-pH stability fields for hematite, magnetite, and siderite in the iron-water-CO_2 system at 25°C and 1 atm total pressure (Zhang et al, 1997). During the growth of the Fe(III)-reducing bacteria, pH decreased from 8.0 to 6.5 and Eh decreased from ~40 mV to –550 mV (Fig. 1). Microbial processes with lactate and fly ash under a higher bicarbonate buffer (140–210 mM) resulted in lower Eh values than microbial process with a lower bicarbonate buffer (30–70 mM) (Fig. 1), suggesting greater microbial reduction of Fe(III) in association with the increased bicarbonate buffering capacity.

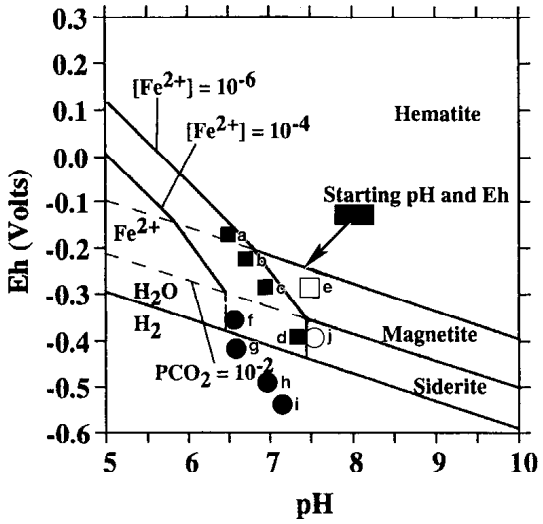

Fig. 1. Eh-pH stability fields for hematite, magnetite, and siderite in the water-iron-CO_2 system at 25°C and 1 atm total pressure (modified from Zhang et al., 1997). (a: 30 mM HCO_3^-, TOR-39; b: 70 mM HCO_3^-, TOR-39; c: 140 mM HCO_3^-,TOR-39; d: 210 mM HCO_3^-, TOR-39; e: Control; f: 30 mM HCO_3^-, g: 70 mM HCO_3^-; h: 140 mM HCO_3^-, i: 210 mM HCO_3^-; j: Control).

Similarly, the microbial utilization of hydrogen under a H_2-CO_2 atmosphere resulted in significantly lower Eh values (<–450 mV) than lactate utilization under a N_2 (~200 mV) and a N_2-CO_2 (~300 mV) atmosphere (data not shown), suggesting greater microbial reduction of Fe(III) in association with H_2 oxidation. The observation of microbial siderite and calcite formation using metal-rich fly ash in a higher bicarbonate buffer (210 mM) and under a H_2-CO_2 atmosphere was consistent with the Eh measurement. The presence of a H_2-CO_2 atmosphere and the high bicarbonate buffer (210 mM) provided more reducing conditions and significant buffering capacity allowing the complete reduction of Fe(III) in metal-rich fly ashes than did the N_2/N_2-CO_2 atmosphere and low bicarbonate buffer (30–140 mM). Thus, the Eh-pH diagram shows that carbonate minerals including calcite and siderite precipitation is likely facilitated by the microbial alternation of Eh conditions, pH conditions, or both and creating conditions of potentially localized supersaturation with respect to a mineral phase (Zhang et al., 1997).

Chemical analysis of water-soluble metals in the culture media after incubation revealed that the leaching of Ca and Fe from fly ash was significantly reduced in the presence of a H_2-CO_2 atmosphere (Fig. 2) and in HCO_3^- buffered media (>140 mM) (data not shown). This effect was likely a consequence

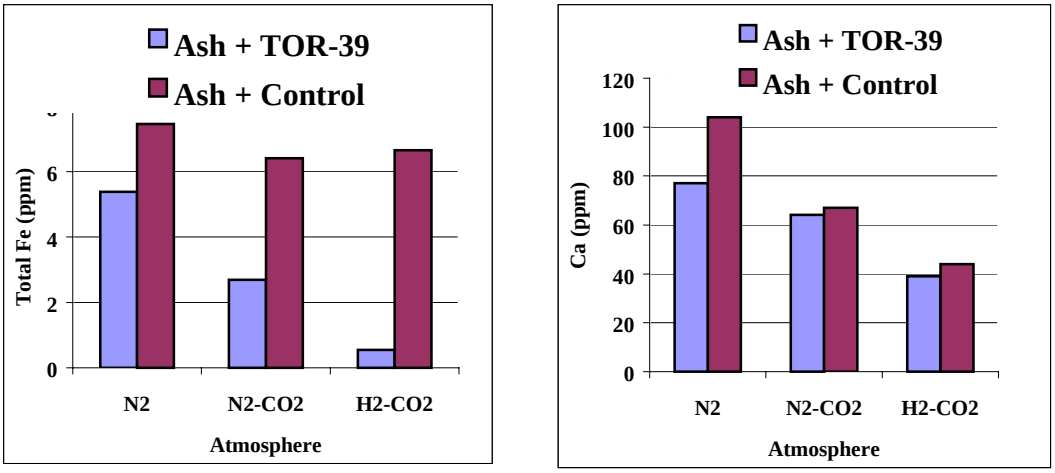

Fig. 2. Water soluble Ca and Fe after microbial precipitation and mineralization processes using fly ash (left: ORNL steam plant fly ash (95%) + lime (5%); right: Johnsonville fly ash).

of microbial metal reduction and the precipitation of carbonate minerals in the presence of appropriate electron donors such as hydrogen, lactate, and glucose.

Biomineralization under the different atmospheres and bicarbonate concentrations: XRD analysis showed that the Fe(III)-reducing bacteria precipitated calcium carbonate using Bull Run power plant fly ash (95%) with lime (5%) under a H_2-CO_2 atmosphere at 60°C incubation temperature (data not shown). SEM with EDX spectra showed that calcium carbonate precipitated by bacteria using fly ash and lime (Fig. 3). No carbonate minerals were formed using fly ash and lime without bacteria (Fig. 3). SEM and EDX analysis also showed that the Fe(III)-reducing bacteria facilitated the precipitation of calcite using Ca-rich Springerville fly ash (15%) under a H_2/CO_2 atmosphere and a high bicarbonate buffer (210 mM) (data not shown). The Fe(III)-reducing bacteria facilitated calcite precipitation using Ca-rich fly ash or Ca-poor fly ash plus lime under a H_2-CO_2 atmosphere and a high bicarbonate buffer (210 mM):

$$Ca(OH)_2(cr) => Ca(OH)_2(aq) + CO_2(aq) => CaCO_3(cr) + H_2O$$

XRD analysis showed that increased bicarbonate buffer (210 mM HCO_3^-) facilitated biomineralization of siderite using Fe-rich Johnsonville fly ash (25% Fe_2O_3) and ORNL steam plant ash (15% Fe_2O_3) under a N_2 atmosphere at 65°C. SEM with EDX spectra showed that microbially-facilitated precipitation of iron carbonate with the Fe-rich fly ashes under a H_2-CO_2 atmosphere (Fig. 4). In environments with high bicarbonate concentrations, the microbial production of Fe(II) from Fe-rich fly ash may stimulate siderite formation.

$$Fe^{2+} + HCO_3^- => FeCO_3 + H^+$$

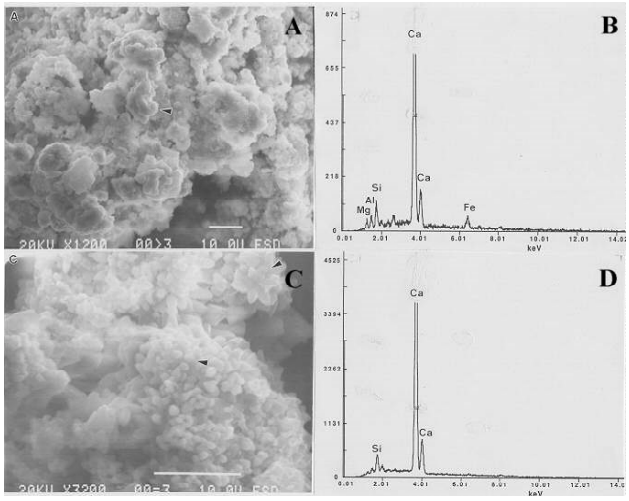

Fig. 3. SEM/EDX analysis of fly ash plus lime used for microbial precipitation of carbonate minerals under a H_2-CO_2 atmosphere (A and B: without bacteria; C and D: with bacteria).

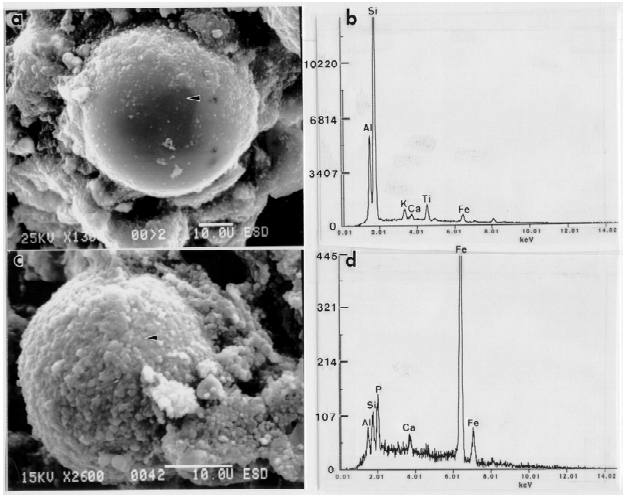

Fig. 4. SEM/EDX analysis of Johnsonville Fe-rich fly ash used for microbial precipitation of carbonate minerals using 210 mM bicarbonate buffer (A, B: with bacteria; C, D: without bacteria).

This study indicates that siderite and calcite precipitation using metal-rich fly ash lime is generally associated with the bacterial metabolism of organic matter and hydrogen coupled with microbial Fe(III) reduction in the presence of reducing environments and high bicarbonate buffer or a H_2/CO_2 atmosphere. High alkalinity and Fe(II) ions, as prompted by bacterial activity seem important to biologically facilitated precipitation of carbonate minerals such as calcite and siderite. The microbial production of Fe(II) and lower redox potential also stimulates siderite precipitation (Fredrickson, 1998).

The atmosphere and bicarbonate buffer concentration, in conjunction with biomineralization processes, exhibited profound influences on the types of minerals and the rate of carbonate mineral precipitation. Total carbon analysis of Ca-rich fly ash used for carbon sequestration showed that total carbon content in fly ash directly correlated with pCO_2 (Fig. 5). The capacity of Fe(III)-reducing bacteria to precipitate carbonate minerals, such as calcite and siderite, using metal-rich fly ash creates the possibility of more effective CO_2 sequestration than would be possible with photosynthetic systems in alkaline ponds. In addition to microbially facilitated precipitation of carbonate minerals using fly ashes, the microbial utilization of organic matter and hydrogen to produce sparingly soluble carbonate minerals may also contribute to direct or indirect precipitation of redox sensitive metals in fly ash ponds.

Scale-up experiments (1-L scale experiment) using thermophilic metal-reducing bacteria have proved successful at sequestering carbon while using Ca and Fe-rich fly ash (Fig. 6). Biomineralization processes for carbon sequestration dramatically reduced water soluble metals such as iron, calcium, and other metals under blankets of carbon dioxide. These upscaled experiments show potential for dramatic

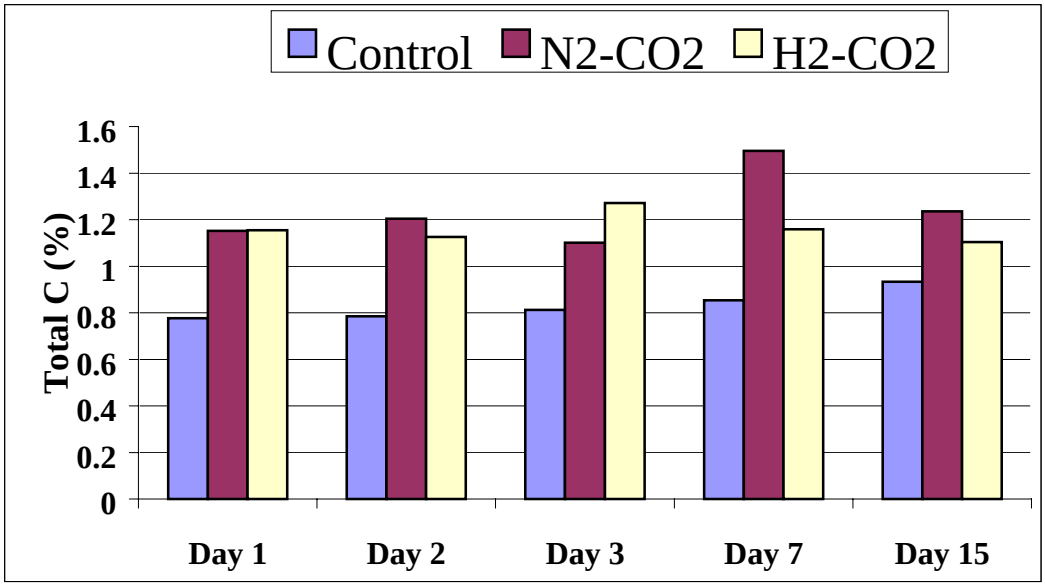

Fig. 5. Total carbon analysis of Ca-rich fly ash used for carbon sequestration in the presence of atmosphere (control) and 20% CO_2 (80% N_2-20% CO_2 and 80% H_2/20% CO_2) for 15 days incubation

Fig. 6. Scale-up carbon sequestration experiment using Ca-rich fly ash and Fe(III)-reducing bacteria (TOR-35) at 60°C (left 1-L bottle: with bacteria and right 1-L bottle: without bacteria).

improvements of carbon and metal sequestration by complementing existing fly-ash handling with biomineralization processes.

The capacity of iron-reducing bacteria to precipitate carbonate and metal containing minerals using fly ash creates the possibility of more effective CO_2 and metal sequestration than would be possible with

photosynthetic systems in alkaline ponds and far greater than current technologies. In environments with high bicarbonate concentrations, the microbial production of Fe(II) from Fe-rich fly ash may stimulate siderite formation. Ca-rich fly ash or lime facilitated the calcium carbonate crystallization by the organisms altering local Eh, pH, and nucleation conditions. Biological carbonate mineral formation using fly ash and lime materials indicated that bacteria may complement the capture of carbon dioxide from fossil fuel plants while potentially stabilizing fly ash wastes and solving red water problem in leachate from fly ash ponds. Interestingly, the results also suggest that many fly ash streams are less than saturated with respect to carbon dioxide. While biologically facilitated mineralization resulted in dramatic impacts, a significant portion of the total sequestration (30–60%) could be accomplished by saturating the fly ash waters with carbon dioxide. Future efforts will include discussions with TVA and the Paradise plant as to the potential utility of engineered upscaling of both biotic and abiotic mechanisms of increased carbon and metal sequestration in fly ash streams.

APPLICATION

Assuming significant upscaling issues a set of fly ash ponds, 8–10 m (25–30 ft) depth with residence times of weeks, may handle 10,000 tons of ash per day (ash from >40,000 tons of coal per day). One may sequester 1/3 of the approximately 20,000 tons of carbon dioxide bubbled through the ponds each day as some will surely escape. Sequestration mechanisms would include algal precipitation, anaerobic microbial sequestration, and abiotic geochemical precipitation. Enhancing the bio- and geo-chemical precipitation of carbonate minerals and carbon dioxide sequestration could assist meeting recently established energy efficiency goals. Accordingly, one could estimate sequestering a pound of carbon per cubic meter of pond each day. Such an efficiency would represent approximately 10% of the efficiency of our microbial cultures observed in the laboratory in the absence of significant abiotic geochemical precipitation. By circulating warm process waters and heating the deeper portions of the ponds to 30–45°C the biogeochemical carbon sequestration rates could increase. While most of the cost advantage represents offsets from disposal costs of fly ash the aggregate may have value as fill materials.

PUBLICATIONS

Roh, Y., T. J. Phelps, A. D. McMillan, C. Zhang, C. J. Rawn, R. J. Lauf, and J. Bai. 2001. Microbial Synthesis and the Characterization of Metal-Substituted Magnetites. Solid State Communications. 110:529–534.

Roh, Y., T. J. Phelps, A. D. McMillan, and R. J. Lauf. 2001. Utilization of Biomineralization Processes with Fly Ash for Carbon Sequestration. 1st Nat. Conference on Carbon Sequestration. http//www.netl.doe.gov/events/01conferences/carbseq/carbseq01.html.

Zhang C., J. Horita, D. R. Cole, J. Zhou, D. R. Lovley, and T. J. Phelps. 2001. Temperature-dependent oxygen and carbon isotope fractionations of biogenic siderite . Geochim. Cosmochim. Acta. 65:2257–2271.

Zhou, J. Z., S. Liu, B. C. Xia, C. L. Zhang, A. V. Palumbo, and T. J. Phelps. 2001. Molecular characterization of thermophilic ironreducing enrichment cultures from deep subsurface environments. J. Appl. Microbiol. 90:96–105.

Hazen, T., Y. Roh, and T. J. Phelps. 2002. Reducing Boron toxicity by microbial sequestration. DOE's J. Undergraduate Research (Manuscript in Press).

Roh, Y., R. D. Stapleton, C. Zhang, A. V. Palumbo, T. J. Phelps, M. Fields, and J. Zhou. 2002. Iron Reduction by Extremophiles: Geochemical and biotechnological implications. Book Chapter for: The Biogeochemicatry of Iron Cycling in the Environments. J. D. Coates and C. Zhang eds., Kluwer Academic Press (Manuscript in Press).

Roh, Y., C.-L. Zhang, H. Vali, R. J. Lauf, J. Zhou, and T. J. Phelps. 2002. Chemical and environmental factors on iron biomineralization: magnetite and siderite formation. Clays Clay Min. (Manuscript Submitted).

Roh, Y., G. Li, H. Huang, T. J. Phelps, and J. Zhou. 2002. Metal reduction and mineral formation by thermophilic Fe(III)-reducing bacteria from deep subsurface environments. Appl Environ Microbiol (Manuscript Submitted).

Roh, Y., T. J. Phelps, and R. J. Lauf. 2002. Carbon Sequestration Utilizing Ca-rich Coal Fly Ash (Manuscript in Preparation).

Roh, Y., T. J. Phelps, and R. J. Lauf. 2002. Utilization of Biomineralization Processes with Fly Ash for Carbon Sequestration (Manuscript in Preparation).

PENDING PATENT

Lauf, R. J., T. J. Phelps, C. Zhang, and Y. Roh. 2002. Mixed oxide nanoparticles and method of making. Patent Pending (U.S. Patent Application Serial No. 09/428,376). PATENT CLAIMS were allowed in October 2001.

REFERENCES

Fredrickson, J. K., Zachara, J. M., Kennedy, D. W., Dong, H., Onstott, T. C., Hinman, N. W., and Li, S., 1998. Biogenic iron mineralization accompanying the dissimilatory reduction of hydrous ferric oxide by a groundwater bacterium. Geochim Cosmochim Acta. 62:3239–3257.

Liu, S. V., Zhou, J., Zhang, C., Cole, D. R., Gajdarziska-Josifovska, P, and Phelps, T. J. 1997. Thermophilic Fe(III)-reducing bacteria from the deep subsurface: The evolutionary implications. Science. 277:1106–1109.

Phelps, T. J., Raione, E. G., White, D. C., and Fliermans, C. B. 1989. Microbial activity in deep subsurface environments. Geomicrobiology J. 7:79–91.

Rossello-Mora, R., Caccavo, F. Jr, Springer, N., Spring, N., Osterlehner, K., Shuler, D., Ludwig. W., Amann, R., and Schleifer, K. H. 1994, Isolation and taxonomic characterization of a halotolerant facultatively iron-reducing bacterium. Syst. Appl. Microbiol. 29:233–263.

Stapleton, R. D., Jr., Z. L. Sabree, A. V. Palumbo, C. Moyer, A. Devol, Y. Roh, and J. Zhou. 2002. Metabolic capabilities and distribution of *Shewanella* isolates from diverse marine environments. Limnology and Oceanography (Submitted).

Zhang, C., Liu, S., Phelps, T. J., Cole, D. R., Horita, J., Fortier, S. M., Elless, M., and Valley, J. W. 1997. Physiochemical, mineralogical, and isotopic characterization of magnetite iron oxides formed by thermohpilic bacteria. Geochim. Cosmochim. Acta. 61:4621–4632.

MESOSCALE CHARACTERIZATION OF NATURAL AND SYNTHETIC GAS HYDRATES

C. J. Rawn, B. C. Chakoumakos, A. J. Rondinone, M. J. Lance, and H. Wang
Oak Ridge National Laboratory

INTRODUCTION

Since the beginning of FY 2002 the project "Mesoscale Characterization of Natural and Synthetic Gas Hydrates" has focused on outfitting scientific instruments, already available at ORNL, with ancillary equipment to allow for the physical and chemical characterization of gas hydrates. This report highlights the instruments that have come online with ancillary equipment allowing for low temperature and/or high-pressure experiments. These extreme environments are necessary due to the conditions at which natural hydrates exist. Below outlines the progress to date assembling a high-pressure system for Raman experiments and modifying a laboratory x-ray diffractometer for low temperature experiments. Also discussed are initial low-temperature experiments using a hot disk analyzer and high-pressure diffraction experiments using a diamond anvil cell.

Some of the initial experiments have been conducted using structure I and structure II trimethylene oxide (TMO) clathrate hydrate samples synthesized at ORNL. TMO clathrate hydrate samples are stable at ambient pressure and moderately low temperatures and can be considered robust compared to other hydrates. TMO clathrate hydrates are particularly useful for gaining hands-on experience before attempting experiments with more exotic clathrate hydrates (e.g., naturally occurring samples) that have lower decomposition temperatures.

High-Pressure/Low Temperature Raman Scattering

In addition to the existing the low temperature stage and diamond anvil cell that can be used in conjunction with the Raman we have purchased a pressure cell (Fig. 1) where hydrates can be formed from water and gas. The gas booster, regulators, and flow meters have been assembled on to a mobile cart and the system has completed it safety review and is now ready to be tested.

X-ray Powder Diffraction Experiments

Low Temperature Laboratory X-ray Powder Diffraction Experiments

A laboratory x-ray diffractometer with a theta-theta goniometer has been modified with a closed-cycle He refrigeration unit, vacuum pumping station, and temperature controller. Cold samples have been successfully loaded and data has been collected as a function of temperature. Samples are loaded onto the

Fig. 1.

low temperature stage in a flowing He glove bag to prevent frosting (Fig. 2). The minimum temperature that can be obtained is approximately 10 K and the maximum temperature during loading can be kept under approximately 150 K.

Fig. 2.

The sample is located in a high vacuum environment where the possibility of volatilization could occur. Data were collected on a sample immediately loaded onto the sample stage then recollected after 24 hours to check for volatilization. The diffraction data showed no evidence that the sample was decomposing on the sample stage. This is an important observation and indicates that other hydrates can be studied under the vacuum conditions at low temperatures. Currently data is being collected on a mixed methane-ethane hydrate sample that has been in storage for several months. The diffraction pattern shows sII hydrate and ice are present. Data collection will be at several temperatures below 160 K to compare with previous thermal expansion results, obtained with neutron powder diffraction.

High Pressure Synchrotron Energy Dispersive X-ray Diffraction Experiments

A four-post Diamond Anvil Cell (DAC) (Fig. 3), has been purchased and the first set of high pressure experiments have been conducted at the National Synchrotron Light Source (NSLS) located at Brookhaven National Laboratory. TMO structure I and II were both successfully synthesized in the DAC at ambient temperature and with pressures above 2 GPa. Energy Dispersive Diffraction (EDD) data were collected on the TMO structure I at 3.32, 4.36, 6.61, and 10.09 GPa and on TMO structure II at 4 and 10.41 GPa. Due to a small sampling of crystals we were only able to find three reflections belonging to the TMO I phase. From the observed reflections the *a* lattice parameter was refined and a preliminary bulk modulus has been calculated.

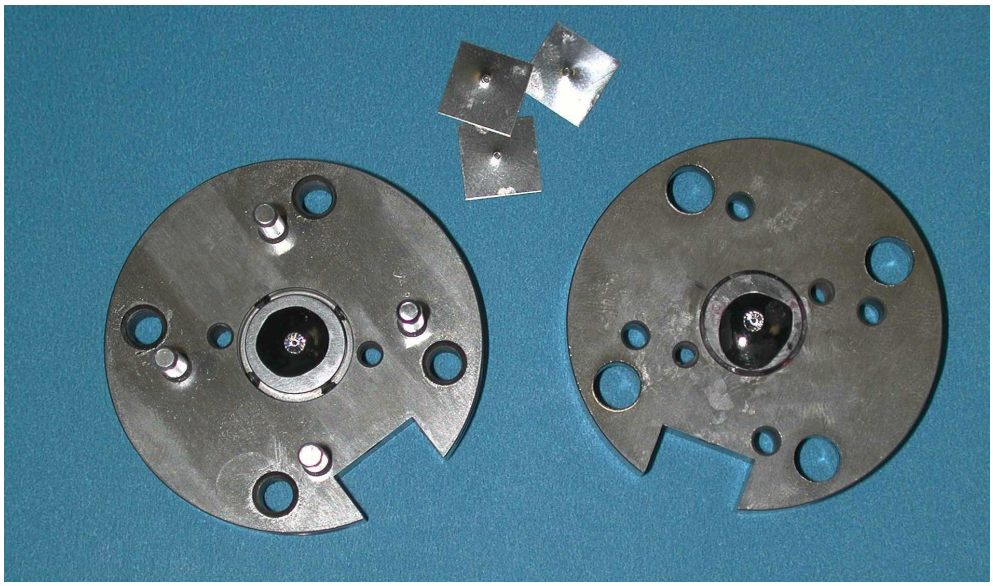

Fig. 3.

Thermal Transport Measurements

Thermal conductivity of ice has been measured using the Hot Disk method in preparation for future measurements on naturally occurring hydrates. Since ice resembles both the chemical composition and structure of hydrates, these measurements provide important background information and guidelines for handling extreme environment samples. One of the advantages of the Hot Disk method is it that offers non-destructive testing of hydrates leaving the samples undisturbed for additional property characterization.

With ice we have explored testing using both the double-sided and single-sided methods and the results are compared in the Table 1.

Table 1. Thermal conductivity of ice at –34°C

Double-sided method				
Test	1	2	3	Average
K (W/mK)	2.391	2.397	2.383	2.391
Single-sided method				
Ice 1 (W/mK)	2.469	2.408	2.397	2.425
Ice 2 (W/mK)	2.487	2.434	2.380	2.434

These results show good reproducibility and that the single-side method can be used to measure thermal conductivity of ice or hydrates. The double-sided method set-up is shown below.

Double-sided method

In the first test, we used the standard Hot Disk method in which two ice specimens were used and the Kapton sensor/heater was place between the two samples (Fig. 4). The test conditions were: 0.5 Watt and 10 seconds.

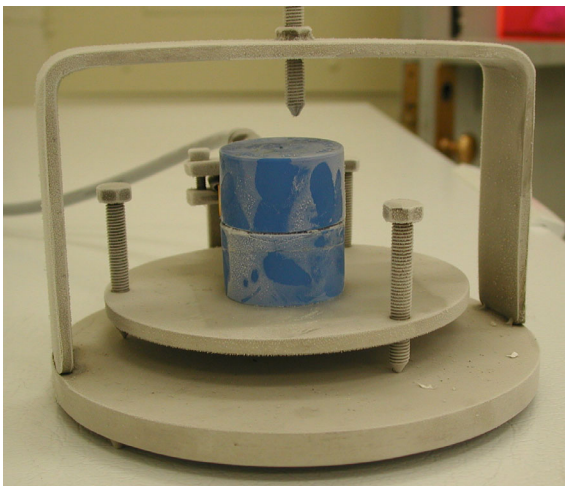

Fig. 4.

Single-side method

In this test, only one specimen is required. A backing material with known thermal conductivity and thermal diffusivity is used. We chose Styrofoam as backing material. The same test conditions were used for both the double-sided and single-sided methods

Obtaining Natural Samples

We are currently exploring the possibility of obtaining naturally occurring artic permafrost gas hydrates samples from the Mallik Core from Tom Mroz (NETL) and seafloor gas hydrate samples from the Gulf of Mexico from Dr. Roger Sassen (Deputy Director, Resource Geosciences at Texas A&M University).

ENVIRONMENTAL ANALYSIS SUPPORT

R. L. Miller
Oak Ridge National Laboratory

INTRODUCTION

Activities in environmental analysis support included assistance to the National Energy Technology Laboratory (NETL) at Morgantown and Pittsburgh in reviewing and preparing documents required by the National Environmental Policy Act (NEPA) for projects selected for the Clean Coal Technology (CCT) Program and for the Low Emission Boiler System (LEBS) Program. An important activity for the CCT Program was the preparation of an Environmental Impact Statement (EIS) for a project to demonstrate the integration of a direct ironmaking process with the production of electricity at Geneva Steel's existing plant in Vineyard, Utah. An important activity for the LEBS Program was the preparation of an EIS for integrated coal-fired technologies for electric power generation at the proof-of-concept scale adjacent to the Turris Coal Company's existing underground coal mine near Elkhart, Illinois.

ENVIRONMENTAL SUPPORT TO THE CLEAN COAL TECHNOLOGY PROGRAM

Work for the National Energy Technology Laboratory (NETL) during this period included the preparation of an Environmental Impact Statement (EIS) to evaluate the potential environmental effects associated with constructing and operating a project selected by DOE under the Clean Coal Technology (CCT) Program. The project would demonstrate the integration of a direct ironmaking process with the production of electricity using coal in an efficient and environmentally responsible manner. Direct ironmaking eliminates the intermediate step of producing coke from coal. The EIS will be used by DOE in making a decision on whether or not to provide cost-shared funding to design, construct, and demonstrate the HIsmelt (High Intensity smelting) technology proposed by the CPICOR Management Company at Geneva Steel's existing plant in Vineyard, Utah. CPICOR is an acronym for Clean Power from Integrated Coal/Ore Reduction. The site is located immediately west of Orem, Utah, about 5 miles northwest of Provo, Utah, and about 35 miles south-southeast of Salt Lake City. The proposed project would be demonstrated during a 2- to 4-year period starting in late 2004.

The overall objective of the project is to demonstrate the feasibility of the HIsmelt technology at a size large enough to allow the ironmaking industry to make decisions regarding commercialization of the technology. The new HIsmelt facility would use iron ore and coal to produce about 3,300 tons of molten

iron per day. Consequently, the existing blast furnace No. 3 would be placed in standby status (i.e., it would not operate whenever the HIsmelt facility is operating), while blast furnaces No. 1 and No. 2 would be available to continue in operation without modification. Offgas from the HIsmelt facility would be used as a fuel in the existing boilers to produce steam for in-plant use by Geneva Steel and to generate up to 300 MW of electricity using a combination of new and existing turbines. Not only would the electricity satisfy internal process needs at the Geneva Steel plant, but the remainder would be available for export to the existing power grid. The project is expected to provide Geneva Steel and offsite consumers with a low-cost, efficient, and environmentally sound source of additional electric generating capacity.

The HIsmelt technology produces molten iron directly from iron ore and coal in a single integrated operation, which eliminates the intermediate step of producing coke from coal. Iron ore, coal, fluxes (i.e., limestone, dolomite, lime, and/or dolime) and oxygen-enriched hot air are injected into a closed molten-bath reactor. The metal bath is the primary reaction medium in which carbon from the coal reduces iron ore to iron. The fluxes keep the materials molten in the reactor. Molten iron that collects in the bottom of the bath is continuously tapped from the reactor vessel to maintain a constant level of iron inside the vessel. Slag (the molten by-product generated from coal ash, fluxes, iron oxide, and other impurities) is tapped periodically and used to coat and control the internal cooling system and reduce heat loss.

The reactor vessel is aligned vertically in the HIsmelt technology. The coal is injected into the bath where carbon in the coal dissolves rapidly. The dissolved carbon reacts with oxygen from the injected iron ore to form carbon monoxide and iron. The high-temperature reactions release large quantities of buoyant coal gases (e.g., carbon monoxide and hydrogen) that create a large liquid fountain as they entrain and propel droplets of slag and molten iron upward into the post-combustion zone of the vessel. The result is strong mixing within the metal bath, which provides thermal uniformity. Because the iron reduction reaction in the molten bath is endothermic, additional heat must be generated and returned to the bath to sustain the reduction process and maintain an acceptable hot metal temperature. This additional heat is generated in the post-combustion zone by combusting the carbon monoxide and hydrogen released from the bath with oxygen-enriched hot air blast (2,200°F) that is injected down through piping from the top of the vessel. This reaction heats the metal and slag droplets in the post-combustion zone which, in turn, heat the bath after gravity returns them to the bath. Oxygen enrichment of the hot air blast increases the productivity of the process. Reacted gases, mainly nitrogen, carbon dioxide, carbon monoxide, hydrogen, and water vapor exit the vessel. After scrubbing the reacted gases, the cleaned gases can be combusted to generate electricity. The cleaned gases can also be used to pre-heat and partially pre-reduce the incoming iron ore.

The HIsmelt process possesses several advantages over conventional processes. Because it uses a high-temperature reactor vessel (up to 5,000°F) and eliminates the intermediate step of producing coke from coal, many of the air emissions and solid waste streams associated with traditional coke plant operations are eliminated. The high temperature breaks down and destroys hydrocarbons (e.g., toluene, benzene, and phenols) to minimize hazardous air pollutants typically emitted by coke ovens at temperatures less than 2,800°F. Because the high temperature of the reactor vessel exceeds the threshold for condensation of alkalis, problems in blast furnaces associated with alkaline iron ores and coals from the western United States are eliminated. The process is responsive to short-term operational problems because it can be shut down rapidly and easily restarted. Process efficiency is improved by capturing and recycling particulate matter.

Work on the EIS has included the initial evaluation of environmental issues that could result from construction and operation of the proposed project. During the scoping process at the beginning of work on the EIS, local residents were encouraged to express their concerns about potential effects. The issue of most concern was the potential impact to air quality from the proposed project's emissions. Other concerns that were expressed during the scoping process were the proposed project's use of coal; potential effects of the project on human health; potential impacts of the project on the water quality of the nearby Utah Lake; potential effects on wetlands; transportation, handling, and use of hazardous materials; issues associated with emergency preparedness and response; changes in the types and number of jobs associated with the proposed project; a possible decline in housing values; and potential visual impacts. The public input obtained during the scoping process was used to add to the list of issues requiring assessment. Issues are analyzed in the EIS in accordance with their level of importance. The most detailed analyses focus on issues associated with air quality impacts.

In addition to the proposed project, the no-action alternative (including two reasonably foreseeable scenarios) is being considered in the EIS. Under the no-action alternative, DOE would not provide funding to demonstrate the integration of the HIsmelt direct ironmaking process with the production of electricity. In the absence of DOE funding, there are two options that Geneva Steel could reasonably pursue: (1) Geneva Steel could continue to operate the blast furnaces without modification; and (2) Geneva Steel could modernize the existing blast furnaces to lessen the requirements for coke and install new cokemaking facilities with state-of-the-art pollution controls that are needed to comply with the National Emissions Standards for Hazardous Air Pollutants.

ENVIRONMENTAL SUPPORT TO THE LOW EMISSION BOILER SYSTEM PROGRAM

Work for the National Energy Technology Laboratory (NETL) during this period included the preparation of an Environmental Impact Statement (EIS) to evaluate the potential environmental effects associated with constructing and demonstrating a new coal-fired Low Emission Boiler System (LEBS) for electric power generation at the proof-of-concept scale. The EIS will be used by DOE in making a decision on whether or not to provide cost-shared funding to design, construct, and demonstrate the integrated technologies proposed by a team headed by D.B. Riley, a private sector participant in the LEBS Program. The goal of the LEBS Program is to provide the U.S. power industry with a reliable, economic, highly efficient, and environmentally preferred alternative to current coal utilization technologies.

The proposed project would demonstrate the technologies using a new 91-MW coal-fired power plant to be built adjacent to an existing underground coal mine owned and operated by Turris Coal Company, a member of the project team. The site is situated in central Illinois, about 2 miles southeast of the town of Elkhart and about 17 miles northeast of Springfield. The project would incorporate the following technologies: (1) a slagging combustor, which is U-shaped to increase the combustion reaction time; (2) low oxides of nitrogen (low-NO_x) burners, staged combustion, and coal reburning (injecting about 10–15% of the coal higher in the combustor) for NO_x control during combustion, in combination with a selective catalytic reduction (SCR) post-combustion NO_x control system; (3) a wet limestone scrubbing system for sulfur dioxide (SO_2) capture; and (4) an electrostatic precipitator for particulate removal from the flue gas. The technologies are expected to capture at least 96% of SO_2 emissions, decrease NO_x emissions by 85%, and remove 99.8% of particulate matter.

The proposed project would be demonstrated during a 6-month period in 2004. The facility would be fueled with coal from the adjacent mine, and electricity generated by the facility would be provided to the mine and to the local power grid. The captured SO_2 would be converted to commercial-grade gypsum, which would be marketed as feedstock for wallboard production. Bottom ash from coal combustion would be marketed for commercial applications such as a road base or construction material.

Potential impacts to environmental resources, including air quality, groundwater, and land availability, that could result from construction and operation of the proposed project were analyzed. Key findings include that emissions from the proposed facility would not exceed National Ambient Air Quality Standards (NAAQS) or Prevention of Significant Deterioration (PSD) increments. For the latter set of standards, the emissions would be less than 20% of the allowable degradation. The contribution of

emissions from the proposed facility to acidic deposition and to global climate change is expected to be negligible.

Initial results indicate that the aquifer may be capable of supporting the additional requirements of groundwater withdrawal during facility operation, but declines in groundwater levels may occur in nearby water supply wells, including the village of Elkhart municipal water well, located approximately 1 mile west of the proposed site. In addition, the relatively large additional consumption could degrade water quality in the aquifer, resulting in increased total dissolved solids, heavy metals, and dissolved minerals. However, the effects of drawdown and groundwater quality degradation can be mitigated somewhat by using multiple wells for groundwater withdrawal with sufficient separation from the village of Elkhart well. In addition, the use of field drainage runoff that passes through the Turris property is being pursued as a mitigation measure that could supplement groundwater withdrawal.

With the construction of a new coal combustion waste disposal area at the adjacent mine, sufficient disposal capacity would be available to accommodate all solid wastes generated by the proposed facility during its 30-year commercial operation, even if no bottom ash or gypsum were sold or used. If the proposed waste disposal area is not constructed, the Turris Coal Company would have other options to dispose of the material, including (1) reducing the current level of coal combustion ash received from offsite customers, and (2) transporting solid waste off the site to a permitted landfill.

Impacts to other resource areas would be minor. Flooding at the site is not anticipated, and floodplain encroachment would not occur. There are no significant wetland resources near the proposed site. No appreciable impacts on terrestrial or aquatic ecosystems are expected. There are no historic or archaeological resources known to occur on the project site. Construction and operation of the proposed facility are anticipated to have only minimal impacts on socioeconomic factors in the surrounding area, and no environmental justice impacts are expected. With respect to aesthetic resources, construction of the proposed project would produce slight short-term visual impacts, but visual characteristics would not differ appreciably over the long term from those at the site now. No appreciable impacts are expected with regard to noise, traffic, land use, and human health including worker safety.

A MULTI-PROPERTY VECTOR APPROACH TO ASSESSMENT OF DIESEL FUELS AND EMISSIONS IMPACTS

G. R. Hadder
Oak Ridge National Laboratory

INTRODUCTION

Multiple regression analysis is widely used for expressing the dependence of a response variable on several predictor variables. In spite of its evident success in many applications, multiple regression analysis can face serious difficulties when the predictor variables are to any appreciable extent covariant. Efforts to evaluate the separate effects of fuel variables on the emissions from heavy-duty diesel engines are often frustrated by the close association of fuel properties. Most heavy-duty diesel engine research has been conducted with test fuels concocted in the laboratory to vary selected fuel properties in isolation. While it might eliminate the confounding effect caused by naturally covarying fuel properties, this approach departs markedly from the real world, where reformulation of fuels to reduce emissions will naturally and inevitably lead to changes in a series of interrelated properties. To address these concerns, we have implemented an alternative approach to modeling the effects of fuel characteristics on emissions.

1. EIGENFUEL APPROACH

The alternative approach is based on the use of Principal Components Analysis to describe fuels in terms of vector quantities called *eigenfuels*. Each eigenfuel represents a unique and mathematically independent characteristic of diesel fuel, and the most important eigenfuels can be related to refinery processing and blending. When applied as predictors for emissions in regression analysis, eigenfuels have many advantages, including:

Simplification of the analysis, because the mathematical independence of eigenfuels eliminates correlations among the variables and the complications introduced by multi-collinearity.

Economy of representation, because a smaller number of such vector variables may effectively replace a larger number of original variables.

Greater understanding of the patterns of variation that are important to emissions, and how these patterns relate to refinery processing and blending.

New insight into the optimal economic formulation of fuels to reduce emissions, and improved experiment design for the estimation of fuels effects.

Knowing the extent of interdependence among fuel variables, we should not be surprised by the difficulty of selecting an "optimal" set of variables for a regression model. We may believe that natural cetane or density has an important influence on emissions, but either may be *nearly replaced* by a combination of other variables. Stepwise regression, a commonly used multiple regression analysis technique, searches through a sequence of differing model formulations to find one that is "optimum." With diesel fuel test data, there can be many different sets of variables that perform nearly as well as the one set ultimately chosen.

Figure 1 brings this point into focus. There are 4,095 different regression models that can be formed from twelve fuel properties, and these models form the universe among which stepwise regression searches. It will take all twelve properties to place a model at the very end of the curve. Forty-five different models populate the last 0.02 in R^2, and these models typically involve 7–9 fuel property variables. The coefficients of the fuel property variables can be significantly different among these models, leading to uncertainty about their relative importance in testing and in the cost-effective blending

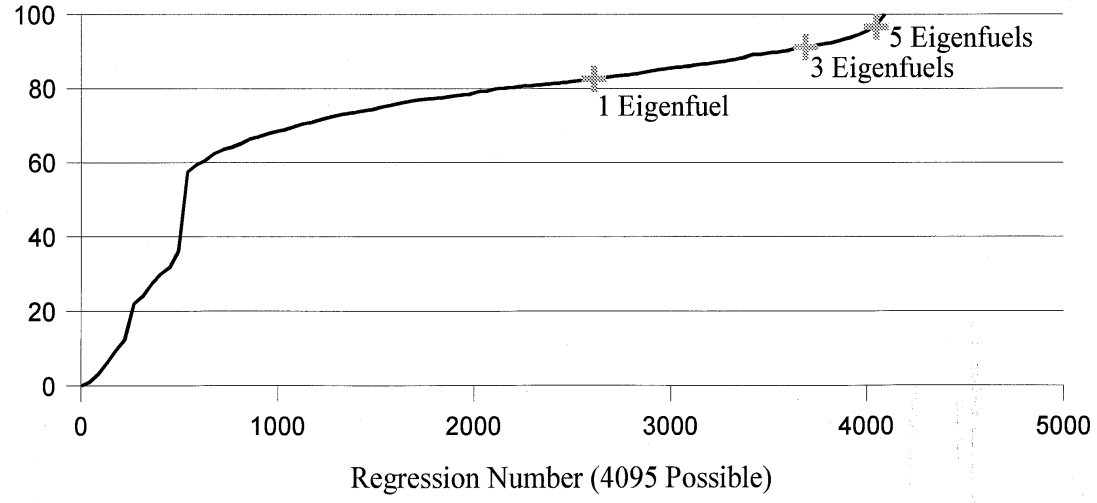

Fig. 1. Comparative Performance of Regression Models (based on twelve fuel properties)

of refinery stocks. However, models based on a small number of eigenfuels perform well, with five eigenfuels explaining nearly 97 percent of the fuels-related variance in NO_x. The eigenfuel coefficients are unambiguous and theoretically correct for test designs and for cost-effective blending of refinery stocks.

2. CONCLUSIONS

A database of heavy-duty diesel engine testing was compiled from the literature and used to demonstrate the eigenfuel methodology, recognizing that the existing data are inadequate to answer fully the many questions related to the effect of fuels on emissions. Within this limitation, we find that the eigenfuel approach leads to new perspectives on diesel fuel-emissions relationships:

Fuel properties are only surrogate variables for underlying causal factors. Much of the emissions reduction seen in past testing comes from reducing highly aromatic cracked stocks in diesel fuel. Because these stocks are low in cetane number and high in density, researchers have tended to attribute the emissions reductions to the increase in cetane number or reduction in density associated with their removal, rather than to the compositional change itself.

How one varies a fuel property can be the most important factor in determining the emissions response. A given fuel property can be changed in many ways, and a unit change in that property can produce markedly different effects on emissions depending on how that change is introduced.

Past studies may understate the impacts of fuels on emissions. If density is varied in several ways—one of which has a strong effect on emissions and the others not all—a study will tend to see only the average, diluted effect.

The eigenfuel approach provides new ways to design test fuels that are far more likely to be representative of future fuels that will be produced in refineries, compared to fuels blended in an effort to vary selected properties independently. These test fuels will express the natural correlations among fuels properties. While these correlations would be confounding factors in conventional analysis, they can be exploited in eigenfuel analysis.

3. PUBLICATIONS

H. T. McAdams, R. W. Crawford, G. R. Hadder. 2000. “A Vector Approach to Regression Analysis and Its Application to Heavy-Duty Diesel Emissions,” SAE 2000-01-1961, Society of Automotive Engineers International Spring Fuels & Lubricants Meeting & Exposition, Paris, France, June 19–22.

H. T. McAdams, R. W. Crawford, G. R. Hadder. 2000. *A Vector Approach to Regression Analysis and Its Application to Heavy-Duty Diesel Emissions*, ORNL/TM-2000/5, Oak Ridge National Laboratory, Oak Ridge, TN 37831, November.

H. T. McAdams, R. W. Crawford, G. R. Hadder. 2002. *PCR+in Diesel Fuels and Emissions Research*, ORNL/TM-2002-16, Oak Ridge National Laboratory, Oak Ridge, TN 37831, March.

CLEAN ENERGY TECHNOLOGY EXPORTS (CETE) PROGRAM ASSISTANCE

T. J. Wilbanks
Oak Ridge National Laboratory

INTRODUCTION

The FY 2001 Report of the U.S. Senate Appropriations Committee on the Energy and Water Development Bill directed that an interagency working group be formed, jointly chaired by the Departments of Energy (DOE) and Commerce (DOC) and the United States Agency for International Development (USAID). This interagency workgroup would be responsible for improving the Federal government's role in promoting exports of clean energy technologies. Other agencies represented on the workgroup include the Departments of State and Treasury, the Environmental Protection Agency (EPA), the Export-Import Bank (Ex-Im), the Overseas Private Investment Corporation (OPIC), and the Trade and Development Agency (TDA). The Senate report requested that a five-year strategic plan be prepared for a clean energy technology exports (CETE) program, as well as calling for subsequent annual reports.

ORNL is assisting the DOE Offices of Energy Efficiency and Renewable Energy; Policy and International Affairs; Fossil Energy; Nuclear Energy, Science and Technology; and Congressional and Intergovernmental Affairs in planning and coordinating DOE's contributions to the interagency Clean Energy Technology Exports (CETE) program. ORNL roles include drafting and assisting in revising the five-year strategic plan for the CETE program; assisting with initial implementation steps, which may include responsibilities for specific activities; and assisting with the design of the CETE performance evaluation approach.

This project supports a program (CETE) that is still only at a strategic planning stage, with FY 2003 and out-year funding uncertain. It anticipates that, as FY 2003 program directions are clarified, ORNL will receive funding as appropriate from FE and other offices.

Supported in part by funds from FE, ORNL has developed and submitted for interagency review six drafts of the Strategic Plan, along with frequent revisions and technical assistance, and organized an off-site meeting for the agency representatives on August 31, 2001. The final draft was submitted on February 27, 2002; and the Strategic Plan was submitted by the CETE Working Group to Congress in April 2002.

BIOGEOCHEMICAL REMEDIATION OF AMMONIA DISCHARGES FROM POWER PLANTS

T. J. Phelps, R. J. Lauf, and Y. Roh
Oak Ridge National Laboratory

INTRODUCTION

Coal fired electrical generation plants often add a process for Selective Catalytic Reduction (SCR) to reduce NOx emissions. By reacting NOx with ammonia across an SCR the NOx becomes chemically reduced to less toxic emissions. Unfortunately, excess ammonia is required to drive the catalytic reaction and that excess ammonia becomes a liquid effluent added to the fly ash slurry discharged to the ash ponds. There is inevitably a small amount of the unreacted ammonia that is thereby placed into the wastewater fly ash slurry system. It is imperative that the ammonia be removed from the waters before discharge into local streams because even a ppm ammonia concentration may be toxic to fish, at times resulting in rapid death of fish passing through an ammonia plume.

During warm weather nitrifying bacteria can proliferate in the fly ash slurry ponds and these nitrifying are likely capable of detoxifying ammonia to nitrogen gas or even nitrate, akin to the biologic processes in an aquariums that removes ammonia. However, known denitrifying bacteria are slow growers and are relatively poor at removing ammonia in cooler waters typical of winters. As power plants upgrade they are often adding these SCR NOx scrubbing systems and the dearth of information on the biogeochemistry of ammonia interactions with cold waters or with fly ash discharges led to the forging of expertise between ORNL, TVA, and the University of Tennessee in the areas of geochemistry, geology, materials sciences, microbial ecology and electrochemistry.

The purpose of this project is to gain an understanding of biogeochemical processes that may affect and/or attenuate ammonia concentrations in fly ash slurries and developing procedures to insure that toxic levels of ammonia are not discharged into area waterways. Importantly, the goal of the TVA and ORNL collaborations is to develop processes that are capable of mitigating ammonia discharges from ash ponds and related aqueous streams associated with ammonia inputs from coal use. The implementation of the Selective Catalytic Reduction process that removes NOx and SOx from flue effluents dictates that the disposition of related waste streams not adversely affect other ecosystem components. The need for this research is because power plant effluents of even 1 ppm can rapidly kill fish in streams and we need to understand biogeochemical determinants of the ammonia disposition under varied physical, chemical, climatic or flow regimes.

GOALS AND EXPERIMENTAL APPROACH

Our recently initiated research is focusing on ammonia containing fly ash slurry streams at an ammonia test facility, (FoSCR) Pilot Test Ponds at Tennessee Valley Authority's Paradise Fossil Plant located near Paradise, Kentucky. This research is closely linked with TVA and their Paradise generation plant. After several meetings with TVA personnel, a shared literature review and a review of previous TVA data we embarked on a field endeavor to track ammonia and its biogeochemical interactions during the testing of ammonia discharges at the Paradise plant.

For this project, we sampled 6 fly ash sediments and 14 water samples within 2 pilot ponds at the Paradise Fossil Plant, Kentucky to gain an understanding of ammonia removal mechanisms in fly ash ponds as well as to identify and characterize promising cultures and ammonia capture processes in ash-containing waters and sediments. Samples included both water and fly ash sediments at various locations within the ponds, during intentional additions of ammonia. The intentional injection of ammonia was to simulate the downstream effects of selective catalytic reduction to control NOx emissions.

RESULTS AND CURRENT ACTIVITIES

Chemical analysis of pond water (Table 1) showed that ammonia is likely being removed and/or precipitated with fly ash sediments in the pilot fly ash ponds. TVA data concur that they are accounting for less than 25% of the ammonia in mass balances. While it is convenient to suggest that the lost ammonia is due to biology, the fact that it occurred within hours of disposition into pond waters, during cold climates, and within days of the restart of ammonia injection further heightens our speculation that ammonia is unaccounted for within the system. The ammonia added to the pond water may be precipitated with metals (i.e., Na, K, Ca, K and others) in the fly ash sediments. Further analyses of fixed ammonia are required to understand ammonia removal/disposition in the fly ash ponds. We are currently focusing efforts on more stringent ammonia extraction procedures for ash samples and for the bottom sediment of pond 1. This sample shows evidence of nitrogen in the samples, and we hope that with a strong sulfuric acid pre-extraction that we can recover ammonia tightly bound with or precipitated onto the fly ash solids.

The pH values of the pond water were alkaline, ranging between 7.59 and 12.2. The source of alkalinity in the pond water with fly ash sediments is thought to be from the high content of Ca in the sediment slurries at NH_4 injection point, and bottom sediments in pond 1 (Table 2). The high Ca concentrations in the pond water with fly ash sediments are thought to be from the easily soluble sublimates on the ash particle surface. This might be attributed to the presence of Ca-solubility controlling phases such as gypsum or anhydrite (Table 3).

Table 1. Chemical composition of water samples collected at Paradise fossil plant

Sample	pH	NH_4-N (ppb)	Nitrate-N (ppb)	Ca (ppm)	Na (ppm)	Mg (ppm)	Fe (ppm)	Si (ppm)
Water, FGD Water Stream	7.67	98	11,424	641	52.2	172	3.32	10.8
Water + Sediment FGD Unit 2 End of Sluice Pipe	7.59	100	13,177	762	27.7	164	4.04	12.7
Water + Sediment Upstream of NH_4 injection	10.95	632	4,898	1,161	112	0.2	14.1	0.56
Water Upstream of NH_4 injection	9.35	32	4,097	84.7	10.6	9.3	0.49	2.89
Water Pond 1-End of Pipe	9.44	2,001	5,506	78.4	10.4	9.0	0.49	2.62
Water Pond 1-Pond Edge	9.5	1,230	5,765	82.4	10.8	9.4	0.49	3.14
Water + Sediment Pond 1–Ash Delta	12.2	2,440	5,803	123	16.2	0.02	0.81	1.76
Water + Sediment Pond 1 Bottom Sediment	11.86	1,571	4,924	1,104	110	0.3	9.1	1.83
Water Pond 1 Water Station A	8.88	927	3,594	123	16.8	24.0	0.73	4.81
Water Pond 2-End of Pipe	9.45	2,244	5,264	79.7	10.7	9.1	0.49	2.14
Water Pond 2-Pond Edge	9.51	2,778	4,228	87	11.7	9.4	0.543	2.0
Water + Sediment Pond 2-Surface Sediment	ND*	3,278	6,526	ND*	ND	ND	ND	ND
Water + Sediment Pond 2-Dike	ND	1,807	5,192	ND	ND	ND	ND	ND
Water Pond 2-Water Station A	8.85	1,340	4,451	114	15.9	21.1	0.68	5.05

*ND, Not determined.

Tables 2 and 3 show geochemical and mineralogical analyses of fly ash sediments collected at various points within the FoSCR Pilot Test Ponds. Concentration of CaO was higher (28.2%) for the flue gas desulfurization (FGD) unit sediments whereas SiO_2 (41.7–45.1%), Al_2O_3 (18.3–18.7 %), and Fe_2O_3 (12.8–13.2%) were respective percentages. Fly ash sediments from coal combustion at the site comprise a mixture of crystalline and amorphous oxides. XRD analysis showed that crystalline phase of FGD unit sediments differs from that of other fly ash sediments within ponds. Crystalline mineral of FGD sediment is mainly gypsum ($CaSO_4 \bullet H_2O$). Other fly ash sediments mainly consisted of mullite, quartz and silicon.

Table 2. Geochemical analysis of fly ash sediments from ash ponds at the TVA Paradise fossil plant

Sample	SiO_2	Al_2O_3	Fe_2O_3	MnO	MgO	CaO	Na_2O	K_2O	TiO_2	P_2O_5
					%					
Sediment FGD Unit 2 End of Sluice Pipe	10.83	4.32	5.16	0.011	1.29	28.19	0.19	0.69	0.292	0.06
Sediment Upstream of NH_4 injection	45.13	18.70	17.20	0.028	2.43	9.74	1.13	1.83	1.293	0.61
Sediment Pond 1–Ash Delta	45.03	18.61	12.82	0.028	2.71	12.82	1.40	1.39	1.284	0.52
Sediment Pond 1 Bottom Sediment	41.68	18.32	13.35	0.025	3.02	13.47	1.48	1.37	1.324	0.56
Sediment Pond 2-Surface Sediment	44.01	18.60	13.38	0.027	2.90	13.38	1.42	1.42	1.309	0.54
Sediment Pond 2-Dike	41.87	18.74	13.05	0.023	3.17	14.13	1.48	1.39	1.369	0.58

*ND, not determined.

Table 3. Geochemical and mineralogical analysis of fly ash sediments from Paradise fossil plants

Sample	Total C (%)	Total N (%)	Mineralogy	Exchangeable NH_4-N (2M KCl extractable)	Exchangeable Nitrate-N (2M KCl extractable)
Sediment FGD Unit 2 End of Sluice Pipe	1.521	BD*	Gypsum	462 ppb	2,287 ppb
Sediment Upstream of NH_4 injection	1.146	0.008	Quartz, Mullite, Silicon	279 ppb	3,949 ppb
Sediment Pond 1–Ash Delta	0.494	BD	Quartz, Mullite, Silicon	224 ppb	2,467 ppb
Sediment Pond 1 Bottom Sediment	2.055	0.013	Quartz, Mullite, Silicon	259 ppb	2,414 ppb
Sediment Pond 2-Surface Sediment	0.463	BD	Quartz, Mullite, Silicon	247 ppb	2,261 ppb
Sediment Pond 2-Dike	0.713	0.002	Quartz, Mullite, Silicon	241 ppb	1,361 ppb

*BD, Below detection limit.

Fly ash samples were analyzed to determine the concentration of carbon and nitrogen (Table 3). Large amounts of carbon (0.5–2%) were captured within fly ash sediments. This study indicates that fly ash can be utilized to sequester CO_2 from flue gas by reacting it with alkali metal oxide in the fly ash ponds (i.e., $Na_2O + CO_2 \rightarrow Na_2CO_2$; $Ca(OH)_2 + CO_2 \rightarrow CaCO_3$).

These results and results of previous TVA tests indicate a phenomenal ammonia loss in short distances and time that though previously attributed to warm climate ammonia oxidizing microorganisms is likely too rapid in the cool weather sampling we are investigating. While impacts of biology would certainly be welcome, it is imperative to get a better closure on the ammonia mass balance and laboratory tests are being conducted to evaluate ammonia precipitation with the Paradise materials. Consideration of relevant thermodynamic and kinetic principles are needed to develop a conceptual design of a method to intentionally increase the sequestration of CO_2 at the power plants, quantify the amount of CO_2 captured, accomplish mass balances of ammonia and ascertain the disposition of ammonia and any of it breakdown products or dominant precipitation products.

Analytical method for quantifying and determining fixed versus soluble ammonium in the fly ash sediments and slurries will be developed/implemented to ascertain a mass balance of ammonia. This is imperative for any understanding and ascertaining the mass flux of ammonia. Understanding and implementing ammonia removal mechanisms in fly ash ponds and would greatly complement TVA efforts as they have yet to account for the ammonia inputs. We will pursue the characterization of nitrifying microbial cultures from the ash ponds to see if they are accounting for the ammonia loss. Bench-scale studies will be performed to develop strategies for and understandings of ammonia removal and carbon sequestration using fly ash collected from the two pilot ponds at Paradise fossil plant.

APPLICATION

In collaboration with TVA we will pursue completing a mass balance for ammonia additions/losses/disposition into and from fly ash slurry systems. Current mass balances of 20–50% are insufficient for understanding, ascertaining or implementing ammonia control strategies be they biological or engineering based control systems. Importantly, we will scrutinize the impacts of ash, time, distance and flux of ammonia in the fly ash processing pond systems using closed headspace laboratory tests and relate those laboratory tests to field studies. We will complete the first phase of the characterization nitrifying cultures from the ash ponds to see if microbial processes are accounting for a significant portion of the ammonia loss with seasons. Bench-scale studies will be performed to develop strategies of ammonia removal and carbon sequestration using fly ash collected from the two pilot ponds at the Paradise fossil plant. By combining interdisciplinary approaches with industry and research expertise we will determine the pathways and critical variables affecting ammonia disposition in fly ash slurries that will enable development of process and procedures for the mitigation of ammonia inputs into the fly ash slurries while protecting waterways. This process may include biological components for ammonia oxidation and/or may engineering controls for enhanced geochemical removal/sequestration.

NATURAL GAS AND OIL TECHNOLOGY PARTNERSHIP SUPPORT

T. W. Schmidt
Oak Ridge National Laboratory

INTRODUCTION

The Natural Gas and Oil Technology Partnership expedites development and transfer of advanced technologies through technical interactions and collaborations between nine national laboratories and the petroleum industry (majors, independents, service companies), and universities.

The Partnership combines the expertise, equipment, facilities, and technologies of the U.S. Department of Energy's national laboratories with those of the US petroleum industry. The laboratories utilize unique capabilities developed through energy and defense research and development, including electronics, instrumentation, materials, computer hardware and software, engineering, systems analysis, physics, and expert systems. Industry contributes specialized knowledge and resources and prioritizes Partnership activities.

The areas of technology are as follows:

- **Diagnostics and Imaging Technology** addresses cutting-edge geophysical methods for improved reservoir characterization with a focus on improved borehole hardware and computational efforts for seismic processing and other exploration issues. The Partnership catalyzed formation of a 25-company collaboration which has become the industry focal point for this technology.
- **Oil and Gas Recovery Technology** addresses a broad range of technologies aimed at improving production from existing fields and with specific emphasis on assisting independent producers. The industry interface is an Industry Review Panel consisting of more than 20 individuals representing independents, majors, and the service companies.
- **Drilling, Completion, and Stimulation Technology** aims at better access to the reservoir through improved drilling and completion technologies. Currently, the laboratories participate in several joint industry projects fostered by two industry organizations: the Drilling Engineering Association (DEA) and the Completion Engineering Association (CEA). In 2002 this technology area has been expanded to cover research and development in gas exploration, production and storage.

- **Upstream Environmental Technology** addresses new technologies that are needed to produce more oil and gas from mature domestic sources while safeguarding the environment. Key issues to be addressed include:
  – produced water
  – stationary source emissions
  – risk assessment
  – tank bottoms and sludge
  – naturally occurring radioactive material (NORM)
  – soil remediation
  – vapor recovery
  – offshore structure decontamination and dismantlement (D&D)
  – drilling wastes.
- **Downstream Environmental Technology** is an area of technology that was developed to address the needs of the U. S. refining industry. This technology area emphasizes advanced processing technologies, such as bioprocessing and particulate emissions.

NATURAL GAS AND OIL TECHNOLOGY PARTNERSHIP
COORDINATION OF BIOPROCESSING PROJECTS

T. W. Schmidt

The Natural Gas and Oil Technology Partnership Bioprocessing program involves projects at four national laboratories: Oak Ridge National Laboratory, Argonne National Laboratory, Idaho National Engineering and Environmental Laboratory, and Lawrence Livermore National Laboratory. To ensure coordination between the different projects, two meetings involving the four laboratories and their collaborating industry partners are held each year.

DISCUSSIONS OF CURRENT ACTIVITIES

T. W. Schmidt and S. M. Robinson

During 2002, T. W. Schmidt participated in the development of the recommendations for funding of the Partnership Programs on behalf of Oak Ridge National Laboratory. In addition to existing projects in Diagnostics and Imaging Technology and Downstream Environmental Technology, T. W. Schmidt and S. M. Robinson assisted in the continued research of the In-Well Oil and Water Separation Project, completion of the Physical Property Measurement of Produced Water Project, the studies of the project to develop an ecological framework to evaluate the impacts of the releases at petroleum exploration and production sites, and measurements using inorganic membranes for hydrogen separations in refinerys. Other activities include program planning with the Partnership, selection of a Partnership Steering Committee, coordination of the Partnership projects in Bioprocessing of Crude Oils, and coordinating all of the national laboratory participation in the Downstream Technology Area. In 2002 one new research project was funded: Modeling of Water-Soluble Organic in Produced Water. More recently ORNL has submitted two proposals to a new research area that focuses on gas exploration, production and storage.

ENVIRONMENTAL COMPLIANCE ASSISTANCE SYSTEM (ECAS) FOR THE NATIONAL PETROLEUM TECHNOLOGY OFFICE

S. M. DePaoli
Oak Ridge National Laboratory

INTRODUCTION

The Environmental Compliance Assistance System (ECAS) is a web site provided through the National Petroleum Technology Office (NPTO). This web site is targeted at the independently owned and operated oil and gas exploration and production (E&P) industry. In general, these E&P facilities are small, family-owned operations, and therefore do not have the capital to support the personnel needed to research and maintain information regarding environmental compliance issues concerned with their industry. This web site has been provided to aid these and other interested parties with regulatory information on the E&P industry; local, state, and federal contacts; waste handling/treatment/disposal options; and to direct them to other related web sites. A link to the ECAS can be found on the NPTO home page (http://www.npto.doe.gov/) or the site may be found directly at http://www.ecas.ws/.

ANNUAL REPORT, 2002

This NPTO funded project is tasked with updating the ECAS system that is currently on the web. The new, completed website is currently on a server at Advanced Integrated Management Services (AIMSI) (accessed through the above address). The NPTO is working on a new environmental webpage to be accessed from their main website. The ECAS website will be a link from this page, and will be incorporated when the NPTO's environmental website is complete.

A logo was designed for the ECAS website by Karen Billingsley of AIMSI Corp. in Oak Ridge under a subcontract on this project, and is shown above. Work on creating the web site began in January 1999. The website was completed in late 2000, and has been publicly accessible for about 1 year. The new site now includes information regarding links to other pertinent sites; federal and state regulatory contacts; regulatory/legislative changes that are pending; and help with waste management and emergency response. Information on regulations is provided through the site. Work continued in 2001 on updating the site's section concerning applicable treatment for wastes generated within the Oil and Gas Industry, as

well as inclusion of summaries of current issues regarding environmental compliance within this industry. During 2002 we will continue to update regulations and current events, and expect to include information regarding treatment methods applicable to waste generated in the oil and gas industries. Tracking of website access has shown it regularly receives in excess of 10,000 hits per month.

CHARACTERIZATION OF SOLUBLE ORGANICS IN PRODUCED WATER

D. A. Bostick and J. McFarlane
Oak Ridge National Laboratory

INTRODUCTION

ORNL, Shell, ChevronTexaco, Phillips, and Statoil are collaborating in a Petroleum and Environmental Research Forum (PERF) project to characterize organic solubility in produced water. The project is aimed at reducing future production of these contaminants, thereby minimizing costs associated with their treatment. ORNL is responsible for analyzing water-soluble organics (WSO) in produced water derived from Gulf of Mexico (GOM) drilling sites. WSO content is being defined through the measurement of equilibrium solubilities in GOM brine at ambient and high pressures and temperatures. These concentrations are then compared to the properties of the deep-water crudes from which they were derived. Industrial partners provide samples of deep-water crudes and produced water, contribute to the selection of methods to characterize the water-soluble organics, compare the deep-well data with historical data obtained from low-pressure wells, and evaluate the data for trends. PERF partners will develop a model to predict the production of water-soluble organics as a function of crude composition and formation characteristics.

The primary tasks for FY 2001 included:

(a) Obtain samples of actual crude/produced water from industrial partners.
(b) Characterize water-soluble organic content in both the oil and in contacted brines by EPA Method SW-846 8270C (Semivolatile Organic Compounds and Polyaromatic Hydrocarbons) and by EPA Method 1664 (Total Recoverable Petroleum Hydrocarbons) as the benchmark protocol for environmental regulation requirements.
(c) Study the effect of water cut, produced water pH and salinity, and crude oil properties on the type and content of water-soluble organics.
(d) Determine the distribution and partitioning of components over a range of temperatures and pressures.
(e) Provide data to industrial partners and assist in the analysis of the data.

These tasks concluded in 2002, as characterization was completed for one deep-well crude and begun for a second source of deep well crude.

DISCUSSION OF CURRENT ACTIVITIES

Background

Soluble organics in produced water and refinery effluents are treatment problems for the petroleum industry. Production facilities and refineries have to meet regulatory discharge requirements for dissolved organics. These problems are expected to increase as environmental regulations become stricter and production from deep-water operations increases. Deep-water crudes have a large polar component, which increases the amount of dissolved hydrocarbons in the produced water and refinery effluents. Early data from GOM wells indicate that dissolved hydrocarbons will increase significantly as deep-water production increases.

Neither the chemistry involved in the production of soluble organics in the petroleum industry nor the toxicity of these compounds is well understood. Several industrial companies, including Shell, ChevronTexaco, Phillips, and Statoil, have developed a collaborative Petroleum and Environmental Research Forum (PERF) project to characterize and evaluate water solubles, aimed at increasing understanding of the production of these contaminants. The project will ultimately result in reduced production of water solubles and allow the development of guidelines for effluent treatment. Quantitative characterization data are needed as the first step in this activity. Between 1999 and 2001, ORNL completed a study of the characterization of crude oils and water solubles in produced water under a variety of experimental conditions. The water-soluble organics were quantitatively determined by accurate measurements of equilibrium solubilities in contacted GOM brine.

ORNL is uniquely well suited to do research on the characterization of crude oils and water solubles, by virtue of its strong in-house concentration of equipment and expertise in high-temperature solution chemistry. A wide range of analytical instrumentation, equipment formerly under control of the DOE NIPER program and the ORNL High-Temperature Aqueous Chemistry group, is available. Starting in 2002, ORNL will assist the PERF industrial partners to develop a model to predict the production of water solubles from formation, crude, and water properties. ORNL also plans to characterize produced water treatment effluent; evaluate the potential impact of increased water solubles on down-stream processing; and measure the toxic effects of water soluble compounds in produced water and refinery effluents.

Progress

The data collected on the contact experiments with the first GOM crude sample are published and have been made available to industrial partners [1]. The water-soluble organic content of produced water was quantified as a function of several experimental parameters. Industrial partners provided ORNL with two samples of GOM deep-water crude. Only a limited volume of produced water was present in the

crude oil samples shipped from drilling sites. Hence, to determine the effect that various drilling conditions might have on WSO content in produced water, a simulated brine containing the principal inorganic components normally found in Gulf of Mexico water was prepared. The GOM simulant was then contacted with as-received crude oil to study the effects of water cut, produced-water pH and salinity, pressure, temperature, and crude oil source on the type of water-soluble organic content in produced water. The test plan involved the analysis of the organic content of simulated produced-water samples derived from oil/brine contacts covering the following operating ranges:

- pressures of 1–100 bar;
- temperatures of 90–200°F (~25–100°C);
- pH level of 6.5 ± 2;
- water cuts of 20, 50, and 80%; and
- salinities of 35,000–150,000 ppm.

The identities of individual semi-volatile organic compounds were determined in all as-received crude and produced water samples using the standard USEPA SW-846 Method (8270C) protocol. These analyses were supplemented with measurements of total petroleum hydrocarbon (TPH) content in the gas (C_6–C_{10}), diesel (C_{10}–C_{20}), and oil (C_{20}–C_{28}) carbon ranges as determined by both gas chromatographic (GC) – flame ionization detection (FID) and infrared (IR) analyses. Inorganic constituents in the produced water were analyzed by ion-selective electrodes and inductively coupled plasma (ICP)–atomic emission spectrometry (AES).

An open liquid chromatographic procedure was used to differentiate the saturated hydrocarbon, aromatic hydrocarbon, and polar components within the extractable TPH. The total organic material was fractionated into methylene chloride–soluble and hexane-soluble material. The hexane-soluble organics were further separated into saturated hydrocarbon, aromatic hydrocarbon, and polar hydrocarbon classes. The proportions of gas-, diesel- and oil-TPH within each fraction were then determined by GC/FID analysis.

Gas chromatographic results indicated that water-soluble organic compounds found in produced water samples were primarily polar in nature and distributed between the low and midrange carbon ranges. Typical levels of total extractable material were about 20 mg/L; that associated with the aromatic fraction was present at 0.2 mg/L and that in the saturated hydrocarbon fraction was present at less than 0.02 mg/L. Formic, acetic, and propionic acids were also found in the produced water by ion chromatography, occurring at a total concentration of 30 mg/L.

Of the five tested parameters, the factor that most controlled the total WSO in produced water was that of aqueous phase pH. Significant quantities of C_{10}–C_{20} range material become more soluble as they deprotonate in a basic aqueous phase, pH>7. Data presented in Fig. 1 are for GC analysis of contact data with the first crude sample. The "TEM" designation refers to the total TPH that is extracted from the brine by methylene chloride. The "C_6-C_{10}" and "C_{10}-C_{20}" symbols denote the quantity of material present in the hexane-soluble ("HEX") fraction within each of the respective carbon ranges. Note the apparent inflection point in the data at pH 7, indicated as a vertical line on the plot. Results presented in Fig. 2 are from the gravimetric analysis of contacts with the second crude sample, for which a pH study was also performed.

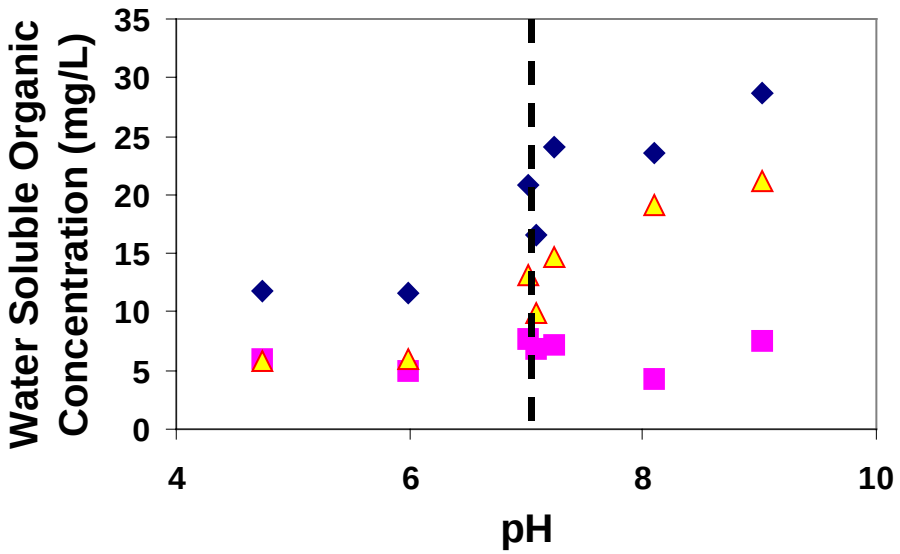

Fig. 1. Plot of water-soluble organic concentration as a function of pH. Fractions corresponding to different carbon size ranges are separately labeled, TEM with rhombuses, C_6-C_{10} with squares, and C_{10}-C_{20} with triangles. These data were taken in contact experiments using the first Gulf of Mexico crude sample, at reference conditions: 25°C, ambient pressure, 4 d contact time, and 80% water cut.

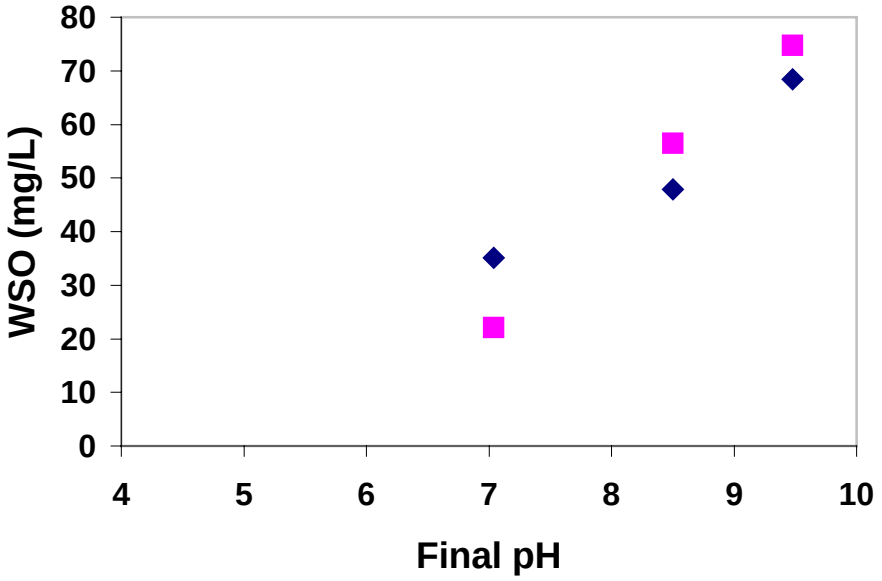

Fig. 2. Gravimetric analysis of methylene-chloride soluble (rhombuses) and hexane soluble (squares) fractions in simulated produced water brines that had been in contact with crude sample 2 for 4 d, at 25°C, ambient pressure, 80% water cut, under various conditions of pH.

The effects of water cut, pressure, temperature, and salinity are given in Figs. 3 through 6. Figure 3 summarizes the data trends for changing water cut or water:(oil+water) volume ratio. There was little change in overall water-soluble organic content in all chemical fractions combined as the water cut increased. This effect was a combination of decreasing solubility of the C_{10}–C_{20} carbon fraction and increasing solubility of the C_6–C_{10} carbonaceous material. Pressure slightly enhanced the water-soluble organic content by increasing the relative quantity of dissolved material in the C_6–C_{10} range (Fig. 4). Temperature primarily altered the relative ratio of soluble organic carbon ranges within the overall envelope, without significantly elevating the total water-soluble organic content in the brines. Temperature data are plotted in the form of a Van't Hoff plot to illustrate changes in apparent heats of solution with temperature (Fig. 5). Salinity appeared to have no effect on the chemical character or the carbon size of water-soluble organics in produced water (Fig. 6).

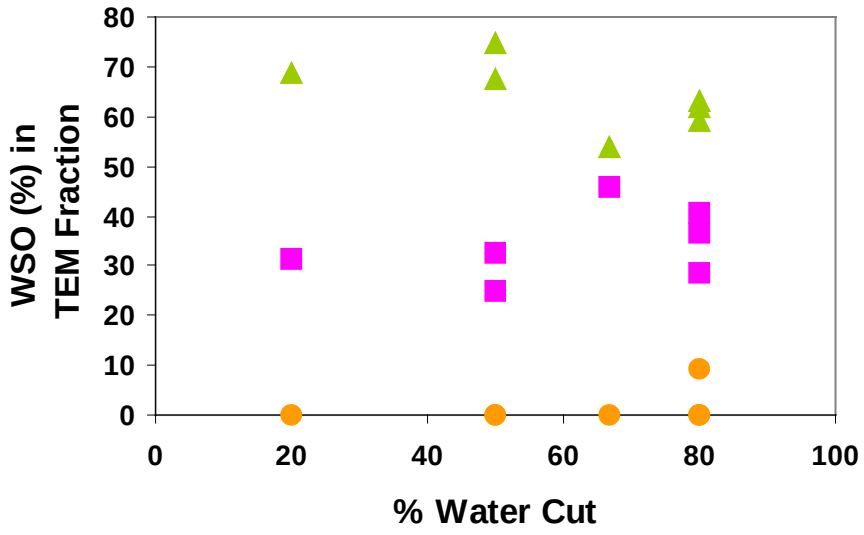

Fig. 3. Percentage of extractable material in various ranges of carbon chain length as a function of water cut: C_6-C_{10} (squares), C_{10}-C_{20} (triangles), C_{20}-C_{28} (circles). Data were taken from contact experiments with the first crude sample, under the reference conditions of 25°C, ambient pressure, and 4 d contact time.

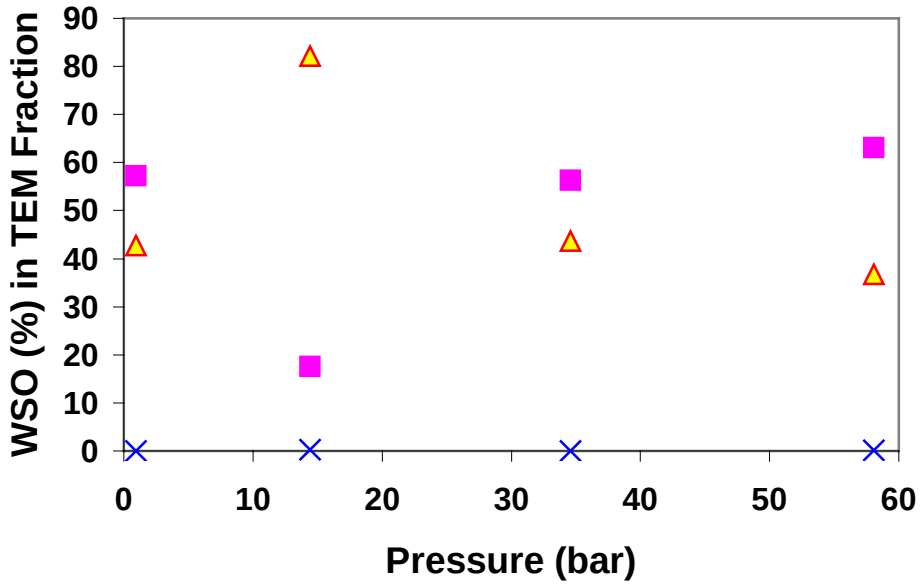

Fig. 4. Percentage of extractable material in various ranges of carbon chain length as a function of applied He pressure: C_6-C_{10} (squares), C_{10}-C_{20} (triangles), C_{20}-C_{28} (crosses). Data were taken from contact experiments with the first crude sample. Apart from pressure, the contacts were carried out under reference conditions (4 d contact time, 25°C, water cut of 80%).

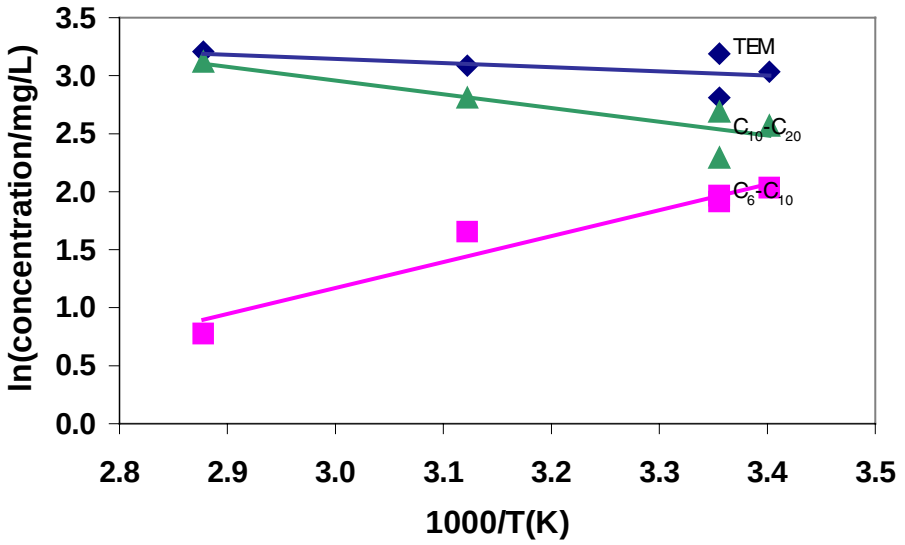

Fig. 5. Concentration as a function of reciprocal T in (K^{-1}) for contacts performed with the first crude oil sample. The total extractable material (rhombuses) is plotted along with the fraction in C_6-C_{10} (squares) and C_{10}-C_{20} (triangles). Apart from temperature, contacts were carried out under reference conditions: 4 d contact time, ambient pressure, water cut of 80%.

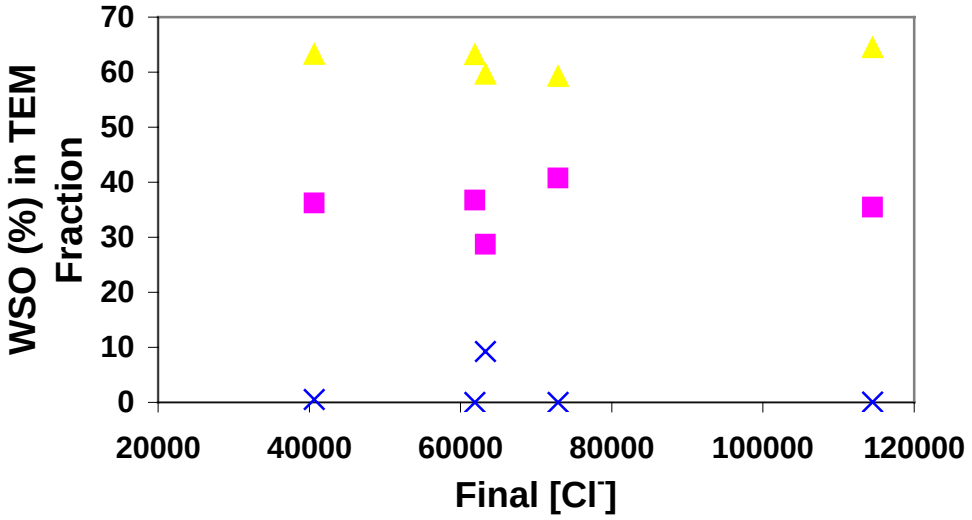

Fig. 6. Percentage of extractable material in various ranges of carbon chain length as a function of brine salinity: C_6-C_{10} squares, C_{10}-C_{20} triangles and C_{20}-C_{28} (x). Data were taken from contact experiments with the first crude sample, at 25°C, ambient pressure, 4 d contact time, and 80% water cut.

In summary, water characterization data were collected from contact experiments involving two separate GOM crude oil samples (i.e., taken from different well sites within the Gulf of Mexico). Results indicated that factors such as pH and temperature primarily determine the WSO solubility in GOM brine. Pressure or water cut may slightly affect the quantity of organic contaminants in brine; however, the noise in the data precludes the development of a quantitative model based on current pressure and water cut data.

Future Progress

Water characterization data were collected for two different samples of deep-water GOM crude. The remainder of these data will be transferred to the industrial partners as they become available. Starting in 2002, ORNL will assist the partners in the development of a model to predict the production of water-soluble organic compounds from formation conditions, crude characteristics and water properties. ORNL is also prepared to obtain additional data on water-soluble organics from other crude/produced water systems to augment the database. The predictive model will allow ORNL will evaluate the potential impact of increased concentrations of polar contaminants on produced water treatment methods and downstream processing, and evaluate the toxic effects of water soluble compounds in produced water discharge.

REFERENCES

1. D. T. Bostick, H. Luo, and B. Hindmarsh. 2001. “Characterization of soluble organics in produced water,” Oak Ridge National Laboratory Technical Memorandum, ORNL/TM-2001/78.

REMOTE SENSING FOR ENVIRONMENTAL BASELINING AND MONITORING

David Reister, Robert Washington-Allen, and Art Stewart
Oak Ridge National Laboratory

INTRODUCTION

Hyperspectral remote sensing is an emerging technology with the potential to identify plant species, map vegetation, characterize soil properties, identify contamination, classify ecological units and habitat characteristics, and differentiate causes of vegetation stress. The main benefit of this project, both to the DOE Fossil Energy Program and to our petroleum industry partners, will be an improved ability to provide detailed environmental data for a region, rapidly, at low cost. Increasingly, environmental data are needed to assess present conditions of lands owned, leased or managed by petroleum companies, and to characterize and quantify changes in the environmental conditions of these lands through time. Present methods of assessing large areas depend extensively on field surveys, which can take weeks or months to complete. Such methods are inconvenient and can be expensive. Further, some areas that are inaccessible or very large are difficult or virtually impossible to monitor accurately using field-survey techniques only.

Investigators from ChevronTexaco, the University of California at Davis (UC Davis), and the Oak Ridge National Laboratory (ORNL) are collaborating to develop remote (airborne or satellite) hyperspectral sensor techniques specifically to characterize conditions at exploration and production (E&P) sites, where vegetation and soil may be impacted by oil or gas production. Project objectives include: (1) identifying hyperspectral signatures of plant responses to hydrocarbons, toxic metals and other stressors; (2) developing advanced analytical methods for evaluating hyperspectral data, so as to more clearly reveal environmental impacts from spectrally "noisy backgrounds;" and (3) demonstrating techniques for revealing environmental impacts by analysis of hyperspectral data. These techniques are not currently available. ChevronTexaco and UC Davis investigators are performing experiments in which plants reared hydroponically are being exposed to metals and hydrocarbons in a controlled-growth facility. The responses of these plants to the pollutants are being measured with a portable spectrometer. Concurrently, ORNL investigators are analyzing hyperspectral data obtained from an oil spill site on the Jornada Experimental Range (see http://usda-ars.nmsu.edu/).

An ideal (but costly) experiment for this project would be to apply petroleum hydrocarbons on a plot, and obtain hyperspectral images of the plants on the plot before and after the spill, to characterize changes in vegetative condition through time. In June 2000, a near-ideal "natural" experiment occurred when a road grader accidentally cut an oil pipeline, allowing oil to spray over a five-acre site at the Jornada Experimental Range near Las Cruces, NM (see Fig.1). Jornada has been operated as a research park by

Fig. 1. Oil spill at Jornada.

the Agricultural Research Service (ARS) since 1912. Thus, the oil-spill accident at this park was a particularly fortuitous event for our project. In 1981, the National Science Foundation selected Jornada as a Long-Term Ecological Research (LTER) site. The Jornada Experiment (JORNEX) was begun in 1995 to collect remotely sensed data from ground, airborne, and satellite platforms. In May 1997, an 11-day field sampling campaign occurred at Jornada. This sampling campaign was designed to collect ground and airborne hyperspectral data to validate satellite images. During the campaign, the Airborne Visible/Infrared Imaging Spectrometer (AVIRIS) sensor was used to collect data at Jornada. Subsequently, this sensor has been used to collect data at Jornada at least twice a year. AVIRIS is an imaging hyperspectral sensor with 224 bands; it is carried aboard a NASA ER-2 airplane (a modified U2 plane) at an elevation of ~20 km. An AVIRIS flight over the Jornada site occurred on June 10, 2000, just ten days after the oil-spill. The Jornada site also was imaged with the AVIRIS sensor before the spill, and hyperspectral data on vegetation and soils at the site have been obtained during site-characterization projects by ARS investigators. Thus, Jornada has a rich set of before-and-after hyperspectral data, both from ground and airborne platforms. We obtained access to hyperspectral data (both field data and remote AVIRIS data) collected at Jornada during previous experiments, and expect to acquire additional

hyperspectral data at the site by making field measurements. As these data are collected, we will develop analytical methods to identify environmental impacts and the source of the impacts.

APPROACH

An AVIRIS image consists of multiple lines, with each line composed of 614 pixels (for the AVIRIS images we used, a pixel is a square, 17.4 m per side). A typical Jornada AVIRIS-flight event yields an image containing 4,489 lines spanning a distance of ~78 km. Each scene from the image is 614 pixels wide and 512 pixels long; thus, a scene cover an area of ~95 km^2 (10.68 km by 8.91 km). For each pixel within the image, the intensity and wavelength of reflected light depends on factors such as the species that are present, the current status of each species within the annual growth cycle (vegetative, flowering, fruiting, senescent), the environmental stresses on the plants, atmospheric absorption of radiation, cloud cover, etc.

Our goal is to use the reflectance spectra of the pixels to make rapid, quantitative determinations of environmental conditions. An appealing conceptual model is that each pixel is composed of a relatively small number of homogeneous regions. The total reflectance then is the sum of the reflectance for each type of homogeneous region, weighted by mixing coefficients (the fraction of the total area that is occupied by each type):

$$\rho_{\mathbf{pixel}} = \rho_{\mathbf{veg}} \mathbf{C}_{\mathbf{veg}} + \rho_{\mathbf{soil}} \mathbf{C}_{\mathbf{soil}} + \rho_{\mathbf{litter}} \mathbf{C}_{\mathbf{litter}} + \varepsilon \qquad (1)$$

In Eq. (1), above, ρ and $\mathbf{C}$ are the reflectance and cover fraction of each endmember, respectively, and ε is an error term. To accumulate a library of potential types of homogeneous regions, field data can be collected with a spectrometer that images pixels 1 m^2 or smaller.

With a library and the mixing coefficients, it is possible to correctly forecast the pixel spectrum. The inverse problem (that is, given a library and a spectral measurement, can we estimate the mixing coefficients?) is more difficult. A fundamental requirement for solving the inverse problem is a linearly independent set of measurements in the library. We are currently developing methods for solving the inverse problem.

DATA SOURCES

The primary data set for the Jornada oil spill is from the AVIRIS flight on June 10, 2000. We contacted Dr. G. P. Asner (Stanford University), the primary source for these data. Dr. Asner informed us that obtaining the data is not a simple matter of downloading a large (1.2 Gigabyte) file from a web site. In an e-mail, he noted: “If you would like to work with data subsetted, geo-located, and converted to

surface reflectance, then I can quickly provide you with an image from May 1997. However, if you would like more recent corrected data, then please know that this is a really major job on my end. The atmospheric correction of AVIRIS data is a science issue, requiring continued field work and algorithm development. I am currently working on spectroscopic imagery from June 2000." Since Asner is not being compensated to correct the data, he asked for our collaboration. We agreed. However, because he is in the process of moving his research group from the University of Colorado to Stanford University, the collaborations cannot begin until next year. In the interim, we have been given accounts on the web site that allow users to access data, and thus have access to the uncorrected data for June 2000 and May 1997.

We have contacted three groups (Asner, ARS, and TEC) that have measured field data at Jornada and asked to analyze their data. Asner's (2000) field-spectroscopic database contains 98,423-spectrum measurements of bare soils, green canopies, and litter canopies for 17 arid and semiarid sites in North and South America, representing a wide array of plant growth forms and species, vegetation conditions, and soil mineralogical-hydrological properties. He has written: "To develop a broadly applicable spectral unmixing approach for arid and semiarid ecosystems, our strategy was first to quantify the biogeophysical variability of the dominant endmembers at as many field sites and under as many conditions as we thought necessary to ultimately acquire statistical confidence in the subpixel cover fractions. Recognizing the multitude of highly variable green and senescent plant canopies and bare soil in these regions, we felt that a thorough survey of their spectral properties would yield the most generalizable endmember data set needed to establish the most predictable spectral region for mixture modeling. The field spectral survey included vegetation types from grasslands, shrublands, woodlands, and savannas in desert, semidesert, temperate, subtropical, and tropical climates. The data set included green and litter canopies of more than 450 herbaceous and woody plant species, representing a wide array of growth forms, physiologies, canopy architectures, intracanopy shading, tissue chemistries, and tissue optical properties." After Asner completes his move to Stanford University, we will explore gaining access to his database.

A recent publication on remote sensing at Jornada (Havstad, 2000) notes that, beginning in 1997, hyperspectral plant canopy and soil reflectance measurements have been collected twice a year at Jornada using an Analytical Spectral Devices (ASD) full-range (350–2500 nm) spectrometer. These data were obtained at 5-m intervals along 150-m vegetation transects, and at temperature-measurement grids in grass, shrub, and transition sites. Separate radiometric measurements were made for the dominant plant species, litter, and bare soil (10 measurements of each selected type) at each site. We contacted Dr. Kris Havstad and Dr. Al Rango at Jornada and asked to help process the data from these measurements. In September 2001, Rango requested permission to release the data, from the ARS headquarters in Beltsville, MD. Our request was discussed and approved at the JORNEX team meeting in March 2002. In April 2002, we received data for the 822 Full Range measurements that were made in September 2000.

The Army Corps of Engineers Topographic Engineering Center (TEC) also greatly enhanced our library by sending us a well-documented data set consisting of 583 measurements of reflectance spectra of grasses, herbs, shrubs, trees, rocks and soils (Satterwhite 1990; Table 1). Many of the data in the TEC library were measurements made at Jornada. The TEC also gave us data on hyperspectral measurements for oil on sand.

Table 1. Distribution of measurements in the Army Corps of Engineers TEC library

Spectrum source	Limited[a]	Full[b]	Total
Grass	36	18	54
Herb	7	25	32
Rock	2	53	55
Shrub	48	21	69
Soil	47	289	336
Tree	0	37	37
Total	140	443	583

[a]Limited-data ranges, from 360 nm to 1100 nm.
[b]Full-data ranges, from 360 nm to an upper limit between 1920 nm and 2500 nm.

ORNL has an ASD spectrometer that can acquire data over a range from 324 nm to 1051 nm. We used this spectrometer to collect data at Jornada in July 2001, adding to our spectral library. The presence of chlorophyll in green vegetation explains the characteristic red-edge signature, which is strong absorption in the red band followed by strong reflectance in the near infrared (see green curve, Fig. 2). At Jornada, woody stems, dead plants, and oily soil all had a characteristic brown spectrum, wherein reflectance increases steadily from 400 nm to 1050 nm (see Brown curve, Fig. 2). This brown spectrum lacks the red-edge signature. Under vegetative stress (the color changes that occur in leaves during autumn is a familiar example), spectra from green vegetation change: reflectance in the red increases, causing the leaves to appear yellow, orange, or red. Concurrently, leaf reflectance in the near infrared declines, which reduces the red-edge signature (see the Red and Yellow curves, Fig. 2).

Asner (2000) demonstrated that green plants are distinguishable from brown plants and soil, by analysis of data in the spectral range from 2100 nm to 2400 nm (SWIR2). Furthermore, petroleum hydrocarbons have a broad absorption band between 1600 nm and 1800 nm. Thus, to distinguish green plants from brown plants and to detect oil, spectral data must be available for 400 nm to 2500 nm. Fortunately, many of the field measurements and those obtained using the AVIRIS sensor contain data within this spectral range.

To illustrate the advantages of full-range data, we will discuss two average soil spectra. Data grouped for the 336 soil measurements revealed two clusters, containing 94 and 76 members, respectively. The

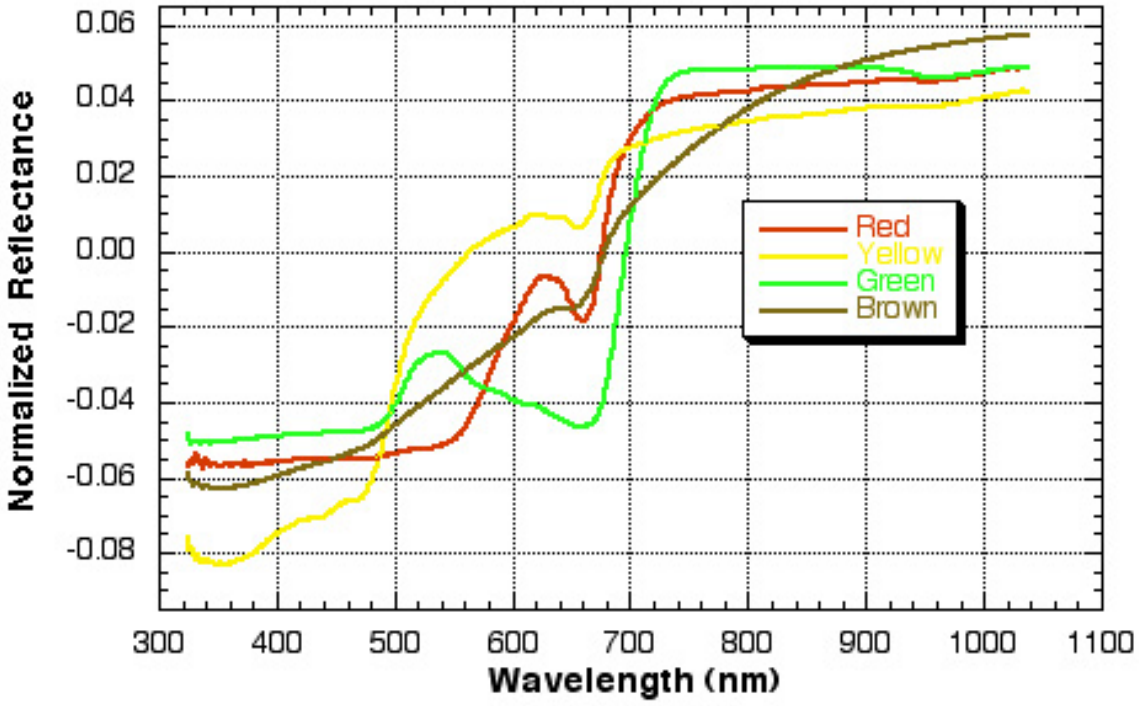

Fig. 2. Normalized reflectance spectra for red, yellow, green, and brown leaves.

chief distinguishing factor for soils in the clusters was water content. The average spectrum for each cluster is shown in Fig. 3. From detailed descriptions of the experimental procedures, we discovered that the samples differed because water had been added to soil samples [for example, in the experiment described on page S-0066 of Satterwhite (1990), the four water levels ranged from 7.4% to 42.7%].

Adding water to soil reduces soil reflectance in the water-absorption regions, centered near 1400 nm and 1900 nm. Since the mean value of each normalized spectrum shown in Fig. 3 is zero, a reduction in reflectance in the water region must be balanced by an increase in reflectance in the non-water regions. In Fig. 3, the reflectance peaks are greater at 1300 nm and 1700 nm, supporting this supposition. Unexpectedly, we observed that an increase in soil water reduced the reflectance peak at 2200 nm.

Asner notes: “Soil spectra collected by Asner had a distinctive absorption feature centered near 2200 nm, which results from combinations and overtones of hydroxyl absorption in the clay lattice structure of soils that dominate many arid and semiarid environments.” In Fig. 3, the reflectance dip at 2200 nm attributed by Asner to the soils’ clay-lattice structure is conspicuous.

Future field-work at Jornada will involve collecting full-range (400 nm to 2500 nm) reflectance data for green plants, brown stems, and soil (with and without oil exposure). We will look for stress particularly in plants within a relatively small area, where plants were exposed to oil but did not die.

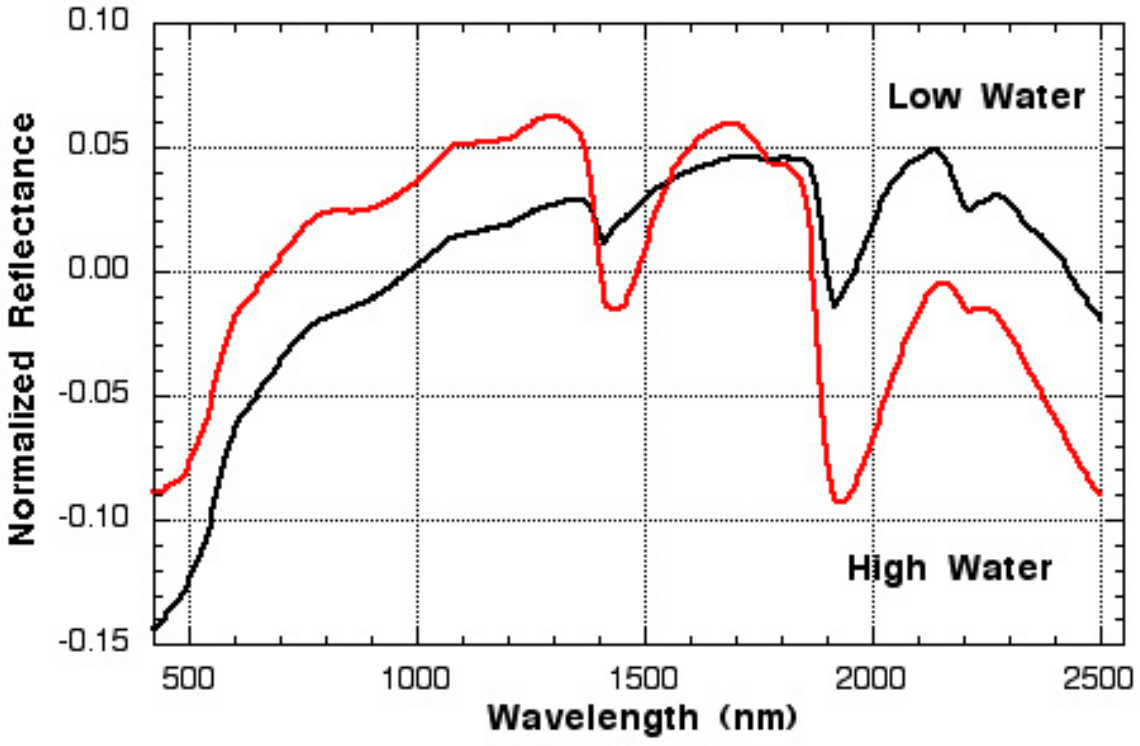

Fig. 3. Reflectance spectra of soil with low versus high moisture content.

STRESS DIFFERENTIATION

In the current project, stress differentiation by analysis of spectra from vegetation is an important objective. This objective would be met by finding a distinctive spectral signature for a plant stressed by metal, versus the distinctive spectral signature for a plant that has been exposed to hydrocarbons. Our resources currently consist of an extensive library of spectral measurements of plants, soil, and leaf litter. The library spectra could include data for plants that are healthy, and/or stressed by environmental factors (drought, heavy metals, hydrocarbons, etc.). We can generalize Eq. (1), by the model that any potential measurement of the reflectance (**r**) for a pixel will be a linear combination of the measurements in the library:

$$\mathbf{A}\,\mathbf{p} = \mathbf{r} \qquad (2)$$

In Eq. (2), **A** is a matrix of library members and **p** is vector of mixing coefficients. If the library has **N** measurements of reflectance and each measurement has **M** bands of spectral data, the matrix **A** will have **M** rows and **N** columns.

We distinguish between a forward problem and an inverse problem. For the forward problem, we know all of the parameters (**p**) and thus can calculate the reflectance. For the inverse problem, we

measure the reflectance and want to estimate the parameters. If one of the parameters is hydrocarbon stress and another parameter is stress from some other factor, solving the inverse problem will tell us if the change in reflectance is due to exposure to hydrocarbons or to the other stressor. In many cases, the forward problem has a unique solution. Often, the inverse problem can have multiple solutions.

A fundamental requirement for solving the inverse problem is a linearly independent set of measurements in the library. Since all green plants have some biochemistry in common, the spectra of many green plants are similar. A square matrix can be inverted when the determinant is not zero. Thus, for an arbitrary shape for the matrix **A**, we elected to analyze the problem using singular value decomposition (SVD). The number of positive singular values is the number of linearly independent columns in the matrix. The variance of the data is the sum of the squares of the singular values. Since small singular values contribute little to the variance, a numerical criterion can be used to determine which singular values are too small to consider.

The SVD of **A** yields three matrices: **U**, **V**, and **W**. **U** and **V** are orthogonal ($\mathbf{U}^T\mathbf{U} = \mathbf{I}$ and $\mathbf{V}^T\mathbf{V} = \mathbf{I}$), and **W** is diagonal. **U** is M by M, **V** is N by N, and the elements of **W** are the singular values, which are non-negative and arranged in decreasing order. The SVD of **A** is:

$$\mathbf{U}^T\mathbf{A}\mathbf{V} = \mathbf{W} \tag{3}$$

The condition number of a matrix is the ratio of the largest to smallest singular values (w_i). For practical reasons, it is helpful to limit the condition number to a reasonable value (i.e., ten or one hundred) rather than a huge number (one million). The rank (K) of the matrix **A** is the number of positive singular values that satisfy the condition number criterion. The columns of **U** ($\mathbf{u}_i$) are an orthonormal basis for the measurement vectors (**r**), and the columns of **V** ($\mathbf{v}_i$) are an orthonormal basis for the mixing coefficients (**p**), and the columns satisfy:

$$\mathbf{A}\,\mathbf{v}_i = \mathbf{w}_i\,\mathbf{u}_i \tag{4}$$

$$\mathbf{A}^T\mathbf{u}_i = \mathbf{w}_i\,\mathbf{v}_i \tag{5}$$

To solve Eq. (2), we expand **r** and **p** using the basis vectors:

$$\mathbf{r} = \sum_i \mathbf{q}_i\,\mathbf{u}_i \qquad \text{where} \qquad \mathbf{q}_i = u_i^T\mathbf{r} \tag{6}$$

$$\mathbf{p} = \sum_i \beta_i \mathbf{v}_i \qquad \text{where} \qquad \beta_i = \mathbf{v}_i^T \mathbf{p} \tag{7}$$

Multiplying Eq. (7) by **A** and using Eqs. (2), (4) and (6), the components of **p** can be determined:

$$\beta_i = \mathbf{q}_i / \mathbf{w}_i \qquad \text{for i = 1,K} \tag{8}$$

Thus, the measurement (**r**) can only determine K of the components of **p**.

While starting out to solve Eq. (2) for **p**, it seems clear that Eq. (6) is much more useful. By analyzing data from a large library of measurements that are highly correlated, it is possible to end up with a small set of coordinates (**U**) that are uncorrelated. The new coordinates are the directions of greatest variance in the data. The first coordinate (u_0) is the mean value of the library, and the second vector (u_1) is the direction of greatest change.

In a library that includes data on non-stressed plants and plants stressed by hydrocarbons and metals, one (or more) of the coordinates should be suitable for differentiating effects due to the different stressors.

We used SVD to analyze a data set containing spectra for vegetation ranging from green to brown. The values of q_1 (the coordinate in the u_1 direction) ranged from –0.4 for the greenest plants, to +0.3 for the brownest plants. Figure 4 displays three curves: u_0 is the mean value, u_{0a} is green (with a negative value of q_1), and u_{0b} is brown (with a positive value of q_1).

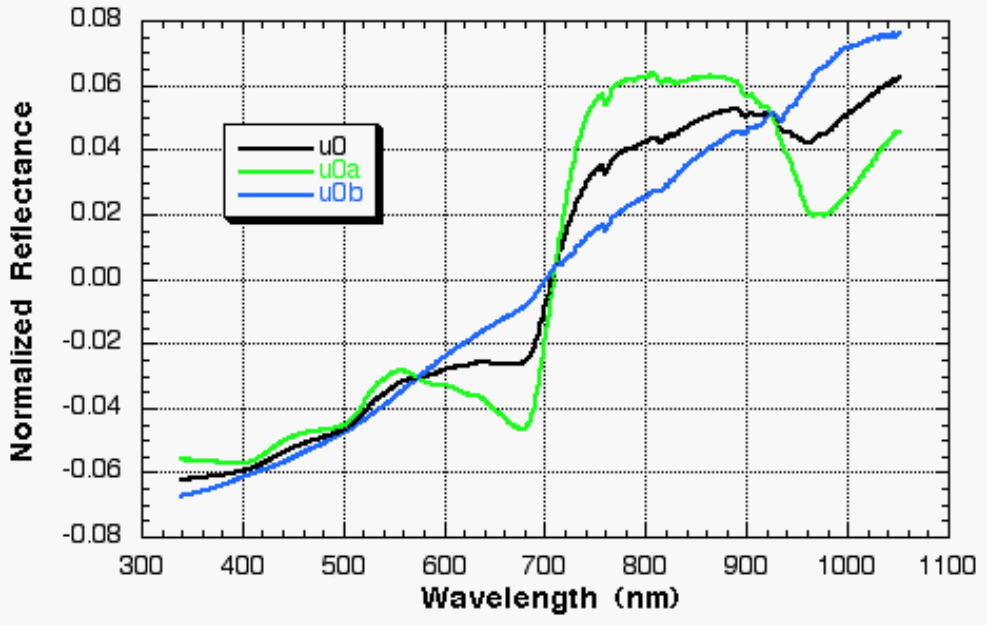

Fig. 4. As q_1 increases from –0.3 to 0.25, the spectra move from green to brown.

We will contrast our approach (i.e., SVD) with Spectral Mixture Analysis (SMA) [Eq. (1)]. SMA is based on an appealing conceptual model of a pixel. Each pixel is considered composed of a small number of homogeneous regions. The total reflectance from the pixel then is the sum of the reflectance for each type of homogeneous region (the endmembers), weighted by the fraction of the total area occupied by each endmember. SMA uses a model that is the same as Eq. (2), but selects a few columns for the matrix **A**. SVD, in contrast, allows use of many (hundreds) of columns. In SMA, the mixing coefficients are positive and sum to unity. In SVD, the mixing coefficients can have any value. We use SVD to find K uncorrelated coordinates (**U**). While the study by Gillespie (1990) mentions that the number of endmembers is one more than the intrinsic dimensionality (i.e., K + 1), subsequent studies by Roberts et al. (1998) and Asner and Lobell (2000) use two and three endmembers. Roberts et al. (1998) notes that three-endmember models provide poorer vegetation discrimination due to an increase in model overlap. The reason for the overlap is that the endmembers are correlated. Since the sum of the weights is one, a two-endmember model has only one free parameter.

The condition that the mixing coefficients must sum to unity is relaxed, in the SVD method, by transforming all of the original reflectance measurements. In the transformation, the mean value is subtracted from each value before the sum of the squares of each component is normalized to one. After the transformation, the covariance matrix becomes a correlation matrix.

ACKNOWLEDGMENTS

This research was supported by the U.S. Department of Energy (DOE) Office of Fossil Energy (Office of Natural Gas and Petroleum Technology) through the National Petroleum Technology Office and the DOE Office of Science (Office of Basic Energy Sciences). ORNL is managed by UT-Battelle, LLC for the U.S. Department of Energy under Contract No. DE-AC05-00OR22725.

REFERENCES

Asner, G. P. and D. B. Lobell. 2000. A biogeophysical approach for automated SWIR unmixing of soils and vegetation. *Remote Sensing of Environment.* **74**:99–112.

Gillespie, A. R. et al. 1990. Interpretation of residual images: spectral mixture analysis of AVIRIS images, Owens Valley, California. Proceedings of the 2nd AVIRIS Workshop, pp. 243–270.

Havstad, K. M. et al. 2000. Jornada Experimental Range: A unique arid land location for experiments to validate satellite systems. *Remote Sensing of Environment* **74**:13–25.

Roberts, D. A. et al. 1998. Mapping chaparral in the Santa Monica Mountains using multiple endmember spectral mixture models. *Remote Sensing of Environment.* **65**:267–279.

Satterwhite, M. B. and J. P. Henley. 1990. Hyperspectral signatures (400 to 2500 nm) of vegetation, minerals, soils, rocks, and cultural features: laboratory and field measurements. ETL-0573. Army Corps of Engineers Engineering Topographic Laboratories, Fort Belvoir, Virginia.

BIOPROCESSING OF FOSSIL FUELS

A. P. Borole
Oak Ridge National Laboratory

INTRODUCTION

The overall objective of this research program is to develop novel technologies for processing fossil fuels using biocatalysis and bioprocessing concepts. As compared to current thermochemical technologies, the bio-based technologies operate at lower temperature and pressure and have the potential to be more energy-efficient. Processes based on oxidative as well as reductive reactions are being investigated for bioupgrading applications, which include sulfur removal, polyaromatic hydrocarbon conversion and nitrogen removal.

Bioupgrading of Heavy Crudes

An enzyme-based process is being investigated for bioconversion of polyaromatic structures present in oil. The first step in the degradation of molecules such as pyrene, anthracene and other polyaromatic hydrocarbons (PAHs) is an oxidative attack on the aromatic ring by oxidase enzymes. This process however, requires cofactors, which are expensive. Use of alternate enzymes such as peroxidases, which use hydrogen peroxide for similar reactions, eliminates requirement or cofactors and was therefore used in this work. Naturally-occurring peroxidases are not very stable and active in organic media. Chemical modifications of the enzymes conducted in the previous year demonstrated that the activity can be improved. However, to achieve the needed improvements, it was necessary to use genetic methods for modification. For this purpose, the enzyme lignin peroxidase was cloned into a yeast host. Although the gene was successfully cloned, expression of the enzyme was found to be a problem. Various methods including media optimization, addition of heme, calcium and iron, variation of leader sequence did not seem to improve expression. Directed evolution of the gene was conducted via point mutagenesis, however, did not yield much success. It appeared that there was an inherent problem with the expression of the lignin peroxidase gene in the yeast. The focus was therefore moved to a different enzyme. An oxidase enzyme cytochrome P450, capable of oxidation of hydrocarbons as well as PAHs, already expressed in E. coli will be used for improving performance in organic media. Secondly, modifications of the enzyme will also be screened for improvements in thermal stability.

Biodesulfurization of Petroleum Feedstocks

The objective of this project is to develop improved enzymes for biodesulfurization of petroleum feedstocks. The goal will be to improve the activity and broaden the selectivity of desulfurization enzymes

using directed evolution as a tool as well as to explore the impact of ring-opening on biological desulfurization. The first year of the project was focused on development of recombinant strains expressing the desulfurization genes (dszABC and dszB), development of ring-opening biocatalysts, assay methods for high-throughput screening of desulfinase enzyme and studying the specificity of the wild-type *Rhodococcus* sp. IGTS8 biocatalyst. The project partners included ExxonMobil, Texaco, and University of Tennessee, Knoxville (UTK). The first task was conducted at ExxonMobil, second at Texaco and the following two at UTK and Oak Ridge National Laboratory (ORNL). The screening technique for biodesulfurization enzyme assay is based on the detection of the sulfur-free product of the reaction using a 96-well plate spectrophotometer. Specificity experiments demonstrated that the following sulfonates are recalcitrant to the dsz enzyme system: 2-methylbutyl methanesulfonate, 2,2-Dimethyl-1,3-dioxolan-4-lymethyl p-toluenesulfonate, 2,3-diphenylpropyl p-toluenesulfonate. These as well as molecules from oxidized diesel will be used to broaden substrate specificity. Preliminary experiments were initiated to study synergistic biodesulfurization-biocracking in collaboration with Texaco.

Biological Hydrogenation of Organosulfur Compounds

This project is aimed at investigating the potential of enzymatic and biomimetic catalysts for hydrogenation and hydrodesulfurization of oil compounds with the goal of upgrading crudes via sulfur removal and improving downstream processing. In the first year of the project, the laboratory for conducting anaerobic microbiology and enzymology was set up followed by some preliminary experiments which included isolation of enzymes. The setup included installing an anaerobic chamber and a gassing station. A thermophilic and a mesophilic hydrogenase enzymes are being investigated for desulfurization. The mesophilic enzyme is derived from *Desulfovibrio gigas (Dg.)* strain. The thermophilic enzyme is derived from a hyperthermophile, *Pyrococcus furiosus (Pf)*. A collaboration with Dr. Mike Adams, University of Georgia, Athens, has been setup to conduct part of the thermophilic work. The initial goal for this project is to modify the two enzymes to enable binding of organosulfur substrates.

Biological Denitrogenation of Petroleum

This project was part of a collaborative effort between the Oak Ridge National Laboratory and PDVSA-Intevep, S.A. The collaboration was made feasible via a Joint Agreement between U.S. Department of Energy and the Ministry of Energy and Mines, Venezuela. The purpose of the collaboration was to increase interaction between the two entities in the area of applied microbiology and enzymology for petroleum biorefining.

The research was focused on the use of bacteria and enzymes for removal of nitrogen from petroleum feedstocks. The scope of the research included the following tasks:

1. Oxidative removal of nitrogen compounds [check on whether typical biodesulfurization (BDS) chemistry works for biological denitrogenation (BDN)]. Conduct literature survey and list the reactions demonstrating biological transformation of organonitrogen compounds.
2. Selection of oxidation, hydrogenation and hydrolysis enzymes. Identify potential enzymes capable of breaking nitrogen-carbon bonds, reducing/oxidizing/hydrolyzing aromatic nitrogen compounds (either biodegradative or bioconversion-type).
3. Evaluation of enzymes selected in 2, for BDN reactions. Conduct research to demonstrate the biotransformation of selected organonitrogen compounds relevant for petroleum bioprocessing application.

A detailed literature survey of biodenitrogenation using bacteria and enzymes was conducted by Dr. Ramirez, followed by experiments to investigate nitrogen removal. The results indicated that microbial removal of quinoline was possible using *Pseudomonas putida* Chin 1K—strain 1 (DSM 6412) and *Comamonas acidovorans*—strain 3 (DSM 6426). The strains were, however, unable to remove carbazole and indole. The concentration of carbazole and specifically indole, may have been inhibitory in the experiments conducted. Further experiments are necessary to confirm this finding.

An additional exploratory experiment to study removal of quinoline from a real petroleum feedstock using the two strains is warranted to demonstrate the use of microbial denitrogenation, prior to further development.

EFFICIENT CLEAN-FUEL PROCESSING USING DESIGNER SOLVENTS

D. W. DePaoli, S. Dai, H. Luo, and B. H. Culbertson
Oak Ridge National Laboratory

INTRODUCTION

This project is focused on the removal of sulfur compounds from gasoline and diesel fuel. Desulfurization of fuels has become a topic of recent concern with the increased environmental hazards sulfur emissions are having on the atmosphere, such as photochemical smog. Sulfur removal will be applied to a substantial fraction of the market as the concentrations of sulfur-containing compounds increase in newly produced crudes and as regulations lower the maximum level acceptable in products. Conventional desulfurization processes become increasingly expensive as target levels decrease; therefore, alternative technologies are pursued. The large potential impact of this work is apparent by considering that a 1 cent/gallon decrease in the cost of sulfur removal, applied to the entire gasoline demand of 8.5×10^6 barrels/day, would translate to approximately $1 billion per year.

In this project we sought an alternative desulfurization technology by exploiting relatively new "designer" solvents – room-temperature ionic liquids. Room-temperature liquid salts surround solutes with ions, not molecules, and, therefore, defy many traditional chemical laws. They can serve as both solvent and catalyst. These traits allow chemical reactions to occur that were previously thought to be impossible. In addition, the unique properties of these materials may be exploited for efficient separations and recycle, reducing significant amounts of energy and waste presently associated with separations of solvents during fuel processing. Their low vapor pressure has the additional advantage of virtually eliminating the volatility of the solvent, greatly reducing solvent loss and airborne hazards. They are, therefore, candidates for tackling the difficult task of removing contaminants to produce ultra-clean fuels.

To date, hundreds of different ionic liquids have been made, and it is estimated that at least a million exist. A wide range of catalyzed organic reactions can be carried out in room-temperature liquids, including alkylation, acylation, reduction, oxidations, oligomerization, and polymerizations. In addition, the potential for separations based on solvent properties of ionic liquids has been demonstrated. However, additional development is needed in both basic chemistry and process engineering for ionic liquid systems before they can be applied industrially.

DISCUSSION OF CURRENT ACTIVITIES

The capability of several room-temperature ionic liquid systems to remove sulfur-containing compounds from liquid fuels by liquid-liquid extraction has been explored. Several ionic liquids were synthesized, aiming at developing a solvent with desired properties, including high partitioning and

selectivity of sulfur-containing compounds, low solubility of fuel compounds, and stability. For the preliminary studies conducted in this project, dibenzothiophene (DBT) dissolved in octane at levels of 10 to 60 ppm was used to model a sulfur-containing fuel. Batch extractions were carried out in which aliquots of the octane/DBT mixture were equilibrated with lesser volumes of immiscible ionic liquid. Representative measurements of liquid-liquid partition coefficients, defined as the ratio of the concentration of DBT in the ionic liquid phase with the concentration of DBT in octane, are shown in the figure below.

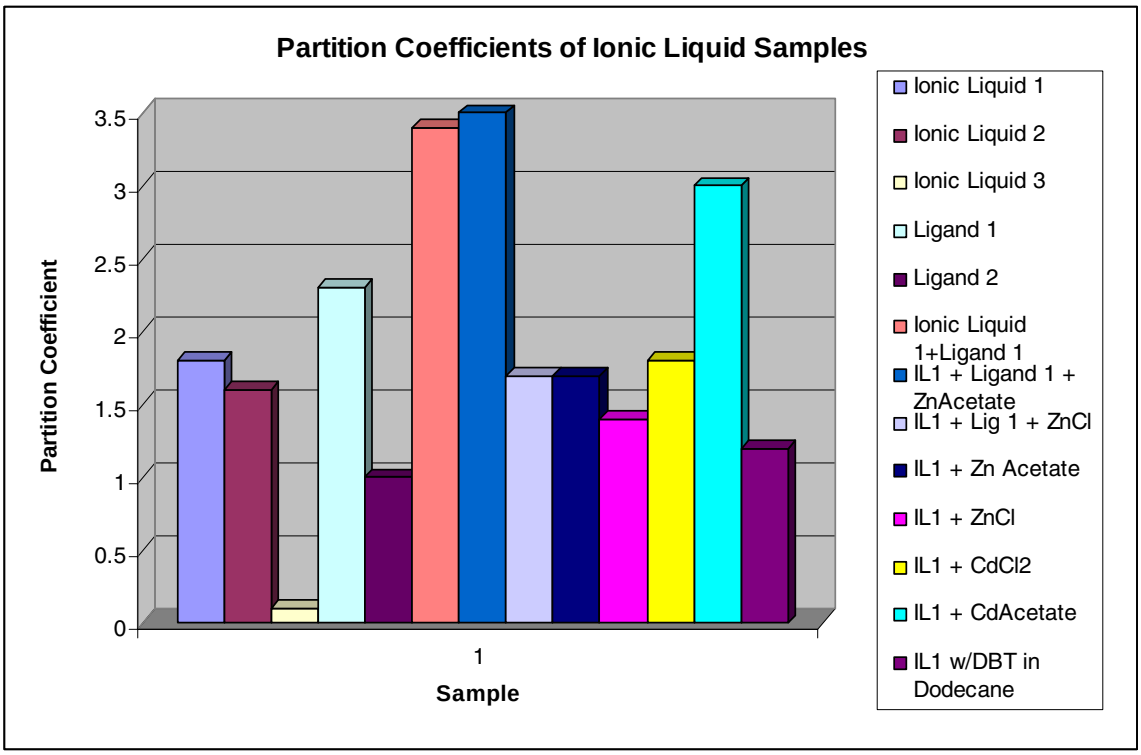

Most of the experiments seen above were carried out using an ionic liquid that has a DBT partition coefficient of 1.7 with octane. Ligands and catalysts were included in some of the experiments to further enhance the partitioning. The highest partition coefficients, approaching 3.5, were similar to recently published data for DBT extraction from diesel fuel (Bossman et al., *Chem Commun*. 2001, 2494-2495). The liquids used in this study have significant advantages due to their stability in contact with air.

For ionic liquids to be used for solvent extraction in industrial practice, they must be regenerable. To date, we have conducted a limited number of preliminary experiments of regenerability. These tests have shown limited removal of the DBT by heating under vacuum and by contacting with another solvent phase. Further regeneration experiments are being conducted.

These studies have indicated that it may be possible to design an ionic-liquid based system for removal of sulfur-containing compounds from liquid fuels. Further basic studies on the partitioning of sulfur-containing compounds with different ionic liquids and bench-scale process testing are needed for further development and evaluation of ionic-liquid-based desulfurization technology.

DEVELOPMENT OF A CENTRIFUGAL DOWNHOLE SEPARATOR

J. F. Birdwell
Oak Ridge National Laboratory

INTRODUCTION

By volume, the largest waste stream generated in the production of crude oil from the U.S. Gulf Coast region is water comprising that which is present in the oil-bearing formation and that which is used in the injection process. In 1991, Gulf Coast production generated in excess of 8 billion barrels of wastewater containing salts, chemicals, solids, and trace metals, in addition to oil. Annually, more than 250 million barrels of produced (waste) water are discharged to surface waters in Louisiana and Texas.

Two alternative approaches for addressing the problem of produced water disposal exist: (1) develop improved (more efficient, less expensive) methods for treatment prior to surface or subsurface release, and (2) reduce the volume of produced water by separating water from the product stream prior to delivery to the surface. Technologies currently being considered for produced water treatment include hydroclones, reverse osmosis, membrane filtration, gas flotation, carbon adsorption, bioreactors, chemical oxidation, back-extraction, and UV oxidation. Each of these technologies is complicated and expensive. Furthermore, it is anticipated that treatment processes will have to incorporate several operations involving one or more of these technologies to meet increasingly stringent water discharge standards. Therefore, elimination of the largest possible fraction of produced water from the product stream prior to delivery to the surface is the most effective means of reducing waste treatment and disposal costs.

The objective of the subject project is the application of separations equipment that has been developed for use in liquid-liquid extraction operations to in-well recovery of oil produced by enhanced, secondary recovery techniques. In its original application, the apparatus (a centrifugal solvent extraction contactor) combines the phase mixing and separation operations necessary for efficient transfer of solutes between immiscible liquids. Centrifugal contactors of various sizes (having rotor diameters from 2 to 25 cm) have been built and operated at the U. S. Department of Energy's Savannah River Site, Oak Ridge National Laboratory, Argonne National Laboratory, and Idaho National Engineering and Environmental Laboratory. Figure 1 is a photograph of a prototype contactor with a 5.5-cm diameter rotor. These devices have several characteristics that make them an attractive candidate for use in downhole oil/water separation. These characteristics include: (1) excellent phase separation capability, (2) demonstrated reliability in remote applications with >20,000 hours of operation without maintenance, and (3) the ability to process materials at high throughputs with low residence time and volume (i.e., compactness).

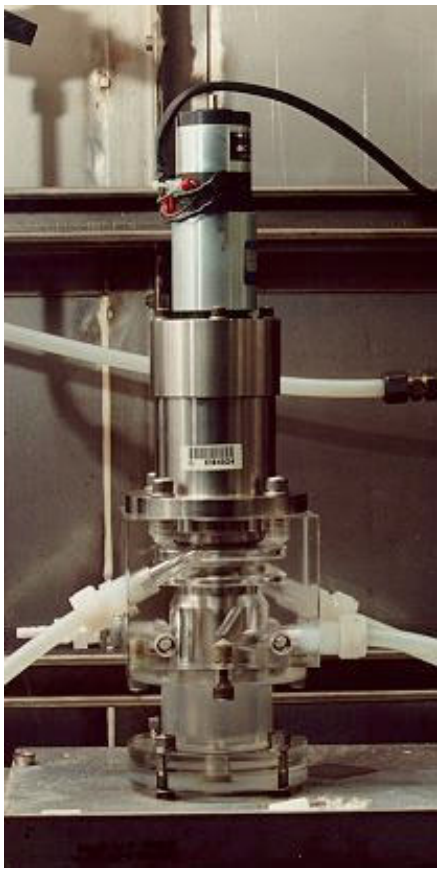

Fig. 1. Prototype 5.5-cm–dia centrifugal contactor/separator.

Several modifications to the centrifugal contactor are needed to optimize it for use as a centrifugal downhole separator (CDHS). The primary need to be addressed is increasing the throughput of the device while remaining within inherent space constraints. As an extraction device, throughput increases are normally achieved by increasing the diameter of the rotor in order to increase residence time and centrifugal separation force. In the downhole application, it is necessary to achieve throughput increases by increasing the rotor length. Additional throughput increases can be obtained by limiting mixing of the phases prior to introduction into the separator.

Additional issues pertinent to the downhole application that are to be addressed include the ability to minimize introduction of solids into the separator and modification of the rotor to reduce solids retention, and the configuration of separator connections needed to facilitate pumping of recovered oil to the surface.

MATERIALS AND METHODS

Several model V-2 centrifugal separators (having 2-inch rotors) have been obtained from a commercial vendor (CINC, Inc., Carson City, NV). A Petroleum Environmental Research Forum (PERF)

industrial partner has supplied two crude oils for use in separations testing. One is a Gulf of Mexico light crude with an API gravity of 34.06°, specific gravity of 0.8547 at 60°F, and a viscosity of 9.0 cP at 77°F. The other is a heavy North Sea crude with an API gravity of 19.3°, specific gravity of 0.948 at 60°F, and a viscosity of 400 cP at 77°F. Substitute ocean water for use in testing has been formulated according to ASTM Standard Specification D1141-90. Most of the testing performed to-date has used the lighter oil, based on recommendations from industrial partners, who have indicated that addition of water to heavy oils is generally needed to facilitate pumping to the surface.

The separator has been tested under a variety of operating conditions. Typically, the water and oil inventories are kept separate and are mixed just prior to delivery into the separator. Discharge solutions are continuously recycled to the feed tanks, permitting testing for extended periods. Samples of discharge solutions are collected in API centrifuge tubes, are acidified with 0.125 mL of 1 N HCl, and are centrifuged for 10 minutes at 4500 rpm. Water contamination of the oil discharge stream is measured by direct reading using the graduations on the centrifuge tubes. Oil contamination of the water stream is determined by dissolving the oil from the water samples in two 1-mL aliquots of hexane, evaporating the hexane, and weighing the oil residue.

RESULTS

The project is currently working against functional criteria that were developed with input from the Department of Energy and representatives from the PERF. These functional criteria were listed in the preceding year's progress report, and have been updated to reflect work performed in the current reporting year (Table 1).

Results reported previously indicate that separation performance is improved at elevated (above ambient) temperatures, and that addition of gas to the inlet stream did not affect phase separation. The latter finding is attributable to the presence of a liquid-free column along the center axis of the rotor during operation. As a result, the light-phase flow path is not obstructed through the rotor, allowing for two-phase (gas/liquid) flow.

Activities in the reporting year have been focused toward design and testing of modifications to increase the throughput of the unit. Using a mathematical model of separator hydraulics, the effect of length increases on throughput has been evaluated and an extended-length device has been fabricated by modifying one of the commercially available units. Testing of this unit is just getting underway.

Of perhaps greater significance, a modified feed configuration has been devised and tested. Specific details of the design cannot be released pending completion of documents required to protect intellectual property rights. In general, the modification reduces the mixing effect which the rotor has on entering fluids. Consequently, the liquid material entering the rotor is not a dispersion of the feed phases, as is the

Table 1. Functional Criteria for Development of the CDHS

Industry-supplied criteria	Achieved to-date	Comments
Flow rate: 2,000 to 10,000 bbl/d	15 bbl/d	Throughput has been limited by use of a small, vendor-supplied unit. An extended length rotor has been fabricated for testing. A modification made to the feed mechanism has been found to greatly reduce mixing of feed. Additional throughput may be achieved by increasing rotational speed.
Diameter: 6 inches maximum for 7-inch diameter well	2 in. dia. by 4-in. rotor 2 in. dia. by 6-in. rotor	An extended length rotor has been fabricated. A design modification is in progress that will provide the mechanical stability required for longer rotors.
Temperature: 100 to 180°F.	75–150°F.	Increasing operating temperature was found to improve separations using heavy North Sea crude
Water-to-oil ratio: 1:10 to 10:1	1:19 to 10:1	The bench-scale separator has been operated over the stated criteria range without loss of separating efficiency
Is gas processing feasible?	Yes	Tests have been performed at gas levels up to 21% (v/v) without loss of performance
Solids: 0–3% (sand to clay)	3% sand Feed modification made to reduce solids uptake	3% sand was processed through a hydroclone as a pretreatment step. The recent modification of the feed mechanism reduces solids uptake
Product quality: <2000 ppm cross-phase contamination	Achieved in tests to-date	Separation efficiency can be increased by dimensional adjustments and speed increase
Reliability: 18 months between failure	27 mo. or greater time between failure	Mean time to failure has been determined from prior DOE tasks. Units currently in use as extraction equipment have greatly exceeded 27 mo. in chemically harsh environment.

case in the prior state of the art. Because the feed stream is not dispersed, the residence time required within the rotor to achieve separation is greatly reduced. Based on preliminary observations and hydraulic calculations, it is estimated that the throughput of the device can be increased by at least a factor of ten without any increase in rotor length or rotational speed.

Work to confirm and improve upon projected and preliminary results using the feed configuration modification, the extended-length rotor, and higher-speed rotor operation is continuing.

SUMMARY

Work is currently underway to optimize a centrifugal device originally designed as a liquid-liquid extractor for use as an oil/water separator. The modifications that are being made particularly reflect size and configuration constraints imposed by in-well use of the device. Preliminary testing using a commercial device with few modifications has confirmed acceptable phase separation performance on light and heavy crude oils. Testing at elevated temperatures and with introduced gas has indicated no loss of separation performance. Pretreatment of the inlet stream to remove solids has been demonstrated.

Recently, equipment modified to increase throughput has been obtained for testing. In addition, a novel feed configuration has been devised that has been found to reduce the extent to which the feed streams are mixed by rotor-generated shear forces. Testing to quantify the effect of the modifications on throughput and separation performance is now underway.

IMPROVING TOOLS AND METHODS FOR ECOLOGICAL RISK ASSESSMENT AT PETROLEUM-CONTAMINATED SITES

R. A. Efroymson, D. S. Jones, and W. W. Hargrove
Oak Ridge National Laboratory

INTRODUCTION

This project, FEAC319, began in May of 2000 with support from the U.S. Department of Energy (Fossil Energy Program, National Petroleum Technology Office, Tulsa, OK; Kathy Stirling, Project Manager; Nancy Comstock, additional DOE manager). The project is intended to provide risk assessment tools and methods to the Petroleum Environmental Research Forum (PERF) project 99-13, "Expanding the Science Basis of Risk." Although the kickoff meeting for this project was planned for 1999, it did not occur until February of 2001. At the time of this writing, ChevronTexaco, ExxonMobil, BP, Unocal, and the Canadian Association of Petroleum Producers have contracts in place, in addition to Proprietary Agreements with Lawrence Berkeley National Laboratory and Oak Ridge National Laboratory. FEAC319 has four ongoing tasks: (1) to develop a framework for Net Environmental Benefit Analysis, (2) to develop plant uptake models for chemical contaminants that are found at downstream sites, (3) to develop or to evaluate spatial analysis models and tools for risk assessment of vegetation and wildlife, and (4) to finalize a review of soil ecotoxicity values for petroleum mixtures in soil.

Remedial activities at refinery or other downstream locations may be more expensive than necessary for at lease three reasons. First, models for estimating ecological exposure are not readily available, so excessively conservative estimates of exposure and risk are sometimes made. Second, certain remedial actions such as soil removal and the associated destruction of habitat may result in greater risk to ecological populations or processes than the continued presence of the original, aged contamination. Third, certain ecological functions may be replaced by on-site or off-site restoration.

Net Environmental Benefit Analysis (NEBA). NEBA attempts to answer the question: what type and scope of remediation, restoration, or natural attenuation of chemicals in environmental media would cause the least damage or most benefit to the value of habitat, local populations, and valued ecological functions? NEBA involves calculating a net environmental benefit of remediation or ecological restoration, compared to natural attenuation (no action) or another regulatory baseline. Remedial alternatives include traditional methods such as excavation, and less invasive options, such as microbial bioremediation (nutrient additions and tilling), phytoremediation, natural attenuation, wetland enhancement, and planting of native species. The recolonization of areas damaged by contamination, excavation or tilling may depend on the extent of fragmentation of a landscape.

The term “NEBA” was probably coined by agencies and industries evaluating options for marine oil spills. A report was published by the National Oceanographic and Atmospheric Administration (NOAA) in 1990 entitled *Excavation and rock washing treatment technology: net environmental benefit analysis.* In that study a group of scientists and engineers comprised of Exxon, NOAA, and State of Alaska scientists evaluated the environmental tradeoffs associated with excavating and washing hydrocarbon-contaminated sediments that were deeply buried along parts of the Alaskan shoreline affected by the Exxon Valdez oil spill. Several precedents for NEBA exist, but they provide little, specific methodological guidance for the assessment of contaminated sites. These range from federal and state government examples (e.g., Texas Natural Resource Conservation Commission) to industry examples. A framework for Net Environmental Benefit Analysis, analogous to the EPA framework for ecological risk assessment, has not been developed prior to the effort under this project.

Plant uptake models. A primary gap in any ecological risk assessment for terrestrial wildlife is in the quantification of chemical concentrations in wildlife foods. It is advisable to measure these concentrations at a site of concern. However, because funding or seasonal constraints may limit the number and type of measurements that may be made at a site, it is useful to have models available to estimate contaminant concentrations in plant materials and invertebrates, based on concentrations in soil, soil characteristics, and taxonomic characteristics. Elements and compounds of concern at downstream petroleum sites include: polycyclic aromatic hydrocarbons, lead, nickel, selenium, mercury, and vanadium. Published soil-plant uptake factors tend to overestimate bioaccumulation and risk when concentrations of elements in soil are high and to underestimate uptake at lower concentrations. In addition, soil and/or plant characteristics have not previously been incorporated into uptake models.

Spatial modeling. The exposure of ecological receptors to chemical contaminants has spatial dimensions. Wildlife exposure models include dietary uptake but rarely the habitat preferences that also determine exposure. Refineries, landfarms, or pipelines may be located at the center of a single habitat type (e.g., grassland), in which case the sizes of the habitat patches are important, or at the edge of two or more habitats (e.g., wetland and urban), which may have varying use by a particular species. The premise of this task is that organisms experience the environment spatially, as a patchwork. Patches may be good, as in the case of habitat for the animal, or patches may be bad, as in the case of buildings or spilled contaminants. The integrated effect of the patchwork landscape on a particular species will depend on the spatial arrangement of those patches of varying quality. Some pertinent questions are: (1) what is the role of wildlife movement and preferential uses of different habitat in determining exposure; (2) what is the role of the fragmentation of habitat in determining exposure; and/or (3) how do habitat loss and contamination interact to determine risk to wildlife? Spatial modeling will provide more realistic estimates of ecological exposure, so that fewer conservative assumptions may be used in risk assessments.

Ecotoxicity values. Ecotoxicity benchmarks for petroleum mixtures (i.e., ecotoxic concentrations in soil) can be used to help determine which impacted sites might require an ecological risk assessment. Several studies of the ecotoxicity of petroleum in soils have been conducted in the past decade, including toxicity tests of plants, soil invertebrates, and other organisms in field-contaminated and laboratory-contaminated soils. This information has not previously been assembled. Such a review is a necessary precursor to determining research gaps and ultimately selecting concentrations of petroleum hydrocarbons that may be used as screening levels for ecological risk assessments at petroleum exploration and production sites, refinery sites, pipeline locations, or other petroleum-mixture-contaminated locations.

It is assumed that improved methods for ecological risk assessment should lower costs of remediation by decreasing the need for conservative assumptions in estimates of ecological exposure.

DISCUSSION OF CURRENT ACTIVITIES

Net Environmental Benefit Analysis. Net Environmental Benefit Analysis (NEBA) provides a methodology for revealing and comparing benefits and risks of alternative management options. NEBA of chemically contaminated sites has been defined as the comparison of risks and benefits associated with any pair of three principal alternatives, as well as combinations of these: (1) leaving contamination in place; (2) physically, chemically, or biologically remediating the environment through traditional means; and (3) improving ecological value through on-site and off-site restoration alternatives that do not directly focus on removal of chemical contamination. The initial focus of this task was narrowed to the development of a framework for NEBA; petroleum industry representatives indicated that such a framework would provide a useful product. We drafted part of a manuscript on this topic in October 2001, with Joseph Nicolette of CH2M Hill, a NEBA practitioner, as a coauthor. This task will be completed with FY02 funds.

We have chosen to adopt risk assessment terminology to describe the NEBA framework to facilitate the use of NEBA by risk assessors. The NEBA framework described here has a single problem formulation stage to define the management goals of the assessment, the assessment endpoint entities, the stressors or beneficial agents of interest, temporal and spatial scales of analysis, and the plan for comparison between alternatives, including proposed, comparative metrics for ecological states. Parallel characterizations of exposure for each alternative include chemical concentration dynamics (e.g., estimates of rate, extent, and metabolites of biodegradation) and changes in bioavailability. Parallel characterizations of effects (benefits and risks) for the alternatives include the dynamics of ecological recovery, as well as direct restoration dynamics. NEBA, by definition, includes a final step of comparing ecological states among alternatives. A flow chart for NEBA will be included as part of the final paper.

Plant uptake models. To evaluate the relationship between the contaminant concentration in soil and plants, single-variable and multiple regressions were performed using SYSTAT 7.0 (SPSS 1997). Earlier in this project, models were developed for vanadium, with soil pH as the only soil characteristic, and lead, with three soil characteristics (i.e., pH, percent organic matter, and cation exchange capacity) and a common co-contaminant (cadmium). The current reporting period includes efforts to refine the vanadium models through the collection of additional data and efforts to incorporate soil characteristics into the uptake model for selenium. This report focuses on the latter effort.

A single-variable model for selenium was developed previously (BJC 1998, Efroymson et al. 2001) and was updated using funds from FEAC319. Multiple regression analyses were conducted for selenium in soil and three soil characteristics (i.e., pH, percent organic matter, and cation exchange capacity). A series of two-variable models were developed, each containing soil selenium concentrations and one of the soil characteristics. A multiple regression analysis was also conducted.

Preliminary results of log-log regression analyses of soil and plant selenium concentrations suggest that this model may be useful for predicting plant concentrations of selenium. The single-variable regression based on all 157 data points in the data set, was statistically significant ($p < 0.001$, $r^2 = 0.627$). pH contributed significantly to the two-variable regression model ($p < 0.001$) and helped explain more of the variance in plant selenium concentrations ($r^2 = 0.824$) than did the single-variable model. The two-variable regression model including percent organic matter was also statistically significant ($p < 0.001$ overall and $p < 0.01$ for both variables). This two-variable model explained more variance ($r^2 = 0.757$) in plant selenium concentrations than the single-variable model, but less than the two-variable model that included pH. The two-variable regression model including cation exchange capacity was also statistically significant ($p = 0.018$), but cation exchange capacity did not contribute significantly to the model ($p = 0.829$) and the amount of variance explained ($r^2 = 0.276$) was substantially reduced.

The multiple regression model that included all three soil characteristics was not statistically significant ($p = 0.083$) and explained relatively little of the variance in plant selenium concentrations ($r^2 = 0.291$). This may be partly due to the small number of observations ($n = 28$) for which all three soil characteristics were available. The three-variable multiple regression model that included pH and organic matter, but not cation exchange capacity, also was not statistically significant ($p = 0.111$, $n= 29$) and explained relatively little of the variance in plant selenium concentrations ($r^2 = 0.210$).

Based on these results, the two-variable regression model that included pH and soil selenium concentrations was the best of the models tested above. Figure 1 shows the plot of selenium concentrations in plants versus soil for the 120 data points for which soil pH was available, and the associated single-variable regression line.

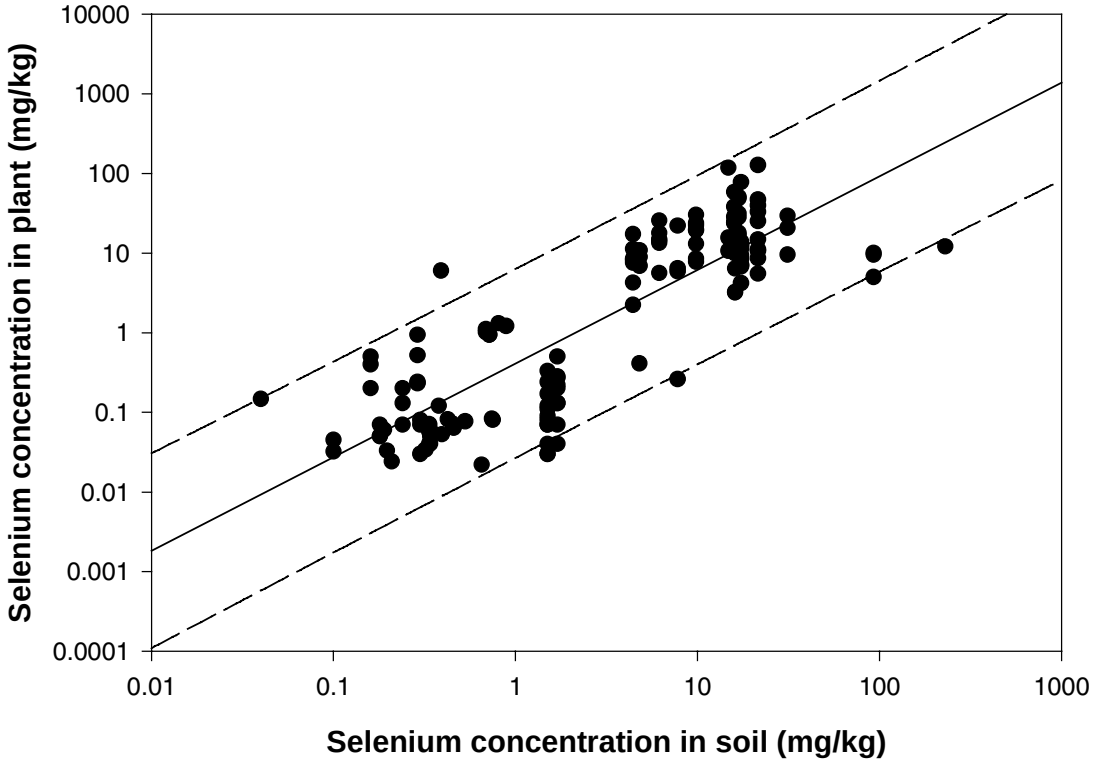

Fig. 1. Selenium concentrations in plants and co-located soil samples. Only those data points for which soil pH was available are included (n = 120).

Petroleum industry representatives have also indicated interest in the uptake of organic chemicals by wildlife foods, and this task may shift toward organic chemicals in the future.

Spatial analysis tools and models. An initial candidate study site was the Chevron land in Port Arthur, TX. However, this option was abandoned because of sensitive regulatory negotiations occurring there. A second site that was under consideration was the Nature-Conservancy-owned Tallgrass Prairie Preserve (TPP) in Osage County, OK, but because this site was not agreed upon because it is an upstream site. An additional candidate study site was a Chevron diesel pipeline spill location at the USDA Jornada Experimental Range near Las Cruces, New Mexico. However, this isolated spill was determined not to be ideal for landscape-scale analysis. A more theoretical study was proposed because of the lack of a study site with spatial data. This proposal is described below. However, work has not proceeded because the specifics of the proposal are still under consideration by DOE, with recommendations by PERF partners.

A landscape map analyzer tool was proposed to identify and map corridors and barriers to animal movement across any map of land cover categories (e.g., roads, grass, industry, etc.) or more specific features (e.g., spills). Applications of the tool to the petroleum industry lie in the identification of key areas for ecological restoration; spill remediation or wildlife barrier construction; or avoidance areas for road, pipeline or refinery facility development. Corridors are the "roadways" most commonly used by animals as they travel through an area. Corridors represent frequent movement paths among discrete patches of suitable habitat in a diverse matrix of land cover categories. Despite its importance, the idea of landscape corridors remains largely conceptual. No analytical tool exists which can examine a real-world map, quantify landscape connectance, and identify wildlife corridors. The proposed tool would work by simulating virtual animals, termed "walkers," which are imbued with the movement characteristics and preferences of those animal species.

The tool was based on the idea of island biogeography, whereby habitat categories are isolated patches embedded in a matrix “sea” of all other patches of all other categories. Bird or mammal walkers would try to get from one “island” patch of favorable habitat to another “island” in the archipelago, to define and locate often-used movement corridors. The spatial arrangement, number, area, and juxtaposition of patches of contamination, industrial development, roads, and other real-world landscape features would affect the movements of walkers and the routes of corridors across the map.

Three types of results are proposed for each analyzed map: (1) the collective "footprints" of all walkers successfully dispersing, summed to map corridors; (2) a matrix of pair-wise rates of transfer from each patch to each other patch in the map; and (3) a set of importance values for each patch in the landscape, in terms of the addition that patch makes to overall connectivity across the map. The absence of corridors would show barriers to movement, and absolute barriers would be explicitly included in the modeling process. The transfer matrix would indicate whether particular patches are population “sources” or “sinks,” which would indicate the overall effect of this patch on the demography of the animal population.

The patch importance values would be an important potential result of the tool. We would calculate a connectivity index for the map with the patch present, then conceptually remove the patch and recalculate map-wide connectivity to compute an importance value for each patch in the map. Patches with high importance could be protected or preferentially remediated; patches with low importance would be more favorable for industrial growth and development. In the case of an invasive species, the sense of the importance values would reverse. Patches important for connecting movements of a weedy species could be made inhospitable for the invader. In addition, the tool could lead to mitigation measures, such as the identification of key areas for habitat restoration or barrier construction.

Serial and parallel versions of the code are under consideration. The parallel version would allow the analysis of very large maps or maps with large numbers of habitat patches. Visual map products would be provided for a DOE-hosted web site to highlight the project.

Ecotoxicity benchmarks. Project funds were used to revise a journal article on ecotoxicity benchmarks for plants and soil invertebrates (Efroymson et al. 2000 draft) that was originally written under FEAC303 "Biological quality of soils containing hydrocarbons and efficacy of ecological risk reduction by bioremediation alternatives." The article was accepted by *Environ. Toxicol. Chem.* but withdrawn after results were presented at a PERF 99-01 meeting in October 2000 and received substantial review comments from petroleum industry representatives. The article was revised in June of 2001 and again in November of 2001, based on additional petroleum industry comments. The paper has become a review of existing ecotoxicity values and guidance to regulatory agencies and others regarding recommended considerations in the derivation of soil ecotoxicity benchmarks.

Data on the toxicity of total petroleum hydrocarbons (TPH) to plants and soil invertebrates were reviewed for possible application to benchmark development. Toxicity data included Lowest Observed Adverse Effects Concentrations (LOAECs); estimated 25^{th} percentile effective concentrations (EC25s), EC20s, and median lethal concentrations (LC50s); effective concentrations that caused greater than a 20% level of effect; and No Observed Adverse Effects Concentrations (NOAECs). The variabilities in petroleum material, chemical analytical methodology, age of hydrocarbon-soil contact, nutrient amendment, and measured effects levels did not permit much aggregation of the data. Tenth, twenty-fifth, and fiftieth percentiles of toxicity and no-effects data were presented for unaggregated results. Some toxicity values for plants exposed to various refined petroleum mixtures in soil were below the 10000 mg/kg TPH level that is sometimes recommended as a protective criterion for plants exposed to crude oil waste. Toxicity to invertebrates often occurred at concentrations of TPH lower than those associated with toxicity to plants. Lighter mixtures generally were associated with lower ranges of effects concentrations than heavier mixtures such as heavy crude oil. Existing toxicity data were not sufficient to establish broadly applicable TPH ecotoxicity screening values with much confidence, even for specific mixtures.

The following guidance was suggested for regulatory entities or other interested parties that are considering establishing screening benchmarks for ecotoxicity:

1. A party with interest in developing screening benchmarks must consider what entities to protect.
2. The regulatory agency or other interested party must choose two levels of protection: (1) an approximate response level and (2) a percentile that represents the acceptable percentile of the community that may exhibit the response.

3. A decision should be made about which analytical data to use. Considerations include the accuracy and availability of data obtained using various methodologies.
4. The regulatory agency or other interested party should decide whether toxicity data for TPH or petroleum fractions are most useful (and available) for estimating toxicity of aged mixtures in soil.
5. Screening benchmarks should be established with detection limits in mind.
6. Regulatory agencies and other interested stakeholders should strongly consider collecting new ecotoxicity data for petroleum hydrocarbons in soil.
7. Given the paucity of existing ecotoxicity data for TPH, a well-conducted field survey may currently be a more useful screening tool than a benchmark comparison.

REFERENCES

BJC (Bechtel Jacobs Company). 1998. Empirical models for the uptake of chemicals from soil by plants. ES/ER/TM-198. Oak Ridge National Laboratory, Oak Ridge, TN, USA.

Efroymson, R. A., B. E. Sample, and G. W. Suter II. 2001. Bioaccumulation of inorganic chemicals from soil by plants: regressions of field data. *Environ. Toxicol. Chem.* 20:2561-2571.

SPSS 1997. *SYSTAT 7.0 for Windows: Statistics*. SPSS Inc., Chicago, IL. 751 pp.

DEVELOPING AN ECOLOGICAL FRAMEWORK TO EVALUATE THE IMPACTS OF RELEASES AT UPSTREAM EXPLORATION AND PRODUCTION SITES: THE EFFECT OF SIZE AND DISTRIBUTION

R. A. Efroymson, H. I. Jager, T. L. Ashwood, E. A. Carr, W. W. Hargrove, and R. A. Washington-Allen
Oak Ridge National Laboratory

INTRODUCTION

This project, FEAB321, began in July of 2000 with support from the U.S. Department of Energy (Fossil Energy Program, National Petroleum Technology Office, Tulsa, OK; Nancy Comstock, Project Manager). The framework and ecological modeling are collaborative research between Lawrence Livermore National Laboratory (Tina Carlsen, Principal Investigator) and Oak Ridge National Laboratory. The project has several long-term goals: (1) to develop an ecological framework for evaluating impacts of brine and/or oil spills at petroleum exploration and production (E&P) sites, utilizing population models based on patchiness of landscapes and/or trophic transfer; (2) to develop early exit criteria from the ecological risk assessment process (if possible), based on size and distribution of spills in the context of potentially patchy habitat; and (3) to provide guidance for mitigation measures that may be taken by a company prior to exiting a site. The primary tasks of the past year have been (1) to obtain spatial distributions and areal statistics for spills, wells, roads, vegetation types, and fencing at the Tallgrass Prairie Preserve (TPP) near Pawhuska, Oklahoma, (2) to develop a plan for individual-based modeling of key vertebrate species of the TPP; and (3) to begin to incorporate vegetation, disturbance regimes, and species life-history characteristics into a computer code. Essentially, this project is intended to inject ecology into ecological risk assessment, a field that has been dominated by conservative assumptions about exposure and toxic responses. The project will contribute to Petroleum Environmental Research Forum (PERF) project 99-01, “Ecological Evaluations for Upstream Site Remediation Programs.” Improved methods for ecological risk assessment should lower costs of remediation by decreasing the need for conservative assumptions in estimates of ecological exposure.

BACKGROUND

The exposure of ecological receptors to chemical contaminants has a spatial context. Wildlife exposure models include dietary uptake but rarely the habitat preferences that also determine exposure. The premise of this project is that organisms experience the environment spatially, as a patchwork. Patches may be beneficial, as in the case of suitable habitat for the animal, or patches may be detrimental, as in the case of some hydrocarbon or brine spills. In addition, background processes, such as controlled burns and grazing by bison, can contribute to patchiness of habitat. Areas denuded of vegetation are non-

habitat for most vertebrates. The integrated effect of the patchwork landscape on a particular species will depend on the spatial arrangement of those patches of varying quality.

DISCUSSION OF CURRENT ACTIVITIES

Case study site. The subject of the case study for this project is the Tallgrass Prairie Preserve (TPP) in Pawhuska, OK. The TPP is approximately 37,000 acres of mostly intact prairie grassland with approximately 600 historic wells (about 120 in current production) and isolated spills of hydrocarbons and brine. The Nature Conservancy, which owns the site, has attempted to restore ecosystem function through controlled burns and grazing by introduced bison. Tallgrass prairie vegetation forms comprise about seven percent of oil and gas well locations in the U.S., and related plant communities such as short-grass prairie and north, mixed-grass prairie comprise another thirteen percent (Fig. 1). Thus, our case study site is representative of about one out of five upstream oil and gas locations.

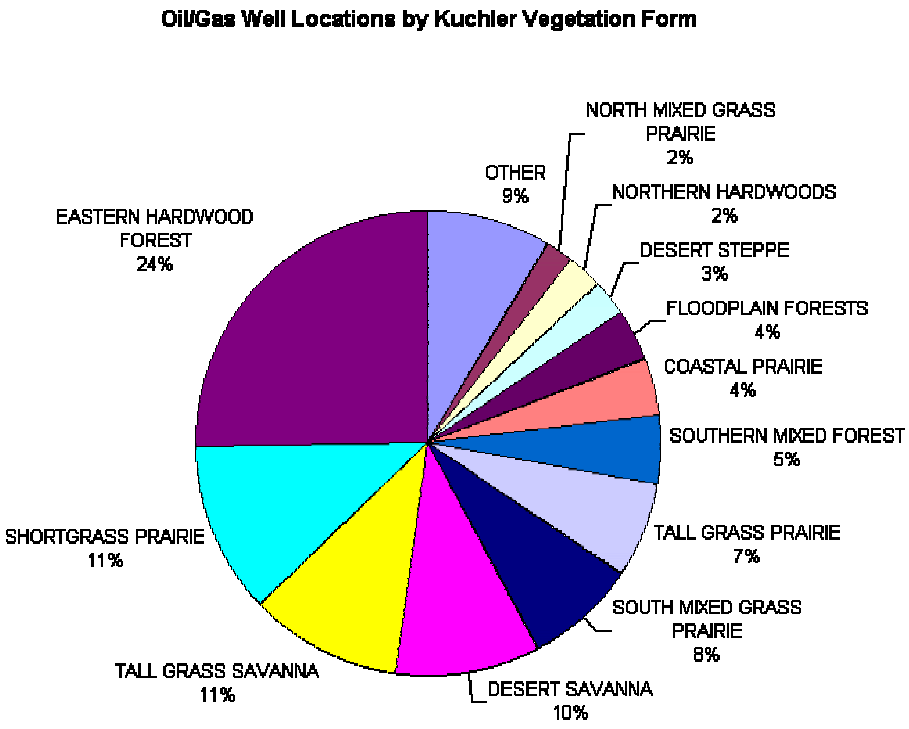

Fig. 1. Predominant vegetation forms in ¼ mile by ¼ mile cells in which productive and unproductive oil and gas wells in the U.S. are located. Data on well locations in USGS (1995), were obtained from David Ferderer at USGS.

Geographic Information System (GIS). A web-based interface for the GIS, that includes map layers provided by ORNL, was released by Lawrence Livermore National Laboratory (LLNL). The web site, entitled "Managing Ecological Impacts at Exploration and Production Sites" is accessible at http://gis.llnl.gov/mei/ to project team members, DOE sponsors, and PERF 99-01 partners. The GIS includes the following types of data, described more fully in last year's *Fossil Energy Program Annual Progress Report*: (1) soil survey, (2) vegetation type, (3) digital ortho quarter quad photos, (4) Landsat Multispectral Scanner data (North American Landscape Characterization data from USGS/EPA/NASA), (5) Normalized Difference Vegetation Index for six years, (6) prescribed burn history (annual 1991-1999), (7) management usage and years of bison grazing, (8) bison pastures with dates opened, and (9) land ownership. Some of these layers are not yet available on the web site. Airborne Visible/Infrared Imaging Spectrometer (AVIRIS) hyperspectral data have been obtained from the USGS, and these have been radiometrically corrected by USGS but not yet georectified.

Site Statistics. The project team and sponsors visited the TPP in June of 2001 to tour the site and obtain positions (through Global Positioning System hardware and software) of wells and spill boundaries. Preliminary site statistics were calculated using the GIS. The calculated site statistics include total preserve area, pasture data (numbers, sizes, fencing lengths), length and area covered by roads, length of streams, number and area of wells, burn rate, brine spill number and area, and vegetation coverage (woodland, savanna, prairie, pasture, crop and other) (Table 1).

Spill Generator. A brine and hydrocarbon spill generator is under development. The spill generator will create artificial spills on the TPP landscape at frequencies and with spatial distributions that are consistent with (1) the spatial distributions of wells and pipelines, (2) the timing of spills from historical data, (3) known vulnerabilities of pipelines of different categories, and (4) the time to recovery of restored and/or unrestored spills. In the simplest case, spills are assumed to occur randomly on any section of pipeline of a given length. Artificial spills will comprise the disturbance regime in some model runs, and actual spills will comprise the disturbance regime in others.

Ecological Modeling. The presence of oil or brine spills may affect population density and persistence of animal populations through several mechanisms. Patches of spills may impact animal movement, food availability, shelter availability and availability of refuge from predators. Habitat loss may lead to local extinction at low population densities ("Allee effect") because of the inability to find mates or breeding territories.

Several types of model structures were considered for use in modeling the effect of habitat loss on animal populations in the TPP (and relevant to other oil and gas exploration and production facilities). These included: (1) models that simulate species presence or absence with probabilistic state variables, (2) population models with aggregated state variables, (3) cellular automata, and (4) individual-based

Table 1. Site Statistics for TPP

Total Preserve Area = 15,720 ha (38,000 acres)[1]	
Pasture Data[2]	**Burns**[3]
Number of Pastures = 65	Median burn rate = 6,700 ha/y
Total length of fencing around all pastures = 209 km	
Median pasture area = 66 ha	**Spills**[4]
Largest pasture = 1981 ha	Number of brine spills = 126
Number of bison paddocks = 6	Total spill area = 17 ha
Total area of bison paddocks = 3949 ha	Median spill size = 0.02 ha
Median bison paddock area = 310 ha	Largest spill = 4.9 ha
Largest bison paddock = 1981 ha	
Smallest bison paddock = 50 ha	**Vegetation**[5]
	Woodland = 1,866 ha
Roads[6]	Savanna = 1,919 ha
Total length of roads on preserve = 198 km	Prairie = 11,198 ha
Area covered by roads = 73 ha	Pasture = 153 ha
	Crop = 5 ha
Streams[7]	Other = 4 ha
Total length of mapped streams on preserve = 60 km	
Wells[8]	
Number of oil wells within preserve boundary = 337	
Area = 2.5 ha	

[1]Tallgrass Prairie Preserve (TPP) web site (www.oklahomanature.org/tallgrassScience/html).

[2]Source: GIS coverage from Pete Earls, Oklahoma State University. Fencing calculated as sum of line lengths in coverage, assuming that all pasture boundary lines are fenced.

[3]Source: Annual burn coverages from 1991 through 1999, intersected with boundary coverage from TPP web site.

[4]Annual burn coverages provided by Pete Earls, Oklahoma State University.

[5]Source: Spills coverage from Bryan Tapp, University of Tulsa.

[6]Source: Oklahoma GAP.

[7]Source: Roads layer from OK GAP intersected with boundary coverage from TPP web site. Area based on assumed width of 3.7 m (12 ft).

[8]Source: Streams layer from OK GAP intersected with boundary coverage from TPP web site.

GIS coverages from Bryan Tapp, U. of Tulsa, intersected with boundary coverage from TPP web site. Well area assumes average of 74 m^2 per well.

models (IBMs). From an applied perspective, the strength of IBMs is in their ability to simulate mechanistic linkages between the physical environment, as modified by human activities, and animal populations. This strong linkage with real human-altered landscapes requires the model to use actual, spatial GIS data as input. Both ORNL and LLNL chose to develop spatially explicit IBMs for terrestrial vertebrates and to do the coding in C++, an object-oriented programming language. Object-oriented (OO) languages have several advantages, including: (1) the structure of the code, which mimics that of natural

objects comprising an ecosystem (e.g., individual animals); (2) modularity, which facilitates modeling as a team; and (3) economic allocation of memory, which permits modeling of complex dynamics and inclusion of large numbers of variables.

The structure of the model template for ORNL and LLNL models is described in Fig. 2. The cell, as well as its immediate surroundings, is conceived as the source of food resources and shelter for individual animals. The model will simulate population changes over time in response to disturbances by fire, petroleum spills, and brine spills. Modeled events will include local biological processes that influence individual animals (e.g., mortality, reproduction, aging, mating choice) and external or landscape-wide events (e.g., disturbances, redistribution of organisms).

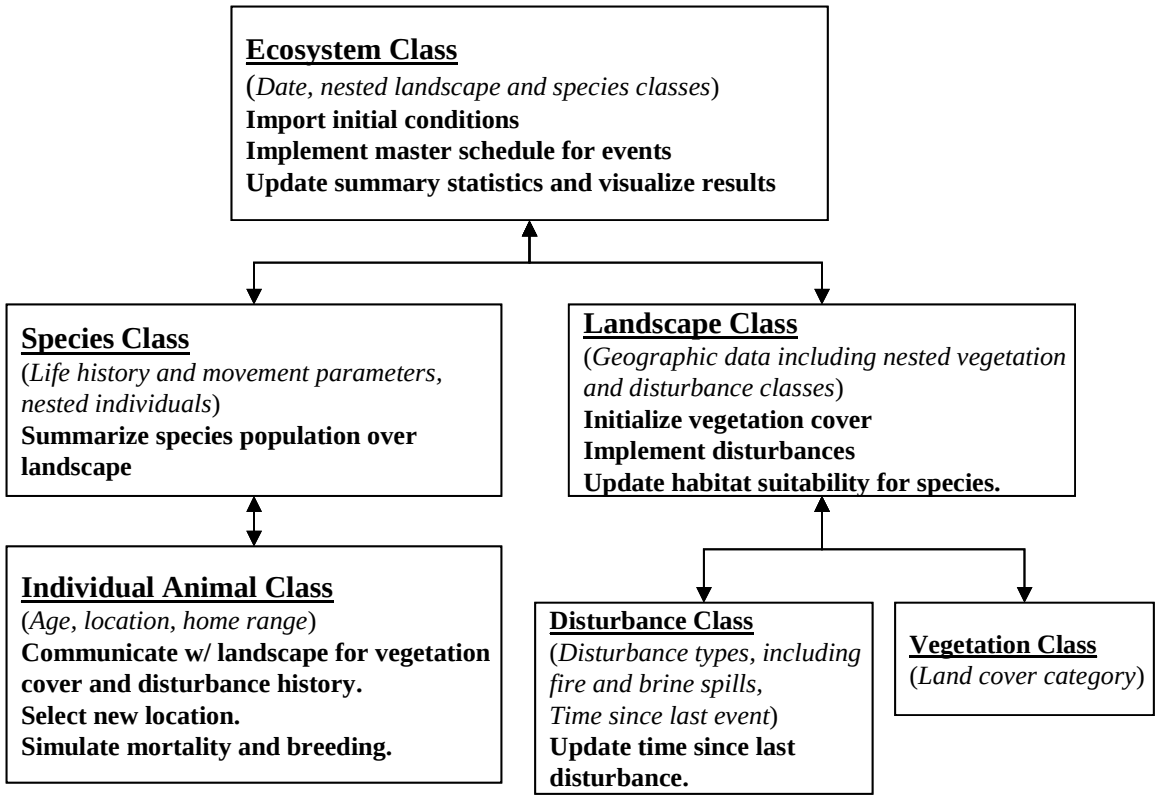

Fig. 2. Diagram of the proposed model template. Objects in the model are defined by classes that include data members (*italics*) and member functions (bold). Each class is represented by a box in the diagram.

Trophic interactions (e.g., vegetation growth and reduction due to grazing, herbivory, and bioenergetics) are a focus of the model in development by LLNL. The prairie vole (*Microtus ochrogaster*), a monogamous herbivore, feeds on grassland vegetation and is preyed upon by predators such as owls and badgers.

Differences in the susceptibility of species with different life histories and habitat requirements to habitat loss is the focus of the model in development by ORNL. A process for selecting representative species from those that occur on the Tallgrass Prairie Preserve has been developed. The goal is to choose species that represent different spatial life histories (i.e., mating systems) that may differ in susceptibility to habitat loss. Mating systems include: polygyny (harem defense polygyny, scramble-competition polygyny, resource-defense polygyny, lek polygyny), promiscuity, and monogamy (obligate monogamy and facultative monogamy). In addition, species that are the focus of this modeling effort must move at a scale that is potentially affected by the size and distribution of the spills at the TPP. Three candidate species include: (1) American badger (*Taxodea taxus*), a mustelid predator with a polygynous mating system and solitary social structure; (2) Greater prairie chicken (*Tympanuchus cupido*), a polygynous leking species in which males form a social hierarchy and perform booming displays to attract females; and (3) grasshopper sparrow (*Ammodramus savannarum*), a territorial breeder with high mate and nest fidelity. These are not threatened or endangered species; thus a risk to the population rather than a risk to the individual is of primary concern. At present, the spatial model developed at ORNL has been implemented for the first species, the American badger.

We have implemented a movement algorithm that includes two components: (1) dispersal and acquisition of a home range/breeding territory by juveniles when they become adults, and (2) daily movements within the home range of adults that have acquired home ranges. Each cell in the TPP landscape can belong to zero, one, or more adult home ranges, depending on the characteristics of the species. For species that exhibit strong territoriality, a “social fence” may prevent even casual movement through the territory of another adult. For other species, such as the badger, territories are too large to prevent casual movements, but home ranges do not overlap with those of other adults of the same sex.

Habitat quality is used to define the animal’s home range and its daily survival rates. Each cell in the landscape is assigned a quality index that depends on vegetation cover and density of conspecifics. For most species, cells with brine spills are less suitable than those without. Our movement algorithm requires home ranges to contain a minimum average quality within a restricted total area. Survival probabilities are lower for animals when they are in low quality cells, reflecting a reduced availability of prey or an increased risk of predation.

Model results will contribute to generalizations about the effect of the size and distribution of brine and oil spills on the demographics of wildlife populations. Exclusion criteria and/or mitigation measures for E&P sites may be recommended, based on results of population modeling. The models will comprise part of the ecological framework for E&P sites that is the final deliverable for this project.

FUNDAMENTAL CHEMISTRY OF HEAVY OIL

W. V. Steele
Oak Ridge National Laboratory

INTRODUCTION

Catalytic hydroprocessing continues to be the core method for upgrading of feedstocks with high aromatic content. European environmental organizations have already established standards in this area and the U.S. is expected to follow in the near future. The reduction of aromatics in heavy petroleum upgrading will require careful management of hydrogen during hydroprocessing. Effective hydrogen management requires an understanding of the relationship between the distribution of the hydrogenated products in the process streams and the conditions of their formation, i.e., temperature and pressure.

To counteract the adverse effects of carbon rejection methods, refiners have the option of hydrogen-addition (hydroprocessing) methods. However, hydroprocessing consumes large quantities of hydrogen. As refineries reconfigure to produce the new "clean fuels" ("reformulated fuels," i.e., those with oxygenates present), hydrogen shortages are occurring, and new sources of supply are required. The addition of oxygenates to gasoline means that less octane is required from the reformer, lowering the severity of the operation and the amount of hydrogen formed. Also, the mandated reduction of aromatics content by the U.S. government in the 1990 Clean Air Act Amendments has resulted in a further reduction of reformer operating severity, hence, severely reducing hydrogen production. Other contributions to the problem in managing hydrogen result from mandated lower gasoline temperature endpoints and reduced sulfur levels. Hence, the use of hydrogen exactly where it will "do the most good" is paramount. Over-hydrogenation will have to be minimized.

The purpose of the cooperative work between the Design Institute of Physical Property Data (DIPPR)® and the Thermophysical Property Group within the Separations and Materials Research Group at ORNL is to develop thermodynamic and thermophysical property data for use in leading edge chemical technology. The property measurements are directed by the DIPPR Project Steering Committees responsible for Project 821-Pure Component Liquid-Phase Vapor Pressure Measurements and Project 871-Pure Component Ideal-Gas Enthalpies of Formation. The objective of Project 821 is to obtain precise and accurate liquid-phase vapor pressure data for selected pure components. The objective of Project 871 is to measure the enthalpies of combustion and derive the enthalpies of formation in both the condensed and the idea-gas phases of "key" compounds that have been chosen to elucidate the enthalpy of particular atomic groupings. These group contributions can then be used to estimate data on large families of related compounds each containing that particular atomic arrangement.

DIPPR, now in its 23rd year of funded research, is the oldest of the American Institute of Chemical Engineers' (AIChE) active Industry Technology Alliances. In 2002, DIPPR has 31 sponsors from industry and government bodies. Its purpose is to make possible, through joint sponsorship, thermophysical property data measurement, correlation, and dissemination. The objective of the Design Institute for Physical Property Data (DIPPR)® is to develop the world's best set of critically evaluated thermophysical and environmental property data to satisfy industry needs. Data developed in DIPPR projects have become the data of choice for leading chemical process simulators and are used throughout the world.

DISCUSSION OF CURRENT ACTIVITIES

Background

Worldwide demand for petroleum products continues to expand as the nations develop. However, if the demand is analyzed in terms of the three major classes of petroleum cuts: light products such as gasolines; petrochemical feedstocks, middle distillates such as jet fuels and diesels; and heavy products such as fuel-oils and lubricants; then there has been a drastic shift in emphasis toward the light end. Whereas in 1972, both the light products and the middle distillates accounted for approximately 30% of the market. Analysts believe that by the turn of the century the light products will have 38%, the middle distillates 40%, leaving only 22% for the 1973 major component the heavy-ends.

Whether it is an East Coast refinery importing crude oil from Nigeria, or a U.S. Gulf Coast refinery importing crude oil from Saudi Arabia, or even a U.S. West Coast refinery operating on Alaskan North Slope crude, over the last decade or more for which records are available (1986–96), the quality of the crude oil processed by refineries has declined. If the decline in the quality of crude processed in U.S. refineries is denoted in terms of the API gravity, the gravity has decreased by an average of 0.15° per year in the decade 1986–95.[1] Furthermore, the decline appears to have accelerated back to the rate applicable in the early 1990's. Measured as a five-year average (1989–93), the API gravity had declined by 0.22° per year. After leveling at 31.3^{o} for the next four years, in 1996 it was back on the line pointing to a value of 30.5° for the API gravity in the year 2000. As the API gravity of crude oil falls, the aromatic content (carbon content) increases and the correlations derived for the light crudes begins to break down. The failure of the correlations is well documented in the literature. New or revised correlations are necessary for continued high thermal efficiency in the refining of present and future crudes.

Within the petroleum industry, catalytic hydroprocessing continues to be the core method for upgrading of feedstocks with high aromatic content, as well as for heteroatom removal through HDS and HDN. Meetings such as the 3-day symposium, "Recent Advances in Heteroatom Removal," presented at the Division of Petroleum Chemistry meeting as part of the ACS biannual meeting held in Dallas, March

1998, demonstrate the extensive interest by the petroleum and catalysis industries in this area. In a review of fuel-quality specification for transportation fuels, Touvelle et al. of Exxon Research and Engineering discussed trends in the regulation of aromatics in fuels. Although benzene content is carefully scrutinized, the total aromatics content is not regulated specifically in the U.S. In contrast, European environmental organizations have already established standards in this area and the U.S. is expected to follow in the near future.

The reduction of aromatics in petroleum and particularly in heavy petroleum will require careful management of hydrogen during hydroprocessing. Effective hydrogen management requires an understanding of the relationship between the distribution of the hydrogenated products in the process streams and the conditions of their formation, i.e., temperature and pressure. To meet this need, a dual-track approach involving both state-of-the-art property measurement and advanced Ab Initio computations is proposed.

The property measurement program previously funded by DOE Fossil Energy in Oklahoma has accumulated extensive results for partially hydrogenated two, three and four-ring aromatics. The majority of these results have not been published; particularly those which allow calculation of hydroaromatic distributions under processing conditions. Ab Initio computational coding is in its infancy in this area. Accurate atomistic modeling of hydroaromatic systems will use the codes and techniques we have developed for parallel molecular simulations on the ORNL Paragons and other parallel supercomputers. Using our simulation capabilities, we believe we can substantially surpass the best prior efforts in realism and quantitative, predictive accuracy. These simulations will build on existing ORNL world-class efforts on simulating high temperature liquid and supercritical aqueous systems.

The experimental database and the fundamental understanding from the simulations will be brought together to develop useful models for correlating data and predicting stability under hydroprocessing conditions. The two fundamental questions to be addressed in this research are: (1) What are the “ideal condition” for meeting low aromatics levels and still meet sulfur levels, smoke point, etc., (2) How does the model react to changes in the complex heterogeneous and multi-component systems (i.e., addition of a new crude oil from, say, Nigeria to the refinery)?

Results from this research will allow the industrial participants to lead the field in catalyst development and process condition controls in processing particularly middle distillates. It can be anticipated that severe operating conditions such as high temperatures, low space velocities, and high pressures can be mediated as the result of insights developed with the program. For example, at low temperatures and high space velocities, the amount of monoaromatics in the product can be higher than in the original feed. This is not unexpected since every mole of triaromatic compound that is saturated would add a mole to the diaromatics, each diaromatic compound hydrogenated would add a mole to the

monoaromatic category, and as the number of rings decrease, the rate of saturation should also decrease. Interaction between the various options can be simulated in the model and options such as increased catalytic activity balanced again two- or even three-stage process designs.

The project has been set up in the CRADA form with an initial lifetime of three years. Subcommittees comprised of DIPPR Project supporters, DOE Fossil Energy Staff, and ORNL staff will decide at the annual AIChE/DIPPR meeting in November a list of compounds for study in the following year in each of the two project areas. Compounds will be chosen to represent whole families containing the necessary functionalities and to facilitate extension of available data bases, rather than to fulfill the specific needs of any single member company.

PROGRESS

Work is in progress on a number of fronts within this project. An initial literature search is being performed to ascertain the relative importance of various aromatic compounds and sulfur-containing compounds in the range of heavy petroleum being imported to refineries in the U.S. Emphasis will be placed on finding the degrees of condensation and substitution of the compound types. The results of the study will be used to define the scope of the experimental work and the reaction schemes to be studied. Available literature data are being collected and process conditions defined where applicable. Properties for the majority of the species have not been published in the open literature, particularly those that allow calculation of hydroaromatic distributions under processing conditions. Hydroaromatic distributions will be derived where possible and a list of gaps in the database highlighted. This work will conclude with the reporting of sets of compounds to be studied to widen the applicability of the derived correlations.

Work is also in progress to ascertain the practicality of using the range of heavy petroleum being imported to refineries in the U.S. to produce both 5 ppm sulfur gasoline and a “clean diesel” with the following specifications: 50 ppm sulfur with lower density, lower PAH (polyaromatic hydrocarbons), lower boiling point, and higher cetane number than the “best diesel being produced for the California market. Preliminary results of calculations of the conditions necessary to obtain various sulfur levels in diesel using hydrodesulfurization are given in Table 1. In the table the baseline is assumed to be the conditions (temperature/pressure/catalyst activity) required to produce 500 ppm sulfur diesel.

Table 1. Conditions necessary to produce certain sulfur ppm levels in diesel

Sulfur content	Catalyst activity	Temperature F	Hydrogen pressure
Baseline 500 ppm	100%	Baseline	Baseline
350 ppm	130%	+15F	120%
200 ppm	190%	+30F	170%
100 ppm	300%	+55F	300%
50 ppm	450%	+70F	600%

To obtain the required sulfur level, only one of the listed options would be required. Obviously, the hydrogen pressure increase option is not realistic. Note also that the increase in temperature would mean that the amount of aromatics would increase, requiring even greater hydrogen pressure to premeditate the effect.

Another option other than hydrodesulfurization to meet the sulfur level is alkylation of the sulfur-containing molecules raising the boiling point of sulfur-containing fraction and removing the sulfur in the resid. Or, the sulfur-containing compounds can be removed by selective adsorption using a catalyst containing a zero-valent transition metal. Presently, both methods of sulfur removal are being presented by refiners as new technology options. Results from this research project will aid in both research areas (property measurements will give examples of boiling point of substituted benzothiophenes with both degree of substitution and actual position of substitution). Initial calculations point to several metals being particularly capable of reversible adsorption of benzothiophenes and dibenzothiophenes under very moderate reaction conditions. Further computational chemical calculation during FY 2001 will expand on these initial ideas.

Finally, work is also in progress on what the PI of this project calls “The 2015 Refinery” where all processes within the bounds of the refinery are as environmentally sound as possible. The 2015 refinery would for example not have any alkylation units with the associated problems of HF-or H_2SO_4. Fuels would be manufactured via olefin formation and upgrading. Possibilities then increase of producing “zero sulfur” gasoline and even cleaner-burning naphthenic fuels.

In the reporting period, the CRADA was signed and both project committees have met during the AIChE meeting in Los Angeles in November 2000. Lists of possible compounds for measurements were tentatively drawn up at those meetings and finalized after subsequent literature surveys were conducted to ensure the quantity and quality of any available data. Samples of each of the chemicals chosen for study have been obtained and purification via spinning-band distillation or (in case of solid samples) zone-refining are in progress. The property measurements are due to commence in early May 2002.

Results from earlier work completed at Bartlesville, Oklahoma, have cleared full committee review and will be published in the *Journal of Chemical & Engineering Data* in May 2002. The titles of the 6 papers are:

- DIPPR Project 821. Vapor Pressure of Organic Compounds of Industrial Interest. The 1995 Project Results. Vapor pressure, heat capacity, and density along the saturation line measurements for Benzenamine, butylbenzene, sec-butylbenzene, tert-butylbenzene, 2,2-dimethylbutanoic acid, tridecafluoroheptanoic acid, 2-butyl-2ethyl-1,3-propanediol, 2,2,4-trimethyl-1,3-pentanediol and 1-chloro-2-propanol. By W. V. Steele, S. E. Knipmeyer, and A. Nguyen.

- DIPPR Project 821. Vapor Pressure of Organic Compounds of Industrial Interest. The 1996 Project Results. Vapor pressure, heat capacity, and density along the saturation line measurements for ε-caprolactam, pyrazine, 1,2-propanediol, triethylene glycol, phenylacetylene, and diphenylacetylene, by W. V. Steele, S. E. Knipmeyer, and A. Nguyen.

- DIPPER Project 821. Vapor Pressure of Organic Compounds of Industrial Interest. The 1997 Project Results. Vapor pressure, heat capacity, and density along the saturation line measurements for cyclopropane carboxylic acid, N,N-diethylethanolamine, 2,3-dihydrofuran, 5-hexen-2-one, perfluorobutanoic acid, and 2-phenylpropionaldehyde. By W. V. Steele, S. E. Knipmeyer, and A. Nguyen.

- DIPPR Project 871. Thermodynamic Properties and Ideal-Gas Enthalpies of Formation. The 1995 Project Results. Methyl benzoate, ethylbenzoate, (R)-(+)-limonene, tert-amylmethyl ether, transcrotonaldehyde, and diethylene glycol by W. V. Steele, A. B. Cowell, R. D. Chirico, S. E. Knipmeyer, and A. Nguyen.

- DIPPR Project 871. Thermodynamic Properties and Ideal-Gas Enthalpies of Formation. The 1996 Project Results. Trans-Methyl cinnamate, α-methyl cinnamaldehyde, methyl methacrylate, 1-nonyne, trimethylcetic acid, trimethylacetic anhydride, and ethyltrimethylacetate by W. V. Steele, A. B. Cowell, S. E. Knipmeyer, and A. Nguyen.

- DIPPR Project 871. Thermodynamic Properties and Ideal-Gas Enthalpies of Formation. The 1997 Project Results. 1,4-Diisopropylbenzene, 1,2,4,5-tetraisopropylbenzene, cyclohexanone, oxime, dimethyl malonate, glutaric acid and pimelic acid by W. V. Steele, A. B. Cowell, S. E. Knipmeyer, and A. Nguyen.

REFERENCE

1. S. W. Benson, *Thermochemical Kinetics*, 2nd Edition; Wiley: New York, 1976.

ADVANCED TECHNIQUE FOR IMPROVING THE BIOLOGICAL QUALITY OF PETROLEUM CONTAMINATED SOILS

Arthur J. Stewart
Oak Ridge National Laboratory

INTRODUCTION

"Advanced Technique for Improving the Biological Quality of Petroleum Contaminated Soils" started in May 1999 with support by the U.S. Department of Energy (Fossil Energy Program, National Petroleum Technology Office, Tulsa, OK; Nancy Comstock, Project Manager). It provides data and technical guidance to Petroleum Environmental Research Forum (PERF) project 99-01, "Ecological Evaluation for Upstream Site Remediation," sponsored by Chevron (http://www.perf.org/). Participants in PERF Project 99-01 currently include ChevronTexaco, ExxonMobile, Phillips Petroleum and BP Amoco, in addition to the Department of Energy. The objective of PERF Project 99-01 is ". . . to develop and/or improve methods for ecological risk evaluations and assessments via the development of early exit criteria for excluding sites from ecological risk assessment, and using field surveys to determine appropriate cleanup standards for total petroleum hydrocarbons (TPH) or salts in site soils." To complement PERF Project 99-01, the "Advanced Technique…" project focused on the following question: What types of soil amendments or biological treatments might be used to improve the biological quality of oily soils found in petroleum landfarming operations?

Petroleum landfarms are sites where waste petroleum hydrocarbons are biotreated by direct application to the ground. The materials are tilled into the soil, along with nutrients, to encourage biodegradation of the hydrocarbons by soil microbes. Soil "bulking agents" and gypsum are usually applied as well, to improve ion balance and physical properties of the soil. One problem associated with petroleum landfarming is that while lower molecular weight petroleum compounds volatize and/or are biodegraded efficiently, higher molecular weight petroleum compounds tend to biodegrade much more slowly. Thus, a consequence of continued application of petroleum hydrocarbons to landfarm soil is the gradual accumulation of high-molecular weight petroleum compounds. Unrefined petroleum is not very toxic on a per-unit-mass basis, but at high concentrations it can increase soil water repellency, which can have negative effects on plant growth. As a result, bioremediated oily soils may be less productive than desired, and may not support a taxonomically or functionally diverse community of soil invertebrates. Ultimately, the concentration of petroleum hydrocarbons approaches an upper-bound permitted limit (typically 10,000 ppm as TPH). When this occurs, the landfarm can no longer be used for treating additional waste petroleum, and alternative uses for the land are then desired. It is possible that regulators

would be more willing to consider alternative land-use possibilities if the soils are of demonstrably good quality with respect to their ability to support communities of plants and soil invertebrates.

DISCUSSION OF CURRENT ACTIVITIES

This report is both an annual report and the project's concluding report. Over the past 12 months, we completed the last definitive experiments, and reported the results of the study. As part of the past 12-months' activities, the project's principle investigator also accomplished the following: (1) Attended two PERF meetings, made a site visit to a landfarm operation near Rangely, Colorado, and participated in a DOE NPTO/NETL workshop on produced water and air quality in Houston, Texas; (2) met with Dr. Kerry Sublette (University of Tulsa), to discuss the possibility of remediating brine-damaged soils with a combination of vegetation and earthworms; (3) attended the annual meeting for the Society for Environmental Toxicology and Chemistry in Baltimore, Maryland; and (4) completed arrangements for hosting a minority internship student (Ms Michelle Kerr; Jefferson Community College, Louisville, KY), during June–August 2002. Details for these activities are given below.

Throughout the project, I have used project funds to attend appropriate PERF meetings. Over the 12 months, I attended PERF meetings in Brea, CA (October 2001) and San Ramon, CA (February 2002). Other travel accomplished with project support was a trip to Houston, TX, to attend the DOE NPTO/NETL workshop on produced water quality and air quality issues at upstream sites (January 2001), and a trip to Baltimore, MD, in November 2001, to attend the annual meeting of the Society for Environmental Toxicology and Chemistry (http://www.SETAC.org). The SETAC annual meeting is significant because SETAC is an important "open forum" within which industry representatives, scientists, and environmental regulators can professionally interact.

In June 2001, a co-worker and I also visited a ChevronTexaco landfarm operation near Rangely, Colorado (Fig. 1). This landfarm was the source of the petroleum-contaminated soil that was used throughout the project. The site visit was valuable in that it allowed us to better understand the details and practicalities of landfarm operation.

The PI's discussion with Dr. Kerry Sublette occurred at the University of Tennessee's Center for Biomarker Analysis in February 2002 and focused on the idea that vegetation and earthworms might be used together to increase the rate of ecological recovery of brine-damaged soil. This idea stemmed logically from research conducted to support the "Advanced Technique…" project, because one of the most interesting findings from the "Advanced Technique…" project was that plants (tall fescue) seeded into an oily soil did better (i.e., had more root and shoot growth) when earthworms were present. Furthermore, the "Advanced Technique…" project showed that earthworm survival in the oily soil was greater if plants were present, when straw was used as an organic amendment. Thus, biotic manipulations

Fig. 1. Project PI (left), learning about petroleum landfarm operations from a ChevronTexaco environmental engineer. Irrigation structures can be seen in the background. The soil is disked periodically to improve aeration, and must be kept moist enough to promote soil-microbe activity.

used together (such as the addition of straw and earthworms, particularly in conjunction with vegetation) might hasten remediation, or guide recovery to more desirable outcomes. We thought that earthworms plus straw plus plants might also accelerate the recovery of soils that have been damaged by other pollutants, such as brines.

Dr. Mac Callaham, an ORAU Postdoctoral Fellow who worked on the project, gave several poster presentations highlighting key results of the investigations, as noted in last year's annual project report. However, in June 2001, after leading the preparation of the manuscript that provides the results of the experiments conducted to support the "Advanced Technique…" project, Dr. Callaham accepted a position with the U.S. Forest Service. The manuscript he led was accepted following minor revision, and is now scheduled for publication in *Environmental Toxicology and Chemistry* in July 2002 [1]. As soon as reprints are available to us, we will make them available to anyone who so requests.

Throughout the project, the PI has been attentive to the fact that the "Advanced Technique…" project is the hands-on type of project that can provide exceptional science-education opportunities for students. Assistance from students can benefit projects, too, simply because student time is much less costly than PI time. Furthermore, some of the science-education programs funded through DOE allow PIs to assign "free" or cost-shared students to projects. In such cases, mutual benefits are realized: the student benefits by participating in ongoing research, and the project benefits by "extra hands" at reduced cost.

Although the "Advanced Technique…" project is ending, the PI was able to get one last "free" internship student (Ms Michelle Kerr), who will assist the project during June 3 through August 9, 2002. Ms Kerr, a DOE-CCI participant from Jefferson Community College (Louisville, KY) will conduct tests to determine the sensitivity of earthworm to brine constituents in soil; her assistance is "free" to the project because the DOE's (Office of Science Education) Community College Initiative (CCI) is paying for her costs. The various students (and a visiting scientist) who contributed to "Advanced Technique…" since the project started in 1999 are listed in Table 1; only one of these individuals (Dr. Mac Callaham) was supported by project funds.

Table 1. Students and visiting scientists contributing to the "Advanced Technique…" project since June 1999

Student name	Start date	General area of contribution	Education level[a]	Sponsor information
Susan Humphries	June 1999	Revegetation potential of petroleum landfarm soil	UG-CC	DOE-CCI; no project cost
Bi-Chi Do	June 2000	Endophyte effects on growth of tall fescue	UG-CC	DOE-CCI; no project cost
Mac Callaham	June 2000	ORAU Postdoctoral Fellow	PD	Supported at project cost
Melissa Knight	June 2000	Use of earthworms for soil-quality tests	HS	ORISE SEED; no project cost
Clara Alarcón	September 2000	Bioassay techniques for oily soils	MS, VS	PDVSA-Intevep; no project cost
Carmen Infante	May 2001	Microbial tools for environmental clean-up	PhD, VS	PDVSA-Intevep; no project cost
Michelle Kerr	June 2002	Tolerance of earthworms to brine in soil.	UG-CC	DOE-CCI; no project cost

[a]Education-level codes are: UG-CC = undergraduate community college; PD = postdoctoral; HS = high school; MS-VS = Master of Science, visiting scientist; and PhD-VS = Doctorate, visiting scientist.

Finally, the PI plans to attend a DOE-PERF workshop in Houston (May 30, 2002); the focus of this workshop is on the bioremediation of crude oil and fuels in soil, a topic that relates directly to subject matter in the "Advanced Technique…" project.

As noted previously, the main technical accomplishments of the project are summarized effectively in the paper scheduled for publication in the July 2002 issue of *Environmental Toxicology and Chemistry*. The most useful product of "Advanced Technique…" were data supporting the idea that the biological quality of biotreated oily soils may be increased, post-treatment, by the use of simple organic amendments (such as straw) plus bio-manipulations that include (for example) a cover crop and addition of earthworms. The general principle of the strategy developed by conducting the "Advanced Technique…" project dovetails with and extends the concept of phytoremediation, a vegetation-focused

technique currently being evaluated as a means for hastening the recovery of oil-contaminated land. References [2–7], below, provide access to literature we found to be particularly relevant to the project.

REFERENCES

1. M. A. Callaham, Jr., A. J. Stewart, C. Alarcón, and S. J. McMillen, "Effects of earthworm (*Eisenia fetida*) and wheat straw (*Triticum aestivum*) additions on selected properties of petroleum contaminated soils." *Environmental Toxicology and Chemistry* (in press).
2. S. S. Humphries, K. D. Gwinn, and A. J. Stewart, "Effects of endophyte status of tall fescue tissues on the earthworm, *Eisenia fetida.*" *Environmental Toxicology and Chemistry.* **20**:1346–1350 (2001).
3. C. G. Jones, J. H. Lawton, and M. Shachak, "Organisms as ecosystem engineers." *Oikos* **69**:373–386 (1994).
4. S. O. Bain, K. R. Butt, and R. M. Morris, "Survival and reproduction of *Lumbricus terrestris* L. in colliery spoil and sewage sludge." *Pedobiologia* **43**:729–734 (1999).
5. K. R. Butt, J. Frederickson, and R. M. Morris, "The earthworm inoculation unit (EIU) technique, an integrated system for cultivation and soil-inoculation of earthworms." *Soil Biology and Biochemistry* **29**:251–257 (1997).
6. J. P. Curry and D. C. F. Cotton, "Earthworms and land reclamation," pp. 215–228 in *Earthworm Ecology, From Darwin to Vermiculture*, J. E. Satchell (ed.), Chapman and Hall, London (1983).
7. R. Martens and F. Zaradril, "Screening of white-rot fungi for their ability to mineralize polycyclic aromatic hydrocarbons in soil." *Folia Microbiologia* **43**:97–103 (1998).

NEW ACOUSTIC WAVE PIPE INSPECTION SYSTEM

Venugopal K. Varma, Raymond Tucker, Steve Kercel, Thomas Thundat, and Ali Passian
Oak Ridge National Laboratory
and
Joseph Rose and Xiaoliang Zhao
Pennsylvania State University

INTRODUCTION

The safety of the Unites States' natural gas supply is of prime importance since 30% of the energy produced in the country is derived from it. Natural gas is supplied through a vast, million-mile pipeline network. Pipeline companies have an impressive safety record due to the proactive role of standards and inspection of pipelines. Since the pipelines are getting old, there is a great need to identify corrosion, cracks, and other defects that can cause potential problems.

There are two main ways of testing the integrity of pipelines. One is destructive inspection and the other is non-destructive testing. The destructive testing procedure uses a hydrostatic inspection technique to verify that a pipeline is within the safety margin for operation. The procedure does not however locate defects that are just above the threshold of the safety margin. In addition, the testing disrupts the pipeline's normal operation. For this reason it is not a preferred method. Generally, such techniques are good for offline inspection of pipelines before they are put into use. On the other hand, non-destructive inspection (NDI) techniques detect flaws that can cause potential failure in future. This way, NDI provides information on the integrity of the pipeline as well as a measure of its current safety margin.

There are two main methods of non-destructive testing of pipeline. They are (1) Magnetic Flux Leakage and (2) Ultrasonic method. This project uses the ultrasonic wave guide using EMAT's (Electro Magnetic Acoustic Transducers) to detect the flaws.

FLAW DETECTION

The project uses a horizontal shear wave generated using EMATs to detect flaws. The EMAT produces a shear force on the carbon steel pipe wall due to a combination of Lorentz and Magnetorestive forces. A schematic of an EMAT is given in Fig. 1. The force is given by the equation **F = J x B,** where F is the force vector, J is the current vector and B is the magnetic field vector.

In order to detect both circumferential and axial flaws, two separate EMAT sets are deployed The two sets of EMATS produce two waves traveling along the circumferential and axial direction.

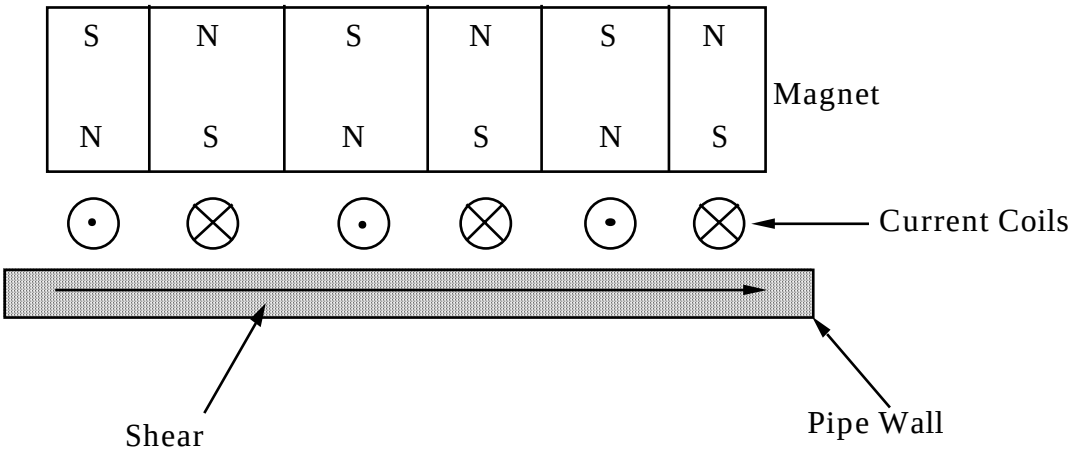

Fig. 1. Schematic of a horizontal shear EMAT.

The objective of the experimental set-up is to quantify the flaw (width, depth) and determine the severity of the condition. The EMAT will also be able to detect metal loss and pitting damages inside the pipeline. Figure 2 shows the EMAT inside a 10 in. diameter pipe for flaw evaluation.

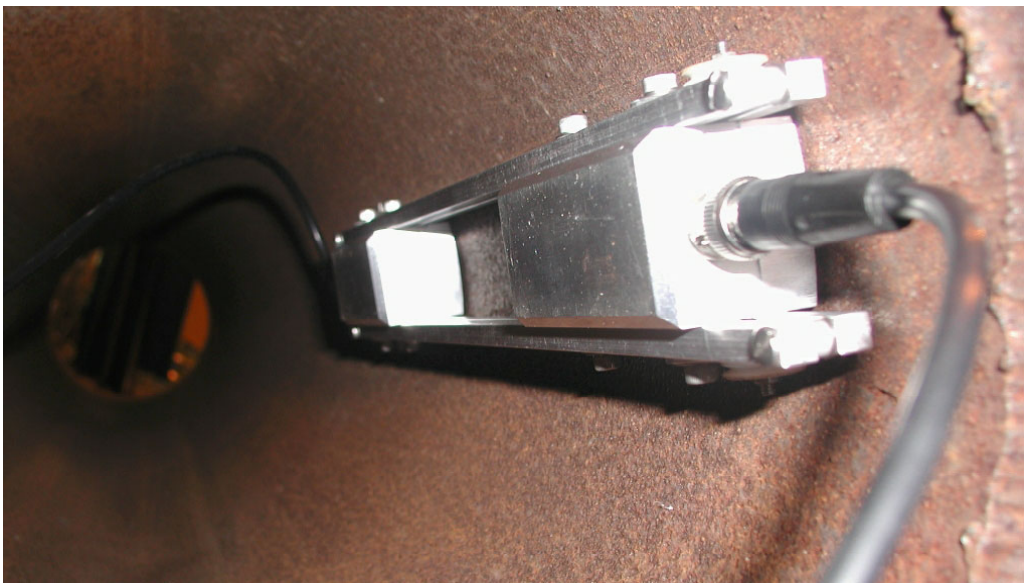

Fig. 2. EMAT configured inside a pipe to detect flaws.

The flaws used for these tests are machined grooves to calibrate the waveform signature for a known defect. These calibration data can then be used to predict an uneven flaw on a pipe.

The shear wave traveling along the thickness of the pipe wall is interrupted by flaws it encounters. Part of the signal is reflected while the other gets transmitted. The ratio of the transmitted to the reflected

component of the wave is dependent on the type and shape of the flaw. Figure 3 gives a transmitted component of the shear wave for a 10 in. pipe with 1/8 in. wide flaw with varying depth of defect obtained from computer modeling.

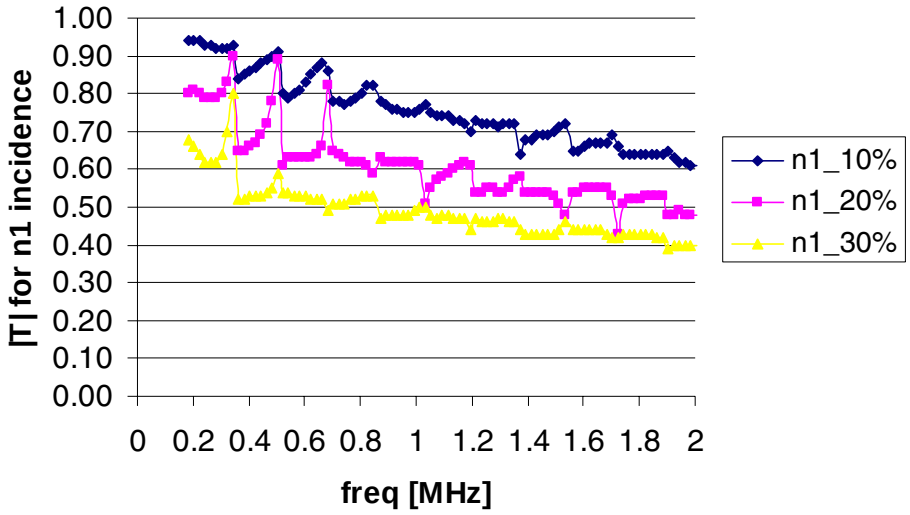

Fig. 3. Transmission coefficients of shear wave on a 1/8 in. wide flaw.

After the raw data is obtained from the data acquisition system, wavelet analysis is used to quantify the flaw. Wavelet analysis will also help compress the data stored during analysis of the pipeline. Pre-filtering the data, and storing only those that are relevant for flaw detection/analysis can reduce the amount of information stored.

CRACK DETECTION

Introduction: Apart from flaw detection using EMATs, the project also is working on the detection of cracks using microcantilevers. Microcantilevers are micron sized (μm) devices that have a fundamental frequency of vibration in the KHz range. The gas escaping from the crack has an acoustic signal that is dependent on the size of the crack. By tuning the cantilever to match its frequency to that of the escaping gas, pipeline cracks can be detected and characterized. Current acoustic detection systems are bulky, fragile, and expensive. A detection system that provides high performance in a rugged, affordable package will be very attractive for pipe inspection. A novel micro-electro-mechanical system (MEMS)-based acoustic sensor that uses a tunable, high Q microcantilever array is being pursued under this project.

Test Results: An 8 in. diameter pipe with one end closed and the other end connected to the plant air was used for the initial testing of cantilever sensors. A small crack was fabricated on the pipe using a drill. The cantilever was placed outside the pipe to detect the acoustic signal produced by the escaping air. Initial tests on pin hole cracks through which gas escapes has been effectively detected using this approach. The cantilever need not be placed next to the crack and even with a stand off distance of approximately 4 in., the cantilever was able to detect the presence of a crack.

During the deployment of this sensor, it will be integrated with the flaw detector and the PIG that travels inside the Natural Gas pipeline. Hence, the next step in this research is to place the cantilever inside the pipe and conduct a similar study. Also, the cracks that develop in Natural Gas pipelines are not regular geometric shapes and in order to see the variation of the frequency between various crack shapes, multiple cracks will be fabricated on a single pipe. By allowing gas to escape through only one crack at a time, the frequency variation of the acoustic signal to crack size will be quantified. A resistive type cantilever is used for these experiments. Another important information that will be gathered is the effect of multiple cracks on the acoustic frequency seen by the cantilever.

CURRENT STATUS OF THE PROJECT

- All hardware necessary for the flaw detection is in place
- Pipes with circumferential and axial flaws have been fabricated
- Preliminary data have been taken and experiments are being conducted to fully characterize the machined flaws with EMAT sensors
- 2-D modeling of the acoustic wave transmission through a flaw is complete and 3D modeling is currently being pursued
- Crack detection hardware is ready and preliminary data have been obtained for the microcantilever sensor

REAL-TIME BUBBLE SIMULATIONS FOR FLUIDIZED BEDS

S. Pannala, C. S. Daw, and W. A. Shelton
Oak Ridge National Laboratory

INTRODUCTION

Fluidized bed reactors are widely used in the chemical industry and are essential to the production of key commodity and specialty chemicals such as petroleum, polymers, and pigments. Fluidized beds are also going to be widely used in the next generation power plants in aiding conversion of coal to clean gas. However, in spite of their ubiquitous application, understanding of the complex multi-phase flows involved is still very limited. In particular, existing computer simulations are not sufficiently accurate/fast to serve as a primary approach to the design, optimization, and control of industrial-scale fluidized bed reactors. Availability of more sophisticated computer models is expected to result in greatly increased performance and reduced costs associated with fluidized bed implementation and operation. Such improved performance would positively affect U.S. chemical/energy industry competitiveness and increase energy efficiency.

To improve fluidization simulation capabilities, two different projects are undertaken at ORNL with the specific objective of developing improved fluidization computer models. On one hand, a very detailed multiphase computer model (MFIX) is being employed. On the other hand a low-order bubble model (LBM) is being further developed at ORNL with the eventual aim of real time diagnosis and control of industrial scale fluidized beds.

BACKGROUND

Since the publication of Davidson and Harrison's classic book, "Fluidized Particles," [Davidson and Harrison (1963)], the two-phase model of fluidization has been the most widely used concept to describe the behavior of bubbling fluidized beds. The model assumes that the bed can be described by a phase containing the particles called the "emulsion phase" and a second phase containing the gas beyond what is needed for minimum fluidization of the particles. The model resembles a liquid column with gas bubbles rising through it. The model is simple and elegant and has an intuitive appeal that is extremely helpful in understanding the basic physics of fluidized beds.

Since the introduction of the two-phase model, there have been numerous studies and publications to explain practical aspects of bed performance. Chemical conversion, heat transfer, solids mixing, flows around internals, particle entrainment, and jet behavior has all been explained on the basis of the two-phase assumption. An obvious limitation of many applications is that they assume a single "average" bubble size, while it is known, in fact, that there is a wide range of bubble sizes present at any time.

Various authors [Clift and Grace (1970), Wen and Fan (1975), Glicksman et al. (1981), and Rafailidis et al. (1991)] have recognized the importance of bubble interactions, coalescence, and the distribution of bubble sizes. Available computational power, however, limited their studies to simple cases of only a few bubble interactions.

Recently [Halow et al. (1998)] developed a two-phase bubble model that simulates many dynamic features of bubbling beds at near real-time speed. This low-order model is based on classical two-phase bubbles that behave according to a simple set of deterministic rules defining how each bubble moves and interacts with its neighbors. In their implementation, these rules are similar to those used in cellular automata (CA), except that the bubbles are allowed to move freely and there is no fixed spatial grid. Thus, in effect, the dynamics are tracked in a local Lagrangian frame of reference. The bottom boundary condition of the bed specifies how bubbles are initially injected into the bed, and the rising bubbles are then free to rise, interact, and coalesce. Bubbles reaching the top of the bed exit and disappear according to the upper boundary condition. Global patterns of emergent behavior appear as the net effect of iterating all of the multiple interactions over time.

In studying the simulated bubble patterns from this model, we have observed unexpectedly rich behavior that is reminiscent of emergent behavior in biological and societal systems suggesting that emergent behavior modeling approaches might improve our understanding of fluidized beds.

Emergent behavior refers to collective patterns exhibited by a large group of agents following simple rules for interactions [Resnick (1994), Reynolds (1987), Toner and Yuhai (1998)]. Often cited examples are the flow of traffic (where the rules govern the behavior of each driver) and the flocking of birds (where the rules define each birds flight path relative to its neighbors). Some general characteristics of low-order models for emergent systems are:

(i) The model consists of multiple interacting copies of a limited number of agents.
(ii) The configuration of the agents and components change as time evolves (the model is dynamic).
(iii) Interactions are constrained to a succinct set of deterministic rules.
(iv) Because the interactions are non-linear and sensitive to initial conditions, the collective behavior of many agents cannot be predicted from the behavior of an “average” individual agent.

Emergent systems will generally exhibit a variety of “states” in which some set of interactions have set up a pattern (or non-pattern) of behavior. And usually some set or sets of external perturbations will lead to the transition into or out of one state to another. Important advantages of using low-order models to study emergent behavior are that such models can reveal the essential underlying physics and such models are very amenable to fast computation and, when appropriate, parallelization.

The main goal of the Low-order bubble model is to capture the large-scale global behavior of the fluidized beds, as these features are important in addressing many problems commonly investigated. Large-scale global features can dominate bulk mixing, heat transfer, mass transfer, chemical reactions etc., in a fluidized bed. In addition, global features can be used as diagnostics for small-scale phenomena (e.g., detecting onset of solids stickiness or agglomeration by shifts in solids circulation). Global features are also critical to validation of detailed CFD codes and low-order models can help interpret physical reasons for code/experiment differences. Better understanding of global dynamics may lead to new control strategies (e.g., how does solids circulation affect agglomeration, how does distributor design affect circulation). Since the LBM is extremely fast, it can be used for on-line diagnostics and control of a very large beds used for various industrial processes.

RESULTS AND DISCUSSION

Mathematically, the formulation is not analytically solvable. There is one equation for each bubble that is in the bed and so for many simulations this can amount to hundred or thousands of equations. Each equation is a first order O.D.E. coupled nonlinearly to another equation through the bubble separation distances. While analytically complex, the problem is readily solvable numerically. Currently, with Pentium IV computers, the simulation runs near real-time for thousands of bubbles formed in a second.

A first order explicit time integration is currently used and it is sufficient for our use as the code is run at small enough time-steps to capture the transient behavior of the fluidized bed. A quick sort algorithm is used for sorting bubbles to determine the nearest leading and trailing bubbles. This algorithm seems to be efficient for this sorting process and this part of the code takes very little time. The original code (Halow et. al, 1998) was using visual basic. This code has been translated to Fortran 90 so that is more portable, modular and efficient. Detailed profiling was performed and the efficiency of the code was improved by two orders of magnitude to give the ability to model large-systems with thousands of bubbles almost real-time. The flowchart of the current code is detailed in Fig. 1. The algorithm is inherently suited for parallel computations and at a later point if need arises - it can be easily parallelized to do even bigger and detailed simulations.

Large-scale beds with different cross-sections (square and circular) were simulated for various cases. Most of these results were presented at the AIChE annual meeting in November, 2001 (Pannala et. al., 2001). Some of the salient results are presented here.

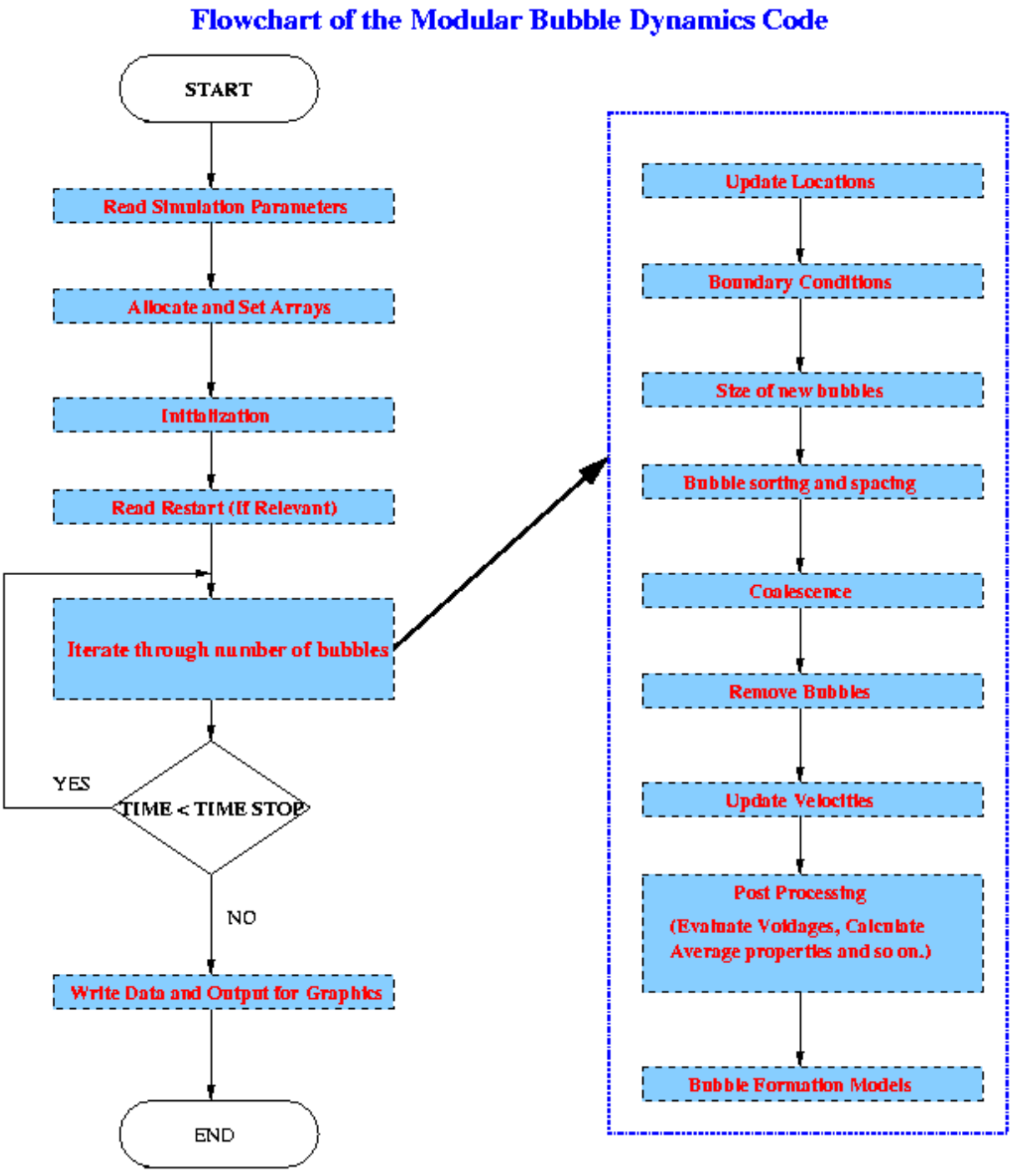

Fig. 1. Flowchart of the lower order bubble model code.

The following are the details of the 3-D simulation with square cross-section.

- 200 cm width bed
- Bed L/D equal to 3.0
- U_{mf} = 6 cm/sec
- U/U_{mf} = 2
- 2.5 cm bubbles released at randomly from distributor
- Spacing of Tuyeres (injectors) = 25 cm

Figure 2 illustrates the bubble distribution at various axial locations of the bed. At 100-cm height the bubbles start interacting from bubbles injected from the neighboring injectors. The interaction extends between the neighboring chains as the coalesced bubbles start interaction and bigger bubbles are formed. The process continues till the bubbles become even bigger through the coalescence process and a description of this process is summarized in Fig. 3.

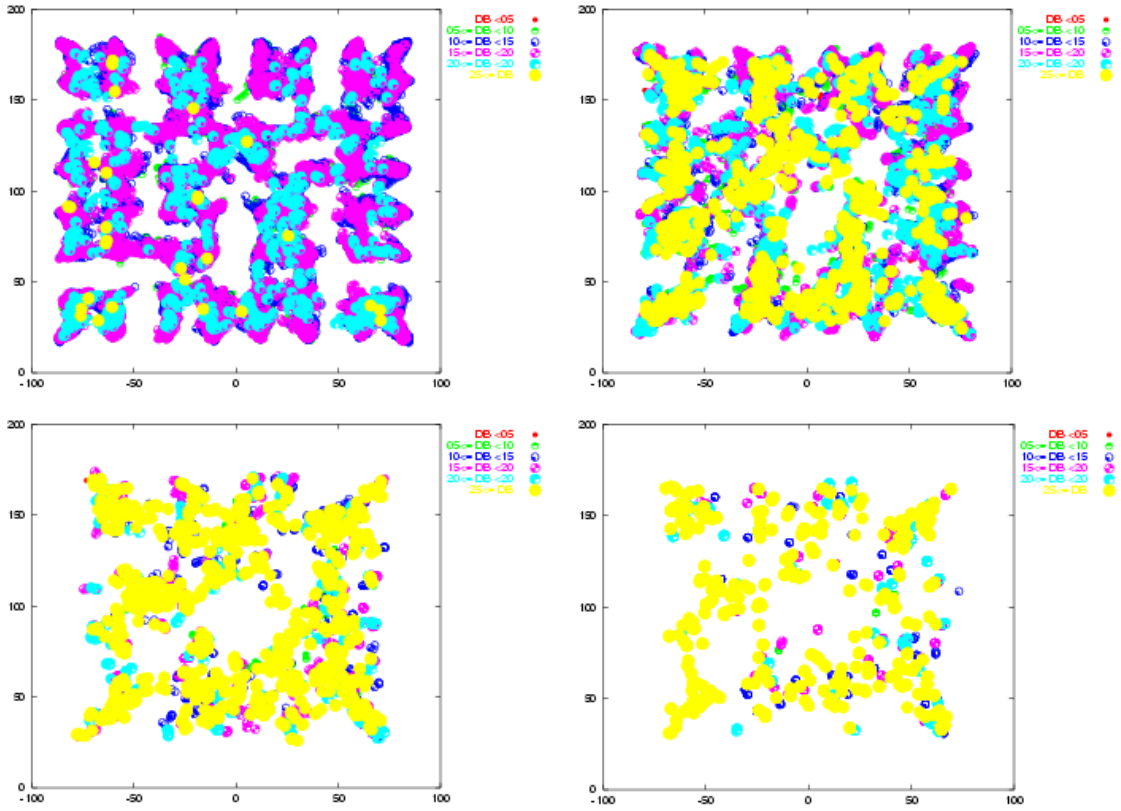

Fig. 2. Bubble distribution at various heights (a) 100 cm, (b) 200 cm, (c) 400 cm, and (d) 600 cm.

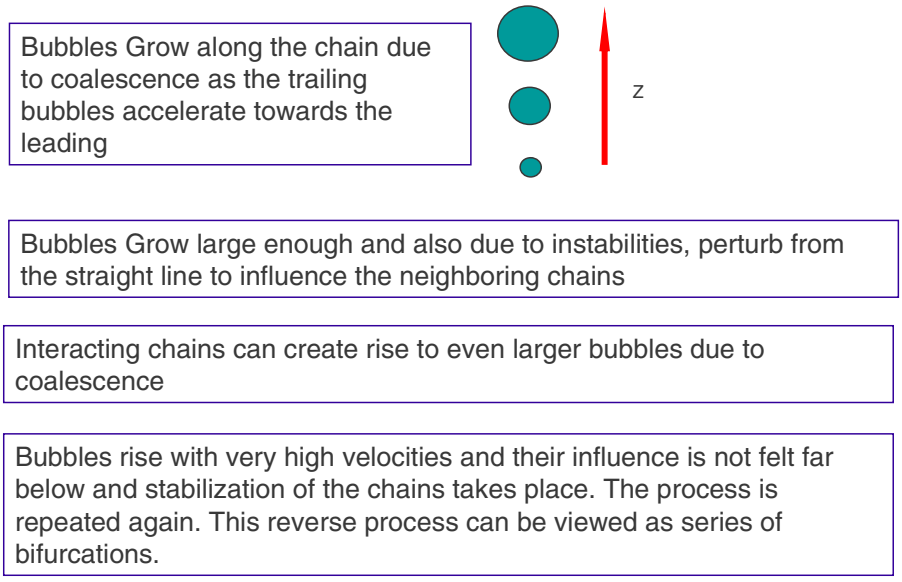

Fig. 3. Schematic explaining the formation of channeling and the emergent behavior.

Simulations of these large-scale beds show that LBM captures global features like channeling and emergent behavior. It has also been found that square beds behave differently from the circular beds because of imposition of the boundary conditions. The next steps include simulating chemical processes and the chemical conversion rates. These results will be compared to some known experiments. Using the model various parametric studies will be performed to map a space of optimal performance of the fluidized beds.

REFERENCES

Clift, R. and J. R. Grace, "Bubble Interaction in Fluidized Beds," *Chem. Eng. Prog. Symp. Ser*. **66**, 14 (1970).

Davidson, J. F. and D. Harrison, Fluidized Particles, Cambridge University Press, 1963.

Glicksman, L., W. Lord, J. Valenzuela, A. Bar-Cohen, and R. Hughes, "A Model of the Fluid Mechanics in Fluidized Bed Combustors," *AIChE Symp. Ser*. **77**, 139 (1981).

Halow, J. S., E. J. Boyle, C. S. Daw, and C. E. A. Finney, 3-Dimensional Simulation of Fluidized Beds, Fluidization IX Durango, Colorado, May, 1998.

Pannala, S., Daw, S. and Halow, J., “Near Real-time Simulations of Large Fluidized Beds with a Low Order Bubble Model,” Session 199b, *AIChE Annual Meeting*, Reno, Nevada, November 4-9, 2001.

Rafailidis, S., R. Clift, and E. J. Addis, “Study of the Influence of Bubble Formation at the Distributor on Fluidized Bed Behavior,” *AIChE Symp. Ser*. **87**, 47 (1991).

Resnick, M., Turtles, Termites, and Traffic Jams: Explorations in Massively Parallel Microworlds, The MIT Press, 1994.

Reynolds, C. W., “Flocks, herds, and schools: A distributed behavioral model,” *Computer Graphics* **21**, 25 (1987). See also http://hmt.com/cwr/boids.html

Toner, J. and Yuhai T., “Flocks, herds, and schools: A quantitative theory of flocking,” *Physical Review **E*** **58**, 4828 (1998).

Wen, C. Y. and L. T. Fan, Models for Flow Systems and Chemical Reactors, Chap. 10, pp. 358–389, Marcel Dekker, New York, 1975.

COMPUTATIONAL FLUID DYNAMICS FOR MULTIPHASE FLOW

S. Pannala, E. D'Azevedo, and C. S. Daw
Oak Ridge National Laboratory

INTRODUCTION

Fluidized bed reactors are widely used in the chemical industry and are essential to the production of key commodity and specialty chemicals such as petroleum, polymers, and pigments. Fluidized beds are also going to be widely used in the next generation power plants in aiding conversion of coal to clean gas. However, in spite of their ubiquitous application, understanding of the complex multi-phase flows involved is still very limited. In particular, existing computer simulations are not sufficiently accurate/fast to serve as a primary approach to the design, optimization, and control of industrial-scale fluidized bed reactors. Availability of more sophisticated computer models is expected to result in greatly increased performance and reduced costs associated with fluidized bed implementation and operation. Such improved performance would positively affect U.S. chemical/energy industry competitiveness and increase energy efficiency.

To improve fluidization simulation capabilities, two different projects are undertaken at ORNL with the specific objective of developing improved fluidization computer models. On one hand, a very detailed multiphase computer model (MFIX) is being employed. On the other hand a low-order bubble model (LBM) is being further developed at ORNL with the eventual aim of real time diagnosis and control of industrial scale fluidized beds.

MFIX (Multiphase Flow with Interphase eXchanges) is a general-purpose computer code developed at the National Energy Technology Laboratory (NETL) for describing the hydrodynamics, heat transfer and chemical reactions in fluid-solids systems. It has been used for describing bubbling and circulating fluidized beds, spouted beds and gasifiers. MFIX calculations give transient data on the three-dimensional distribution of pressure, velocity, temperature, and species mass fractions. MFIX code is based on a generally accepted set of multiphase flow equations. However, in order to apply MFIX in an industrial context, key additional improvements are necessary. These key improvements correspond to the two ORNL efforts: (1) To develop an effective computational tool through development of a fast, parallel MFIX code and (2) Develop infrastructure for easy collaborative development of the MFIX code and exchange of information between the developers and users.

BACKGROUND

I. Development of a Fast, Parallel MFIX Code

While MFIX has successfully demonstrated to accurately describe fluid flow and reactive chemical processes in small experimental models, a typical model simulation of an industrial scale fluidized bed in three dimensions, using MFIX, requires several days of processing on a fast single processor workstation, thereby severely limiting the grid resolution. Relaxation of this limitation through implementation of fast parallel algorithms has become an essential ingredient to enable practical use in describing industrial processes.

At each time step, MFIX solves a set of nonlinear equations that couple mass, energy and momentum exchange, to the conservative velocity fields. The highly nonlinear response of solid phase material to solid pressure near the packed regime greatly adds to the stiffness and difficulty of solving these nonlinear equations. The simulation time step is greatly reduced if there is slow convergence in the nonlinear solver.

II. Collaborative Tools for MFIX Website and Code Development

A wide range of developers from industry, universities and national labs are involved in developing the MFIX code. In order to facilitate this collaboration, a set of web-based tools have to be put together for seamless integration of the various components. In addition, a website interface would have to be set up to help free exchange of information between the developers, researchers and users.

RESULTS AND DISCUSSION

ORNL along with its collaborators (NETL, Aeolus, Inc.) has been involved in migration of MFIX to modern high-performance parallel architectures. A hybrid parallel version of MFIX has been developed using MPI communication library and OpenMP compiler directives on shared memory environments. The code has been ported to Linux Beowulf cluster, IBM SP, SGI multiprocessors, and Compaq clusters. Various optimizations and developments are made to improve performance and reduce communication costs for simulations using MFIX. Most of these results have been reported at the SIAM conference (D'Azevedo et. al.). Two cases are discussed here. The first one is an ozone decomposition simulation using a grid—$76 \times 112 \times 16$ or 130 thousand cells. The domain is decomposed both in the radial and axial directions. The simulation was performed on the Alpha cluster at ORNL. This COMPAQ cluster has 64 "Alpha EV67" nodes and each node has four 667 MHz and 2 GB of memory. The multi-processor machine has 2 TB of fiber channel disk. As can be seen in Fig. 1, the scaling for this relatively small problem is quite good up to 16 processors.

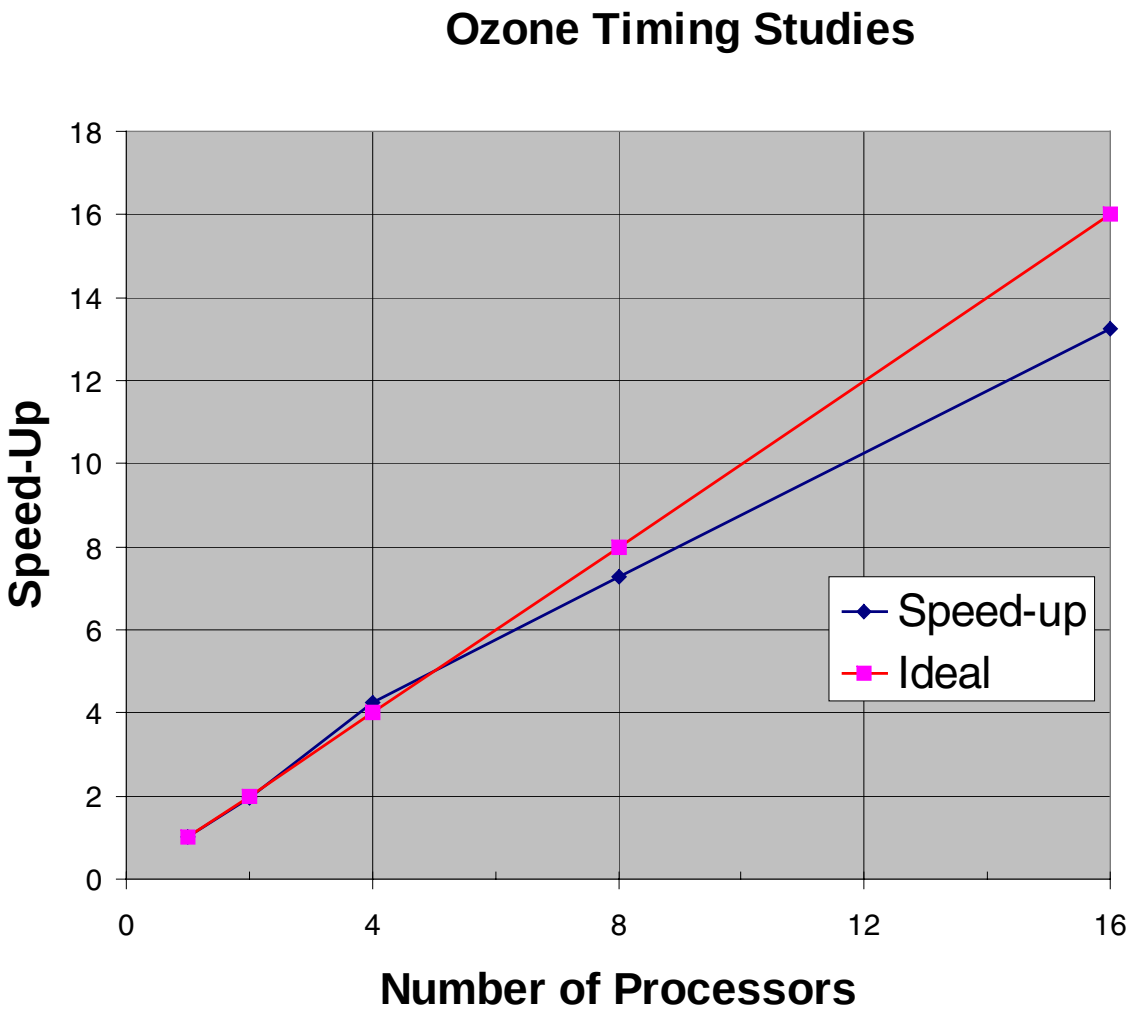

Fig. 1. Scaling studies for the ozone decomposition simulation.

The next problem (Fig. 2) is simulation of a square-cross section Circulating Fluidized Bed (CFB). The problem has 1.08-million grid points ($60 \times 300 \times 60$). The grid has been decomposed in all three directions. The problem scales reasonably well till 32 processors and tends to flatten out beyond that. Performance is not remarkable at 128 processors but the wall-clock time is considerably less (10 minutes compared to 10 hours on 1 processor) leading to fast turn-around of results. These are not the most optimized results and different decomposition and pre-conditioner options are being tested out.

CVS (concurrent version system) has been used for seamless integration of the various components of the development work. Web/Java based tools have been used to make this process easier and facilitate the virtual collaboration between these diverse set of developers and researchers. In addition, a website (www.mfix.org) has been started to help free exchange of information between the developers, researchers and users. Over 60 researchers have downloaded MFIX and some of them are active

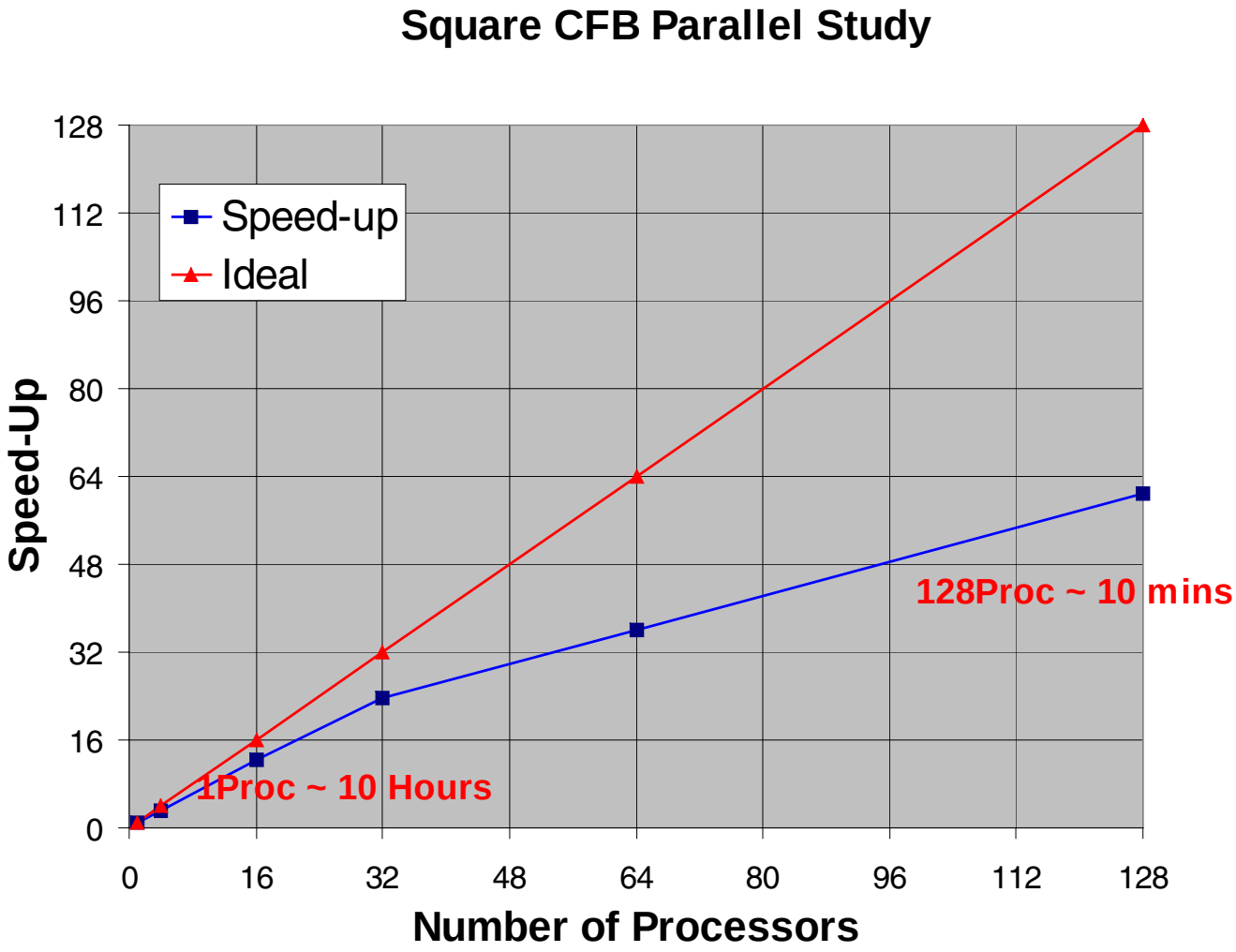

Fig. 2. Scaling studies for the square cross-section CFB.

participants in various discussions through the mailing lists. These researchers are from National Labs, Universities, Industry, and Research Labs around the world (see Table 1). The MFIX code and the collaborative experience was submitted for the R&D 100 awards by NETL.

The efforts will be continued into next year. In addition, implementation of various non-linear coupled solvers for faster convergence would be explored.

Table 1. Affiliations of researchers who have downloaded MFIX code from www.mfix.org

Aeolus Research	IIT, Delhi	Reaction Engineering
ANL	Instituto de Investigaciones Electricas	San Diego State University
Carnegi Mellon University	Instituto Mexicano del Petroleo	Texas A&M University
Colorado School of Mines	Iowa State	The University of Akron
Computational Dynamics Limited	Laboratoire Magmas et Volcans	University of Washington
Consiglio Nazionale delle Ricerche	LANL	Universite de Rennes1
Dalhousie University	Millenium	University of Bristol
Delft University of Technology	Michigan Tech	UNIVERSITY OF CALGARY
Edinburgh University	National Research Council of Canada	University of Milan
ExxonMobil Research & Engineering	NETL	University of Saskatchewan
FLUENT	ORNL	US Steel
Foster Wheeler Development Corp.	Politecnico di Milano	Wroclaw University of Technology
National Academy of Sciences of Belarus	Princeton	West Virginia University
IIT, Bombay	Pittsburgh Supercomputing Center	

REFERENCE

D'Azevedo, E., Pannala, S., Syamlal, M., Gel, A., Prinkey, M., and O'Brien, T., "Parallelization of MFIX: A Multiphase CFD Code for Modeling Fluidized Beds," Session CP15, *Tenth SIAM Conference on Parallel Processing for Scientific Community*, Portsmouth, Virginia, March 12–14, 2001.